Imperial College London

Life-cycle modelling of lithium-ion batteries for electric vehicles

by

Evangelos Kallitsis

Imperial College of Science, Technology and Medicine

Department of Earth Science and Engineering

A thesis submitted to Imperial College London for the degree of

Doctor of Philosophy

November 2022

This page is intentionally left blank

In memory of my grandfather,

Evangelos Avramidis (1930-2022),

for staying positive during hard times.

This page is intentionally left blank

Abstract

The transition to clean energy and electric mobility is driving unprecedented demand for Li-ion batteries (LIBs), creating a need for sustainable manufacturing hubs and supply chains. The dynamic nature of the LIB market creates the need to account for the environmental impacts of value chains and technological options. In this direction, Life Cycle Assessment (LCA) is a crucial tool to support decision-making towards avoiding shifting environmental burdens from one part of the planet to another or diminishing current environmental problems to create new ones**.** A detailed and modular engineering-system inspired life cycle model for automotive traction LIBs was developed in this research. First, the LCA of LIB production component model was developed accounting for the environmental burdens of producing lithium nickel-manganese-cobalt (NMC) oxide batteries and quantifying the impact of the Chinese domination in LIB manufacturing. Novel NMC batteries were shown to exhibit similar threats to humans and ecosystems as the commercialised ones, occurring mainly from the metals used in the battery cells, with an obvious environmental benefit being realised due to their improved energy densities. The production of LIBs in China was shown to come at a high environmental cost of 40% higher Global Warming Potential (GWP) than earlier literature suggests. Second, an LCA and techno-economic analysis of LIB utilisation in electric vehicles was performed, accounting for different thermal management solution. It was demonstrated that by optimising the battery thermal management system, the battery life cycle cost and carbon footprint can be reduced by 27 % and 25%, respectively. Third, hydrometallurgical and pyrometallurgical recycling chains for spent automotive traction LIB packs were analysed and the respective LCA inventories were developed. Pyrometallurgical processing of spent automotive traction battery cells was shown to have a larger GWP, due to its higher energy intensity. Battery recycling was found to be highly beneficial from an environmental perspective, with a net benefit being achieved in 11 out of 13 environmental impact categories, as compared to battery production without recycling. Overall, this thesis provides quantitative evidence to enable the promotion of sustainability throughout the entire LIB value chain, as well as transparent and reproducible models for each stage of their life cycle.

This page is intentionally left blank

Statement of originality

The work included in this thesis is original and has not been submitted for the requirements of any other degree. Results obtained in the course of this research have been presented in a series of peer-reviewed publications and a white paper, which are discussed in different chapters of this thesis as shown below.

Chapter 2

Kallitsis, E., Lander, L., Edge, J., Bravo Diaz, L., Brown, A., Kelsall, G., Offer, G., Korre, A. (2022) Safe and sustainable lithium-ion batteries. doi.org/10.25561/95548.

Chapter 4

Kallitsis, E., Korre, A., Kelsall, G., Kupfersberger, M., & Nie, Z. (2020). Environmental life cycle assessment of the production in China of lithium-ion batteries with nickel-cobalt-manganese cathodes utilising novel electrode chemistries. *Journal of Cleaner Production*, *254*, 120067. doi.org/10.1016/j.jclepro.2020.120067.

Chapter 5

Kallitsis, E. (2022). On the energy use of battery Gigafactories. *Journal of Cleaner Production*, 132573. doi.org/10.1016/j.jclepro.2022.132573.

Chapter 6

Lander, L.*, **Kallitsis, E.***, Hales, A., Edge, J. S., Korre, A., & Offer, G. (2021). Cost and carbon footprint reduction of electric vehicle lithium-ion batteries through efficient thermal management. *Applied Energy*, *289*, 116737. doi.org/10.1016/j.apenergy.2021.116737.

Chapter 7

Kallitsis, E., Korre, A., & Kelsall, G. (2022). Life cycle assessment of recycling options for automotive Li-ion battery packs. *Journal of Cleaner Production, 371,* 133636. doi.org/10.1016/j.jclepro.2022.133636.

(Note: * indicates equally contributing authors)

This page is intentionally left blank

Copyright Declaration

The copyright of this thesis rests with the author. Unless otherwise indicated, its contents are licensed under a Creative Commons Attribution-Non Commercial 4.0 International Licence (CC BY-NC).

Under this licence, you may copy and redistribute the material in any medium or format. You may also create and distribute modified versions of the work. This is on the condition that: you credit the author and do not use it, or any derivative works, for a commercial purpose.

When reusing or sharing this work, ensure you make the licence terms clear to others by naming the licence and linking to the licence text. Where a work has been adapted, you should indicate that the work has been changed and describe those changes.

Please seek permission from the copyright holder for uses of this work that are not included in this licence or permitted under UK Copyright Law.

This page is intentionally left blank

Acknowledgements

First and foremost, I would like to express my deepest gratitude to my supervisor, Professor Anna Korre, for making my doctoral studies an enjoyable journey. She inspired me to undertake this journey and motivated me throughout to improve and contribute to the scientific community. She taught me the importance of taking initiative and encouraged me to develop as a researcher. We have been through good and hard times together, and she was always there to support me and share her experienced point of view. She also encouraged me to teach and supervise, an opportunity which has left me with a series of good memories. Her work ethic, agility and "never give up" attitude will accompany me for a lifetime.

I am also grateful to my co-supervisor, Professor Geoff Kelsall, for always being willing to advise and provide valuable insights towards improving the quality of this work. His rigorous thinking and scientific expertise helped me obtain a better understanding of modern electrochemistry. I would also like to thank the UK Engineering and Physical Sciences Research Council (EPSRC) for providing constant financial support throughout the course of this journey.

This thesis was undertaken throughout challenging times for humanity and having the academic family of the Minerals, Energy and Environmental Engineering Research Group (MERG) by my side has been essential in overcoming obstacles and enjoying my everyday life at the College. I would especially like to thank my coffee partner, Denis Martins Fraga, for always being there to discuss issues ranging from our academic life to sports, and the past and current members of MERG: Professor Sevket Durucan, Dr. Ernesto Santibanez Borda, Yu Zhang, Quentin Wolf, Dr. Zhenggang Nie, Dr. Wenzhuo Cao, Dr. Maria Lathouri, Dr. Betul Yildirim, Dr. Harshit Agrawal, Xuehao Yuan and Junjun Li, for all the unforgettable times we spent together.

Part of this research was undertaken in collaboration with the Electrochemical Science and Engineering (ESE) group at Imperial College London. It has been a great experience to closely collaborate with Dr. Laura Lander, who I thank for her scientific input and her positive attitude.

I am also grateful to Professor Gregory Offer and Dr. Jacqueline Edge for the fruitful collaboration.

I had the opportunity to share my research through the Energy Futures Lab (EFL) and the Institute of Molecular Science and Engineering (IMSE) on a series of occasions. I am thankful towards both institutes for encouraging me to reach wider audiences, beyond the traditional academic communities and to appreciate the importance of scientific communication.

On a more personal note, I wish to thank my family for their constant support and love. The optimism and smile of my mother, Olympia, has been a constant source of energy for me throughout the years. The career of my father, Joannis, has been a true inspiration for me, to aim and generate impact, and has taught me that unconditional giving can produce optimal outcomes. My agile and ambitious older brother, Konstantinos, has been a constant source of motivation in undertaking new challenges. Their warmth and hugs during my visits to our home in Greece have been a key in powering this journey.

Last but not least, I would like to thank my partner Paola Alejandra Saenz Cavazos, as her beautiful smile and unconditional love make me forget even the hardest day at work. Undertaking our MSc and then PhD degrees in parallel has enabled us to support, understand and motivate each other. I am blessed to have her by my side.

Table of contents

Chapter 1 Introduction and objectives 28
1.1 Introduction 28
1.2 Research objectives 33
1.3 Thesis overview 34
Chapter 2 Lithium-ion batteries for electric vehicles: technology and value chain 37
2.1 Battery cell fundamentals 37
2.2 LIB technologies 41
2.3 LIB pack design 44
2.4 LIB value chain 48
2.4.1 Materials for lithium-ion batteries 48
2.4.2 Lithium-ion battery production 54
2.4.3 LIB utilisation in electric vehicles 58
2.4.4 End-of-life for LIBs 59
Chapter 3 Life Cycle Assessment of Li-ion batteries 63
3.1 Life cycle assessment framework 63
3.1.1 Goal and scope definition 64
3.1.2 Life cycle inventory analysis 67
3.1.3 Life cycle impact assessment 69
3.1.4 Interpretation 73
3.1.5 Reporting the results 74
3.2 Life cycle costing 75
3.3 LCA studies on LIB production 76

3.3.1 General overview 76
3.3.2 Methodological choices 80
3.3.3 Reported results across LCAs of battery production 81
3.4 Studies on the LIB utilisation phase 82
3.4.1 ICEVs vs EVs 83
3.4.2 Methodological choices 84
3.4.3 Reported results across LCAs of EVs 85
3.5 Studies on LIB end-of-life 87
3.5.1 General overview 88
3.5.2 Methodological choices 88
3.5.3 Reported results across LCAs of LIB recycling 90
3.6 Methodological choices of this research 91
Chapter 4 Lithium-ion battery production LCA 94
4.1 Background and Motivation 94
4.2 Methods 97
4.3 Results and analysis 104
4.3.1 Cradle-to-gate impacts for all scenarios 104
4.3.2 Contribution analysis 105
4.4 Discussion 108
4.4.1 Chinese LIB manufacturing inventories 108
4.4.2 Breakdown and analysis 109
4.4.3 Future perspectives 112
4.5 Conclusions 113
Chapter 5 Reducing the GHG intensity of battery manufacturing 114
5.1 Background and motivation 114
5.1.1 Critical literature review 115

5.1.2 Pack vs cell level 115
5.1.3 GHG footprint of battery materials and the effect of energy density 116
5.2 Results and analysis 117
5.2.1 Meta-analysing literature data on the energy use of battery Gigafactories 117
5.2.2 Reducing the cradle-to-gate carbon footprint of LIBs 119
5.3 Discussion 120
5.4 Conclusions 122
Chapter 6 Cost and carbon footprint modelling for electric vehicles 123
6.1 Background and Motivation 123
6.2 Methods 126
6.2.1 Battery life cycle costs and emissions 127
6.2.2 Battery and TMS technologies 132
6.2.3 Determination of the maximum cell temperature 133
6.2.4 Capacity fade modelling 134
6.3 Results and analysis 135
6.3.1 Battery cycling life 135
6.3.2 Life cycle emissions and costs 139
6.4 Discussion 141
6.4.1 Sensitivity analysis 141
6.4.2 Impact of thermal gradients on LCC and CF 144
6.4.3 Modified cell design for tab cooling 144
6.5 Conclusions 148
Chapter 7 Lithium-ion battery recycling LCA 150
7.1 Background and Motivation 150
7.2 Methods 154
7.2.1 LCA methodology 154

7.2.2 Inventory analysis 157
7.2.3 Materials recovery and crediting 158
7.3 Results and analysis 161
7.3.1 Environmental impact of recycling 161
7.3.2 Environmental benefit of recycling 164
7.4 Discussion 166
7.4.1 Reducing the environmental impact of battery production 166
7.4.2 Sensitivity analyses 167
7.4.3 LIB recycling environmental performance and comparison with preceding studies 172
7.4.4 Recovered materials value 173
7.4.5 Data gaps, limitations and future perspectives 175
7.5 Conclusions 177
Chapter 8 Innovation and contributions of this research 179
8.1 Recommendations for future research 182
References 184
Appendices 210
Appendix A: LIB production inventory tables 210
Appendix B: LIB recycling inventory tables 223

List of figures

Figure 1. Growth of lithium-ion battery demand by application projected until 2030 and challenges related to the increased amount of batteries (Kallitsis et al., 2022b). 29

Figure 2. Demand share for EV battery chemistries in Europe, modified after Element Energy (2019). 30

Figure 3. Thesis structure and interconnections between individual chapters.....36

Figure 4. Schematic example of a partially discharged Li-ion battery and corresponding analogue electronic circuit (Kallitsis et al., 2022b). 38

Figure 5. Schematic of potential distribution in example LIB when open circuit potential difference ΔE, and potential differences during discharging (Ud) and charging (|Uc|), at current density j (Kallitsis et al., 2022b). 39

Figure 6. Schematic example of effect of fractional depth of discharge on battery open circuit potential difference (Kallitsis et al., 2022b).....40

Figure 7. Timeline of the commercial history of LIB positive and negative electrode materials. Where possible, the bars provide a comparison between materials, according to five performance indicators, with 1 bar being the poorest and 5 bars the strongest (note: 1 bar for cost means highest price) (Kallitsis et al., 2022b). 41

Figure 8. Expected battery technology commercialisation scheme according to IEA (2018). 43

Figure 9. Typical mass composition of a LIB pack (Ellingsen et al., 2014). 45

Figure 10. (a) Schematic overview of air and liquid cooling thermal management systems with their respective components and (b) heat extraction direction for surface and tab cooling (Lander et al., 2021b). 47

Figure 11. Elemental mass composition of a typical 253 kg NMC333-Gr battery pack used in automotive traction applications (Kallitsis et al., 2022a) 49

Figure 12. Raw materials extraction processes for materials commonly used in LIBs (Kallitsis et al., 2022b). 52

Figure 13. Cradle-to-gate stages to produce a lithium-ion battery for electric vehicles (Kallitsis et al., 2022b). 54

Figure 14. Main process steps to assemble lithium-ion battery cells and packs (Kallitsis et al., 2022b) 56

Figure 15. Recycling process flow chart showing possible pathways to new cells and packs, including pyrometallurgical, hydrometallurgical and direct recycling (Kallitsis et al., 2022b). 62

Figure 16. Schematic diagram of iterative LCA framework showing the four phases of LCA according to ISO14040:2006 (ISO, 2006a). 64

Figure 17. Midpoint vs endpoint impact categories covered from the ReCiPe 2016 method (Huijbregts et al., 2016). 71

Figure 18. Overview of reported carbon footprints of battery production across literature studies. 81

Figure 19. Fuel and vehicle cycles for electric vehicles. Reprinted with permission from Wu et al. (2018), Copyright 2018, with permission from Elsevier. 84

Figure 20. Life cycle GHG emissions of current and future EVs per vehicle kilometer (vkm) driven accounting for uncertainty. The boxes contain 50% of the results, whereas the whiskers show the 5th and 95th percentiles and the red line shows the median result. Y axis labels show the background database that was used for the calculation: Ecoinvent uses the current electricity scenario, whereas Baseline and ClimPol show middle-of-the-road and aggressive climate policy scenarios for the future electricity sector, respectively. Reprinted with permission from Cox et al. (2018), Copyright 2018, with permission from the American Chemical Society…86

Figure 21. Life-cycle GHG emissions ICEVs and EVs registered in Europe, United States, China and India in 2021 and projected to be registered in 2030. Reprinted under Creative Commons License (CC BY-SA 4.0) from (Bieker, 2021), Copyright 2021, International Council on Clean Transportation. 87

Figure 22. Cradle-to-gate product system studied. Unit process boundaries indicate: black, inventory data were taken Ellingsen et al. (2014); blue, inventory data adopted from Majeau-Bettez et al. (2011) with corresponding heat and electricity requirement updated based on Dai

et al. (2019a) . Shading indicates: grey, inventory data identical to those of the cited paper in all scenarios, except for the background production processes; white, inventory data modified to serve the goals of this study (Kallitsis et al., 2020). 101

Figure 23. Percentage contribution of coal, natural gas, hydropower, nuclear and wind power to the Chinese electricity mix (Kallitsis et al., 2020). 103

Figure 24. Comparison between the calculated impacts of the BCG scenario to Ellingsen et al. (2014) based on the ReCiPe 1.08 Midpoint characterisation method (Kallitsis et al., 2020). 105

Figure 25. Cradle-to-gate impacts of battery production in China, reported quantitatively for different functional units and disaggregated to key background processes. The Baseline (BSL) scenario reflects the production of a 26.6 kW h NMC333-Gr and is comparable directly with literature studies. The nominal capacities of NMC333-SiGr, NMC622-SiGr and NMC811-SiGr were 40.9, 46.2 and 52.9 kW h respectively. Copper is used for the cathode current collector, cell container and packaging. Aluminium is used for the anode current collector, cell container and packaging; electricity for cell manufacturing; manganese and nickel for the cathode active material; silicon for the anode active material; printed wiring board and electronic component for the Battery Management System (Kallitsis et al., 2020). 108

Figure 26. Battery production Carbon Footprint (CF) in kg CO2 eq (kW h)-1 predicted for NMC333-Gr and NMC811-SiGr, and pilot-/Gigascale. Green indicates CF reduction from European Al use; yellow indicates CF reduction from hydroelectric power use. Reference years are based on the battery commercialisation projections of the IEA (Kallitsis et al., 2022b). 119

Figure 27. Methodological procedure for the life cycle cost and carbon footprint model applied in this study (Lander et al., 2021b). 127

Figure 28. Experimental (dots) and fitted (solid line) data for NMC333/Gr cell at 298 K, 308 K and 318 K based on de Hoog et al. (2017), (Lander et al., 2021b). 136

Figure 29. (a) predicted vs experimental RCD and (b) Coefficient of Variation (CV) vs FECs for fitting Eq. 6.14 to experimental data based on de Hoog et al. (2017), (Lander et al., 2021b). 137

Figure 30. Battery capacity as a function of FECs for air (blue line), tab (pink line), surface (orange line) and immersion (green line) cooling (Lander et al., 2021b). 139

Figure 31. Battery pack costs excluding the TMS, together with the additional cost of TMS as estimated from BatPac (Lander et al., 2021b). 140

Figure 32. (a) LCC (in $ km-1) and (b) CF (in kg CO2 eq km-1) for AC, TC, SC and IC, with battery, vehicle, electricity and maintenance contributions (Lander et al., 2021b). 140

Figure 33. (a) LCC and (b) CF sensitivity analyses for surface cooling varying the battery pack cost/footprint (green), electricity cost/footprint (blue) and lifetime (purple) by ±50%; the dashed line indicates the base value for SC as shown in Figure 32 (Lander et al., 2021b). ..143

Figure 34. Degradation rate plotted against cell cooling coefficient (CCC) for two- sided SC and TC of two lithium-ion pouch cells (Lander et al., 2021b). 146

Figure 35. (a) LCC (in $ km-1) and (b) CF (in kg CO2 eq km-1) for different TMS cooling options, with battery, vehicle, electricity and maintenance contributions (Lander et al., 2021b). 147

Figure 36. EoL recycling product system studied for the recovery of valuable metals from a spent automotive traction battery pack (collection of spent battery packs to generation of secondary materials) (Kallitsis et al., 2022a). 157

Figure 37. (a) Mass composition of the 253 kg NMC333-Gr automotive traction battery pack, (b) recoverable fractions and waste occurring from the hydrometallurgical case and (c) displaced primary materials from the recovered metal fractions of the battery pack; stoichiometric elemental contributions are displayed for the cathode materials (Kallitsis et al., 2022a). 160

Figure 38. Schematic representation of the material and product flows of an integrated LIB production and recycling system; the utilisation phase is excluded from the calculations and is shown in grey (Kallitsis et al., 2022a). 161

Figure 39. Environmental impacts of an NMC333-Gr battery pack recycling in China, disaggregated to key contributing processes. Battery cells are treated with either hydrometallurgical or pyrometallurgical processing in the two cases (Kallitsis et al., 2022a). 163

Figure 40. Environmental benefits of an automotive NMC333-Gr battery pack recycling in China, disaggregated to key contributing processes. Environmental benefits arose from the displacement of primary material based on the EoL recycling approach (Kallitsis et al., 2022a). 165

Figure 41. GWP of LIB production compared to production with EoL recycling for the hydrometallurgical and pyrometallurgical cases in China, North America and Europe (Kallitsis et al., 2022a). 169

Figure 42. Environmental benefit for battery-grade (BG) vs ore-grade (OG) material recovery in the case of hydrometallurgical treatment (Kallitsis et al., 2022a). 171

Figure 43. Economic value of recovered material for one battery pack using the (a) Hydrometallurgical (total: USD 1 079) and (b) Pyrometallurgical (total: USD 816) processes (Kallitsis et al., 2022a). 175

List of tables

Table 1. Description of midpoint impact categories used throughout this thesis, modified after Huijbregts et al. (2017) 72

Table 2. Overview of LCA studies on LIB production for automotive traction applications. 78

Table 3. Overview of the methodological choices for the development of the LIB production, utilisation and end-of-life models. 91

Table 4. Reported GWP of NMC LIB manufacturing across different studies (Kallitsis et al., 2020). 96

Table 5. Input parameters to calculate resulting energy storage capacity of advanced LIBs (Kallitsis et al., 2020). 98

Table 6. Energy storage capacity and energy density of novel electrode chemistries compared to the baseline (Kallitsis et al., 2020). 100

Table 7. Reported energy use for cell production across studies focusing on NMC batteries produced in the Giga-scale (Kallitsis, 2022). 118

Table 8. Summary of inputs to the utilisation LCC model (Lander et al., 2021b). 130

Table 9. Summary of inputs to the utilisation LCA model (Lander et al., 2021b). 131

Table 10. Cell and pack properties for an NMC333/Gr chemistry (Ellingsen et al., 2014; Hoog et al., 2017) 133

Table 11. Heat generation Q̇gen, refrigerant inlet temperature and CCC for surface, tab and immersion cooling (Lander et al., 2021b). 135

Table 12. ΔT and maximum cell temperature for each TMS under study (Lander et al., 2021b). 138

Table 13. Full Equivalent Cycles (FECs), travelled distance over lifetime (Dkm) and lifetime in years (n) for a 26.6 kWh battery pack including air, tab, surface or immersion cooling (Lander et al., 2021b). 139

Table 14. Summary of degradation results and cell cooling coefficients of two lithium-ion pouch cells with different geometry (Lander et al., 2021b). 145

Table 15. Reported GWP of NMC battery production and recycling across published studies (Kallitsis et al., 2022a). 153

Table 16. Main data sources and assumptions for the compilation of the recycling LCI (Kallitsis et al., 2022a). 159

Table 17. Environmental impact of battery production, burden and benefit of battery recycling and their combined effect in the environmental footprint of an NMC333-Gr battery pack. The "Total" is calculated as the sum of the production burden, recycling burden and benefit and "Net" refers to the net benefit on battery production when including recycled material,which is calculated as a percentage comparison between the "Total" and the production burden (Kallitsis et al., 2022a). 167

Table 18. Background Ecoinvent datasets used for the investigation of geographic specificity effects to the combined production and recycling GWP (Kallitsis et al., 2022a). 169

Table 19. Displaced material datasets for the battery-grade (BG) vs ore-grade (OG) cases (Kallitsis et al., 2022a). 170

Table 20. Prices of recovered materials from the battery pack in 2019 (Kallitsis et al., 2022a). 174

List of abbreviations

AC	Air Cooling
ADP	Abiotic Depletion Potential
AP	Acidification Potential
BatPac	Battery Performance and Cost model
BCG	Background scenario
BG	Battery Grade
BMS	Battery Management System
BOM	Bill of Materials
BSL	Baseline scenario
C-rate	Cycling rate
CALCD	China Automotive Life Cycle Database
CCC	Cell Cooling Coefficient
CED	Cumulative Energy Demand
CF	Carbon Footprint
CH	Switzerland
CN	China
CV	Coefficient of Variation
DE	Germany
DMC	Dimethyl Carbonate
DOD	Depth-of-Discharge
EC	Ethylene Carbonate
EoL	End-of-Life
EEA	European Environment Agency
EFL	Energy Futures Lab
EV	Electric Vehicle

FDP	Fossil Depletion Potential
FEC	Full Equivalent Cycle
FEP	Freshwater Eutrophication Potential
FETP	Freshwater Ecotoxicity Potential
FPMFP	Fine Particulate Matter Formation Potential
GHG	Greenhouse Gas
GLO	Global
GREET	Greenhouse gases, Regulated Emissions, and Energy use in Technologies model
GWP	Global Warming Potential
HTP	Human Toxicity Potential
IC	Immersion Cooling
ICEV	Internal Combustion Engine Vehicles
IEA	International Energy Agency
IMSE	Institute of Molecular Science and Engineering
IPCC	Intergovernmental Panel on Climate Change
ISO	International Standardisation Organisation
KR	South Korea
LCA	Life Cycle Assessment
LCC	Life Cycle Costing
LCI	Life Cycle Inventory
LCIA	Life Cycle Impact Assessment
LCO	Lithium Cobalt Oxide
LFP	Lithium Iron Phosphate
LiS	Lithium Sulfur
LIB	Lithium-Ion Battery
LiM	Lithium Metal
LiPo	Lithium Polymer
LMO	Lithium Manganese Oxide
LME	London Metal Exchange
LTO	Lithium Titanate
MDP	Metal Depletion Potential

MEP	Marine Eutrophication Potential
METP	Marine Ecotoxicity Potential
NCA	Nickel Cobalt Aluminium oxide
NiMH	Nickel Metal Hydride
NMC	Lithium Nickel Cobalt Manganese Oxide
NMP	*N*-Methyl-2-pyrrolidone
NO	Norway
NPV	Net Present Value
ODP	Ozone Depletion Potential
OEM	Original Equipment Manufacturer
OG	Ore Grade
PC	Propylene Carbonate
PEF	Product Environmental Footprint
PM	Particulate Matter
PMFP	Particulate Matter Formation Potential
POFP	Photochemical Oxidant Formation Potential
PVDF	Polyvinylidene Difluoride
RAS	Asia
RCD	Relative Capacity Degradation
RER	Europe
RLA	Latin America and the Caribbean
RoW	Rest of World
SC	Surface Cooling
SE	Sweden
SEI	Solid-Electrolyte Interface
SOC	State-of-Charge
SODP	Stratospheric Ozone Depletion Potential
TAP	Terrestrial Acidification Potential
TC	Tab Cooling
TCO	Total Cost of Ownership
TETP	Terrestrial Ecotoxicity Potential

TMS	Thermal Management System
USGS	United States Geological Survey
WHO	World Health Organisation
WTW	Well-to-Wheels

Chapter 1 Introduction and objectives

1.1 Introduction

Poorly controlled emissions of gases and particles from human activities in the atmosphere have led to two serious threats human and ecosystems health, climate change and air pollution. The former threatens to cause sea level rise and extreme weather phenomena, posing significant risks such as species loss and extinction, limited food and water supply, flooding and damage to infrastructure (IPCC, 2018). The latter has been found to cause 4.2 million premature deaths annually (WHO, 2014). Rapid, far-reaching and unprecedented changes are vital to limit global warming to 1.5 ^{0}C and there is an imperative need for improving air quality (IPCC, 2018).

The transport sector is a major contributor to greenhouse-gas (GHG) and air pollution emissions. The fossil-fuel based transport accounted for 24% of global GHG emissions in 2015, with approximately 75% of them attributed to road transport (International Energy Agency, 2017). Transport is also responsible for more than half of nitrogen oxide (NOx) emissions and contributes approximately 13% to other air pollution emissions (EEA, 2014). Moreover, it is a significant source of noise pollution (EEA, 2017). These adverse effects, alongside the geopolitically driven limited availability of fossil fuel resources and energy security concerns suggest that present fossil-fuel based transport systems are not sustainable. There is broad agreement in the scientific community that meeting sustainability goals in the transport sector requires a shift on the underlying vehicle technology, with electric vehicles (EVs) considered the most promising alternative to internal combustion engine vehicles (ICEVs) (Mosaberpanah and Khales, 2012) from a technology, infrastructure and cost perspective (Berckmans et al., 2017; Liu et al., 2013). According to the International Energy Agency (IEA) (2018), the EV fleet is predicted to surge within the next decade, reaching 220 million EVs on the road by 2030.

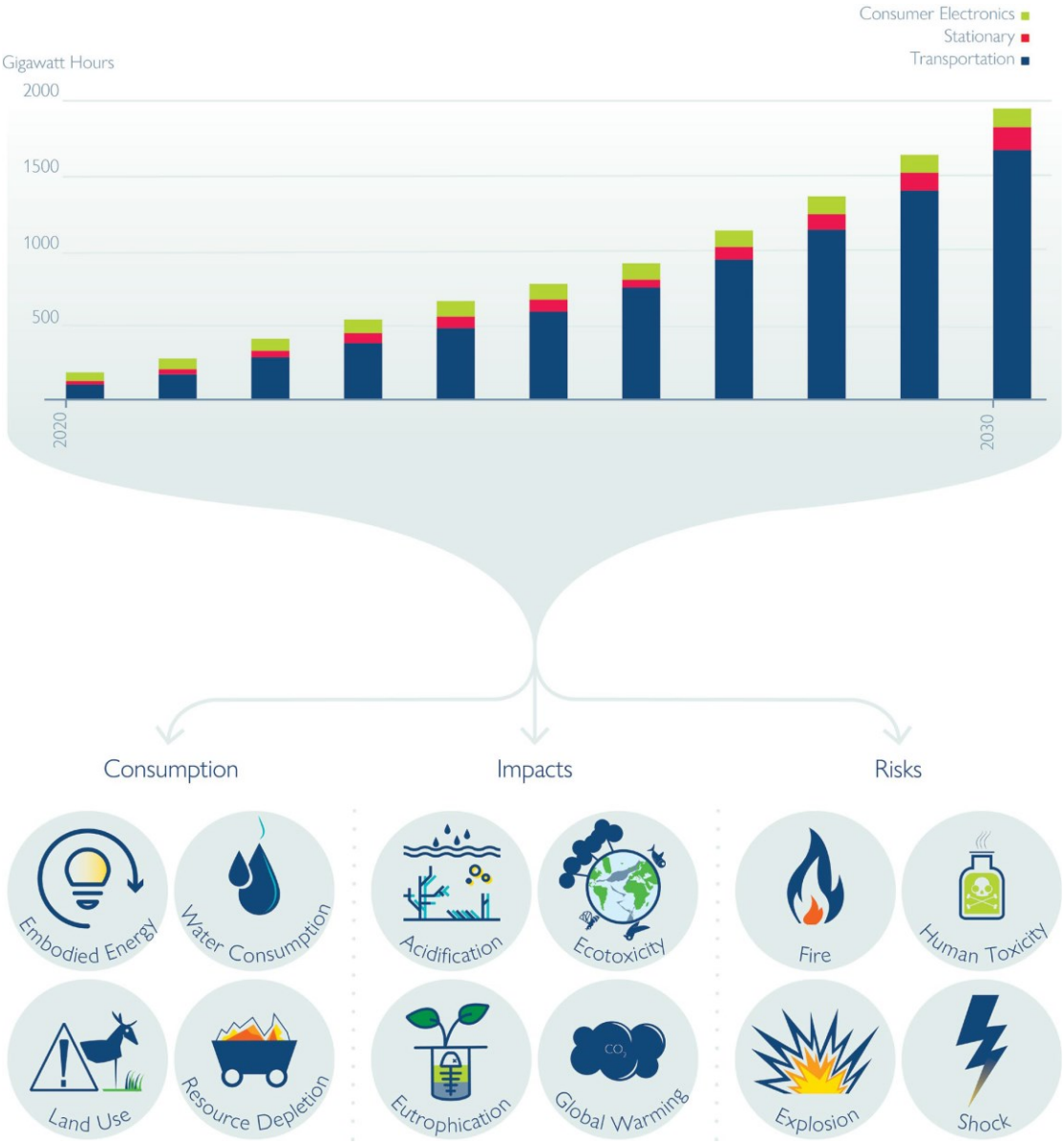


Figure 1. Growth of lithium-ion battery demand by application projected until 2030 and challenges related to the increased amount of batteries (Kallitsis et al., 2022b).

The key enabler of the large-scale uptake of EVs are improved lithium-ion batteries (LIBs), offering higher mass specific energies, volumetric energy densities, potential differences and energy efficiencies (Linden and Reddy, 2002). As illustrated in **Figure 1**, demand for batteries is expected to increase nine-fold by 2030, compared to 2019 levels, primarily driven by the requirement for batteries to satisfy the transformation to electric mobility (World Economic Forum, 2019). LIBs are the predominant choice for automotive applications due to their advanced manufacturing technology availability, evidence of continuous cost reduction and the potential to store increased amounts of energy compared to competing battery technologies (Iclodean et al., 2017; International Energy Agency, 2018).

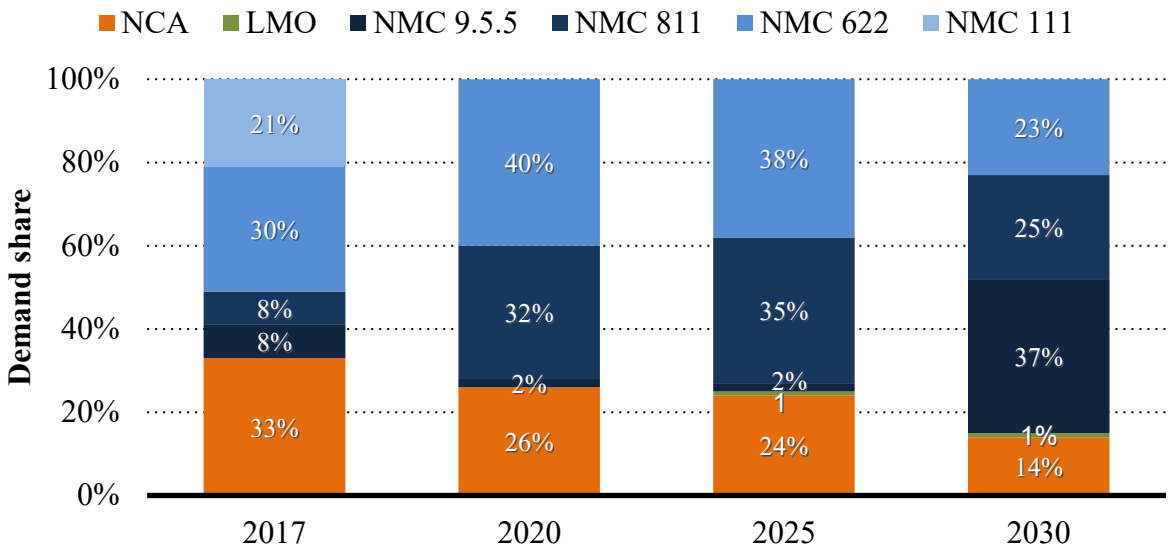


Figure 2. Demand share for EV battery chemistries in Europe, modified after Element Energy (2019).

A series of technologies have been developed since the invention of LIBs in the 1980s by John Goodenough, Stanley Whittingham and Akira Yoshino, who received the 2019 Nobel Prize in Chemistry. As a common denominator, rechargeable batteries consist of one or more electrochemical cells, each containing a positive and negative electrode, separated by a micro-porous membrane and all immersed in an organic electrolyte solution. LIBs are often categorised based on the positive electrode material used in them, with the most relevant chemistries for automotive applications including lithium nickel cobalt manganese (NMC) and nickel cobalt aluminium (NCA) oxides. Also, lower cost lithium manganese oxide (LMO) and lithium iron phosphate (LFP) chemistries have been developed. **Figure 2** illustrates how the demand of these technologies is expected to evolve in the future.

While EVs are known to be zero-emission during their operation, a series of environmental impacts occur throughout the value chain of the batteries that are used in them, as illustrated in **Figure 1**. From the early days of EV adoption, the need to employ wholistic schemes to study the LIB value chain was highlighted in an effort to avoid burden shifting. This has triggered a growing interest in the scientific community in quantifying the environmental impacts occurring through the LIB value chain (Cusenza et al., 2019; Nealer and Hendrickson, 2015; Nordelöf et al., 2014; Peters and Weil, 2018) using life cycle assessment (LCA). The principles and framework for performing such modelling exercises are provided by the International Standardisation Organisation (ISO) 14040 to 14044 standards (ISO, 2014, 2006a, 2003, 2001). When applied to LIBs, an LCA study is subject to prespecified technological, spatial and

system boundaries including: (a) the type of the battery studied, including its chemistry, cell geometry and pack design, (b) the production, utilisation and end-of-life (EoL) location and (c) the value chain steps that are taken into consideration. As the battery value chain is a complex and geographically distributed system, the different steps included in it should be studied separately, including production, utilisation and EoL.

LIB production includes the steps from raw material extraction to battery pack assembly. LCA studies on LIB production have gained attention due to the increased GHG emissions (Nealer and Hendrickson, 2015) and toxicity potential for humans (Nordelöf et al., 2014) associated with it. An early overview of the published LCAs on battery production was given by Peters et al. (2016). The most reliable and transparent studies have been performed by Notter et al. (2010), Dai et al. (2019a) Dunn et al. (2015), Ellingsen et al. (2014), Kim et al. (2016) and Majeau-Bettez et al. (2011). From a technological perspective, those studies focus on standard battery chemistries, allowing for a knowledge gap concerning the industry strive in increasing the nickel content of cathodes and blending the graphitic anodes with silicon. Additionally, few studies have been geographically focused on China (Hao et al., 2017a; Qiao et al., 2019; Xiong et al., 2019; Yu et al., 2018) reporting lower GHG emissions compared to studies focusing on the rest of the world (Ellingsen et al., 2014; Kim et al., 2016; Majeau-Bettez et al., 2011), which is counter-intuitive given China's strong dependence on coal. The environmental implications of the Chinese domination in LIB production remain to be understood. The above create the need for a transparent and reproducible LCA study focusing on LIB production in China, accounting for newly-emerging electrodes with high nickel cathodes and silicon-graphite anodes. Finally, early numbers on the energy use of battery manufacturing plants have reported significanly higher amounts of energy used in the production chain of LIBs (Ellingsen et al., 2014), compared to more recent literature (Dai et al., 2019a), creating the need to apply filtering criteria and quantify the effect of upscaling battery manufacturing from an environmental perspective.

Besides the increased environmental impacts occurring from LIB production, the LIB represents a very significant part of an EVs overall cost, creating an imperative need for accurate LIB cost quantifications through the value chain. Schmuch et al. (2018) reviewed active materials, separators, electrolytes and cell chemistries for automotive batteries from a cost and performance standpoint. Berckmans et al. (2017) performed process-based cost calculations for NMC batteries in an effort to project battery costs up to 2030. The most reliable

and publicly available LIBs costing scheme is offered by the Battery Performance and Cost (BatPaC) model of the Argonne National Laboratory (Nelson et al., 2012), which calculates the cost incurred by the original equipment manufacturer (OEM) accounting for every step in the lithium-ion battery manufacturing process. The cost implications associated with the potential environmental benefits of EVs are not well understood yet. Most of the ongoing research is focusing on the costs incurred by the OEM ignoring those incurred by the time the ownership of the vehicle is transferred to the consumer. An investigation of the total cost of ownership (TCO) is of significant importance in revealing the economic implications associated with the increased market adoption of EVs. Following a life cycle costing (LCC) analysis scheme could reveal hotspots for effective cost reductions in the value chain and could enable a better understanding of them through a detailed cost breakdown.

Both LCAs and LCCs of LIBs are quite sensitive to the lifespan assumed during their utilisation phase in vehicles. Currently car manufacturers are willing to compromise on the attainable cycle number of next generation batteries in order to increase the range per cycle (Schmuch et al., 2018) and thus tackle range anxiety for the consumers. However, from an environmental perspective, a long battery lifetime is highly important because it partly determines the EV's carbon footprint. The high environmental burdens occurring from the LIB production chain can be typically offset by a high battery lifetime (Peters et al., 2016; Romare and Dahllöf, 2017; Zackrisson et al., 2010). Also, the production costs of LIBs will lead to a higher TCO for LIBs with shorter lifespans. Therefore, the unresolved issue regarding the uncertain lifespan of LIBs begs the question of whether next-generation batteries will be responsible for a much higher impact-intensity from an environmental standpoint and an increased cost to the end-user.

The upscaled LIB production capacity has led to an increased interest on their post-usage fate. The dominant choices include recycling (Gaines, 2014), repurposing for a second use (Ahmadi et al., 2017) and disposal. Battery recycling appears to be the dominant technology option for end-of-life treatment of automotive LIBs, as it can divert batteries away from landfills, towards industrial-scale hydrometallurgical and pyrometallurgical processes, which are already being deployed around the world (Chen et al., 2019; Harper et al., 2019). Additionally, battery recycling offers a stream of raw materials, which is crucial in regions with limited availability of primary resources, such as Europe, and provides efficient means of handling scrap from battery Gigafactories (Peel and Sanderson, 2020). From an environmental standpoint, battery recycling can be beneficial in the case that the environmental burdens occurring from the end-of-life treatment chain are lower than the benefits arising from the generation of secondary

materials. A series of LCA studies on NMC LIB recycling have been performed so far (Accardo et al., 2021; Ciez and Whitacre, 2019; Cusenza et al., 2019; Mohr et al., 2020; Sun et al., 2020). As a common denominator, literature reports focusing on the recovery of the battery electrode materials (Ciez and Whitacre, 2019; Mohr et al., 2020), which constitute less than half of a battery pack's mass, neglect significant fractions of aluminium, copper and steel that could be recovered from the battery pack's packaging, thermal management system (TMS) and battery management system (BMS). This creates the need for an environmental investigation of a circular battery value chain on a pack level, from the point it reaches its end-of-life, accounting for collection, transportation, sorting and dismantling of the cells from the battery pack, and materials recovery processes. Additionally, an open question exists regarding the geographic specificity of the EoL treatment chain, given that different local electrical energy and material footprints influence the environmental burden of recycling chains, but also its benefit, as displaced material footprints differ significantly across locations.

1.2 Research objectives

The overarching aim of this thesis was to study the production, use and end-of-life stages for LIBs using the LCA methodology. The primary focus was on current and future NMC battery chemistries, as they are the dominant technology for automotive applications (McKinsey&Company, 2018). Each life cycle stage was studied in detail and the life cycle component models developed were combined with cost calculations to provide holistic quantitative insights where necessary. The objectives of the research include:

a) The compilation of a fully transparent LCA inventory model based on the state-of-the-art in the literature in order to assess the environmental impacts associated with the production of current and non-commercialised LIBs in China.
b) The refinement of energy use data of battery Gigafactories based on filtering criteria on production scale and battery chemistry, and the quantification of the effect of upscaling battery manufacturing plants based on the production LCA model developed in this thesis.

c) The development of a use phase life cycle model calculating the costs and environmental impacts occurring during the utilisation of LIBs in an EVs, accounting for battery degradation effects which have been overlooked in the literature so far.
d) The development of a battery recycling life cycle model and the investigation of the environmental burdens and benefits of battery recycling on a pack level focusing on hydrometallurgical and pyrometallurgical treatment schemes, enabling to examine the role recycling plays in reducing the overall environmental impact of the battery pack when combining it with battery production.

1.3 Thesis overview

This thesis presents research regarding the LCA modelling of the automotive LIB value chain and discusses relevant cost aspects. The main structure of the thesis is depicted in **Figure 3**.

Chapter 2 provides a literature overview of the technological, market and value chain aspects associated with automotive LIBs. An introduction to the dominant battery technologies for automotive applications is followed by a brief description on the operation of battery cells and the design of battery packs. Finally, the main steps included in the automotive LIB value chain are outlined, including battery production, utilisation and end-of-life.

Chapter 3 outlines the ISO-compliant life cycle assessment framework and its applications in the LIB research domain. First, the theoretical background of life cycle assessment is introduced together with some aspects regarding life cycle costing. Second, key methodological choices in LCA studies of automotive LIBs are outlined for battery production, utilisation and end-of-life. Concluding the chapter, key modelling choices for the application of LCA to study LIB production, use and recycling in this thesis are highlighted.

Chapter 4 summarises the model development for the battery production LCA and reports the results for current and non-commercialised battery chemistries in China. The specific literature gaps are identified, followed by a description of the LCI developed (shown in detail in Appendix A) and of the various scenarios studied. Finally, the results are presented and discussed in detail and conclusions are made on the impact of Chinese LIB manufacturing and of novel electrode batteries.

Chapter 5 looks at the energy use and associated GHG emissions of battery cell production. Published data on the energy use of battery Gigafactories are meta-analysed and filtering criteria are suggested based on energy density and production scale. Additionally, energy use numbers for Giga-scale battery manufacturing facilities are inputed to the LIB LCA model to estimate the environmental benefit of upscaling battery manufacturing operations. The Chapter ends with proposing a series of measures that would lead to reduced GHG intensities for battery cell manufacturing.

Chapter 6, explores the environmental and cost implications of the LIB utilisation phase, including the effect of different cooling systems on battery lifetime. The development of an LCA and LCC model for the use phase of LIBs in EVs is presented and results on their overall cost and carbon footprint are discussed. The contribution of critical parameters such as the electricity mix used to charge the vehicle, the battery production footprint and the lifetime of the installed battery are analysed through a sensitivity analysis and their contribution to the total environmental footprint and cost of an EV is explored.

Chapter 7, outlines the development of the battery LCA model for LIB end-of-life processes together with economic aspects. End-of-life treatment chains for automotive traction battery packs is discussed, taking into account market-leading hydrometallurgical and pyrometallurgical processes. Previously applied system boundaries across literature studies are expanded to describe the whole end-of-life treatment chain, from the point of collection of LIB packs to the recovery of secondary material. The specific literature gaps are identified, followed by a description of the LCI developed (shown in detail in Appendix B) and of the various scenarios studied. Finally, the results are presented and discussed in detail and conclusions are made on the environmental competitiveness of hydrometallurgical and pyrometallurgical processes and the importance of recovering materials included in the LIB pack's supporting structures, such as aluminium and copper.

The main contributions of this thesis, including its conclusions and recommendations for future work are outlined in Chapter 8.

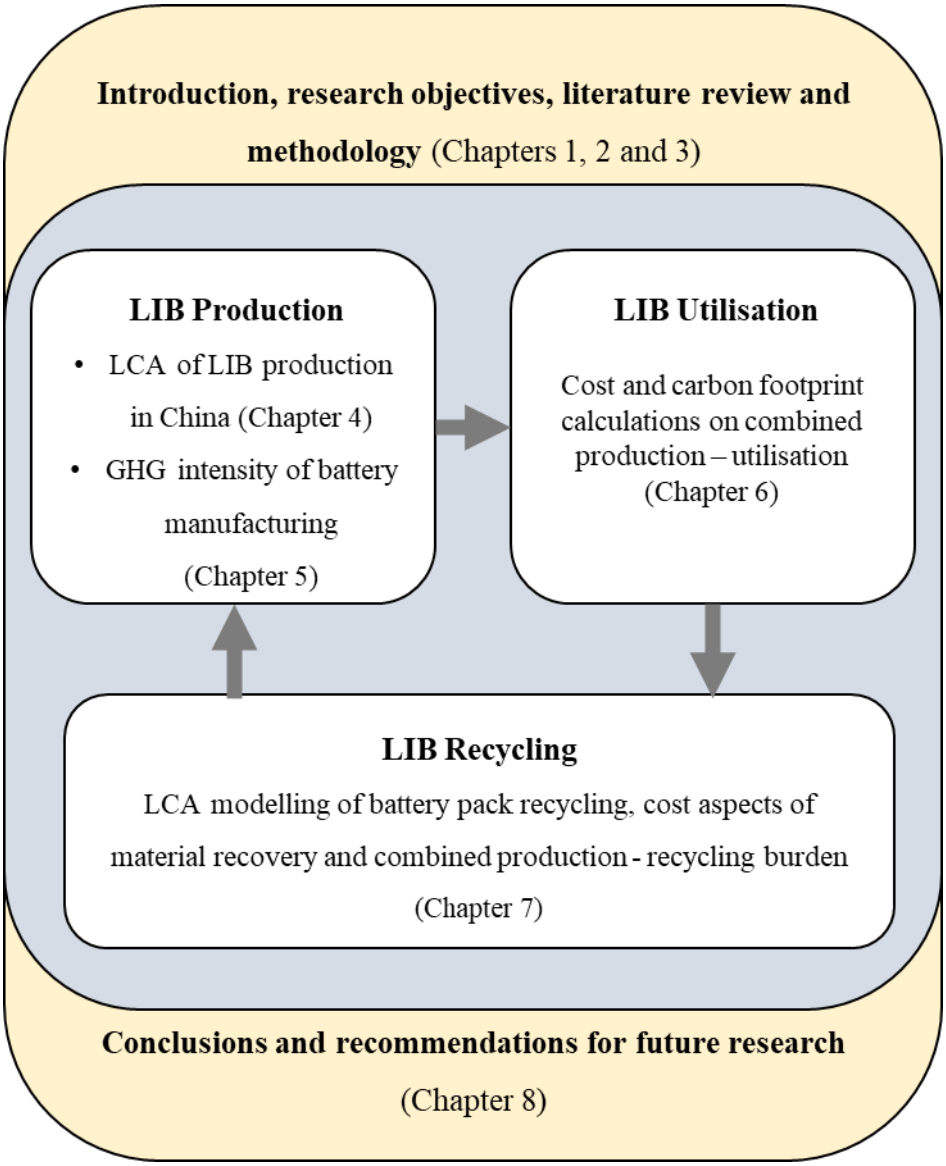


Figure 3. Thesis structure and interconnections between individual chapters.

Chapter 2 Lithium-ion batteries for electric vehicles: technology and value chain

In this chapter, an introduction to the dominant battery technologies for automotive applications is followed by a brief description on the operating principles of battery cells and the design of battery packs. Next, the main steps included in the automotive LIB value chain are outlined, including battery production, utilisation and end-of-life. This chapter is partly based on the "Safe and sustainable lithium-ion batteries" white paper prepared for the Energy Futures Lab (EFL) and the Institute of Molecular Science and Engineering (IMSE) at Imperial College London (Kallitsis et al., 2022b), including the author's contributions.

2.1 Battery cell fundamentals

Rechargeable batteries consist typically of one or more electrochemical cells, each containing a positive (cathode during discharge, anode during charge) and negative (anode during discharge, cathode during charge) electrode, separated by a micro-porous membrane and all immersed in an organic electrolyte solution containing lithium salts dissolved in organic carbonate solvents. Oxidation (loss of electrons) and reduction (gain of electrons) reactions occur at the interfaces between the electrolyte and each of the electrodes; oxidation occurs at anodes and reduction at cathodes. By arbitrary convention, oxidation currents and overpotentials ($E_a - E_{a,eqm}$) are defined as positive, and reduction currents and overpotentials ($E_c - E_{c,eqm}$) as negative.

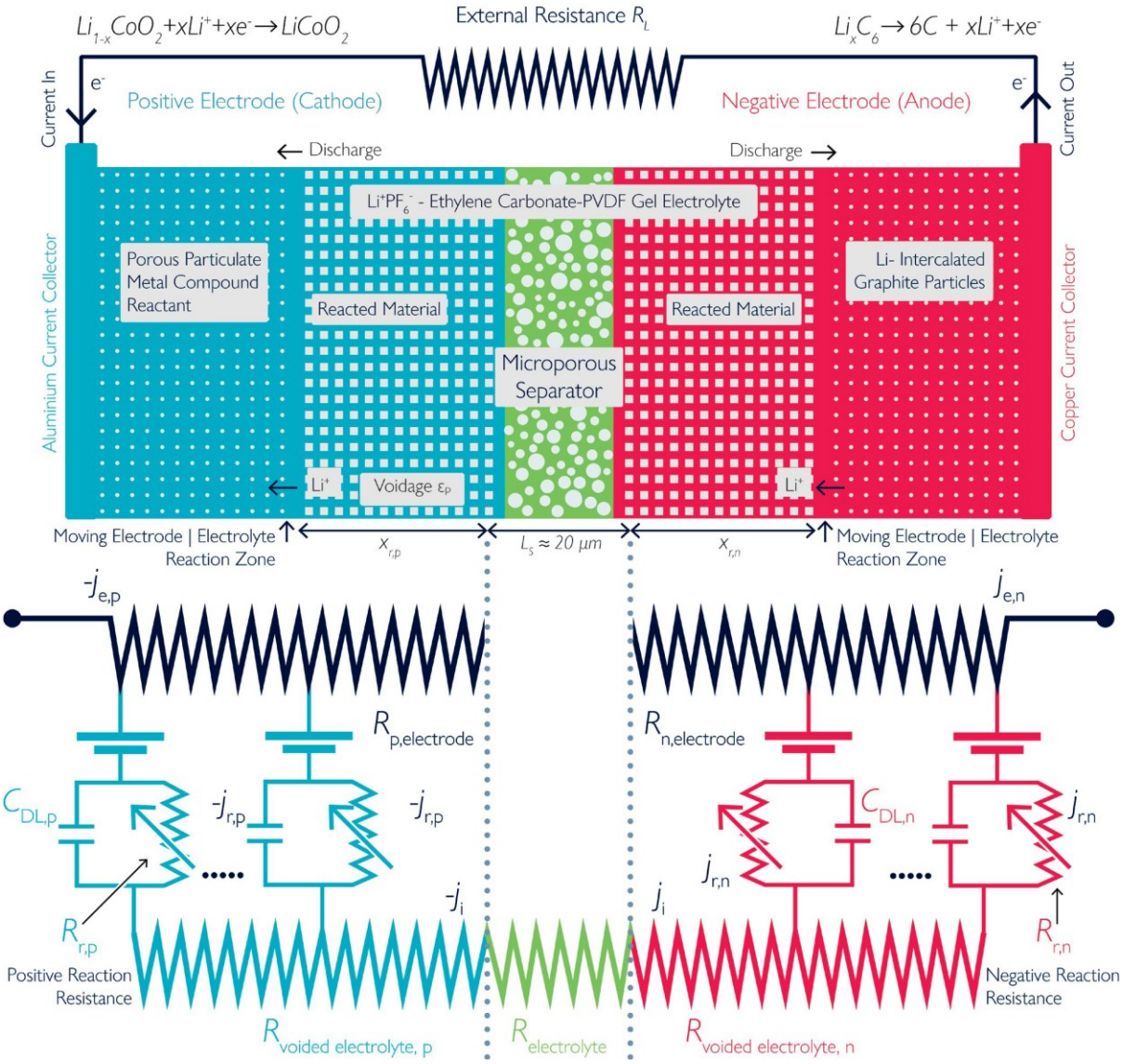


Figure 4. Schematic example of a partially discharged Li-ion battery and corresponding analogue electronic circuit (Kallitsis et al., 2022b).

LIBs take their name from the lithium cations, Li^+, which intercalate into the electrodes and migrate between them through the electrolyte during charge/discharge. As for Li^+ ions, during battery discharge, electrons (e^-) move from negative to positive electrodes, through an external circuit, as shown schematically in **Figure 4**. When current density j is drawn from a battery, positive and negative electrode reactants are consumed, causing the reaction zone to move away from the separator, through which ionic current path lengths are a minimum, towards the anode and cathode current collectors. Assuming very fast reactions, so overpotentials $|\eta| \rightarrow 0$, ohmic potential losses ($\Sigma\, j.L_t / \sigma$) occur due to ionic current density flowing through electrolyte solution of ionic conductivity σ with increasing, time dependent path lengths L_t in porous

reacted layers, as well as through the microporous separator. As shown schematically in **Figure 5**, those ohmic potential losses at positive (cathode) and negative (anode) electrodes decrease discharge potential differences (U_d), so $U_d < \Delta E$ (open circuit potential difference). Conversely, on subsequent charging, the (reversed) applied current causes oxidation to occur at the positive electrode, which then operates as an anode, and reduction occurs at the negative electrode, operating as cathode; the potential losses then cause: $|U_c| > \Delta E > U_d$. This is in addition to the decrease of open circuit potentials with increasing conversion of positive and negative electrode materials (**Figure 6**); charging causes the reverse effect.

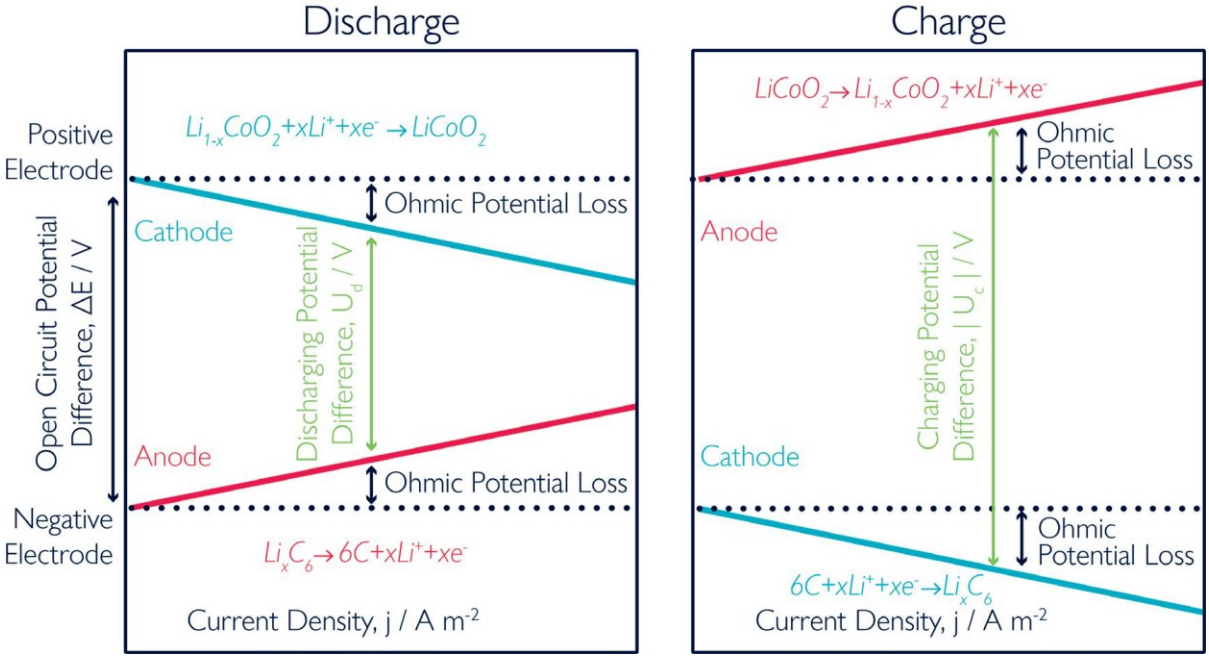


Figure 5. Schematic of potential distribution in example LIB when open circuit potential difference ΔE, and potential differences during discharging (U_d) and charging ($|U_c|$), at current density j (Kallitsis et al., 2022b).

Assuming there are no charge losses to parasitic reactions, such as solvent decomposition or secondary electrode reactions, charge yields at cathode and anode are unity, so the electrical ('round trip') energy efficiency of discharge-charge cycles can be defined by:

$$\Phi^e = \frac{U_d}{|U_c|}$$

Hence, to maximise energy efficiencies, ohmic potential losses and the resulting thermal energy dissipation should be minimised, enabling chemical energy conversion efficiencies to be maximised. However, the then infinitely small current densities would result in infinite long charging times, so current densities need to be optimised to optimise capital and operating

costs. As explained above, the positive and negative electrode are called cathode and anode by arbitrary convention, respectively. The terms are used interchangeably throughout this thesis.

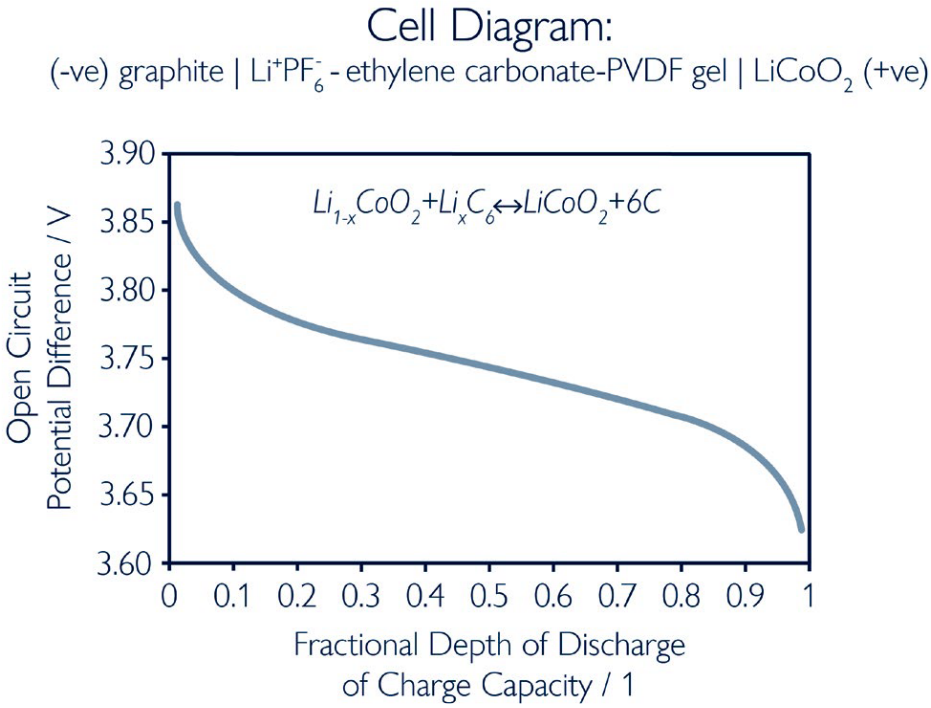


Figure 6. Schematic example of effect of fractional depth of discharge on battery open circuit potential difference (Kallitsis et al., 2022b).

The battery cell is enclosed by a protective casing made of aluminium, iron or composite plastics (Gopalakrishnan et al., 2017). The anode in LIBs consists of a coat of negative electrode paste and a thin copper current collector. The anode paste typically contains natural graphite powder, small amounts of polymeric binder (~5 wt%) and a slurrifying solvent. The cathode consists of a coat of positive electrode paste and a thin current collector made of aluminium. The cathode paste is typically made from the active material, some carbon conductive additive (4-10 wt%), a polymeric binder (5-10 wt%) and a slurrifying solvent. The liquid electrolyte is constituted of lithium hexafluorophosphate ($LiPF_6$) salt mixed with ethylene/dimethyl carbonate mixed organic solvent. Polyvinylidene difluoride (PVDF) is widely used as a polymeric binder to hold the electrodes together and is therefore partially contained in both electrode pastes while *N*-Methyl-2-pyrrolidone (NMP) is used as a solvent to ensure a uniform texture. The NMP solvent is evaporated once the pastes are applied to their respective current collectors. No solvent remains in the final battery and ~99.5% of NMP can be recovered and reused. Separators for LIBs are needed to isolate the positive and negative electrodes and prevent electrical short-circuits; they are usually made of polymeric materials (e.g. polyolefins or polypropylene).

2.2 LIB technologies

LIB technologies are often categorised based on the positive electrode materials used. **Figure 7** shows the family of electrode materials presently used commercially. The most common negative electrode is (lithiated) graphite, but other materials such as silicon and lithium titanate (LTO) are also deployed. NMC and lithium nickel-cobalt-aluminium oxide (NCA) positive electrodes are combined either with graphite, or more recently with silicon for increased energy density / specific energy and decreased costs. For long lifetimes and high power, LFP cathodes can be combined with LTO anodes, but this decreases energy densities.

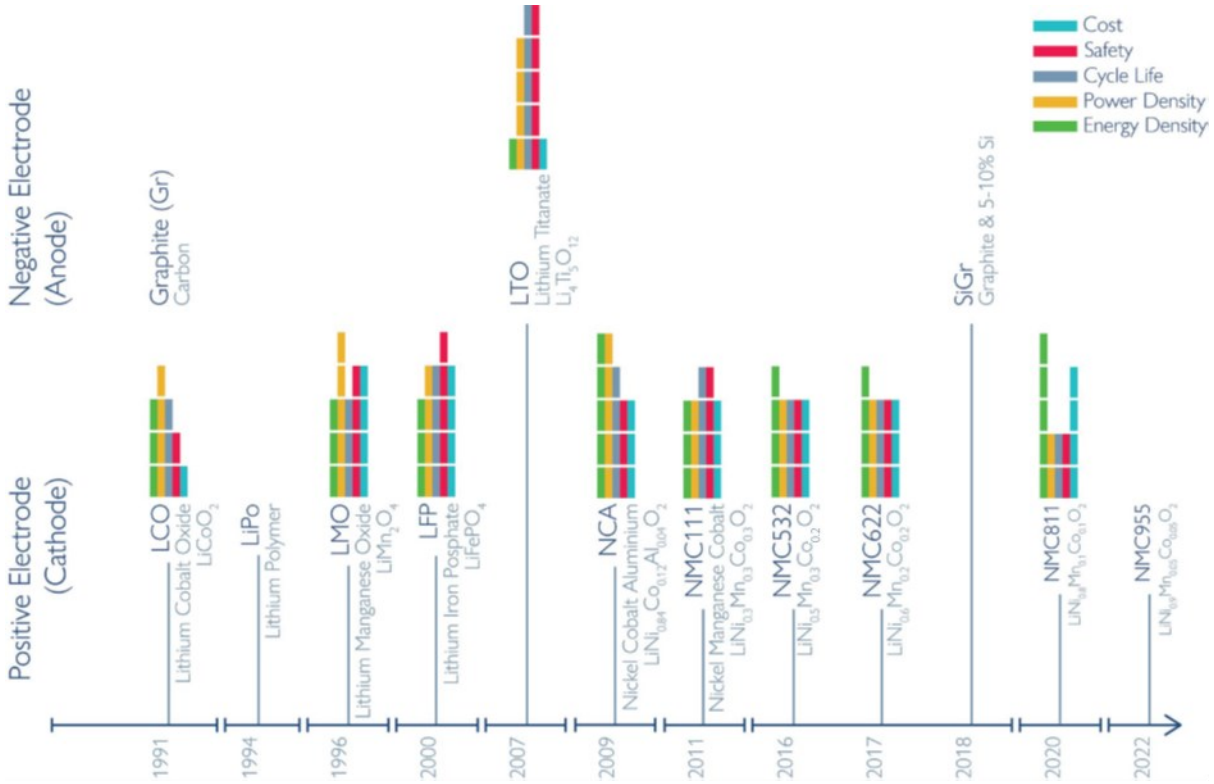


Figure 7. Timeline of the commercial history of LIB positive and negative electrode materials. Where possible, the bars provide a comparison between materials, according to five performance indicators, with 1 bar being the poorest and 5 bars the strongest (note: 1 bar for cost means highest price) (Kallitsis et al., 2022b).

Liquid electrolytes used at present include the salt lithium hexafluorophosphate ($LiPF_6$), dissolved in organic solvents such as ethylene carbonate (EC), dimethyl carbonate (DMC) and propylene carbonate (PC). While lithium cobalt oxide (LCO) cathodes are still used in portable electronics, their structural instabilities makes it difficult to extract their theoretically high energy densities without compromising lifetime (Opitz et al., 2017). One mitigation strategy is

to change the composition of LCO, adding Ni^{II} and Mn^{II} to form composites with higher structural integrity and capacity, enabling overall enhanced performances (Daniel et al., 2014; Ohzuku and Makimura, 2001; Shaju et al., 2002; Yabuuchi and Ohzuku, 2003).

Since their introduction, NMC formulations have emerged as a dominant choice in the battery industry, expected to account for more than 70% of battery capacity to be produced by 2025 (McKinsey&Company, 2018). In order to further decrease cost and increase performance of NMC LIBs, the standard formulation of NMC333 - the numbers meaning that it consists of one-third each of Ni, Mn and Co metal atoms - for automotive applications is modified to transition gradually from expensive cobalt and increase the amount of nickel, providing higher capacity. NMC532, NMC622 and NMC811 were developed, with promising improvements in energy densities but, at the same time, decreased thermal stability and increased degradation rates (Bak et al., 2014; Li et al., 2020; Myung et al., 2017). Another motivation for increasing the nickel content is to decrease concentrations of cobalt, which is associated with higher prices and socio-economic issues (Sovacool, 2019). The development of NCA was another breakthrough, offering higher energy densities compared with LCO (Guilmard et al., 2003; Madhavi et al., 2001; Weaving et al., 2001) and deployed in Tesla EVs. However, thermal instability and capacity fade at elevated temperatures are still limiting its wider deployment (Itou and Ukyo, 2005; Nitta et al., 2015). As highlighted in a 2018 report by the IEA, NMC together with NCA are expected to be the dominant choices for LIBs used in automotive applications (**Figure 8**).

Further improvements of LIBs in terms of cost and performance can be achieved through optimisation of the negative electrode chemistry (International Energy Agency, 2018). The market dominant graphite anodes are blended with silicon (SiGr) resulting in increased energy storage capacities. SiGr anodes have proven to be a very effective way of increasing energy storage capacity and consist a promising short term improvement (Dash and Pannala, 2016; Si et al., 2017; Xu et al., 2017) under the condition that stability issues associated with swelling phenomena are overcome (Chae et al., 2017; Dash and Pannala, 2016). The industry seems to be optimistic towards increasing the Si content of negative electrodes, with SiGr composites expected to reach commercial scale within the next decade, which include increased amounts of Si (figure 8). Negative electrodes including pure Si have also been proposed, with their commercial realisation consisting an important leap towards performance improvements of LIBs (Turcheniuk et al., 2018).

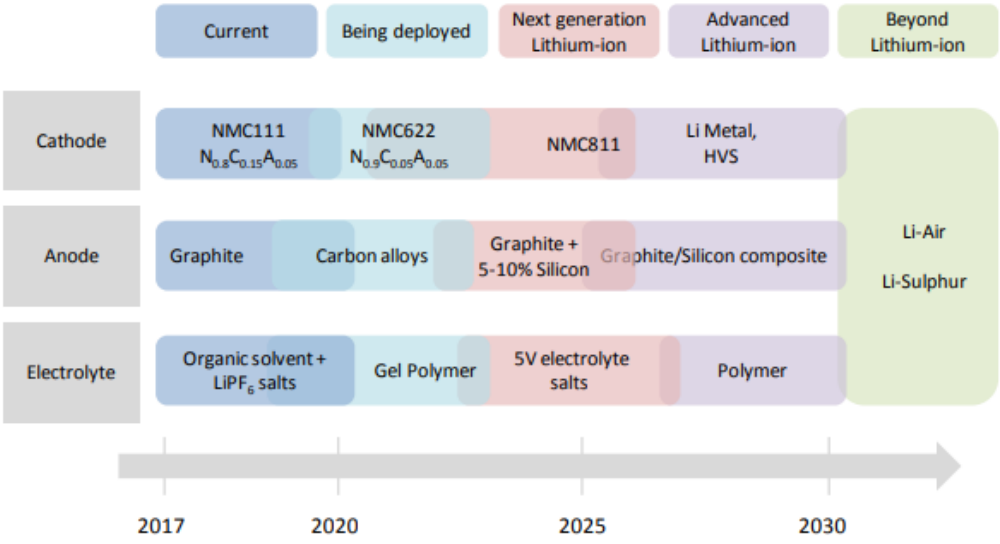


Figure 8. Expected battery technology commercialisation scheme according to IEA (2018).

Moving away from unstable liquid electrolyte solutions, prototypes of LIBs using polymer-based electrolytes - so-called lithium-polymer (LiPo) batteries - were developed in the late 1970s (Kasemchainan and Bruce, 2018; Long et al., 2016). LiPo batteries consist of the same positive and negative materials as conventional LIBs, but the lithium salt is dissolved in a polymer matrix, such as (poly)ethylene oxide, instead of an organic solvent. LiPos tend to be made as pouch cells, packaged in a foil-like bag, having the advantage of higher energy densities and form flexibility, in contrast to the solid metal casings of cylindrical or prismatic cells, which makes them ideal for applications in portable electronic devices.

Solid-state batteries are gaining increased attention in and beyond the research community. Their name is derived from the solid-state electrolyte(s), replacing the traditional liquid organic electrolyte solution. Cathode materials are typically the same as in current LIBs and common anodes consist of graphite, Si, LTO or Li-metal (Kasemchainan and Bruce, 2018; Manthiram et al., 2017). It is only when using a Li-metal or Li-Si alloy negative electrodes that theoretical energy densities are increased, making them an appealing alternative to present LIBs. However, present issues include poor lifetimes, unwanted side reactions, limited scalability of manufacturing processes for thin solid electrolytes and difficulty of ensuring intimate contact between the solid components during cycling and manufacture (Kerman et al., 2017; Schnell et al., 2018). To achieve even higher energy densities, it is necessary to combine a lithium-metal (LiM) negative electrode with a high energy density positive electrode (Fotouhi et al., 2017; J. Liu et al., 2019; Wild et al., 2015) such as Li-Air, in which oxygen is reduced at the

cathode, or lithium-sulfur (LiS) (Fotouhi et al., 2017; Manthiram et al., 2014) in which the sulfur is reduced at the cathode. For LiS cells, a major drawback is the so-called polysulfide shuttle effect, causing loss of active material, anode corrosion and limiting lifetime significantly (Marinescu et al., 2018), with its mitigation being the subject of intensive research (Fan et al., 2018; Rosenman et al., 2015). While the theoretically ultrahigh specific energy of Li-Air is attractive, in practice, this battery system suffers from limited performance and short cycle lifetimes (Asadi et al., 2018). Ongoing intensive research efforts aim to gain a more fundamental understanding of how to increase Li-Air performance and extend its usable life before a commercially viable prototype can be made (Bruce et al., 2012; International Energy Agency, 2020). Li-S and solid-state batteries have already been commercialised, finding applications, for instance, in small, unmanned aircrafts and scooters. However, their potential is not yet fully exploited and further research is required (Larcher and Tarascon, 2015). Such chemistries are expected to appear in electric vehicles beyond 2030, as shown in **Figure 8**.

2.3 LIB pack design

A battery pack is an assembly of electrochemical cells which enable the conversion of stored energy to electricity (Väyrynen and Salminen, 2012). Hundreds of battery cells are connected in series and in parallel inside the battery pack in order to build up the voltage and amperage needed for automotive use. The assembled cells are complemented by the supporting structures, namely the BMS, TMS and the protective pack housing (Romare and Dahllöf, 2017; Väyrynen and Salminen, 2012). The typical mass composition of a LIB pack for automotive use is shown in **Figure 9**. The battery cells offer the operational basis of the battery pack, constituting approximately 60% of it by mass. The next most important contribution to the mass of a LIB pack comes from the protective packaging.

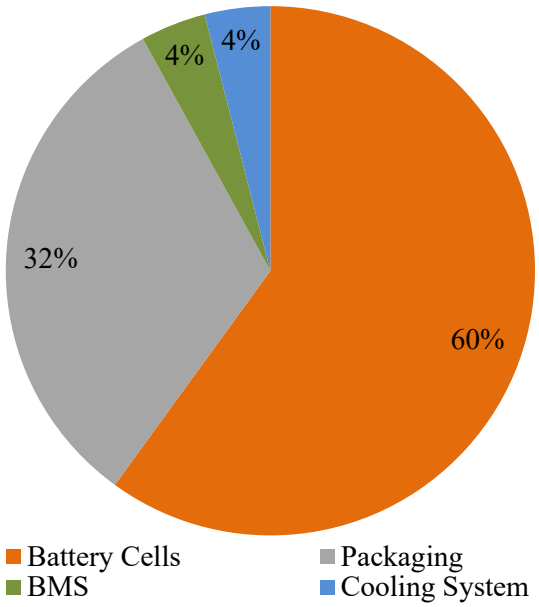


Figure 9. Typical mass composition of a LIB pack (Ellingsen et al., 2014).

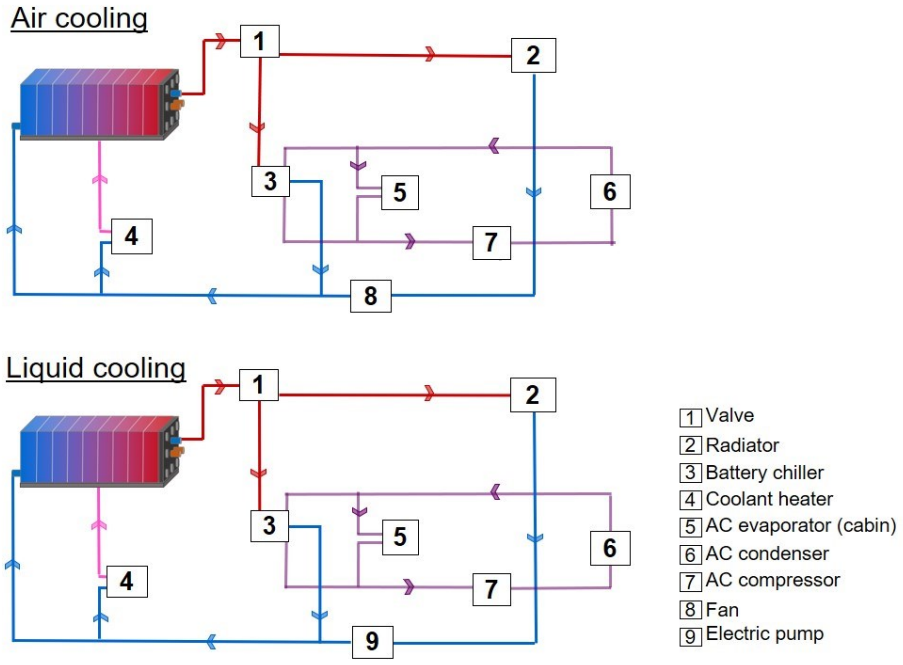
Battery cells are combined to build up battery modules, which are consequently assembled into battery packs. In a typical battery module, low voltage battery cells are combined to produce mid-range voltage, up to 50 V. Battery cells usually come into either cylindrical, prismatic or pouch geometries (Maiser, 2014). The former can be produced in higher volumes and better quality, while the latter can be packaged with better volume efficiency and offer a better heat transfer surface area. Battery cell geometries are chosen depending on the required design of the battery pack with another key integration issue being whether many small cells should be used or fewer large ones. Effective integration of battery cells into modules a pack has a key role in ensuring improved performance, increased lifetime, safety and reduced costs.

The BMS consists the battery pack's brain, as it is responsible for monitoring and controlling the potential differences between cells and the temperature of cells within the pack. It ensures that manufacturer-specified voltage and temperature limits are not exceeded by the battery system (Pesaran et al., 2009). The BMS is typically made of various electronic components such as circuit boards, printed wiring boards, semiconductors, insulated copper wires, sensors and stainless-steel containers.

The TMS plays a crucial role in ensuring that the battery pack operates within a favourable temperature range. In brief, high temperatures result in accelerated degradation rates for LIBs, while low temperatures result in reduced power and energy capabilities which affect the driving range and performance (Pesaran et al., 2009). The accelerated degradation rates in high

temperatures have been shown to result by chemical side reactions such as solid-electrolyte interface (SEI) growth on the anode and electrolyte, while lower temperatures result in lithium plating and loss of lithium inventory (Lander et al., 2021b). Therefore, the key role of the TMS is to heat the batteries in cold temperatures or cool them in high temperatures.

Dominant thermal management strategies for EVs include either air cooling or indirect liquid cooling. Air cooling uses air flow to cool down the battery cells and is generally low-cost and simple to implement in a range of battery pack geometries. However, it often results in reduced heat removal capabilities from the battery pack. Indirect liquid cooling channels a liquid refrigerant through the battery pack and is the preferred choice in modern EV packs due to its improved heat removal capabilities but is expensive to build into the battery pack design; the main differences between air cooling and liquid cooling are shown schematically in **Figure 10a**. Recently, immersion cooling and tab cooling strategies have attracted increased attention due to their improved cooling efficiencies (Xia et al., 2017). A schematic representation of surface and tab cooling is shown in **Figure 10b**. The main components of the TMS are the radiator, clamps and fasteners plus plastics for sealing. The coolant solution is typically made from glycol and water on a 1:1 ratio by mass. Packaging is required for structural and protective reasons, and it mostly requires aluminium, steel or polymeric plastics.



(a)

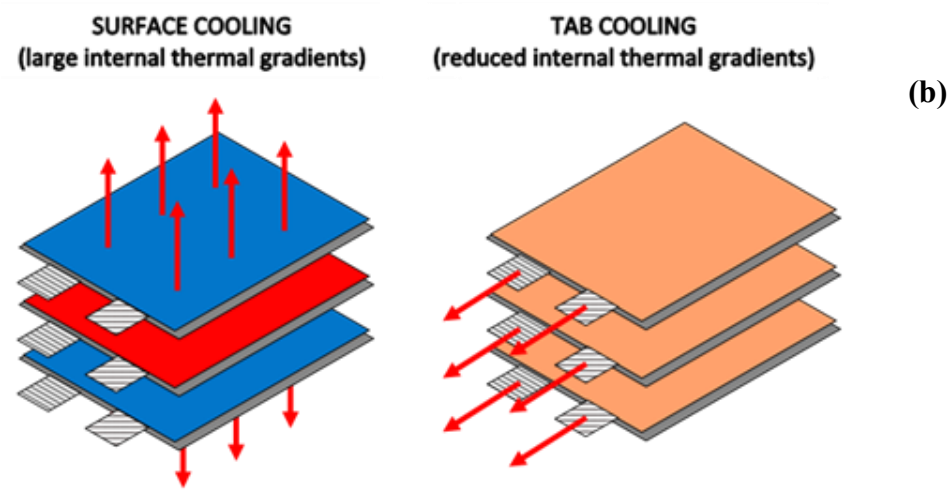


Figure 10. (a) Schematic overview of air and liquid cooling thermal management systems with their respective components and (b) heat extraction direction for surface and tab cooling (Lander et al., 2021b).

The packaging of the battery pack is responsible for ensuring thermal stability, vibration isolation and impact resistance. Battery packs come in various shapes and sizes in order to fit to the overall design of the EV. Typically, the packaging is divided into three subcomponents; the battery retention, module packaging and battery tray (Ellingsen et al., 2014). The module packaging consists of inner and outer frames, busbars, module fasteners, and a module lid. The inner and outer frames form nylon cassettes that are placed around the battery cell container to provide protection and structural support. Additionally, each frame includes an aluminium heat transfer plate to ensure optimal thermal conduction. A series of cassettes are stacked after one another to form a battery module. At the top of the cassettes, the tabs are welded to the busbars. The module fasteners include steel screws, caps, nuts, and retention rods, as well as nylon washers. Together with the module lid, the fasteners are used for assembly of the individual battery modules. The battery retention system keeps the battery modules in place within the battery tray, using straps, restraints, and foams. In addition, the heat transfer plates made of steel are considered a part of the battery retention system. All battery components are placed inside a steel battery tray, which is closed with a sealed lid (Ellingsen et al., 2014). Effective design of the battery pack's packaging is crucial in ensuring easy disassembly after the end-of-life which plays an important role in increasing the recyclability of the battery pack.

2.4 LIB value chain

Technological developments on lithium-ion batteries for electric vehicles require transformative changes throughout their value chain. First, a range of materials used in LIBs are harvested from raw materials mined from the earth's crust or recovered from waters. These elements primarily include lithium (Li), nickel (Ni), cobalt (Co), manganese (Mn), aluminium (Al), copper (Cu) and graphite (Gr). Next, the cell components anode, cathode, electrolyte and separator are produced and are combined in the cell manufacturing process. Further on, assembly takes place in order to produce the battery module and pack. The battery pack is integrated into an EV for an extended use period. Once the pack reaches its end-of-life in vehicle integration, the battery pack's constituents are either repurposed for a second life or recycled.

2.4.1 Materials for lithium-ion batteries

The LIB life cycle starts with mining and processing key battery materials Li, Ni, Co, Mn, Al, Cu and Gr which are extracted from the earth's crust. Li, Ni, Co and Mn are typical materials used in battery cathodes and Gr is the dominant choice for battery anodes. Al is used in the cathode current collector, battery pack housing and TMS while Cu is used in the anode current collector, cell container and battery pack housing. An indicative elemental composition of a typical NMC333-Gr battery back used in automotive traction applications is shown in **Figure 11**. The main production pathways for key LIB materials are shown in **Figure 12** and are discussed in this section.

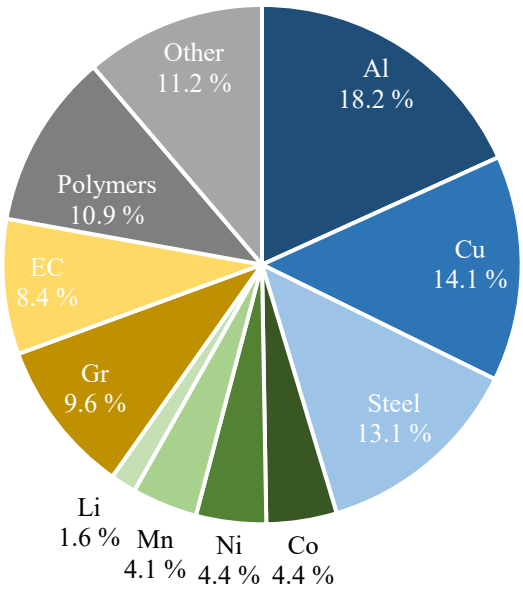


Figure 11. Elemental mass composition of a typical 253 kg NMC333-Gr battery pack used in automotive traction applications (Kallitsis et al., 2022a)

Lithium and its chemicals have historically been produced around the world from either brine or ore principal feedstocks. The former is the dominant production pathway due to low operational costs. Approximately 70 % of the world's resources are found within the "Lithium Triangle", a region of the Andes Mountains including parts of Argentina, Chile and Bolivia (Tran and Luong, 2015). Brines located within this region are processed to produce high-grade lithium salts, providing more than 60 % in the global market. The production sequence for Li brines starts with pumping the brine out of the ground, which typically contains 0.02 – 0.1 wt. % Li. After a solar pond evaporation sequence and precipitation of by-products NaCl, KCl and NaCl·KCl, the Li content in the salt reaches 6 wt. % Li. The LiCl salt gets purified and treated with sodium carbonate (Na_2CO_3) to precipitate high purity lithium carbonate (Li_2CO_3) (Tran and Luong, 2015). Lithium carbonate is a stable white powder that is a key intermediary in the lithium market because it can be converted into specific industrial salts and chemicals, including lithium hydroxide (LiOH) which is commonly used in the preparation of LIB cathode material (Tran and Luong, 2015). LiOH is produced by a series of reaction steps of Li_2CO_3 with a mixture of CaO and water. Lithium chemicals can also be produced from lithium-containing ores, with spodumene being the most common mineral that has been commercially mined and processed to produce lithium compounds around the world (Tran and Luong, 2015). After these ores are mined, mainly through open pit mining, they get processed through a sequence typically including comminution, flotation, magnetic separation, optical sorting or

heavy media separation to produce concentrates containing 4 – 6 wt. % Li_2O (Tran and Luong, 2015). These concentrates are consequently sent to roasting and leaching processes to extract lithium into solution. Metal hydroxides, salts, or acids are added with the concentrates during thermal treatment to yield leachable compounds of lithium sulfate, carbonate or chloride (Tran and Luong, 2015). Purification mainly via precipitation is then carried out to remove impurities and is followed by concentration using ion exchange or evaporation. Finally, electrodialysis, crystallisation, or carbonation are performed to produce battery-grade lithium bearing chemicals, such as Li_2CO_3 and LiOH (Tran and Luong, 2015).

Nickel-containing ores are mined from either open pits or underground mines, depending on the mineralogy, and either get concentrated using mineral processing techniques or used directly. Most nickel is produced from sulfides and laterites, which are processed through pyrometallurgical and hydrometallurgical techniques. The largest deposit of sulfides exists in Norilsk, Russia with substantial deposits being found China, Canada, Australia and Southern Africa. Ore grades of produced sulfides are typically below 1 %, which are typically upgraded to concentrates grading 5 % to 20 % through physical separations by griding and froth flotation (Paulikas et al., 2020a). The sulfide concentrates get typically processed through pyrometallurgical smelting and hydrometallurgical refining to produce class I nickel, which can be further processed to yield battery-grade nickel sulfate ($NiSO_4$). Laterites are geographically concentrated in New Caledonia, Australia, Philippines and Indonesia, which represent approximately 60 % of global nickel reserves and about 70 % of production (Paulikas et al., 2020a). The majority of deposits grades above 1 %, which is higher than sulfides, and include cobalt as well. Depending on the deposit, laterites are processed either hydrometallurgically (limonites) or pyrometallurgically (saprolites). While laterites are higher grade than sulfides, they cannot be readily upgraded to concentrates prior to smelting, as nickel occurs in silicates or oxides, which makes the pyrometallurgical process very energy expensive (Paulikas et al., 2020a). Only hydrometallurgical processing of laterites results in class I nickel, which is relevant to LIBs, as their pyrometallurgical processing typical results in low-quality ferronickel. Class I nickel produced either from sulfides or laterites is converted to battery-grade $NiSO_4$, through a dissolution, evaporation and crystallisation sequence. $NiSO_4$ is the feedstock for the preparation of the cathode powder used in LIBs.

Copper exists worldwide in a number of geological environments. Chile is by far the world's largest producer of copper, with China, Peru, United States, the Democratic Republic of Congo (DRC) and Australia being the next on the list (Paulikas et al., 2020a). Most of copper

production comes from sulfide ores, which get concentrated through grinding and froth flotation. The concentrate, containing about 30 wt. % copper, is sent to a smelter where it gets converted to 98 % pure blister copper through a series of high-temperature steps. Copper blister is then reduced to copper anode and gets cooled into a slab, which is further purified through electrorefining to create a 99.99 % pure copper cathode (Paulikas et al., 2020a). Minor pathways to produce copper come from oxide ores, which are typically treated hydrometallurgically, usually by sulfuric acid heap leaching where the ore is crushed, arranged in piles, and showered with sulfuric acid (Paulikas et al., 2020a). The resulting solution is collected and further processed by solvent extraction and electrowinning.

Cobalt is a by-product of nickel and copper production. More than 55 % of mined cobalt comes from the Kinshasa region of the DRC, which is sent to China, Finland or other countries for processing and refining (Paulikas et al., 2020a). Cobalt is typically produced from three types of ore deposits, stratiform copper, nickel sulfide and nickel laterite deposits. The primary production route comes from stratiform copper deposits, where sulfide and oxide forms of cobalt are often found together in the same mineral deposit. The ores are mined and then get concentrated using milling and flotation. Sulfide concentrates get processed pyrometallurgically and are then treated together with oxide forms using hydrometallurgical processing. After an acid leaching/solvent extraction sequence, a cobalt-rich solution is produced, which gets precipitated to remove impurities and is further refined through different routes to produce a series of final products, including battery-grade $CoSO_4$, which is produced through evaporation, crystallisation and drying.



Figure 12. Raw materials extraction processes for materials commonly used in LIBs (Kallitsis et al., 2022b).

Manganese is mined in open pits, in the form of oxide or carbonate ore, which get processed through a calcination, leaching and purification sequence. The Kalahari manganese district in South Africa contains 70 % of the world's total manganese resources. The primary pathway to produce battery-grade $MnSO_4$ starts with the electrolytic preparation of primary MnO_2, including the reduction to MnO and consequent leaching with sulfuric acid to form $MnSO_4$. The acidic solution is purified by oxidation with MnO_2 and neutralised with lime. The $MnSO_4$ solution is then filtered, its concentration adjusted and subjected to electrolysis, to yield the $MnSO_4$ powder grade required in the preparation of the battery cathode precursors (Bohnet, 2003). There is also a technically harder route to produce battery-grade $MnSO_4$, which entails chemical refinement of ore as shown in **Figure 12**.

Aluminium oxide (alumina) is extracted from bauxite through a digestion process, using caustic soda, followed by calcination to remove the water content from the hydroxide. Primary aluminium production is achieved by smelting alumina, an electrolytic process which breaks down the strong chemical bond between aluminium and oxygen atoms using a powerful electric current. Liquid metal is produced from the process, which gets purified, alloyed to specification and then cast into ingots.

The global graphite market consists of 20-40 % of natural graphite mined out of the earth's crust, with the remainder being synthesised from coke (synthetic graphite). The former is very relevant to battery applications, as approximately 80 % of the anode market is satisfied from natural graphitic-material (European Carbon and Graphite Association, 2018). Natural flake graphite, containing 2 to 30 wt.% graphitic carbon, is mined through open pits or underground, and gets concentrated through milling and flotation (Jara et al., 2019). Occasionally, leaching is performed to further concentrate the graphite and achieve high purity (98 wt.%), but this step is often not required (Surovtseva et al., 2022). High purity graphite (99.95 wt.%) is required for LIB anode preparation, which is produced through hydrofluoric acid leaching, halogen or alkali roasting, or thermal treatment in an inert atmosphere (Surovtseva et al., 2022). On the other hand, synthetic graphite production is achieved using petroleum needle coke as feedstock. The process sequence starts with the production of green coke, which is produced either as an intermediate product of oil refining or through catalytic cracking of heavy oils (Dante, 2015). Green coke gets consequently calcined to produce needle coke with a purity of 97 to 99 wt.%, which gets consequently graphitized at above 2500 °C to produce high-quality and high-purity graphite (Bogacki et al., 2012). Most LIB anode producers use a blend of synthetic and natural graphite, balancing costs and performance.

2.4.2 Lithium-ion battery production

The production of lithium-ion battery packs is a multi-stage process chain spreading across several countries and including more than fifty individual raw materials. The cradle-to-gate stages to produce an automotive traction LIB are depicted in **Figure 13**. This section focuses on the materials processing, component manufacture, and cell, module and pack assembly stages. It is focused specifically in NMC batteries, as these have been the primary focus of the thesis.

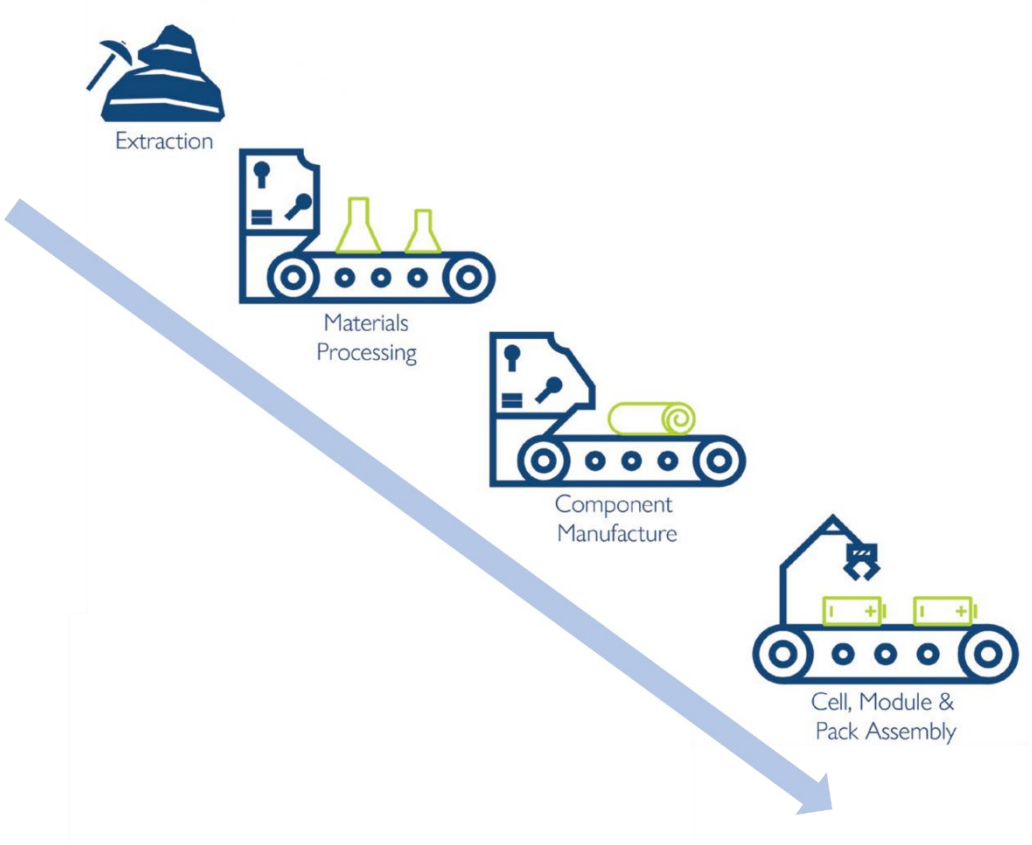


Figure 13. Cradle-to-gate stages to produce a lithium-ion battery for electric vehicles (Kallitsis et al., 2022b).

After raw materials are extracted from mined ores and get processed, as discussed in section 2.4.1, the battery-grade chemicals need to be combined to produce the anode and cathode powder. For LIB cathodes, $NiSO_4$, $CoSO_4$ and $MnSO_4$ are combined with either LiOH or Li_2CO_3 to produce the cathode powder ($LiNi_{1-x}Mn_xCo_yO_2$). The first industrial step for synthesising NMC cathode powder involves the reaction of $NiSO_4$, $CoSO_4$ and $MnSO_4$ with NaOH and NH_4 to produce $Ni_{1-x}Mn_xCo_y(OH)_2$ via co-precipitation (Dai et al., 2019a). The process starts by mixing $NiSO_4$, $CoSO_4$ and $MnSO_4$ in a tank reactor, with NaOH and NH_4OH,

being consequently added to the solution which gets heated to approximately 50 °C to precipitate $NMC(OH)_2$ (Dai et al., 2018). The solid is then filtered out, washed and dried to produce NMC precursor. Na_2SO_4 is a by-product of the process, produced by feeding the filtrate to a four effect evaporator (Dai et al., 2018). The excess ammonia is removed from the wastewater in an ammonia stripping tower and gets recycled for subsequent precursor production (Dai et al., 2018). The NMC precursor then gets mixed with Li_2CO_3 (LiOH might be used depending on the plant) and after a two-step calcination process where additives are inputted, the cathode powder is produced. Material efficiencies for both steps are reportedly close to 100 % (Dai et al., 2018). A simplified version of the main reactions performed in the co-precipitation and calcination steps, respectively, is:

$$(1-x-y)\,NiSO_4 + y\,CoSO_4 + x\,MnSO_4 + 2\,NaOH \rightarrow Ni_{(1-x-y)}Mn_xCo_y(OH)_2 + Na_2SO_4$$

$$Ni_{(1-x-y)}Mn_xCo_y(OH)_2 + \frac{1}{2}\,O_2 \rightarrow LiNi_{(1-x-y)}Mn_xCo_yO_2 + H_2O$$

On the anode side, refined particles produced either through synthetic or natural graphite routes can be fed to battery cell production without any further processing.

Next, the battery components are manufactured and, together with the supporting structures, are used in the battery cell and pack assembly line. The main production steps involved in the component manufacturing and cell assembly stages are presented in **Figure 14** and are further discussed in detail below:

In the first step, the active material powders for the anode and the cathode get mixed with carbon, the binder and additives in a chemical vessel. To produce the NMC cathode paste, the NMC oxide powder (80 – 85 wt%) gets mixed with the PVDF binder (5-10 wt%), and carbon black additives (4-10 wt% carbon black) in a dry mixing step. Consequently, NMP solvent is added to the mixture in order to disperse and homogenise the battery materials in a solvent. A similar mixing process is followed for the production of the anode paste from graphite powder, with the main difference being that deionised water can be used as a solvent instead of NMP. In common industrial practice, different mixers are used for the anode and the cathode to avoid cross-contamination and reduce non-productive time associated with cleaning (Jinasena et al., 2021). Currently, ongoing research is focused on dry material coating techniques to avoid the use of NMP solvent in the cathode mixing process, which include electrostatic spray

deposition, laser techniques and semi-solid casting (Kallitsis et al., 2022b).The slurrified, ideally homogeneous cathode and anode paste mixtures are pumped to the coating machine.



Figure 14. Main process steps to assemble lithium-ion battery cells and packs (Kallitsis et al., 2022b)

The second step includes coating the anode and cathode pastes on the current collector foils. These foils are mostly produced off-site, are up to 20 μm thick and are purchased in rolls by battery manufacturers. Al and Cu foils are used for the cathode and anode, respectively. The machines spread the paste to a thickness of 150 μm to 300 μm depending on battery design, type and manufacturer, with the main coating mechanisms including slot die, doctor blade, anilox roller or a spray coater depending on the manufacturer (Jinasena et al., 2021). The coated electrodes get consequently transferred to the drying chamber to get the desired thickness by evaporating the solvent.

The third step includes drying and calendering. The coated foils are dried in a drying tunnel through convective air heating, infra-red or laser heating. The dryer length can be up to 100 m long, consisting of various temperature zones, typically between 50°C and 180°C, to improve efficiency and the quality of drying (Jinasena et al., 2021). Consequently, the electrode films get compressed to tune the porosity and homogenise material properties. This calendering process is performed using a set of rollers which apply a predetermined amount of pressure

(approximately 2500 N mm^{-1}) (Jinasena et al., 2021). Before and after the calendaring process, the electrode films are cleaned using brushes or air flow.

In the fourth step, the calendered electrode rolls are cut into separate rolls along the width of the films using highly precise cutting, notching, punching or laser tools. Fraying of edges and unnecessary loss of material is undesirable. The separate individual rolls get consequently cleaned and rewound, and get vacuum dried to remove any remaining solvent amount.

The fifth step includes the assembly of electrodes in stacks of anode-cathode sandwich structures, separated by the polymeric separator. For pouch cells, the individual anode and cathode rolls are cut into separate electrodes and then get alternatively stacked on top of each other using a separator sheet in between (Tagawa and Brodd, 2009). For prismatic and cylindrical cells, the anode and cathode rolls are wound together with the separator in a winding process step, resulting in what is called a jelly roll (Tagawa and Brodd, 2009).

Consequently, the current collectors are welded and the stack or jelly roll is placed inside the pouch or prismatic cases and gets sealed. For cylindrical cells, the jelly rolls are placed inside the casing and then get welded on the top and bottom of it (Jinasena et al., 2021).

The sixth step includes filling the electrolyte into the cell and sealing it. The sandwich structures are injected with the liquid electrolyte under vacuum, which should wet and soak in the electrodes and separator, which is achieved by applying a pressure profile to the cell to activate capillary effects. In order to achieve optimal electrolyte wetting, pouch cells get roll pressed while a vibrating table is used for prismatic and cylindrical cells (Tagawa and Brodd, 2009). This is the slowest step in the overall production chain. The cells get consequently sealed using vacuum sealing for pouch cells and crimping, beading or welding for prismatic and cylindrical cells (Jinasena et al., 2021). Most of the cell production described above takes place in a dry room with stringent air filtration requirements and consequently high energy demands.

For safety reasons, cells are always manufactured in a fully discharged condition. The next step is to charge the cells using a “cycler”. A series of charge-discharge cycles with gradually increasing voltage are applied to the cells over a period of 2 to 4 weeks. This step is necessary to test and condition the cells for assurance of operability, quality control and categorisation. Finally, cells are graded by means of discharge, resistance and capacitance measuring and categorised so that EV battery packs have identical cell characteristics.

In the final step the battery cells are packed into modules and packs together with the required electronic, thermal and physical support structures (BMS, TMS, packaging). Key considerations regarding the assembly of battery packs have been discussed in section 2.3. Any excess parts, defective cells or non-homogeneous electrodes are disposed.

2.4.3 LIB utilisation in electric vehicles

The assembled battery packs are transported to car manufacturers in order to get integrated to EVs for an extended use period. The LIB utilisation phase's energy consumption, environmental and cost performance is highly sensitive to a series of factors, with the most important ones including the electricity mix used to charge the vehicle, the energy consumption and the lifetime of the installed battery. During this phase, the battery becomes an integral part of the EV. Therefore, the discussion includes factors associated with both the battery pack and the EV.

The energy consumption is a critical parameter determining the performance of an EV. It is difficult to accurately quantify the vehicle energy consumption as it depends on several internal factors including (dis-) charging conditions, battery degradation, internal efficiency, regenerative braking and external factors including the vehicle's weight, ambient temperature, use of auxiliaries and driving style (Badin et al., 2013). Realistic models to simulate the energy consumption have been developed (Badin et al., 2013; De Cauwer et al., 2015; Fetene et al., 2017), which together with the collection of real world data on market-leading passenger vehicles (Li et al., 2016; Weiss et al., 2020) contribute towards our understanding of the key influencing factors to promote energy efficiency in EVs. Additionally, the electricity mix used for charging consists the most important external factor influencing the EVs environmental footprint. Even though EVs are considered emission free under EU legislation, this is clearly not representative of the real-life emissions occurring on power plants producing the energy to power them. Depending on the location, the price and carbon footprint of the electricity mix vary significantly, leading to large variations in the EVs overall environmental and cost performance.

The internal efficiency is particularly important as it not only influences the EV's energy consumption, but also affects the car's range and required battery capacity and, thus, vehicle weight and cost. The total internal efficiency is a combination of separate component efficiencies: charging efficiency (90%), battery efficiency (95%), engine efficiency (90%) and

drive train efficiency (95%) result in a total efficiency of 73% (Helms et al., 2010). Ellingsen et al. (2016) argued that more realistic cell-specific use energy efficiency data is needed to obtain more reliable LCA results. Peters et al. (2017) also call for the systematic inclusion of internal efficiencies and losses in LCAs as they have substantial impacts on LCA results. Moreover, battery efficiency has also been shown to be more important for overall EV energy consumption than battery weight (Zackrisson et al., 2010).

Despite the many favourable properties of LIBs, uncertain lifetime performance and degradation still present an impediment to the long-term success of the EV industry. A battery is typically considered to have reached its end-of-life for automotive application when the remaining capacity reaches 80% of its initial nameplate capacity. Degradation must be minimised to ensure EV commercialisation by satisfying vehicle lifetime, reduce total cost of ownership, minimise driver's range anxiety and also reduce the EV's environmental footprint. LIBs undergo complex electrochemical and mechanical degradation mechanisms, which are particularly pronounced in such highly demanding operational conditions (Uddin et al., 2016). Generally, battery aging can be split into usage-dependent (cyclical) and usage-independent (calendar) degradation (Ahmadian et al., 2018; Grolleau et al., 2013). Cycle aging is a function of discharge-charge cycles and is consequently affected by battery pack size, vehicle energy consumption and driver preferences. Calendar aging occurs during pure static conditions such as storage (Keil et al., 2016). Depending on the usage-profile and battery chemistry, either cycle or calendar aging might be the dominant degradation mechanism.

2.4.4 End-of-life for LIBs

Once LIBs reach 80% of their initial capacity, they are dismantled from the vehicles as they are considered to have reached their end-of-life. Such batteries might be refurbished and repurposed for other applications to be given a second life. Alternatively, the metals included in the battery cells are extracted through a series of recycling steps or the battery packs are disposed in a landfill without any processing, which is highly unfavourable from an environmental perspective.

The feasibility of second life applications depends on how much useful capacity is left to the battery (Podias et al., 2018) and applications include EV fast charging, self-consumption, area regulation and transmission deferral, depending on the useful capacity remaining in the battery (Casals et al., 2019). In a fast-charging application, a used LIB offers extra power to support

charging from the grid. Self-consumption includes residential storage applications to store energy from renewable sources, while in regulation the LIB system provides grid stability services. In transmission deferral, the LIB charges during off-peak periods and supports a grid transformer when the energy demand is higher than its capability.

To avoid end-of-life LIBs entering landfills, where metal ions and organic compounds could leak and contaminate the soil and groundwater, they should ultimately be recycled systematically (Kallitsis et al., 2022b). Moreover, battery recycling and extraction of their valuable metals helps buffer fluctuating material costs and rebalances geographically uneven raw material distribution and battery production, while avoiding unnecessary transportation between sites (Chen et al., 2019; Harper et al., 2019). Reusing recycled materials for battery production displaces extraction and processing of raw materials and their associated costs and environmental impacts. While most end-of-life lead-acid batteries are recycled, present recycling rates for LIBs is far smaller, due to low collection rates and inadequate recycling processes (Melin, 2019).

Recycling LIBs is a challenging task due to the variety of metals included in the batteries and the difficulty associated with separating and recovering them. The first step towards recycling is collecting the batteries from the point of use and transporting them to the recycling facility. Next, the collected battery packs are identified and sorted based on their battery type (Chagnes and Pospiech, 2013). In order to enable large-scale recycling in the future, this step will have to be automated and facilitated by effective product labelling. Once sorted, spent LIBs need to be discharged because the packs can carry dangerous voltages with inherent adverse chemical reactions and safety risks. Immersion in salt-saturated solutions like NaCl or Na_2SO_4, or alternatively, liquid nitrogen is a common and simple method to discharge spent LIBs. After discharging, the next step is a series of physical and mechanical separation processes, the pre-treatment steps. These are needed to disassemble battery packs and separate them into smaller components. Depending on the recycling process, batteries might get discharged at pack, module or cell level. Pre-treatment steps include (fine) crushing, shredding, milling and sieving as well as magnetic separation, froth flotation or eddy current separation and others (Chagnes and Pospiech, 2013; Choubey et al., 2017; Georgi-Maschler et al., 2012; Shin et al., 2005; Vieceli et al., 2018; Xu et al., 2008). Depending on battery configuration and recycling method, it is possible to recover steel cases, plastics and electronics contained in the modules before or after the disassembly/pre-treatment. Next, the cells are recycled using one of the three dominant

methods: pyrometallurgical, hydrometallurgical and direct recycling. The recycling processes are depicted in **Figure 15**.

In a pyrometallurgical process, whole or shredded LIB cells are processed through smelting of the battery components and high value cathode materials Co, Ni and Cu are recovered while others are lost to the slag (Meshram et al., 2014). In the smelter, the electrolyte and plastics included in LIBs are burned off to supply heat, graphite and aluminium in the batteries act as reductants for the metals and get oxidised, while Co, Ni and Cu end up in the matte (mixed alloy) (Dai et al., 2019b). The matte gets consequently processed through a hydrometallurgical sequence including acid leaching, solvent extraction and precipitation. Depending on the process, the compounds included in the slag, such as Li might be recovered through additional unit processes (Dai et al., 2019b).

Hydrometallurgical recycling consists of a leaching, ion exchange, solvent extraction and precipitation sequence to recover metals as pure salts (Chagnes and Pospiech, 2013; Choubey et al., 2017; Lv et al., 2018; Xu et al., 2008). Other than lithium(I) ions, metal ions in their higher oxidation states in positive electrode materials such as $LiCoO_2$, $LiMn_2O_4$, $LiMnO_2$, $LiNiO_2$ are insoluble in aqueous solutions, so they have to be reduced to lower oxidation states in order to dissolve Co^{2+}, Mn^{2+} and Ni^{2+} ions, for further processing and separation. As sulfuric acid (H_2SO_4) is the cheapest acid, this is commonly used, with hydrogen peroxide (H_2O_2) as relatively expensive reducing agent. Organic acids such as citric, oxalic and formic acids can function both as reducing agents and as metal ion ‘complexants’, increasing the solubilities of the dissolved metal ions, so enabling less acidic conditions to be used, with the additional benefit of decreasing corrosion rates of steel process equipment (Kallitsis et al., 2022b). After leaching, the various metals may be separated via solvent extraction, chemical precipitation and electrodeposition. Unfortunately, processes with fully ‘closed loop’ liquid phases have yet to be developed, so end-of-pipe effluent treatment processes are required to minimise discharges to the environment.

Direct recycling aims to recover battery components in a functional state, so that they can be reused directly. The cathode material can be removed and revived via solid state synthesis, hydrothermal, electrochemical or chemical lithium re-insertion, without changing its overall structure (Chen et al., 2019; Harper et al., 2019). While such processes are considered to be highly favourable from an environmental and cost perspective, they still face significant

challenges, including of how to process different cathode chemistries together, which currently prevent their commercial realisation.

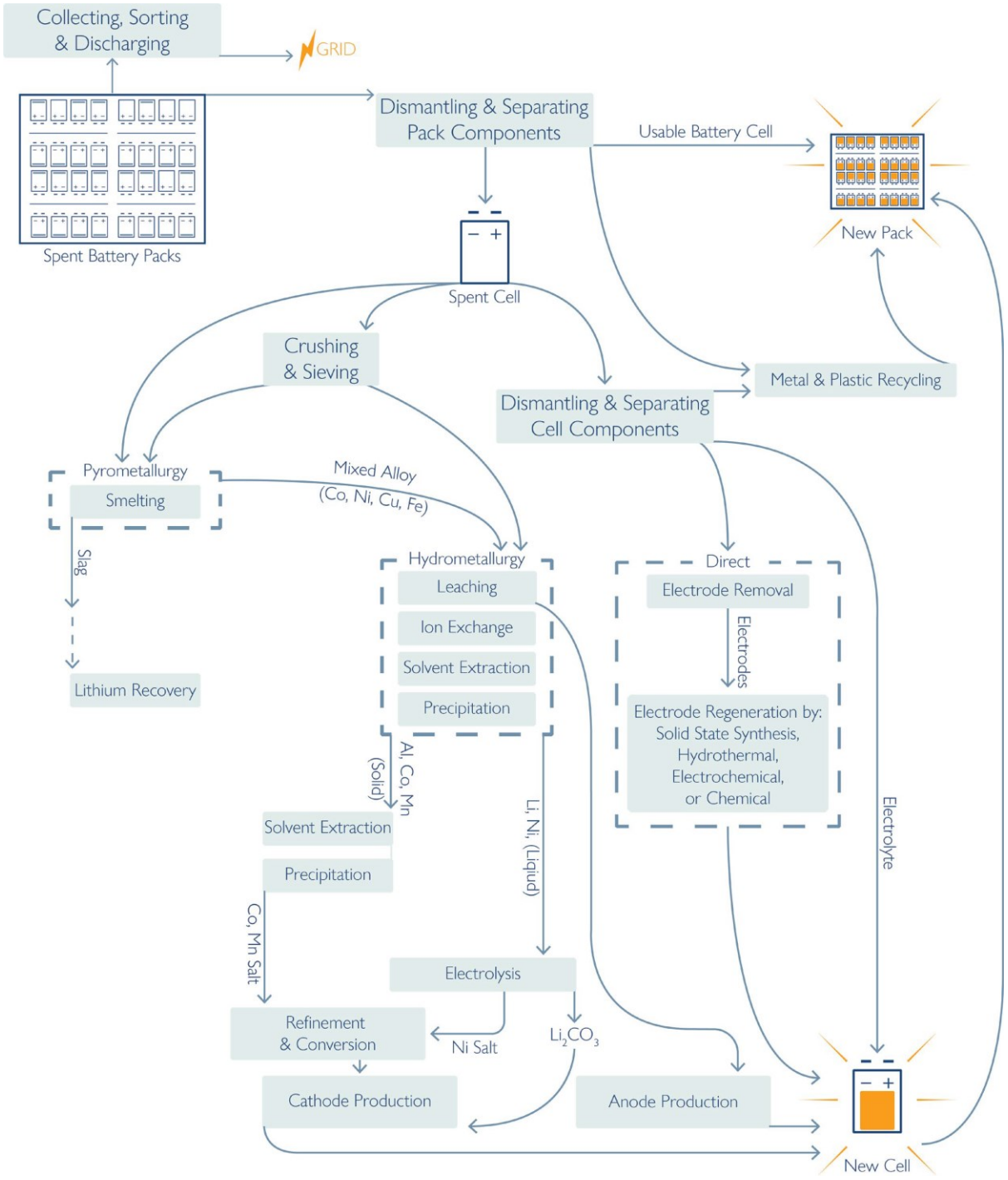


Figure 15. Recycling process flow chart showing possible pathways to new cells and packs, including pyrometallurgical, hydrometallurgical and direct recycling (Kallitsis et al., 2022b).

Chapter 3 Life Cycle Assessment of Li-ion batteries

This chapter introduces the ISO-compliant life cycle assessment framework and its applications in the Li-ion battery research domain. First, the theoretical background of life cycle assessment is introduced together with some aspects regarding life cycle costing. Second, key methodological choices in LCA studies of automotive LIBs are outlined for battery production, use and end-of-life. Concluding the chapter, key modelling choices for the application of LCA to study LIB production, use and recycling in this thesis are highlighted.

3.1 Life cycle assessment framework

LCA is a standardised quantitative and qualitative method used to evaluate the environmental burdens associated with a product, service or activity. To do so, a detailed life cycle inventory (LCI) of material and energy flows is compiled and the associated emissions and wastes released to the environment over a product's lifetime are identified. This information is used to assess the importance of adverse effects and impacts due to resources consumption and emissions. The results are used to compare alternatives, different options and support decision making through the evaluation of potential environmental impacts and the identification of opportunities for environmental improvements.

The ISO 14040 series of standards have been developed to establish the foundations of the LCA methodology and give guidance on how to conduct and report reliable, transparent and replicable results (ISO, 2006a). Their development can be traced back to 1997, when the ISO14040:1997 standard was introduced as an overarching standard encompassing all phases of LCA (ISO, 2006a), together with three more standards supplementing it; ISO14041:1998 dealt with goal and scope, ISO14042:2000 dealt with life cycle impact assessment methods and ISO 14043:2000 on life cycle interpretation methods. In 2006, a revision of the

international standards took place, with the ISO 14040 to 14044 being withdrawn and replaced by the ISO14040:2006 (ISO, 2006a) and ISO14044:2006 (ISO, 2006b). These standards are currently used for conducting LCA studies with the former outlining the principles and framework, and the latter describing further requirements and guidelines for practitioners.

The four phases of LCA include (1) Goal and Scope Definition, (2) Inventory Analysis, (3) Impact Assessment and (4) Interpretation as shown in the framework presented in **Figure 16**. The LCA should be seen as an iterative procedure rather than one-directional e.g. intermediate results obtained from the inventory analysis, impact assessment and interpretation may call for a modification of the goal and scope definition, expansion of the inventory and processes considered, improving the reliability and completeness of the analysis etc.

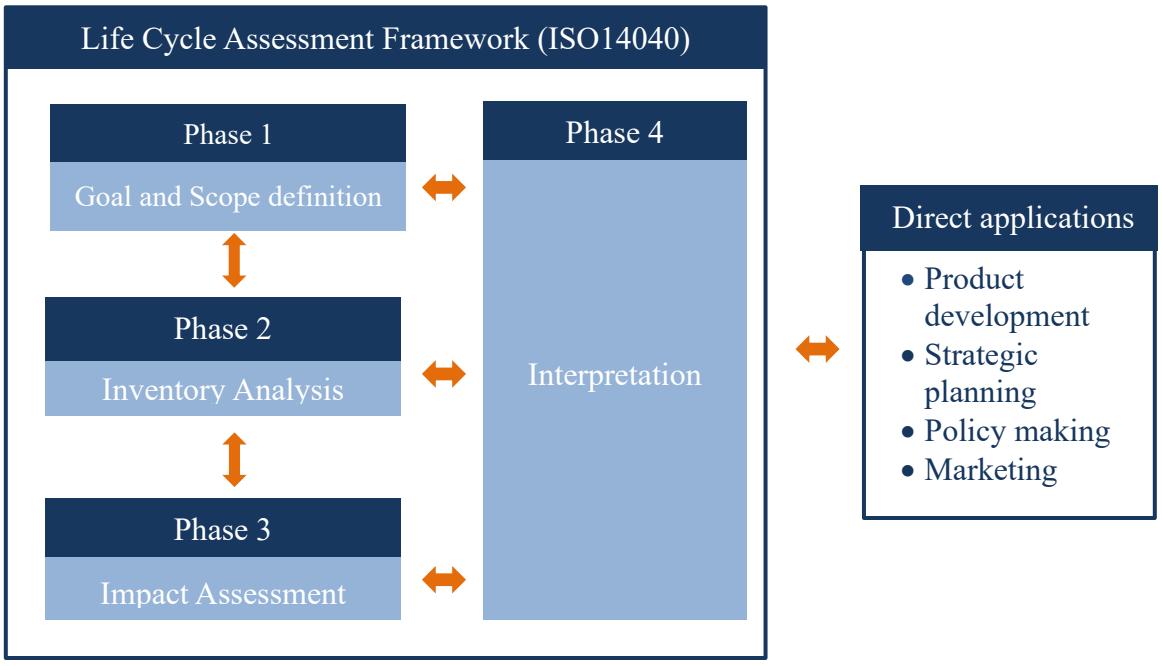


Figure 16. Schematic diagram of iterative LCA framework showing the four phases of LCA according to ISO14040:2006 (ISO, 2006a).

3.1.1 Goal and scope definition

The first step of an ISO-standardised LCA study, is the goal and scope definition where the purpose of the assessment is established and decisions are made regarding the details of the product system being studied (ISO, 2006a). The importance of this phase is often underestimated, as it is much more than a simple introduction to the LCA process (Curran, 2017). It is an important phase as it determines the exact approach to be followed. However,

as LCA is an iterative procedure, the goal as well as the scope can be modified throughout the execution of an LCA study, as data are collected and new insights are revealed.

It is highly important for the goal of the study to be defined at the outset, as it will in turn help with defining the scope and boundaries of the study. According to ISO 14040, the goal definition includes:

- the reasons for carrying out the study,
- the specification of the intended application,
- the identification of the target audience, i.e., to whom the results of the study are intended to be communicated,
- whether the results are intended to be used in comparative assertions with the purpose of being disclosed to the public.

Also, according to the standards, the scope definition defines:

- the product system to be studied,
- the functions of the product system,
- the functional unit,
- the system boundary,
- allocation procedures,
- the investigated impacts,
- the impact assessment methods to be applied,
- the interpretation methods to be used,
- assumptions regarding data and method issues,
- value choices, limitations and data quality requirements,
- the type of critical review and

- type and format of the report required for the study.

The decisions made here have a determinant role on the evolution of the LCA procedure. For example, a critical review of the study might be needed if it is intended to disclose the results to the public and make statements about the environmental superiority of one product over a competing one (Curran, 2017).

Drawing the system boundaries defines where the analysis begins and where it ends, identifying the processes to be included in the technical system. Common system boundaries in LCA studies include cradle-to-gate, with "cradle" indicating the origin of a product, therefore, including any upstream processes, unlike the gate-to-gate system boundary which is commonly used to only refer to the production processes. In addition to the relationship between the technical and natural system, system boundaries must be drawn in other dimensions, such as spatial and temporal. Following that, it should be ensured that the data collected throughout the data collection process are representative or adequate for the purpose of the stated time and spatial boundaries (Curran, 2017).

Another decision that should be made in the goal and scope definition phase, is whether the practitioner is aiming to perform an attributional or a consequential LCA. The former describes the environmentally relevant flows to and from a life-cycle and its sub-systems, while the latter describes how environmentally relevant flows will change in response to certain decisions. The distinction arose in the early 2000s, to resolve debates on what input data to use in LCA and how to deal with allocation problems. Back at that time, it was realised that certain decisions could result in impacts outside of the defined system, as defined by an attributional LCA. Consequential LCA was introduced in order to allow system boundary expansion to encompass likely external consequences of an action or decision. Attributional LCA uses average data and allocation is performed by partitioning the environmental impacts of a process between the life cycles it serves, whereas consequential LCA uses marginal data and avoids allocation through system expansion.

The functional unit is closely tied to defining the goal of the study. It appropriately describes the function delivered by the product or process under study. While the choice of the functional unit might not be as critical for independent LCAs, it immediately becomes more important in comparative assessments of two or more competing products, in which the basis of comparison should be equivalent.

Once the system under study is defined, it is important to identify the types of information needed to answer the questions. Generally, an LCA consists of (a) foreground data, which refer to the processes being under the control of the decision-maker for which an LCA is carried out and (b) background data, which refer to resources being delivered to the foreground system as aggregated datasets, without identifying individual plants or operations within them. Assessing the quality of both foreground and background data is of significant importance in better understanding the reliability of the results and interpreting the outcome of the study.

The goal and scope definition phase should also consider whether the impact assessment phase will be considered, and if yes, the impact categories, impact indicators, and characterisation models should be defined. In what is called a life cycle inventory analysis, the practitioner may choose to stop at the inventory analysis phase, without proceeding to impact assessment, with the purpose of interpreting the inventory results. However, most LCAs feed the inventory results in characterisation models which translate emissions to environmental impact category scores.

3.1.2 Life cycle inventory analysis

Due to the quantitative nature of LCA, Life Cycle Inventory (LCI) analysis has a crucial role in obtaining and modelling accurate data related to the object of study. The widely accepted framework for performing LCI analysis is provided by the ISO14040:2006 standard, which places it between the goal and scope definition and the Life Cycle Impact Assessment (LCIA), stating that this phase includes “data collection and calculation procedures to quantify relevant inputs and outputs of a product system.” (ISO, 2014). Three main steps for performing LCI analysis are listed in the standard:

- data collection,
- data calculation, and
- allocation of flows and releases to the environment.

Given that during the LCI analysis phase the practitioner learns more about the system under study, it is common to iterate with other phases of LCA to update, for example, the definition of the system or the results. Therefore, LCI analysis should be seen as an integral part of the LCA framework rather than an isolated phase to be ticked off (Klöpffer et al., 2021).

The product system comprises the object of focus in LCI analysis, being an interconnected set of processes exchanging energy and/or material flows. The product system is a collection of unit processes, which are the least aggregated units of the system. Each process has output and input flows, with the former commonly including resources from the environment or other flows from the upstream section of the product system. The latter includes emissions to air, water, soil, waste, by-products and flows that are further treated by downstream processes. A specific term is used to refer to flows leaving or entering the natural environment, known as elementary flows. All flows studied in the LCI analysis phase are usually scaled based on the chosen functional unit.

According to Baumann and Tillman (2004), the LCI analysis phase should be performed in three steps. First, a flowchart should be constructed, which depicts the processes included in the product system together with all energy and material flows within the system. Also, the system boundary should be clearly shown, distinguishing between intermediate and elementary flows and defining what is part of the foreground or the background system. Second, inventory data should be gathered for all the unit processes of the product system. This is a time consuming exercise and can be done through a series of ways depending on the type of LCA, including:

- process modelling and design tools,
- engineering calculations,
- estimations/assumptions based on similar operations and
- commercial databases.

The depth and accuracy of data collected is usually higher for the foreground system, where industrial and governmental reports, scientific publications and expert judgements might complement the data collection process. The data associated with the background system are usually more generic and are retrieved from LCA databases.

Third, and after the data collection process is completed, the LCI calculations are performed. Here, a practitioner usually starts from the functional unit of the system, tracing flows forward and backward until they cross the system boundary of the flowchart, where the amount of inputs and outputs is recorded (Klöpffer et al., 2021). Optionally, some preliminary interpretations might be performed in the LCI analysis phase, including hotspot analysis to identify major contributors to the overall energy and material consumption or comparisons to similar systems to benchmark energy and material flows.

3.1.3 Life cycle impact assessment

Life cycle impact assessment (LCIA) is the third phase of LCA according to the ISO14040 standard and aids the translation of elementary flows calculated throughout the LCI analysis phase to a limited but covering set of environmental impact scores. Such scores can support decision-making by enabling, for example, quantitative comparisons between competing products, or by identifying hotspots throughout the life cycle of a product, where the largest environmental impacts are found. The LCIA phase can be separated in five main steps, as described in the ISO14040 standards (ISO, 2014), which include:

1. Selection of the characterisation model to be used, together with the impact categories and category indicators of interest.
2. Assignment of the LCI results to the selected impact categories. This includes matching the elementary flows of the LCI to relevant impact categories selected in step 1, based on their ability to contribute to the environmental problems of concern.
3. Calculation of impact category indicator results (characterisation), which includes the multiplication of each elementary flow assigned to an impact category by a characterisation factor, signifying its importance to the specific impact category. The specific impact categories depend on the characterisation method chosen, but generally all methods include scores related to:
    - abiotic resource depletion,
    - acidification,
    - climate change,
    - ecotoxicity,
    - eutrophication,
    - human toxicity,
    - land use,
    - particulate matter formation,
    - photochemical ozone formation,
    - stratospheric ozone depletion and
    - water use.
4. Optionally, the magnitude of the category indicator results can be calculated relative to reference information, in a process called normalisation according to the ISO14040.

This process is useful in order to compare different impact categories in terms of their relative magnitudes based on a common set of reference information.

5. The final step is also optional according to the ISO14040 standards and includes the conversion of indicator results of different impact categories by using numerical factors based on value choices, in a process called weighting. This is performed to account for varying importance assigned to each impact category and to conclude on studies where trade-offs exist between the results for the different impact categories. The weighting process also facilitates the aggregation of several impact category results to a single score in order to ease the interpretation.

While there are no official ISO guidelines regarding the characterisation models to be used and the impact categories to be included, the practitioner is free to choose as long as it is in line with the ISO criteria. A series of characterisation models have been developed since the conception of LCA in the 1990s, including:

- The CML method that was first developed by the Institute of Environmental Sciences of the University of Leiden in 1992 and has been revised since (van Oers, 2016).

- The ReCiPe method that was first developed in 2008 through a collaboration of industry and academia, and was revised in 2016 (Goedkoop et al., 2009; Huijbregts et al., 2017).

- The Product Environmental Footprint (PEF) method, which was introduced by the European Commission, aiming to provide a harmonised methodology for European environmental footprinting studies (EC-JRC, 2012).

The characterisation methods described above mainly refer to the midpoint, seeking to evaluate the environmental impacts within a point in the cause-effect chain of a particular impact category, therefore, focusing on single environmental problems such as climate change or acidification. On the contrary, endpoint methods provide further aggregation levels, grouping specific environmental problems to three main areas of protection, including damage to human health, damage to ecosystems and damage to resource availability. The difference between the midpoint and endpoint is better illustrated in **Figure 17**, which also describes the damage pathways connecting the two points, as described in the ReCiPe 2016 model.

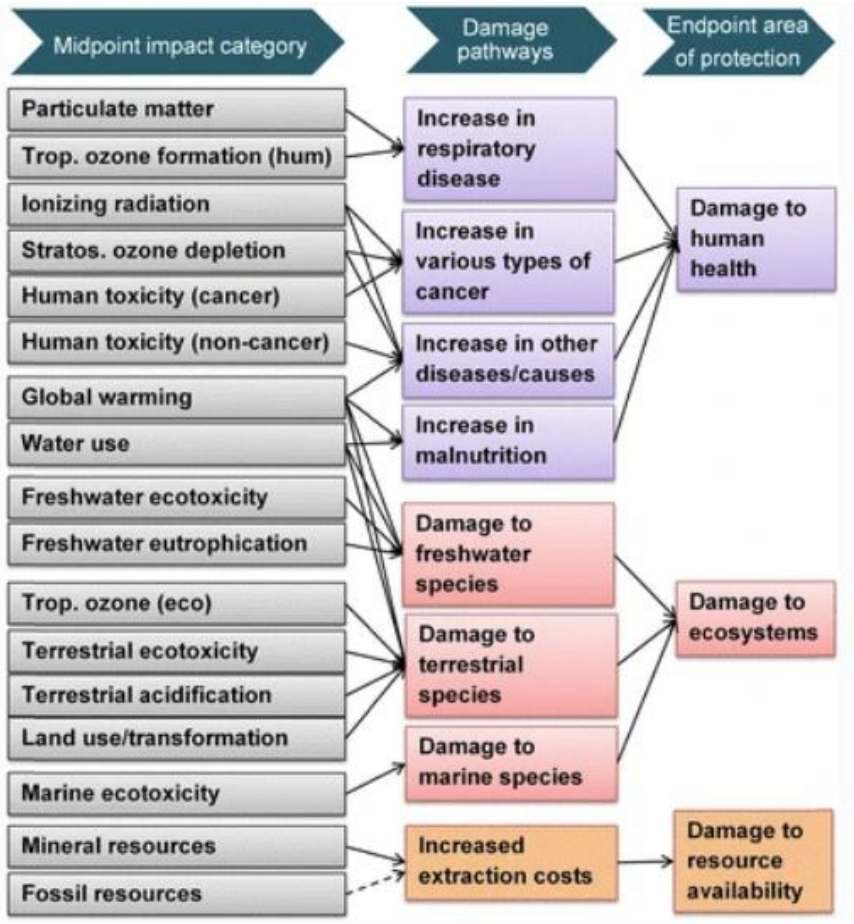


Figure 17. Midpoint vs endpoint impact categories covered from the ReCiPe 2016 method (Huijbregts et al., 2016).

The choice on whether to focus on the midpoint or endpoint mainly depends on the target audience of the LCA. For example, if the results are to be communicated to a high-level manager, it might be more relevant to present them at the endpoint level as there are fewer environmental impact categories to consider making the interpretation easier. Other endpoint methods, such as the Eco-indicator 99 (Goedkoop, 1999), calculate a single damage score, which makes it easier to compare different design alternatives. However, endpoint methods introduce further statistical uncertainties, compromising the reliability of the results. When getting in depth insights on the environmental impact of a product is the ultimate priority, midpoint methods should be used as they provide sufficient level of detail to identify trade-offs or consider differences between impact categories which are aggregated in the same damage category in the endpoint. The main drawback of midpoint methods is that they require in-depth understanding of the multitude of environmental effects to facilitate interpretation and make it harder to draw generalised conclusions. **Table 1** provides a description of the main midpoint impact categories that are reported throughout this thesis.

Table 1. Description of midpoint impact categories used throughout this thesis, modified after Huijbregts et al. (2017).

Impact category	**Units**	**Description**
Global Warming Potential (GWP)	kg CO_2-eq	GWP is a relative measure of how much heat a greenhouse gas traps in the atmosphere. The global warming potential is calculated in carbon dioxide equivalents, meaning that the greenhouse potential of emissions is scaled in relation to CO_2. Since the residence time of gases in the atmosphere is incorporated into the calculation, a time range for the assessment is usually defined to be 100 years with the option to perform calculations for a 20-year time horizon.
Fossil Depletion Potential (FDP)	kg oil-eq	FDP reflects the use of fossil resources and its effect on reducing their availability on a global scale. Therefore, it is measured in oil equivalents.
Ozone Depletion Potential (ODP)	kg CFC-11-eq	ODP represents a relative value that indicates the potential of a substance to destroy ozone gas as compared with the potential of chlorofluorocarbon-11, which is assigned a reference value of 1, resulting in an equilibrium state of total ozone reduction.
Photochemical Ozone Formation Potential (POFP)	kg NMVOC	Non-Methane Volatile Organic Compounds (NMVOCs) can interact with radiation from the sun producing aggressive reaction products, such as ozone, in the presence of nitrogen oxides and hydrocarbons. This effect is captured by the POFP indicator which describes the potential to produce photochemical smog.
Fine Particulate Matter Formation Potential (FPMFP)	kg $PM_{2.5}$-eq	FPMFP describes the change in ambient concentration of particulate matter (PM) after emitting a precursor, such as NH_3, NO_x, SO_2 and primary $PM_{2.5}$. It is commonly expressed in kg of particles less than 2.5 μm ($PM_{2.5}$).
Terrestrial Acidification Potential (TAP)	kg SO_2-eq	The acidification of soils and waters occurs predominantly through the transformation of air pollutants into acids, which leads to a decrease in the pH-value of rainwater and fog (≤5.6). TAP is described as the ability of certain substances to build and release H^+ ions and is given in sulphur dioxide equivalents, commonly calculated over a 100-year horizon.

Impact category	Units	Description
Freshwater Eutrophication Potential (FEP)	kg P-eq	FEP reflects the enrichment of nutrients in the aquatic environment due to the emission of phosphorous.
Marine Eutrophication Potential (MEP)	kg N-eq	MEP reflects the enrichment of nutrients in the marine environment due to the emission of nitrogen.
Freshwater Ecotoxicity Potential (FETP)	kg 1,4-DCB-eq	Ecotoxicity refers to effects of chemical outputs on non-human living organisms. Freshwater, marine and terrestrial ecotoxicity indicators represent potential adverse effects to organisms living in the corresponding environments. They are measured in kg 1,4-dichlorobenzene-equivalents, which is a compound classified as a carcinogen and used as insecticide.
Terrestrial Ecotoxicity Potential (TETP)	kg 1,4-DCB-eq	
Marine Ecotoxicity Potential (METP)	kg 1,4-DCB-eq	
Human Toxicity Potential (HTP)	kg 1,4-DCB-eq	HTP classifies chemicals that cause adverse health effects to humans.
Minerals Depletion Potential (MDP)	kg Cu-eq	MDP reflects the depletion of mineral resources as a result of their increased extraction. It can be measured in kilograms of copper or iron equivalents.

3.1.4 Interpretation

The final step of an ISO-standardised LCA includes the interpretation phase, which provides a systematic technique to assess the results generated from the LCI and LCIA phases. Throughout this phase, the results from the inventory analysis and impact assessment are quantified, checked and evaluated in order to generate a set of conclusions and recommendations from the study. Based on the ISO14040 standards, the interpretation phase should include the following:

- Identification: where results from the LCI and LCIA phases are structured to determine significant issues in line with the goal and scope definition and iteratively with the evaluation element described below. The identification of significant issues might be performed through contribution analysis, dominance analysis or anomaly assessment (Scientific Applications International Corporation, 2006).

- Evaluation: where the reliability of the results generated in the LCI and LCIA phases is enhanced. This is usually established by performing completeness, sensitivity and consistency checks. Also, the results of evaluation should be clearly communicated to the audience of the LCA study to provide a clear and understandable view of its outcome.

- Conclusions, limitations and recommendations: where conclusions are drawn, limitations are identified, and recommendations are made to the audience of the LCA study.

3.1.5 Reporting the results

After the four phases of LCA are completed, the materials should be made available to the audience through a clear and organised report. Not only the results, but also the data, methods, assumptions and limitations associated with the study should be summarised to allow the reader to comprehend complexities and trade-offs. According to the ISO standards the report should include the following elements (Scientific Applications International Corporation, 2006).

1. Administrative information:
    - name and address of LCA practitioner,
    - date of report and
    - other contact information or release information.
2. Definition of goal and scope
3. Life cycle inventory analysis:
    - data collection procedures and
    - inventory calculations
4. Life cycle impact assessment
5. Life cycle interpretation:
    - results,
    - assumptions and limitations,
    - data quality assessment.

Optionally, the study might undergo through external peer-review to identify any issues with its goal and scope, data collection and compilation, assumptions and, the generation and communication of the results.

3.2 Life cycle costing

LCC is a tool enabling the determination of the most cost-effective option amongst competing alternatives based on the TCO. The TCO encapsulates expenses incurred to purchase, own, operate, maintain and dispose a product. All the costs are usually discounted and total to a present-day value known as net present value (NPV). LCC studies are especially useful in the case of products meeting the same performance requirements but differing with respect to initial and operating costs, where they have to be compared in order to select the one that maximises net savings. They can be conducted following either a probabilistic or a deterministic assessment framework. LCCs are often coupled with LCAs in order to determine environmentally friendly and cost-cutting solutions throughout a product's life cycle.

The BatPaC model developed by the Argonne National Laboratory provides a comprehensive way of calculating the manufactured cost of a battery pack for various electrode chemistries (Nelson et al., 2012). The range of chemistries includes NMC333-Gr, NMC622-Gr and NMC811-Gr. The annual materials and purchased items requirements are determined by the design model, which along with the manufacturing and warranty cost comprise the unit cost of a single battery pack. The manufacturing cost is modelled based on a baseline plant of intermediate size and production scale and includes process expenses and costs of operating and manufacturing the facility such as launch costs, working capital, variable overhead, research and development, depreciation and profit. The total cost to the OEM for the whole battery pack is calculated accounting for the additional costs of the cooling system and BMS. The model has increased flexibility in inputting different battery cell configurations and pack designs.

In addition, the EverBatt model developed by the Argonne National Laboratory is a reliable tool allowing the evaluation of the performance of different battery recycling technologies, including hydrometallurgical, pyrometallurgical and direct cathode recycling. For geographic regions, EverBatt currently includes California, U.S. national average, China and Korea. The cost analysis for battery recycling is based on a generalised production cost model for chemical plants, which accounts for equipment, raw materials, labour and utility costs. EverBatt also includes an LCA module, where total energy use, water consumption, air pollutant and GHG emissions are calculated.

3.3 LCA studies on LIB production

After introducing the methodological framework for conducting LCA studies in section 3.1, this section provides a general overview, summarises key methodological choices, data sources and outlines results generated by studies focusing on lithium-ion battery production. Literature studies covering the production of NMC batteries from cradle to the factory gate are discussed herein.

LIB manufacturing has been investigated in numerous LCA studies, most of which are based on engineering calculations, a partial reliance on industry data, precedents from similar industrial processes, assumptions or a mix of these. Review studies by Peters et al. (2016), Porzio and Scown (2021) and Bouter and Guichet (2022) offer a complete overview of methodological choices and key parameters, and summarise results associated with LCA studies on LIB manufacturing. **Table 2** provides an overview of the reviewed studies, including key parameters and methodological choices. The table only includes data related to the production phase of NMC battery chemistries extracted from the above-mentioned review studies; some studies included use phase also; only some studies include other chemistries, described in text; some include recycling which is reviewed in a separate section.

3.3.1 General overview

One of the first studies to perform an LCA of LIBs for automotive traction applications was published by Majeau-Bettez et al. (2011), which was focused on nickel metal hydride (NiMH), NMC and LFP batteries. Their article contributed a public and detailed inventory, which was later picked up by a series of studies to assess the environmental performance of LIBs. Such studies include Ellingsen et al. (2014), who populated their inventory with primary data on producing lithium-ion battery cells and packs to estimate the environmental impact of NMC333-Gr chemistries. Dunn et al. (2015) received energy data from SCS Systems to analyse the dry rooms' electrical energy consumption, one of the most intensive components in the value chain, and estimate the cradle-to-gate energy consumption and greenhouse-gas footprint for a series of LMO, LFP, LCO and NMC battery chemistries. Their assessment was performed using the Greenhouse gases, Regulated Emissions, and Energy use in Technologies model (GREET) (Energy Systems Division Systems Assessment Group, 2016). Other studies based on the GREET model were published by Hao et al. (2017a), who assessed the GHG emissions

of battery production, and Qiao et al. (2019), who combined the cradle-to-gate and well-to-wheel phases to calculate the GHG emissions occurring from electric vehicles in China. A similar approach was followed by Xiong et al. (2019) in order to compare EVs with plug-in hybrid electric vehicles. Yu et al. (2018), modelled the production, use and recycling phases by combining primary and secondary data. Dai et al. (2019a) collected primary industrial data from LIB manufacturers to analyse the environmental impacts of NMC LIBs production, suggesting a series of modifications concerning the production inventories for battery materials. Sun et al. (2020) collected primary data for the cell manufacturing and pack assembly stages from a 30 GW h plant in China to perform an LCA of NMC622 chemistries. Accardo et al. (2021) assessed the environmental impact of producing and using NMC LIBs in electric vehicles based on data from the EverBatt model, which is linked to GREET. Finally, recent bottom-up modelling studies by Degen and Schütte (2022) and Jinasena et al. (2021), have shed light on the energy demand for LIB cell manufacturing, providing flexible tools to benchmark the energy use of different battery chemistries and compare with real-world data.

Table 2. Overview of LCA studies on LIB production for automotive traction applications.

Study	**Battery related parameters**			**LCA methodological choices**			
	Chemistry	**Energy density / kW h kg^{-1}**	**Mass / kg**	**FU**	**System boundary**	**LCIA method**	**LCI data source**
Majeau-Bettez et al. (2011)	NMC442-Gr	0.112 (cell)	50	W h	Production	ReCiPe Midpoint, CED	Battery materials: Ecoinvent 2.2 and own proxies Cell/pack: primary data
				50 MJ charge-discharge	Production and use		
Ellingsen et al. (2014)	NMC333-Gr	0.174 (cell) 0.105 (pack)	253 (pack)	Battery pack kg kW h	Production	ReCiPe Midpoint	Battery materials: Ecoinvent 2.2 and Majeau-Bettez et al. (2011) Cell manufacturing: Primary data and Majeau-Bettez et al. (2011) Pack assembly: primary data
Dunn et al. (2015)	NMC422-Gr	0.155 (cell)	180	km	Production, use and recycling	CED	GREET
Hao et al.(2017a)	NMC333-Gr	0.165 (cell)	170	kW h	Production	GHGs	GREET and literature values for GHG footprint of energy in China
Yu et al. (2018)	NMC (undefinded)	n/a	208	250,000 km (vehicle distance)	Production, use and recycling	CML2001	Battery materials: Own investigations Cell manufacturing: Zackrisson et al. (2010) Pack assembly: primary data
Qiao et al. (2019)	NMC333-Gr	0.143 (pack)	188.7	Vehicle lifetime	Production, use and recycling	GHGs	GREET

Study	Battery related parameters			LCA methodological choices			
	Chemistry	**Energy density / kW h kg^{-1}**	**Mass / kg**	**FU**	**System boundary**	**LCIA method**	**LCI data source**
Xiong et al. (2019)	NMC	0.140 (pack)	444	km	Production, use and disposal	GHGs, CED	Vehicle: Primary data Battery: Peters et al. (2016) , Peters and Weil (2018) and Majeau-Bettez et al. (2011)
Dai et al. (2019a)	NMC333-Gr	0.197 (cell) 0.143 (pack)	165 (pack)	kW h	Production	CED, GHGs, SO_x, NO_x, PM_{10}, water	Battery materials: GREET Cathode and cell manufacturing: primary data Pack assembly: primary data
Sun et al. (2020)	NMC622-Gr	0.180 (cell) 0.115 (pack)	630 (pack)	kW h	Production and recycling	CML-IA baseline V3.02	Battery materials: CALCD, GREET Cell and pack assembly: primary data
Accardo et al. (2021)	NMC333-Gr	0.155 (pack)	226 (pack)	kW h	Production and use	CML-IA baseline V4	Materials and battery production: EverBatt
Jinasena et al. (2021)	NMC333-Gr	n/a	n/a	kW h	Cell production	Energy demand	Bottom-up modelling for the cell assembly process
Chordia et al. (2021)	NMC333- Gr	0.170-0.180 (cell)	67-69 g (single cell mass)	kW h	Cell production	ReCiPe Midpoint	Battery materials: secondary data Electrode materials and cell production: Northvolt reports
	NMC811-Gr	0.210-0.240 (cell)					
Degen and Schütte (2022)	NMC622- Gr	n/a	n/a	kW h	Cell production	Energy demand	Bottom-up modelling for the cell assembly process

3.3.2 Methodological choices

Most studies included in **Table 2** assess the cradle-to-gate battery production system, either focusing on it or as part of modelling the production, use and recycling system. The latter is commonly combined with the well-to-wheel phase for electric vehicles to holistically assess the environmental impacts of e-mobility. Studies explicitly focusing on battery production usually employ a functional unit on a kW h pack or cell capacity basis, while the ones focusing on EVs report their results per km driven throughout the vehicle's lifetime. Even within the same battery chemistry type, such as NMC333-Gr, the energy density varies significantly across literature studies, which affects the kW h functional unit making hard to compare their results. Primary data on cell manufacturing and battery pack assembly have been discussed in a series of studies (Dai et al., 2019a; Ellingsen et al., 2014; Sun et al., 2020), with the remaining studies either relying on the GREET model or preceding literature to compile the foreground bills of materials (BOM). The background data of studies included in **Table 2** are either linked to the Ecoinvent database or GREET, with Sun et al. (2020) relying on the China Automotive Life Cycle Database (CALCD) for their battery materials production inventories. Finally, studies from Degen and Schütte (2022) and Jinasena et al. (2021) focused on the gate-to-gate battery manufacturing system, aiming at assessing its energy demand using bottom-up modelling.

The most commonly applied impact assessment methodologies include the CML and ReCiPe methods. All studies included in **Table 2** reported environmental impacts associated with GHGs, with the next most frequently assessed environmental impact category being the cumulative energy demand (CED). Other environmental impacts such as toxicity and acidification are reported less often. All reviewed studies use midpoint indicators for their impact assessment stage. As recommended by Porzio and Scown (2021), studies should distinguish between energy related emissions, usually tied to combustion, such as GHGs, particulate matter (PM), SO_x and NO_x, and non-energy related emissions. The latter include ecotoxicity and eutrophication impacts tied to the release of chemical compounds to soil and water. Such distinction between energy and non-energy related impacts is crucial, as the former mainly arise through combustion associated with the energy demand of the foreground system, while the latter are mainly tied to mining and materials processing operations.

3.3.3 Reported results across LCAs of battery production

The most frequently reported results across LCAs of battery production include the energy demand and the carbon footprint (or GWP) of the cradle-to-gate system. **Figure 18** summarises the reported carbon footprint across literature studies focusing on battery production.

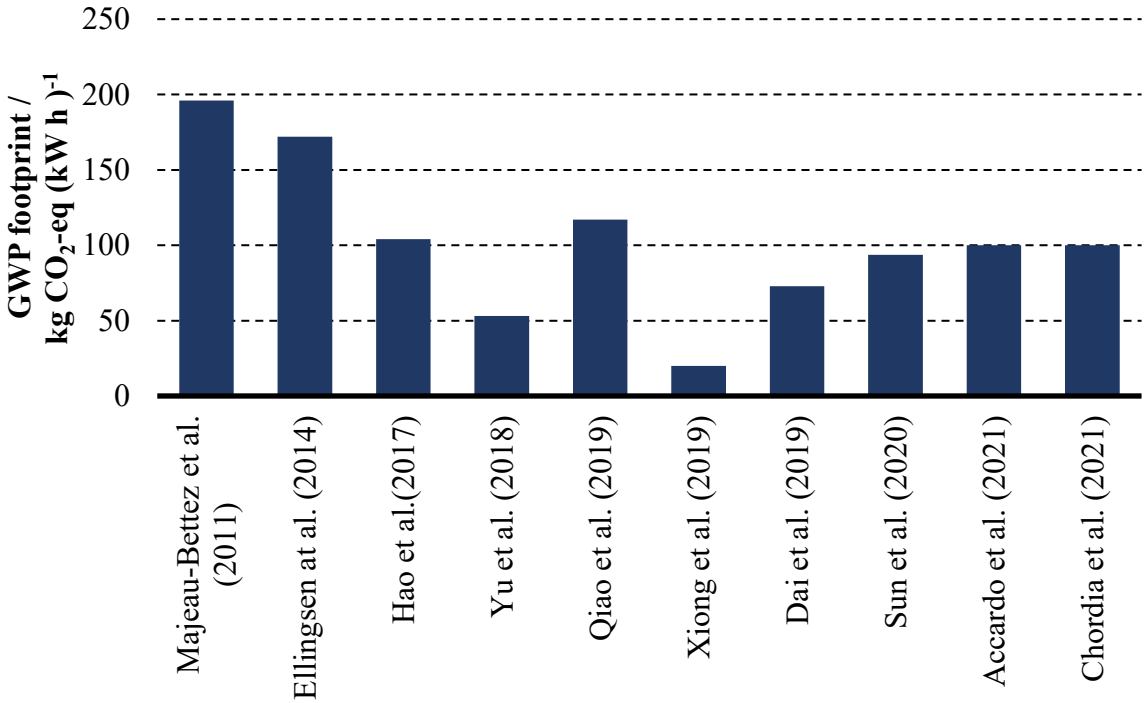


Figure 18. Overview of reported carbon footprints of battery production across literature studies.

Majeau-Bettez et al. (2011) and Ellingsen et al. (2014) reported GWPs for battery production of 196 and 172 kg CO_2-eq (kW h)$^{-1}$, respectively. Both studies were focused on Europe, same as Chordia et al. (2021) and Accardo et al. (2021), with the study of Dai et al. (2019a) being geographically focused on the United States and reporting a GWP of 72.9 kg CO_2-eq (kW h)$^{-1}$. The remaining studies included in **Figure 18** are geographically focused on China. One of the key observations that were made early in this research, is that despite the higher coal intensity in its electrical energy mix, China's LIB manufacturing appears to have a lower GWP production footprint than other regions, which is counter-intuitive and raises the need for more detailed analysis.

A key factor affecting the GWP of battery production is the energy density of the battery chemistry under study. While preceding literature has studied a variety of different battery chemistries within the NMC family, as shown in **Table 1**, the environmental performance of

different battery chemistries had not been benchmarked under the same model and assumptions. This was a major literature gap, especially due to the tendency to increase the nickel content of LIB cathodes and mix silicon in anodes traditionally made of graphite.

Another source of variation associated with the results reported in **Figure 18**, comes from the different energy demand for LIB cell manufacturing modelled across literature studies. Specifically, older studies modelled battery production plants which had not reached full production scale at the time (Ellingsen et al., 2014; Majeau-Bettez et al., 2011), with later literature revealing that the energy demand for cell manufacturing in the Giga scale is significantly lower (Dai et al., 2019a; Sun et al., 2020). Additionally, it was common for literature studies focusing on China to adopt previously published numbers on the energy use of battery production without assessing their representativeness. This becomes more evident when looking at the study of Yu et al. (2018) who reported a significantly lower impact for battery manufacturing of 53 kg CO_2-eq $(kW\ h)^{-1}$, with their manufacturing inventory based on that of Zackrisson et al. (2010), which referred to a completely different battery technology for hybrid electric vehicles, leading to an underestimation. Also, the significantly low value of 20 kg CO_2-eq $(kW\ h)^{-1}$ reported by Xiong et al. (2019) is primarily attributed to the direct use of the results of Peters et al. (2018) without making any modification to account for the local industry average values in China. This raises the need to suggest filtering criteria and assess the representativeness of energy use data for LIB production LCAs.

3.4 Studies on the LIB utilisation phase

This section provides a general overview, summarises key methodological choices, data sources and outlines results generated by studies focusing on using lithium-ion batteries in electric vehicles. Literature studies covering the utilisation (or use) phase in EVs commonly combine the LIB production footprint with the well-to-wheel phase to produce the fuel, accounting for key performance parameters such as the energy consumption and battery lifetime to estimate the environmental footprint. It is also common to assess the use phase footprint in the context of performing a cradle-to-grave LCA of LIBs. Due to varying system boundaries and methodological choices when assessing the use phase, studies are discussed on a case-by-case basis in this section.

3.4.1 ICEVs vs EVs

Back in the time, most of the literature focusing on assessing the environmental footprint of EVs was aiming at comparing with ICEVs in order to quantify possible environmental burden reductions. For example, an early study by Hawkins et al. (2013) found that when powered by a European electricity mix, EVs offer a 10% to 24% decrease in GWP, when compared to ICEVs. They also highlighted key parameters affecting the environmental performance of the use phase, such as the electricity source, use phase energy consumption, vehicle lifetime and battery replacement schedules. The comparison of EVs to ICEVs, had caused controversies not only in the academic literature but also in the popular press. Press articles had questioned the environmental friendliness of EVs, claiming that they emit more than ICEVs (Lomborg, 2013; Sinn, 2019). However, more recent studies, such as the one by Knobloch et al. (2020), have busted this myth suggesting that even if future end-use electrification is not matched by rapid power-sector decarbonisation, EVs can still offer emission reductions in almost all world regions, when compared to ICEVs, shifting the focus from whether EVs offer environmental benefits to how high those emission savings could be. In this direction, Wu et al. (2018) assessed the life cycle GHG emission reductions achieved by EVs relative to ICEVs, for 2010, 2014 and 2020 scenarios, reporting that while EVs had higher GHG emissions in 2010, they lead to a 13.4% reduction in 2020. Marques et al. (2019) performed a comparative assessment of different types of LIBs used in EVs, under realistic capacity fade data, concluding that LFP batteries exhibit a better operational performance than LMO. Xiong et al. (2019) assessed the GHG emissions of pure electric vehicles in comparison to plug-in hybrid electric vehicles in China, reporting that the former are less GHG intensive than the latter. Qiao et al. (2019) combined the cradle-to-gate system with the well-to-wheel phase to study the GHG emissions of EVs, highlighting power grid decarbonisation and battery recycling as major opportunities for environmental impact reductions throughout the entire life cycle. A very detailed statistical study by Cox et al. (2018) quantified current and future scenarios regarding the environmental footprint of EVs, reporting that future EVs are expected to have a 45% to 78% lower climate footprint than current EVs at the time. They also highlighted the electricity used for charging, vehicle size, lifetime, driving patterns and battery size as key sources of variability along the LIB use phase.

3.4.2 Methodological choices

Studies focusing on the EV use phase commonly apply a functional unit based on the distance driven throughout the vehicle's lifetime, therefore reporting their results on a km basis or a vehicle lifetime basis. The life cycle of an electric vehicle is illustrated in **Figure 19**. When modelled in an LCA study, both the vehicle cycle and fuel cycle should be taken into account. The former describes the production of the EVs main parts, such as the car body and the battery, while the latter corresponds to the whole chain to produce and use the fuel, also referred to as the well-to-wheel (WTW) phase. As evident from **Figure 19**, describing the use phase of LIBs in EVs goes beyond just modelling the operation of the vehicle, as the production phase for each input needs to be taken into account, together with the end-of-life phase. As a consequence, most literature studies studying the use phase of LIBs, perform a cradle-to-grave assessment of EVs, combining that with the WTW phase for the fuel (Hawkins et al., 2013; Marques et al., 2019; Qiao et al., 2019).

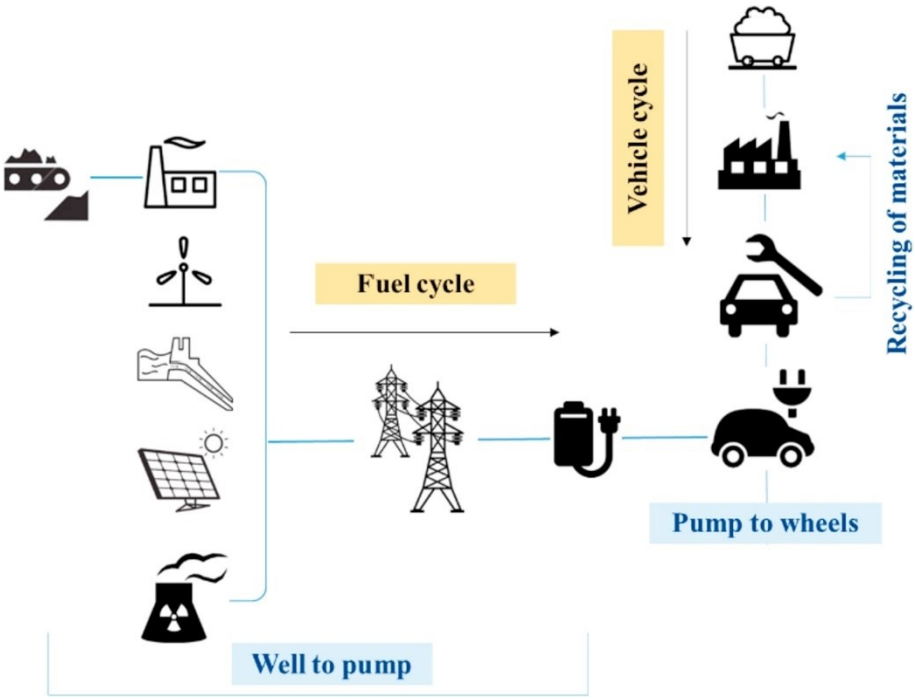


Figure 19. Fuel and vehicle cycles for electric vehicles. Reprinted with permission from Wu et al. (2018), Copyright 2018, with permission from Elsevier.

The most relevant environmental metric associated with the use phase relates to the GHG emissions, not only because of the direct comparison to ICEVs, but also because environmental burdens during the use phase are traced back to the corresponding energy demand. This becomes evident when looking at the studies of Wu et al. (2018), Xiong et al. (2019) and Qiao et al. (2019), which were all focused on GHGs. Hawkins et al. (2013) assessed the

environmental impact across 10 impact categories of interest, based on the ReCiPe characterisation method, while Marques et al. (2019) calculated the global warming, eutrophication and acidification potentials based on the CML method. As suggested by Porzio and Scown (2021), studies should distinguish between environmental metrics tied to energy use and impacts tied to other activities, such as pollutant releases to air, soil and water, with the former being mostly relevant to the LIB use phase.

Most academic literature to date has over-simplified the contribution of battery lifetime as a key parameter affecting the LIB use phase. Studies from Hawkins (2013), Yu et al. (2018), Qiao et al. (2019) and Xiong et al. (2019) assumed a fixed battery lifetime or a vehicle service life associated with it, without backing it with real-world data. However, fixing the vehicle's lifetime in mileage or years could artificially decrease or increase a vehicle's environmental burdens and does not reflect what batteries are realistically capable of, leading to an oversimplification and possibly distorting LCA results. Some studies have aimed at dealing with such issues, with Yang et al. (2018), for example, relying on an analytical model to predict the cycling life of LMO-graphite batteries, to improve the accuracy of the assessment of greenhouse gas (GHG) emissions. Also, Marques et al. (2019) performed a comparative life cycle assessment of LMO and LFP batteries, addressing capacity fade based on experimental data of Wang et al. (2014; 2011). Some progress has been made in realistically modelling battery lifetime in LCAs of EVs, but the topic still is an open challenge for scientists and engineers.

3.4.3 Reported results across LCAs of EVs

Literature studies focusing on the LIB use phase have applied varying system boundaries, parameters and energy mixes, making it impossible to just benchmark their results. Therefore, an effort is made below to group literature studies based on geographical criteria and compare their results, tracing variability to key parameters and assumptions.

Xiong et al. (2019) reported a GHG footprint of 0.237 kg CO_2-eq km^{-1} for an EV utilising an NMC battery chemistry in China. Their study employed a cradle-to-grave system boundary, similar to Qiao et al. (2019), who reported a GHG footprint of 0.273 kg CO_2-eq km^{-1} under similar parameters. The study of Xiong et al. (2019) assumed an EV lifetime of 120,000 km compared to 150,000 km for Qiao et al. (2019) which would normally lead to a lower footprint for the latter. One of the key differences leading to a lower footprint for Xiong et al. (2019) is

that they assumed a significantly low value for the battery production footprint of 20 kg CO_2-eq (kW h)$^{-1}$ compared to approximately 100 kg CO_2-eq (kW h)$^{-1}$ for Qiao et al. (2019). A significantly low footprint of battery manufacturing [53 kg CO_2-eq (kW h)$^{-1}$], together with a much higher lifetime (250,000 km) assumed by the study of Yu et al. (2018) has led to a 0.035 kg CO_2-eq km^{-1} GHG footprint of their EV under study, which is an order of magnitude lower than the studies of Xiong et al. (2019) and Qiao et al. (2019). Indeed, even within China, different regions have varying GHG footprints of the electricity mix, partly explaining the variability in the studies discussed above. Not only the electricity mix, but also varying parameters such as vehicle size, lifetime, driving patterns and battery size cause a highly variable GHG footprint of EVs, as reported by Cox et al. (2018) and illustrated graphically in **Figure 20**. Reasonable GHG footprints of EVs fall within the range of 0.05 to 0.4 kg CO_2-eq km^{-1} based on their study.

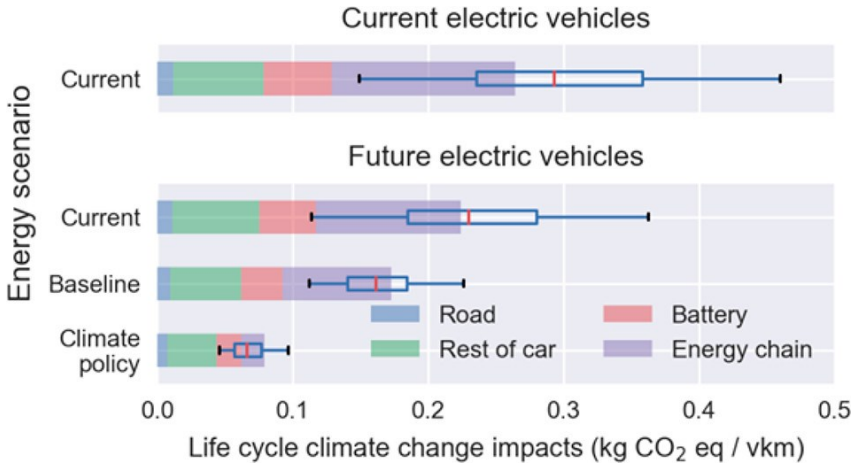


Figure 20. Life cycle GHG emissions of current and future EVs per vehicle kilometer (vkm) driven accounting for uncertainty. The boxes contain 50% of the results, whereas the whiskers show the 5th and 95th percentiles and the red line shows the median result. Y axis labels show the background database that was used for the calculation: Ecoinvent uses the current electricity scenario, whereas Baseline and ClimPol show middle-of-the-road and aggressive climate policy scenarios for the future electricity sector, respectively. Reprinted with permission from Cox et al. (2018), Copyright 2018, with permission from the American Chemical Society.

The geographical variability of the GHG footprint of EVs is illustrated in **Figure 21** (Bieker, 2021). It immediately becomes evident that regions with a lower GHG footprint associated with their electricity mix exhibit a significantly lower GHG intensity for EVs. For example, an EV in the United States has an intensity of 0.1 kg CO_2-eq km^{-1} compared to 0.16 kg CO_2-eq km^{-1} for China and 0.18 kg CO_2-eq km^{-1} for India. Also, the battery and vehicle manufacturing footprints variate across locations but the key cause of variations in the life cycle GHG footprint of EVs across locations is the electricity mix. This is the result of producing results under the

same model and assumptions, as input parameters are a key cause of variation across literature studies as discussed earlier in this section.

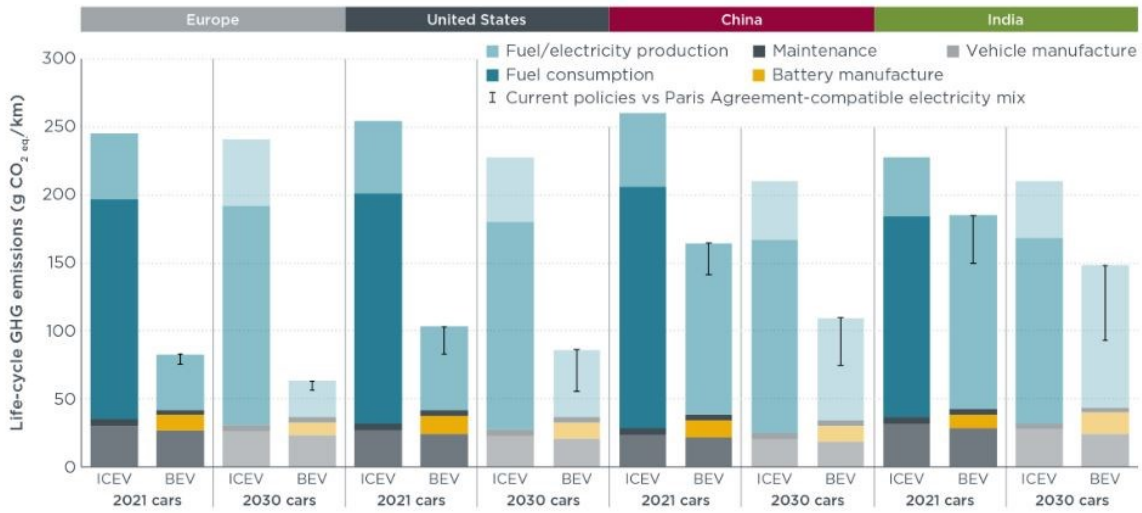


Figure 21. Life-cycle GHG emissions ICEVs and EVs registered in Europe, United States, China and India in 2021 and projected to be registered in 2030. Reprinted under Creative Commons License (CC BY-SA 4.0) from (Bieker, 2021), Copyright 2021, International Council on Clean Transportation.

Overall, the LIB use phase has attracted increased attention due to its significant contribution to the life cycle GHG footprint of EVs. However, most studies have focused on comparative scenarios across locations and battery technologies, arbitrarily specifying key input parameters such as the battery lifetime. In this direction, real-world data should be collected and taken into account to model the number of cycles delivered throughout the LIBs lifespan. This would provide a more realistic picture of the actual mileage achieved throughout an EVs lifetime and provide and idea of the required battery replacements. Also, varying battery production footprints were shown here to be a key source of variability across literature studies, which further supports the case for performing accurate LCAs of LIB production.

3.5 Studies on LIB end-of-life

This section provides a general overview, summarises key methodological choices, data sources and outlines results generated by studies focusing on the end-of-life phase for lithium-ion batteries from electric vehicles. A battery is considered to have reached its end-of-life when it reaches approximately 80 % of its initial capacity to store charge. From there, it can either

by given a second life or be disposed of. Eventually, and as an ideal scenario, EoL LIBs should be fed into battery recycling processes to recover their valuable materials. Currently commercial hydrometallurgical and pyrometallurgical materials recovery processes exist, which are reviewed in this section from an LCA perspective. The discussion is focused on metals recovery processes for NMC batteries for the sake of comprehensiveness.

3.5.1 General overview

The environmental impact reduction potential of recycling technologies is known to depend both on the specific processes used and the particulars of the value chain where recycling is implemented, which has triggered a growing interest in the scientific community of using LCA to investigate the environmental benefits that battery recycling can achieve in different settings. Cusenza et al. (2019) performed a cradle-to-grave assessment of a LIB pack for hybrid electric vehicles utilising a LMO-NMC333 composite cathode material, while Ciez and Whitacre (2019) quantified and benchmarked the net benefit of pyrometallurgical and hydrometallurgical recycling of NMC battery cells, amongst other battery chemistries. Dunn et al. (2015) quantified the possible GHG reduction potential, when producing a NMC battery with recycled material coming from pyrometallurgical processing. Hao et al. (2017b) assessed the EoL phase of EVs in China in the framework of their cradle-to-grave assessment. Sun et al. (2020) performed a cradle-to-grave assessment of NMC333 battery packs in China, similar to Accardo et al. (2021). Quan et al. (2022) performed a comparative assessment of LFP and NMC batteries including second use and different recycling technologies. Another recent study by Du et al. (2022) provides valuable insights on the regeneration of NMC cathode material with a focus on the active material level. Jiang et al. (2022) performed a process-based life cycle assessment to quantify the environmental impacts of hydrometallurgical recycling of LFP and NMC batteries, and reusing materials in their manufacturing in China. Rajaeifar et al. (2021) assessed the GWP and CED and GWP of pyrometallurgical recycling technologies. An earlier comprehensive review by Mohr et al. (2020) highlighted the varying system boundaries and functional units reported by different authors as a reason for variability and the need for transparency amongst LCAs on LIB recycling.

3.5.2 Methodological choices

The methodological approaches to EoL modelling in LCA studies of LIBs have been reviewed by Nordelöf et al. (2019), with their review including 25 peer-reviewed scientific journal and

conference articles. General approaches associated with the LCA method, as well as specifics on how to model the EoL phase for LIBs are discussed herein.

The two methods used to model the EoL phase include the cut off approach and the EoL recycling approach (Nordelöf et al., 2019). The former does not model the fates of recyclable materials all the way to where they recirculate in the production system, therefore having recovery and upgrading processes "cut off" from the product system. In such approach, no credits are allocated for displacing primary materials with secondary materials coming from the EoL treatment system. Instead, benefits are calculated upstream of the product system by assuming that recycled materials provide a share of the overall material demand. In the EoL recycling approach, the material recovery is explicitly modelled instead of being cut off (Nordelöf et al., 2019). In such approach, materials recovery operations are included in the product system, with recovered materials assumed to displace the equivalent amount of primary materials, either upstream of the same product system or in a different one. Therefore, credits in the form of avoided impacts are allocated to the system, mainly in the form of negative environmental burdens. Another distinction made in EoL modelling studies is whether recycling is part of an open loop or closed loop system (Nordelöf et al., 2019). In the former, recycled materials are used in a different product system instead of the one under study, while in closed loop they get recirculated back to the same product system. Based on the review of Nordelöf et al. (2019) most literature studies employ an EoL recycling approach and closed loop approximations.

In terms of methodological choices associated with the LCA scheme, system boundaries across literature studies are primarily focused on materials recovery from battery cells (Ciez and Whitacre, 2019; Dunn et al., 2015; Mohr et al., 2020; Rajaeifar et al., 2021), neglecting a series of processes, including collection, transportation, sorting and dismantling process, associated with the battery pack. This results in open questions regarding the environmental competitiveness of EoL treatment operations when the whole process sequence is taken into account, and the materials which are recovered not only from the battery cells but also from the battery packs supporting structures, such as the TMS, BMS and packaging. Additionally, literature studies on LIB recycling are primarily focused on GHGs (Ciez and Whitacre, 2019; Dunn et al., 2015; Rajaeifar et al., 2021), with more recent studies aiming to extend the analysis beyond GHGs to include other impact categories (Jiang et al., 2022; Mohr et al., 2020; Quan et al., 2022), given the association of non-energy related environmental impacts with battery

materials mining and processing operations (Porzio and Scown, 2021), which are avoided to a certain extent when recycling.

3.5.3 Reported results across LCAs of LIB recycling

Results reported across literature studies on LIB recycling are highly variable. For example, Ciez and Whitacre (2019) reported insignificant GWP intensity reductions achieved through hydrometallurgical and pyrometallurgical processing of NMC battery cells; with the latter resulted in a net increase. However, Mohr et al. (2020) reported a -13.8 and -16.4 kg CO_2-eq $(kW\ h)^{-1}$ net benefit achieved through hydrometallurgical and pyrometallurgical processing of NMC battery cells. Cusenza et al. (2019) reported a -15.4 kg CO_2-eq $(kW\ h)^{-1}$ net benefit for pack level recycling of a LMO-NMC333, while Sun et al. (2020) reported a -30.9 kg CO_2-eq $(kW\ h)^{-1}$ net benefit for hydrometallurgical recovery of NMC622. Accardo et al. (2021) reported recycling to come with a net benefit of -6.2 kg CO_2-eq $(kW\ h)^{-1}$ in Europe. Such variability is a result of varying system boundaries, assumptions and methodological choices across LCA studies of LIB recycling, as discussed in reviews by Mohr et al. (2020) and Nordelöf et al. (2019).

Extending the analysis beyond GHGs, Mohr et al. (2020) examined the abiotic depletion potential (ADP) reduction potential associated with pyrometallurgical and hydrometallurgical recycling operations, reporting that it is relatively higher that that observed for the GWP. They also reported that the ADP has a strong dependence on the specifics of the cell chemistry under study. Jiang et al. (2022) reported that the mineral depletion potential (MDP) and human toxicity potential (HTP) burdens can be reduced significantly when recovering copper from the battery cell anodes. Quan et al. (2022) analysed the Acidification Potential (AP) of hydrometallurgical and pyrometallurgical recycling processes reporting obvious environmental benefits due to the regeneration of cathode materials. They also calculated the Eutrophication Potential (EP), which was high in the case of hydrometallurgical recycling due to increased amounts of ammonia used in the process. Finally, they reported environmental benefits for the photochemical ozone creation potential (POCP) and ozone depletion potential (ODP) impact categories, mainly due to the recovery of cathode materials.

3.6 Methodological choices of this research

Three distinctive life cycle assessments were carried out in this thesis using the respective inventory models developed (a) LIB production LCA, (b) LIB utilisation in EVs and (c) LIB recycling. The methodological choices made are in line with the ISO standards, including the studied product systems and important modelling choices for each of the three studies. The LCAs were complemented by techno-economic calculations using either publicly available modelling tools or by carrying own first-hand engineering calculations. An overview of the main methodological choices for studying the environmental impacts and costs occurring in LIB production, utilisation and end-of-life is given in **Table 3**. A general description of those choices is discussed below and is made more specific in the distinctive chapters of this thesis.

Table 3. Overview of the methodological choices for the development of the LIB production, utilisation and end-of-life models.

	System boundary	**Technologies**	**Functional unit**	**Modelling tools**
		LIB production		
LCA	Cradle-to-gate: from raw materials extraction to battery pack assembly	NMC333-Gr NMC 333-SiGr NMC 622-SiGr NMC 811-SiGr	One battery pack/ kW h of battery pack capacity	Own modelling with inputs from Ellingsen et al. (2014) and Ecoinvent
LCC		NMC 333-Gr	kW h of battery pack capacity	BatPac
		LIB utilisation		
LCA LCC	Cradle-to-gate for vehicle/battery production Well-to-wheel for fuel	Compact EV with NMC333-Gr battery	km driven by the vehicle	Own modelling with inputs from this thesis and literature data
		LIB end-of-life		
LCA	Gate-to-cradle: From battery collection to materials recovery	Hydrometallurgical Pyrometallurgical	kW h of battery pack recycled	Own modelling with inputs from Ecoinvent
LCC				Material costs based on literature values

For LIB production, the LCA was carried out by developing a replicable, transparent and reliable LCI based on a combination of literature data and engineering calculations, while the cost was estimated based on the BatPac tool. The overarching objective was to develop a detailed LCI and LCA to analyse the environmental burdens associated with the production of lithium-ion batteries which utilise novel electrode chemistries and to quantify the effect of LIBs production in China. The geographical boundary was limited to China with material inputs, production processes, electricity mix and other LCI parameters reflecting the Chinese industrial averages. The technology boundaries were defined based on the current LIB production techniques and state-of-the art knowledge of the performance of novel electrode chemistries including NMC811 cathodes and SiGr anodes and are subject to defined modelling assumptions. The functional unit was chosen as the production of one traction battery; however, impacts are also reported in terms of nominal energy capacity (kW h). The product system studied includes raw material extraction, processing to raise the quality to battery-grade materials, component manufacturing, cell production and battery pack assembly, which is in-line with the battery production LCA studies summarised in **Table 2**. The same steps were taken into consideration in order to calculate the cost of producing a kW h of battery pack capacity. The production inventory was compiled based on literature data and first-hand engineering calculations combined with the utilisation of the Ecoinvent database (Wernet et al., 2016). The inventory development process is described in section 4.2 and detailed inventory tables for the battery production system are shown in Appendix A. The effects of the environmental emissions were assessed based on the ReCiPe 1.08 midpoint characterisation method.

Strongly connected with the production LCA, in the LIB utilisation LCA and LCC, the environmental impacts and costs for operating an electric vehicle were calculated by developing a utilisation model accounting for the battery, vehicle, electricity and maintenance costs and environmental impacts, which are calculated for a compact sized EV. The functional unit was chosen as a km driven by the vehicle. The technological boundary was based on the current status for EVs and is representative of a compact vehicle utilising a NMC333-Gr battery chemistry. The system boundary for the components included in the vehicle, including the vehicle body and the battery is set to cradle-to-gate, accounting for all the process steps included in the production of LIBs and the vehicle body. The former was calculated based on the production LCA of this thesis and the later was calculated based on the Ecoinvent database. The system boundary for electricity was well-to-wheel, accounting for all the processes for

delivering electricity to an electric vehicle, including production, transmission and charging. Such system boundaries are standard across LCA studies of electric vehicles, as shown in **Figure 19**. A particular focus is given to battery lifetime as it is an important quantity in the determination of the overall footprint of an EV. In this direction, the technology boundary is extended to include different cooling system options which have a significant contribution to the lifetime of the battery. The effects of the environmental emissions were assessed based on the ReCiPe 1.08 midpoint characterisation method, with a particular focus on GWP, as it is the predominant quantity for comparing transportation alternatives. The cost to the consumer, once ownership has been established, was estimated through engineering calculations accounting for the energy required to power the electric vehicle and maintenance.

In the LIB recycling LCA, the baseline geographical boundary was limited to China, with materials and energy inputs, production processes and other LCI parameters reflecting the Chinese industrial averages. However, the environmental benefit and burden of battery recycling was also explored in the United States and Europe. The product system included the transportation of the spent battery pack, dismantling, discharging of battery cells and materials recovery through hydrometallurgical or pyrometallurgical processing, further expanding the standard system boundaries across literature studies, as discussed in section 3.5. Also, the BMS, TMS and packaging were sent to a metals recycling facility, where the mixed scrap is shredded and sorted, and sent to metal recovery processes. The inventory development process is described in section 7.2 and detailed inventory tables for the battery recycling system are shown in Appendix B. The EoL recycling approach was followed (Nordelöf et al., 2019), which considers that the recovered materials displace primary material upstream in the product system. The impact assessment was performed based on the ReCiPe 2016 Midpoint characterisation method.

For all LCAs conducted in this thesis, the LCA modelling was performed using the GaBi software with the background processes mainly retrieved from the Ecoinvent version 3.5 database (Wernet et al., 2016).

Chapter 4 Lithium-ion battery production LCA

In this section, the development of an LCA model for the production of LIBs is discussed and implemented in the context of such production in China. The specific literature gaps are identified, followed by a description of the LCI developed and of the various scenarios studied. Finally, the results are presented and discussed in detail and conclusions are made on the impact of Chinese LIB manufacturing and of novel electrode batteries. This study has been peer-reviewed and published in the Journal of Cleaner Production (Kallitsis et al., 2020).

4.1 Background and Motivation

Numerous LCA studies in the literature have investigated LIB manufacturing, most of which are based on engineering calculations, a partial reliance on industry data, precedents from similar industrial processes, assumptions or a mix of these. Peters et al. (2016) offer an in-depth review of the interdependence and linkages between published LIB LCA studies, attributing the high variability among studies on different assumptions made on energy density and manufacturing energy demand. They also highlight the fact that important impact categories such as toxicity, acidification and resource depletion are often excluded from studies focusing only on the GWP. The most complete and reliable LCIs were reported by Notter et al. (2010), Dunn et al. (2015), Ellingsen et al. (2014), Kim et al. (2016) and Majeau-Bettez et al. (2011). Dunn et al. (2015) received energy data from SCS Systems to analyse the dry rooms' electrical energy consumption, one of the most intensive components in the value chain. Ellingsen et al. (2014) compiled a highly transparent, peer-reviewed, cradle-to-gate study using real industrial data for NMC batteries. Similarly, Kim et al. (2016) applied original manufacturers' data from LG Chem for a Ford battery pack to analyse the impacts of NMC and LMO batteries. Recently, Dai et al. (2019a) collected primary industrial data from LIB manufacturers to analyse the environmental impacts of NMC LIBs production, suggesting a series of modifications

concerning the production inventories for battery materials. The remaining studies mix primary and secondary data and often combine these with own measurements and data collection, primarily focusing on already commercialised technologies.

Information on the environmental burdens associated with China's role in LIB manufacturing are scarce in published literature. Studies have focused exclusively on electromobility in China, reporting the environmental burdens associated with EV and LIB cycle lives. Hao et al. (2017a) studied the production of a 28 kW h battery pack of three battery chemistries including NMC focusing on the GWP. Qiao et al. (2017) reported the cradle-to-gate energy consumption and GHGs emissions of battery electric vehicles produced in China but did not explicitly specify the nominal storage capacity of the battery integrated in the vehicle. Yu et al. (2018) performed an LCA study of a 208 kg EV power system, from cradle to grave. Qiao et al. (2019) calculated the GHG emissions occurring from electric vehicle's cradle-to-gate and well-to-wheel phases. A similar approach was followed by Xiong et al. (2019) in order to compare EVs with plug-in hybrid electric vehicles. Yin et al. (2019) collected foreground data, from the grey literature, on the manufacturing of critical materials used in LIBs in China; however, they did not proceed to the calculation of the environmental burdens of the LIB manufacturing chain. In summary, the LCA studies focusing on China are incoherent concerning the studied product system and underlying assumptions and lack transparency concerning the data used in their models.

Table 4 compares the GWP footprint (kg CO_2-eq. (battery kW h)$^{-1}$) for the battery manufacturing stage at different locations for reports that allowed the production footprint to be distinguished together with the battery mass and nominal capacity assumed in each study. The indication that despite the higher coal intensity in its electrical energy mix, China's LIB manufacturing has a lower GWP production footprint than in other regions is counter-intuitive and raises the need for more detailed analysis. It also highlights the need to perform comparisons under the same model and assumptions to account accurately for the region-specific impact on LIB production in China.

There are several gaps in the literature concerning the present and future prospect of LIB production. Firstly, even the most seemingly transparent studies on LIB production either do not provide data on the production processes for the raw materials, or use outdated datasets; thus, they do not allow verification of their models or reproduction of their results and estimates. Moreover, no study has been reported that provides a detailed LCI for LIB manufacturing in China. Secondly, the complete set of impacts of producing LIBs in China has

yet to be quantified, creating a major uncertainty in view of the dominance of the Chinese market in battery production and hence the associated environmental burdens. Also, no inter-country comparison exists based on the same model and assumptions, and which could accurately quantify the difference in impact intensity when producing a battery in China compared to the rest of the world. Thirdly, even though nickel-rich cathodes and silicon composite anodes are considered the most promising next-generation LIBs modifications in the near-term, to the author's knowledge there is not a single paper reporting the life cycle performance of such novel chemistries in combination.

Table 4. Reported GWP of NMC LIB manufacturing across different studies (Kallitsis et al., 2020).

Reference	Location	Battery Mass [kg]	Battery Capacity [kW h]	GWP [kg CO_2-eq (battery kW h)$^{-1}$]
Majeau-Bettez et al. (2011)	Europe	-	-	196
Amarakoon et al. (2013)	United States	-	-	121
Ellingsen et al. (2014)	South Korea/ Norway	253	26.6	172
Kim et al. (2016)	South Korea	303	24	140
Hao et al. (2017a)	China	170	28	104
Yu et al. (2018)	China	208	48	53
Qiao et al. (2019)	China	188.7	27	117
Xiong et al. (2019)	China	444	60.5	20
Dai et al. (2019a)	United States	165	23.5	72.9

In the first part of this thesis, a fully transparent inventory was compiled based on the state-of-the-art in the literature in order to assess the environmental impacts associated with the production of current and non-commercialised LIBs in China. Ellingsen's et al. (2014) inventory was used and the raw material production processes were updated based on the latest version of the Ecoinvent database (Wernet et al., 2016). An easy-to-reproduce inventory was compiled this way, which could be used to study various LIB chemistries in future studies. Next, the data was updated in order to reflect the Chinese production conditions and a baseline of LIB manufacturing in China is established. Further modifications on the LIB chemistry were performed in order to study the environmental aspects of introducing silicon in the anode and gradually increasing the nickel content of the cathode. The different chemistries were compared across 13 relevant impact categories based on the ReCiPe 1.08 Midpoint characterisation

method, which are presented in **Table 1**, and the most important contributions in each case are discussed.

4.2 Methods

The standardised reporting methods, according to the LCA ISO standards (ISO, 2006a), were followed in order to create a replicable, transparent and reliable inventory and results. The overarching objective was to develop a detailed LCI and LCA to analyse the environmental burdens associated with the production of lithium-ion batteries which utilize novel electrode chemistries and to quantify the effect of LIBs production in China. The geographical boundary was limited to China with material inputs, production processes, electricity mix and other LCI parameters reflecting the Chinese industrial averages. The technology boundaries are defined based on the current LIB production techniques and state-of-the art knowledge of the performance of novel electrode chemistries including NMC811 cathodes and SiGr anodes, and are subject to defined modelling assumptions. The functional unit was chosen as the production of one traction battery; however, impacts are also reported in terms of nominal energy capacity (kWh). The product system studied included mining and raw material extraction, processing to raise the quality of primary raw materials to battery-grade materials, component manufacturing and assembly of a 253 kg NMC LIB for use in EVs. The steps include raw material extraction, processing to raise the quality to battery-grade materials, component manufacturing to battery pack assembly. A detailed description of the LIB manufacturing processes has been presented in Section 2.4.2.

The mass composition of the produced battery pack is identical to that shown in **Figure 9**. The battery cells and packaging account for 92% of the total pack weight, with the BMS and the cooling system accounting for 4% each. Therefore, increased focus is assigned to accurately describing modifications associated with the battery cells when studying the novel electrode chemistries. The packaging is assumed to remain unchanged while the BMS and TMS are also kept constant between different scenarios.

A set of different scenarios were developed in the direction of fulfilling the goals of this study. The Background (BCG) scenario was developed using the GaBi software and Ecoinvent 3.5 in

order to create an easily reproducible model and directly compare it to pre-existent ones in the literature. The inventory of Ellingsen et al. (2014) was used and background processes were updated based on the Ecoinvent 3.5 database, in order to reflect the production of an NMC333-Gr battery with 26.6 kWh storage capacity in South Korea, which is further assembled in Norway. A direct comparison between the predicted impacts of Ellingsen et al. (2014) and of the current model was performed in order to ensure the validity of it and quantify the effects of updating the background processes. Next, the Baseline (BSL) scenario was developed in order to develop an LCI representative of Chinese LIBs manufacturing. Specifically, the electricity mix as well as the aluminium and copper production were modified to reflect the Chinese industry average. Electrode modifications were subsequently performed in order to encapsulate the effect of introducing silicon in the anode and increasing the nickel content in the cathode.

Important battery performance parameters like specific charge capacity and nominal voltage were extracted from empirical and/or mathematical papers in the literature. A large number of papers was critically reviewed, and values were selected carefully in line with data quality requirements. The chosen range is displayed in **Table 5**. It is noted that the mass-specific charge capacity used is representative of practically achievable charge capacity, not theoretical capacities of the material. It is also important to highlight that **Table 5** presents a snapshot of current LIB technology and ongoing research.

Table 5. Input parameters to calculate resulting energy storage capacity of advanced LIBs (Kallitsis et al., 2020).

Battery Scenario	**Anode**	**Cathode**	**Anode**	**Cathode**	**Anode**	**Cathode**
Active material	SiGr	NMC333	SiGr	NMC622	SiGr	NMC811
Specific charge capacity q_a / q_c [Ah kg^{-1}]	1,000 [a]	160 [b]	1,000 [a]	170 [c]	1,000 [a]	200 [c]
Nominal voltage V_{nom} [V]	3.55 [d]		3.8 [c]		3.8 [c]	

[a] (Dash and Pannala, 2016; Myung et al., 2017), [b] (Manthiram, 2017; Noh et al., 2013), [c] (Myung et al., 2017), [d] (Dash and Pannala, 2016)

Following this, a simple parametrised model was developed to calculate the storage capacity of a LiB pack for different active materials. The total storage capacity of a cell $C_{cell}\ [W\,h]$ is a function of its nominal cell operating voltage $V_{nom}\ [V]$ and its specific (dis-)charge capacity $Q_{cell}\ [A\,h]$. However, the cells (dis-)charge capacity Q_{cell} depends on the specific charge capacity of the materials that are used in the positive and negative electrode. Eq. 4.2 expresses

the cell's charge capacity Q_{cell} as a function of active material mass m [kg] and its mass-specific charge capacity $q\ [A\ h\ kg^{-1}]$, where subscripts a and c indicate anode or cathode, respectively. The charge capacity of negative and positive electrode must balance, which imposes a certain constraint on the overall achievable cell charge capacity Q_{cell}. Because anode materials usually have much higher capacity than cathode materials, it is the choice of cathode material that significantly limits to the overall achievable capacity C_{cell}.

$$C_{cell} = Q_{cell} \times V_{nom} \quad \text{Eq. 4.1}$$

$$Q_{cell} = m_a \times q_a = m_c \times q_c \quad \text{Eq. 4.2}$$

For the purpose of this LCA, it was essential to fix the total battery pack weight. As a result, the battery cell weight contribution must remain constant. In order to facilitate a constant cell weight, this model is based on the simplifying assumption that only the active material mass changes and that current collector weights stay fixed, i.e. constant in size and weight. This constraint is expressed in Eq. 4.3, where k is a constant. The value of k is calculated by summing up active material masses for anode and cathode for the BSL scenario $m_{\alpha,BSL}$ and $m_{c,BSL}$ respectively, and is applied in all further calculations for the remaining scenarios.

$$k = m_a + m_c \quad \text{Eq. 4.3}$$

$$k = m_{a,BSL} + m_{c,BSL} = 25.5 + 58.1 = 83.6 \text{ kg} \quad \text{Eq. 4.4}$$

Based on equations 1,2 and 3, C_{cell} was calculated for all scenarios as:

$$C_{cell} = \frac{q_a \times q_c}{q_a + q_c} \times k \times V_{nom} \quad \text{Eq.4.5}$$

With q_α, q_c and V_{nom} values taken from **Table 5**. The corresponding results are summarised in **Table 6**. The detailed inventory modifications for each scenario are summarised below.

Three scenarios were developed (NMC333-SiGr, NMC622-SiGr, NMC811-SiGr) by modifying the active material in the electrodes with the inventory for all other components (BMS, cooling system etc.) remaining fixed.

Table 6. Energy storage capacity and energy density of novel electrode chemistries compared to the baseline (Kallitsis et al., 2020).

Battery chemistry	**NMC333 -Gr**	**NMC333-SiGr**	**NMC622-SiGr**	**NMC811-SiGr**
Storage capacity [kW h]	26.6	40.9	46.2	52.9
% increase vs. Baseline	-	54	74	99
Pack energy density [kWh kg^{-1}]	0.105	0.162	0.182	0.209

A challenging aspect of modelling the production of novel electrodes is the quantification of the change in energy requirement, when shifting from NMC33-Gr production to novel electrode chemistries. The energy is a function of the throughput of the battery facility, with low throughput facilities exhibiting higher energy intensities. This is because the dominant energy consuming process, dry room conditioning, requires a throughput independent amount of energy (Dunn et al., 2015; Yuan et al., 2017). With that in mind, the energy requirement for the production of battery cells is set to 101 MJ per kg of battery cells produced (Ellingsen et al., 2014) and is kept constant across all battery scenarios, with this being equivalent to fixing the throughput of the facility and the battery weight and varying the nominal energy capacity of each battery technology. This value of energy demand for cell manufacturing is considered to represent the production in a large throughput facility.

A depiction of the studied product system is shown in **Figure 22**. For all scenarios, the battery pack has the weight composition shown in **Figure 9** and the energy requirement for its assembly is kept at 364 kJ per kg of battery pack produced. The production inventories for the BMS, packaging and TMS are identical to those of Ellingsen et al. (2014) and remain unchanged across all scenarios. The processes included in the cell manufacturing chain, are modelled based on the bill of materials and energy requirement of Ellingsen et al. (2014). The latter is calculated as a cumulative number of 101 MJ per kg of battery cells produced, including the energy requirement for the application of solvent to slurrify mixtures, coating of electrode pastes to foils, baking of coated foils, slitting/notching, welding of current collectors to tabs, electrolyte filling, initial cell charging and dry room conditioning. The electrolyte is modelled as a mixture of 88 wt% EC and 12 wt% lithium hexafluorophosphate. The separator's production is modelled as injection moulding of polypropylene granulate and the cell container is mainly consisted of aluminium and copper for all scenarios. The anode is consisted of the negative electrode paste and the negative current collector made of copper. The negative

electrode paste is consisted of battery grade graphite (and silicon for some scenarios), acrylic acid and carboxymethyl cellulose. The cathode is consisted of the positive electrode paste and the positive current collector made of aluminium.

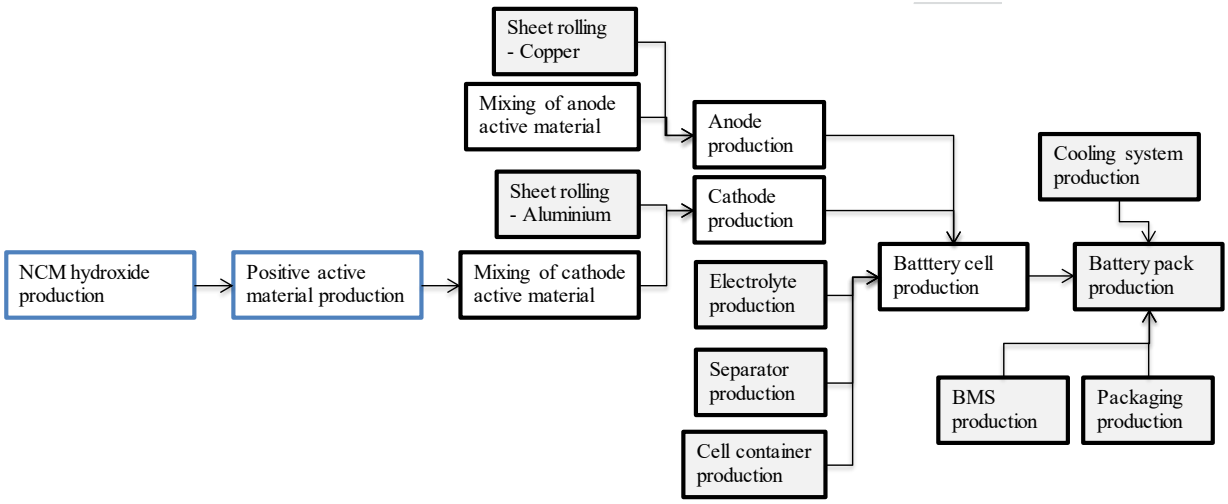


Figure 22. Cradle-to-gate product system studied. Unit process boundaries indicate: black, inventory data were taken Ellingsen et al. (2014); blue, inventory data adopted from Majeau-Bettez et al. (2011) with corresponding heat and electricity requirement updated based on Dai et al. (Dai et al., 2019a) . Shading indicates: grey, inventory data identical to those of the cited paper in all scenarios, except for the background production processes; white, inventory data modified to serve the goals of this study (Kallitsis et al., 2020).

The positive electrode paste is a mixture of positive active material and PVDF. The positive active material is Li-NMC oxide with a varying composition depending on the scenario. It is produced from nickel, cobalt and manganese reacting with sodium hydroxide to form NMC hydroxide, which further reacts with lithium hydroxide (Majeau-Bettez et al., 2011). The anode and cathode current collector production is modelled as sheet rolling of copper and aluminium respectively. As the bill of materials for the manufacturing chains of anode and cathode is scenario-specific, it is presented in detail below.

The BCG scenario's foreground data are based on those of Ellingsen et al. (2014) with the primary difference lying on the utilisation of the latest version of the Ecoinvent database (version 3.5) in order to update the background processes and minimise the proxies for raw material production. The anode is 43 wt% paste and 57 wt% negative current collector. The anode paste is a mixture of 96 wt% battery-grade graphite, 2 wt% acrylic acid and 2%

carboxymethyl cellulose. The cathode is 89 wt% paste and 11 wt% aluminium current collector. The positive electrode paste includes 94 wt% of Li-NMC oxide, with equal molar amounts of nickel, cobalt and manganese, and PVDF binder. The most important BCG scenario modification is associated the production of the raw materials for the battery cells. Ellingsen et al. (2014) adapted the inventory for the positive active material from Majeau-Bettez et al. (2011) with the latter being based on modifications of the inventories for primary nickel from Ecoinvent and the authors' own calculations for manganese. Here, nickel and manganese sulfate production is modelled utilising the latest inventories available in Ecoinvent 3.5, which are based on industry data combined with stoichiometric calculations. Also, background processes for the production of battery grade graphite and lithium hexafluorophosphate are introduced, with the former based on a modified Ecoinvent inventory for industrial graphite, while the latter is neglected in Ellingsen's study. Across all scenarios, 68 wt% of aluminium and 85 wt% of copper are assumed to be primary, with the remaining percentages coming from recycled material. Finally, the recovery of NMP during cathode preparation and the use of water as a solvent in the anode was taken into account and the NMC powder production process was updated based on Dai et al. (2019a).

In the BSL scenario, the energy requirement for the battery cells manufacturing and pack assembly is satisfied from the Chinese market group for electricity process from Ecoinvent 3.5. The coal intensive electricity mix as modelled in this study is shown in **Figure 23**. Aluminium and copper are two frequently recurring metals making up 19% and 14% of the battery pack materials by mass. It is therefore essential to ensure that their corresponding production processes reflect those used in the Chinese market. Aluminium production is adjusted to the Chinese market by introducing the CN: aluminium production, primary, ingot process from Ecoinvent 3.5. The data are based on annual surveys within the global aluminium industry done by the International Aluminium Institute. Copper production is modified in order to reflect the production in Asian conditions, as no specific dataset for China exists. The background process used is RAS: copper production, primary, which reflects copper production in the Asian continent. Also, a series of background production process are modified in the BSL scenario by concentrating to the Rest of World (RoW) instead of Europe/US while the foreground data remain unchanged compared to the BCG scenario.

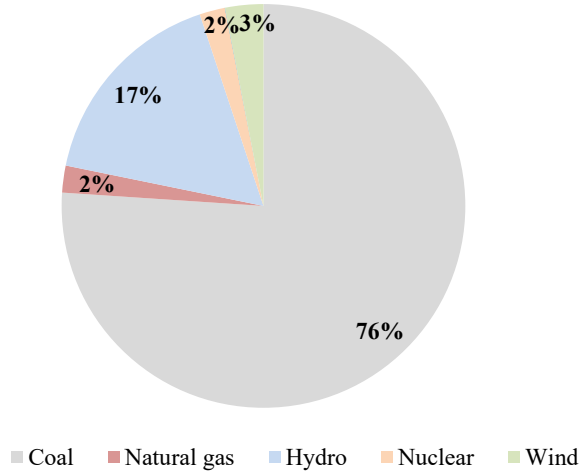


Figure 23. Percentage contribution of coal, natural gas, hydropower, nuclear and wind power to the Chinese electricity mix (Kallitsis et al., 2020).

In order to model the novel electrode scenarios, it is assumed that the production methods of next-generation NMC LIBs need not change significantly as compared to the current. As such, the modifications in the life cycle inventory are only associated with the changes in the composition of the electrodes. For the three novel electrode scenarios (NMC333-SiGr, NMC622-SiGr, NMC811-SiGr) the anode and cathode sub-inventories are modified by altering the ratio of active material and keeping the total weight of each battery component constant. In the NMC333-SiGr scenario, the anode is consisted of 25.5 wt% paste and 74.5 wt% copper current collector. The paste is modified to include 75 wt% graphite, 21 wt% silicon, 2 wt% acrylic acid and 2% carboxymethyl cellulose. The cathode's composition also changes to 91 wt% positive electrode paste and 9 wt% aluminium current collector. In the NMC622-SiGr scenario, 1 kg of NMC hydroxide is produced from 0.34 kg of cobalt sulphate, 0.33 kg of manganese sulphate and 1 kg of nickel sulphate, reacting with 0.87 kg of sodium hydroxide. The anode has a composition of 26.5 wt% negative electrode paste and 73.5 wt% copper current collector, and the cathode of 91 wt% positive electrode paste and 9 wt% aluminium current collector. Similarly, in the NMC811-SiGr scenario, 1 kg of NMC hydroxide is produced from 0.17 kg of cobalt sulphate, 0.16 kg of manganese sulphate and 1.34 kg of nickel sulphate reacting with 0.87 kg of sodium hydroxide. The anode has a composition of 29.2 wt% negative electrode paste and 70.8 wt% copper current collector, and the cathode of 90.7 wt% positive electrode paste and 9.3 wt% aluminium current collector. Detailed inventory tables for all scenarios developed in this work are shown in Appendix A.

4.3 Results and analysis

The environmental burdens associated with the different scenarios of LIBs production are reported in this section and each impact category is broken down to the principal contributions. The results for the BCG scenario are directly compared to those of Ellingsen et al. (2014) in **Figure 24** on a battery pack basis. The BCG and novel electrode scenarios' results are reported in **Figure 25** and the total impacts are broken down to key background process contributions.

4.3.1 Cradle-to-gate impacts for all scenarios

As shown in **Figure 24**, the results for the BCG scenario are in good agreement with those of Ellingsen et al. (2014), with less than 25% variations for GWP, fossil depletion potential (FDP), ozone depletion potential (ODP), POFP, particulate matter formation potential (PMFP), terrestrial acidification potential (TAP), freshwater eutrophication potential (FEP), HTP and MDP, as defined in the figure. The BCG scenario exhibited a 40% to 50% increase across all ecotoxicity categories. Also, the marine eutrophication potential (MEP) of this study was three times lower than that of Ellingsen et al. (2014).

The BSL scenario results shown in **Figure 25** predict that moving LIB production from South Korea/Norway to China (BCG vs BSL) would cause an increase of 40% in the GWP and POFP, 63% in PMFP, a decrease of 46% in ODP and increases of 1 to 36% for the rest of the impact categories. On a per battery pack basis, the three novel electrode scenarios (NMC333-SiGr, NMC622-SiGr, NMC811-SiGr) resulted in slightly higher impacts, but when compared on a kWh basis, significant reductions were predicted as a consequence of the increased energy storage capacities of novel electrode technologies, as shown in **Figure 25**. More specifically, introducing silicon to the anode (NMC333-SiGr) was predicted to cause an impact increase of 16% at most across all impact categories when compared to the baseline; however, as a result of the increased nominal energy storage capacity, significant reductions of 29 to 34% were predicted on a per kW h basis. Increasing the nickel content of the cathode (NMC622-SiGr and NMC811-SiGr) caused an increase of less than 6% in all impact categories, except for PMFP and TAP impacts, which increased by 18% and 31%. The highest nominal energy capacity technology (NMC811-SiGr) resulted in a lower impact for all impact categories of 30 to 50% when compared to the baseline on a kWh basis, except for TAP which decreased by 17 %.

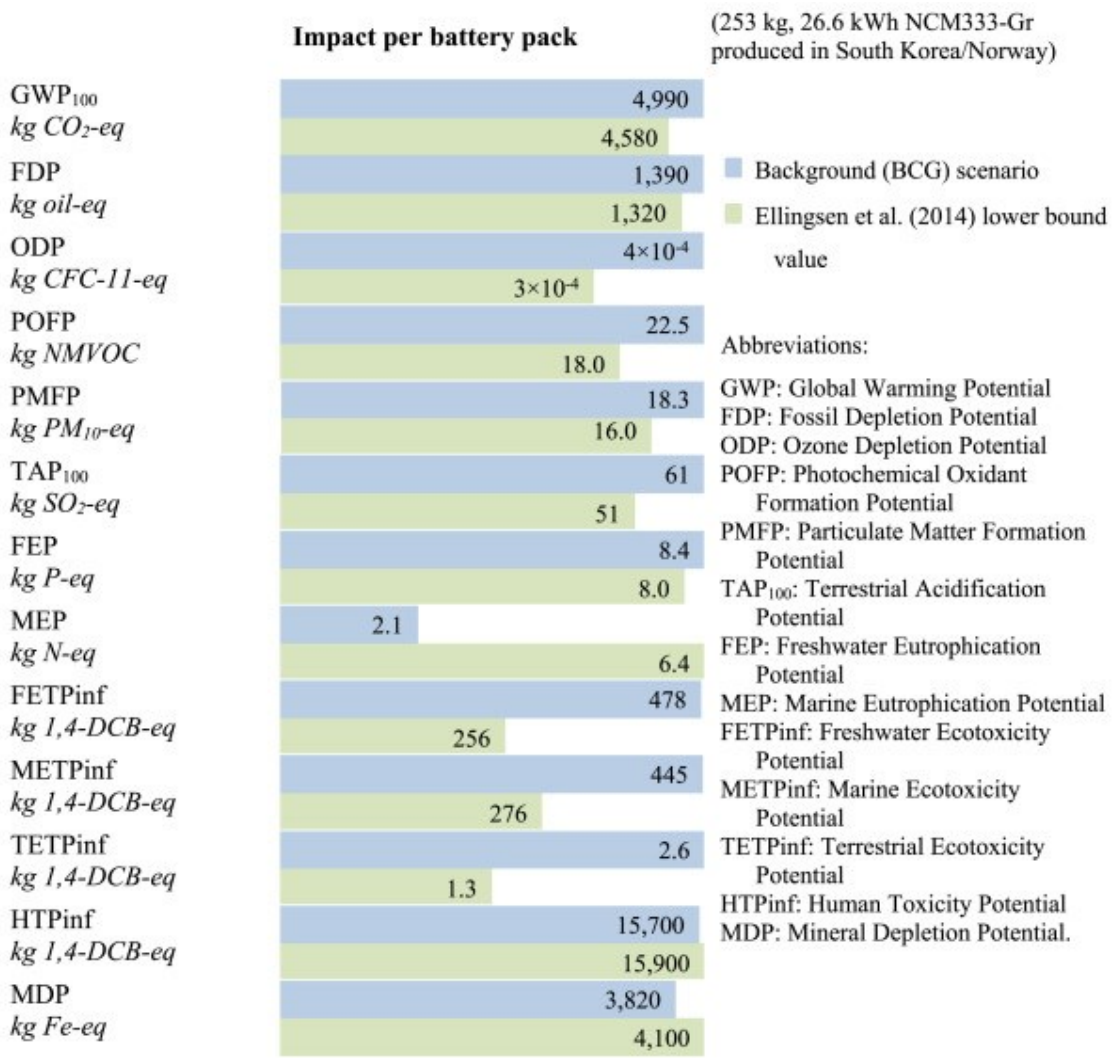


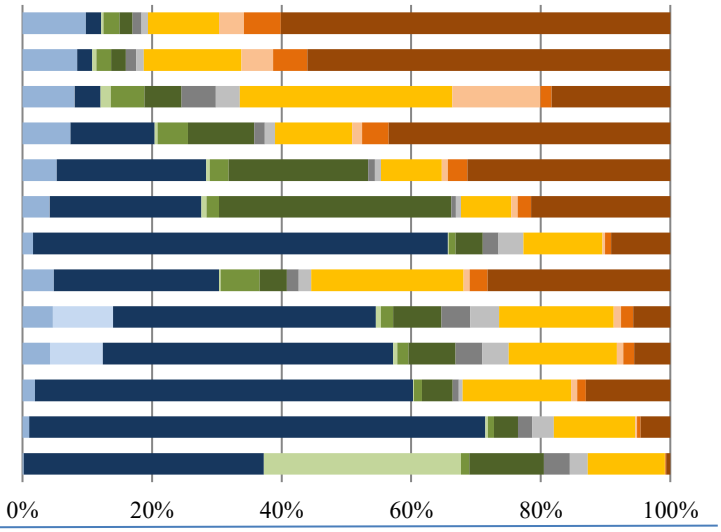
Figure 24. Comparison between the calculated impacts of the BCG scenario to Ellingsen et al. (2014) based on the ReCiPe 1.08 Midpoint characterisation method (Kallitsis et al., 2020).

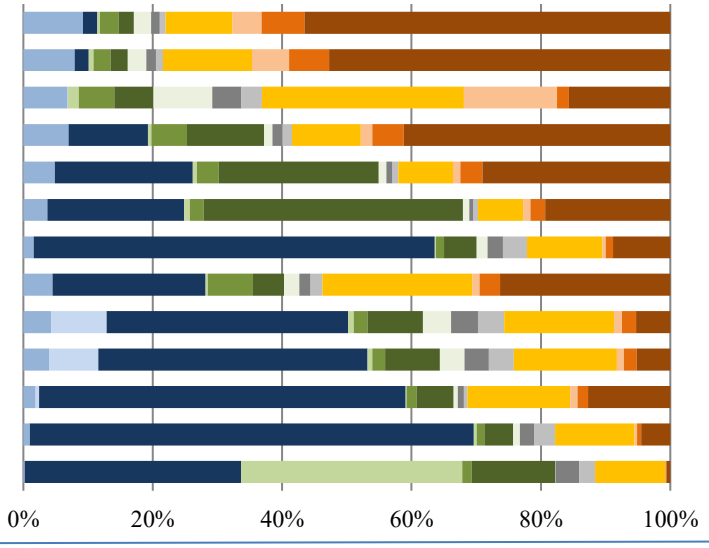
4.3.2 Contribution analysis

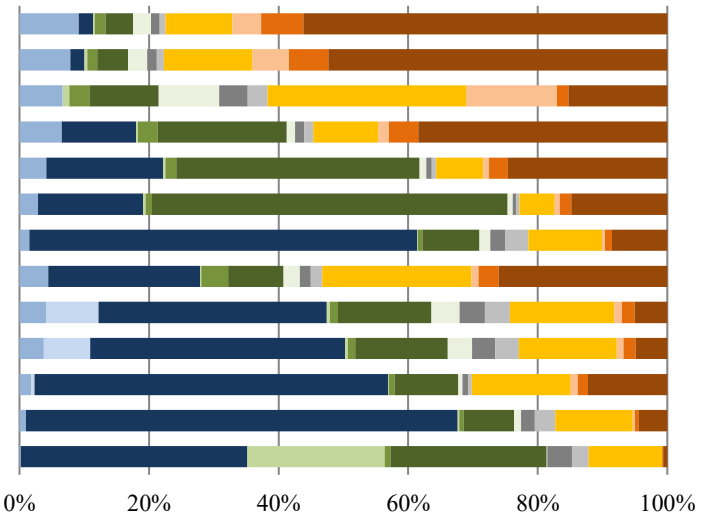
The most important contributions to each impact category for the four battery chemistry scenarios corresponding to China are shown in **Figure 25**. The GWP was dominated by the electrical energy used for cell manufacturing with the next highest contribution coming from primary aluminium production for all scenarios. The contribution analysis was very similar for the FDP. Therefore, the high increase of 40% in GWP when moving cell production to China obviously was connected to the high coal intensity of the local electrical power production and the local energy-intensive aluminium production. The TAP was dominated by nickel sulphate production, so it was predicted to increase gradually on increasing nickel concentrations in LIB cathodes.

More than half of the FEP arose from primary copper production for anode current collectors and increased slightly across the different scenarios as a result of increased nickel content in cathodes, contributing up to 11%. The electrical energy for cell manufacturing and heat provided for co-precipitation were the most significant contributions to the ODP across all scenarios. Copper production exhibited the most significant contribution across all ecotoxicity categories (FETP, METP, TETP) with less significant impacts occurring from electrical power and nickel sulphate production. The latter caused a gradual increase in the overall impact of the nickel-rich chemistries across all ecotoxicity categories. The significantly high HTP was dominated by copper production and increased slightly when introducing silicon-based anodes or increasing the nickel content of cathodes. Small variations were predicted in MEP across all scenarios, with electrical power and copper production contributing as much as 27% and 25%, respectively.

Impact of Production		Functional Unit: Battery pack	Functional Unit: Capacity [kW h]	Contribution Analysis
BSL Scenario				
GWP	*kg CO_2-eq*	6,980	262.4	
FDP	*kg oil-eq*	1,660	62.4	
ODP	*kg CFC-11-eq*	1.75 10^{-4}	6.58 10^{-6}	
POFP	*kg NMVOC*	31.8	1.20	
PMFP	*kg PM10-eq*	29.8	1.12	
TAP	*kg SO2-eq*	83	3.1	
FEP	*kg P-eq*	9	0.34	
MEP	*kg N-eq*	2.35	8.83 10^{-2}	
FETP	*kg 1,4-DCB-eq*	481.0	18.1	
METP	*kg 1,4-DCB-eq*	457.0	17.2	
TETP	*kg 1,4-DCB-eq*	3	0.129	
HTP	*kg 1,4-DCB-eq*	18,600	699.2	
MDP	*kg Fe-eq*	3,970	149.2	
NMC333-SiGr				
GWP	*kg CO_2-eq*	7,350	179.7	
FDP	*kg oil-eq*	1,740	42.5	
ODP	*kg CFC-11-eq*	2.03 10^{-4}	4.96 10^{-6}	
POFP	*kg NMVOC*	33.2	0.81	
PMFP	*kg PM10-eq*	31.8	0.78	
TAP	*kg SO2-eq*	91.0	2.2	
FEP	*kg P-eq*	9.18	0.22	
MEP	*kg N-eq*	2.50	6.11 10^{-2}	
FETP	*kg 1,4-DCB-eq*	515	12.6	
METP	*kg 1,4-DCB-eq*	485	11.9	
TETP	*kg 1,4-DCB-eq*	3.48	8.51 10^{-2}	
HTP	*kg 1,4-DCB-eq*	18,800	459.7	
MDP	*kg Fe-eq*	4,330	105.9	
NMC622-SiGr				
GWP	*kg CO_2-eq*	7,400	160.2	
FDP	*kg oil-eq*	1,760	38.1	
ODP	*kg CFC-11-eq*	2.08 10^{-4}	4.5 10^{-6}	
POFP	*kg NMVOC*	35.6	0.77	
PMFP	*kg PM10-eq*	37.5	0.81	
TAP	*kg SO2-eq*	119	2.6	
FEP	*kg P-eq*	9.50	0.21	
MEP	*kg N-eq*	2.52	5.45 10^{-2}	
FETP	*kg 1,4-DCB-eq*	545	11.8	
METP	*kg 1,4-DCB-eq*	513	11.1	
TETP	*kg 1,4-DCB-eq*	3.61	7.81 10^{-2}	
HTP	*kg 1,4-DCB-eq*	19,400	419.9	
MDP	*kg Fe-eq*	4,150	89.8	







NMC811-SiGr			
GWP	*kg CO_2-eq*	7420	140.3
FDP	*kg oil-eq*	1770	33.5
ODP	*kg CFC-11-eq*	$2.12\ 10^{-4}$	$4.01\ 10^{-6}$
POFP	*kg NMVOC*	37.1	0.70
PMFP	*kg PM10-eq*	41.2	0.78
TAP	*kg SO2-eq*	137	2.6
FEP	*kg P-eq*	9.72	0.18
MEP	*kg N-eq*	2.53	$4.78\ 10^{-2}$
FETP	*kg 1,4-DCB-eq*	566	10.7
METP	*kg 1,4-DCB-eq*	533	10.1
TETP	*kg 1,4-DCB-eq*	3.70	$6.99\ 10^{-2}$
HTP	*kg 1,4-DCB-eq*	19,700	372.4
MDP	*kg Fe-eq*	3,960	74.9

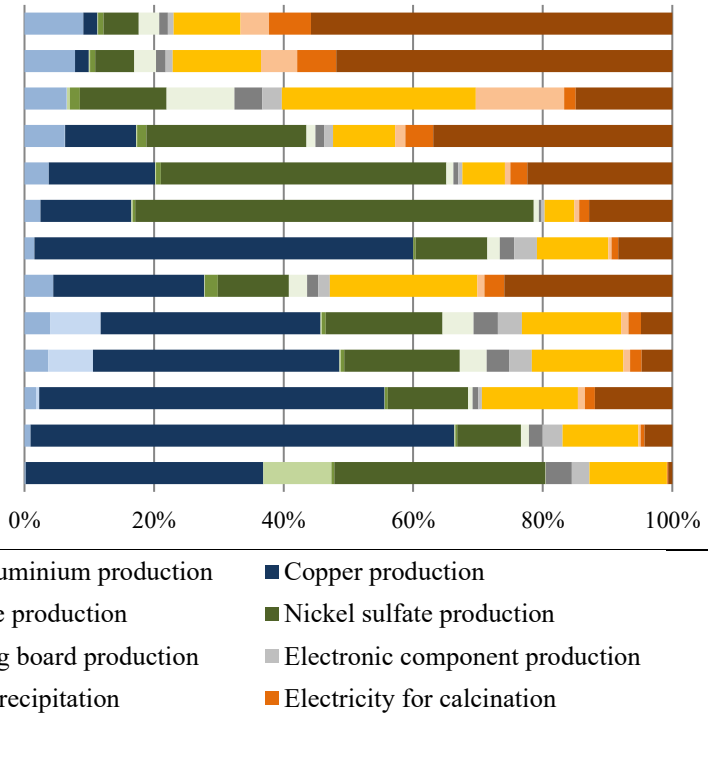


Figure 25. Cradle-to-gate impacts of battery production in China, reported quantitatively for different functional units and disaggregated to key background processes. The Baseline (BSL) scenario reflects the production of a 26.6 kW h NMC333-Gr and is comparable directly with literature studies. The nominal capacities of NMC333-SiGr, NMC622-SiGr and NMC811-SiGr were 40.9, 46.2 and 52.9 kW h respectively. Copper is used for the cathode current collector, cell container and packaging. Aluminium is used for the anode current collector, cell container and packaging; electricity for cell manufacturing; manganese and nickel for the cathode active material; silicon for the anode active material; printed wiring board and electronic component for the Battery Management System (Kallitsis et al., 2020).

4.4 Discussion

4.4.1 Chinese LIB manufacturing inventories

The results reported above show that most of the environmental impacts occurring in the LIB battery cell manufacturing chain in China occur from copper and aluminium used in the current collectors and the materials used in the electrodes; nickel, manganese and silicon. Hence, our

inventory data were compared to those of (Yin et al., 2019). Lithium products, namely lithium hexafluorophosphate and lithium carbonate, are used in the electrolyte and in the cathode active material respectively. Here, electrolyte production, geographically concentrated in China, was modelled using Ecoinvent 3.5 inventory while the Li_2CO_3 was modelled using a global market average. The inventory for lithium hexafluorophosphate production used by Yin et al. (2019) was also based on the Ecoinvent database, while the authors reported an industrial inventory for lithium carbonate. As lithium production is not geographically concentrated to China, combined with lithium products not being included in the main environmental impact contributions, the global average provides a satisfactory representation of lithium production in China. The cathode materials nickel and manganese are modelled based on global averages, while Yin et al. (2019) used the same inventory for nickel, but did not provide any inventory reference for manganese. As future technologies are expected to have an increased nickel content, which increases the impact intensity as shown above, a location-specific nickel production inventory for China is crucial. Also, the production of cobalt is modelled based on proxies in both studies, which fail to capture the toxicity impacts of cobalt mining in the respective local regions. A better description of the cobalt production process is necessary and is expected to further increase the reported HTP. Yin et al. (2019) also provided a foreground process inventory for the production of artificial graphite used in LIB anodes, whereas the production of battery grade graphite in China is modelled here using the respective Ecoinvent inventory. The primary difference of this study with Yin et al. (2019) lies on the exclusive use of the Ecoinvent database, leading to increased ease of reproducibility. Yin et al. (2019) were able to allocate more background production processes to China by utilising information from the CALCD (Liu et al., 2010). Also, we provided holistic inventory for the assessment of the environmental impacts of LIB manufacturing in China, while Yin et al. (2019) focused specifically on battery cell materials.

4.4.2 Breakdown and analysis

One of the most transparent life cycle inventories for the production of traction LIBs has been updated based on the latest version of Ecoinvent 3.5, which is improved by representing more accurately the production of critical cathode materials, e.g. nickel, manganese and is directly compared to its parent inventory. The results for most of the impact categories are in a good agreement with those of Ellingsen et al. (2014), with only couple impact categories diverging, namely MEP, which was a third of that reported by Ellingsen et al. (2014); and the ecotoxicity

categories, which was 40% to 50% higher. The large variation of MEP was attributed to NMP production accounting for 75% of the total MEP impact reported by Ellingsen et al. (2014). An insignificant impact is reported for NMP production as it is assumed that the solvent will be recycled, which reflects the current industrial practice as reported by Dai et al. (2019a). The increase in the ecotoxicity categories was attributed primarily to updates concerning the data and way of modelling of copper production in Ecoinvent, as compared to the previous version. More specifically, Ellingsen et al. (2014) used a global average to reflect the production of primary copper, while in this study's BCG scenario, Latin American production conditions were used in the absence of a global dataset. The development of the BCG scenario provided (a) an up-to-date inventory for the production of LIBs in South Korea/Norway and (b) means for comparing the inter-country impacts of LIB manufacturing based on the same model and assumptions.

The BSL scenario's GWP impact for producing a NMC333-Gr battery in China are comparable directly with those of preceding studies on NMC batteries as shown in **Table 4**. The reported GWP of 262.4 kg CO_2-eq (battery kW h)$^{-1}$ was significantly higher than those of Hao et al. (2017) and Yu et al. (2018) focusing on LIB production in China, but reasonable when compared to studies focusing on regions with less coal-intensive electrical energy mix (Amarakoon et al., 2013; Ellingsen et al., 2014; Kim et al., 2016; Majeau-Bettez et al., 2011), who report GWPs of 120 to 200 kg CO_2-eq (battery kW h)$^{-1}$. Also, when compared to the results of Yin et al. (2019) who calculated the GWP of materials, excluding the energy demand for manufacturing as 108 kg CO_2-eq (battery kW h)$^{-1}$, the calculated GWP for the BSL scenario in this work, excluding the carbon footprint of electrical energy for cell manufacturing as 105 kg CO_2-eq (battery kW h)$^{-1}$, is consistent. Hao et al. (2017a) reported a GWP of 100 kg CO_2-eq (battery kW h)$^{-1}$ for the materials used in the battery, so the primary difference with this study lays on the energy requirement for cell manufacturing. In Hao et al. (2017a) it is unclear whether dry room conditioning is considered. The same group has published a more general study on EVs in China which reports a very similar footprint for the battery manufacturing chain (Qiao et al., 2019). It is considered that the approach followed in this work, using Ellingsen's et al (2014) energy requirement and adjusting the electricity production footprint to China is more reliable and also reports a complete set of 13 impact categories. Yu et al. (2018) report a significantly lower impact for battery manufacturing of 53 kg CO_2-eq (battery kW h)$^{-1}$, which is considered an underestimation, as they base their manufacturing inventory on that of Zackrisson et al. (2010), which referred to a completely different battery technology

for hybrid electric vehicles. The significantly low value of 20 kg CO_2-eq (battery kW h)$^{-1}$ reported by Xiong et al. (2019) is primarily attributed to the direct use of the results of Peters et al. (2018) without making any modification to account for the local industry average values in China and to the significantly high battery capacity (60.5 kW h) of the studied EV, compared to preceding studies.

The impact of LIB production in China was calculated based on the same model to lead to a 40% increase in GWP when compared to the production conditions used by Ellingsen et al. (2014). Impacts across the remaining categories were increased, except from ODP which decreased by 46%. The ODP was halved as a result of the decreased share of natural gas and nuclear power in the electrical energy mix, when compared to the BCG scenario. As China is the dominant producer of LIBs, the impact of the Chinese LIBs production on the climate has been underestimated in the literature so far.

Introducing silicon into the anode is attractive from an environmental perspective, as the results for all the impact categories increase by less than 16% compared to the baseline. The 54% increase in the energy storage capacity of the battery, caused significant reductions of 29% to 34% in all impact categories when compared on a kW h basis. The scenario was similar for the high nickel content chemistries (NMC622-SiGr, NMC811-SiGr) where the TAP increased gradually with increased nickel concentrations in cathodes and improvements in storage capacity caused a decrease on the rest of the impacts on a per kW h basis.

This model is subject to certain assumptions concerning novel battery chemistries and the production of raw materials. First, it is unclear which components of the battery will scale as a function of the energy storage capacity. In this analysis the battery cell production is modified in each case based on electrochemical calculations, but the masses of the other battery components (BMS, Cooling system, Packaging) were kept constant. Whilst this may be an oversimplification, based on results from the literature and from this study, the majority of environmental burdens come from the manufacturing of battery cells, which was modelled accurately. Undisputedly, a larger cooling system will be needed for a larger battery capacity, but this is not likely to lead to significant variations in the impact estimates, partially due to the relatively low share (less than 4%) of the cooling system within the overall battery mass. Also, the amount of energy required for manufacturing the battery cells is uncertain. This is closely connected with the fact that this model assumes that manufacturing technologies would not change significantly for the production of novel electrode chemistries. It is noted, however,

that new production processes, such as dry electrode coating, might emerge at scale and could then come with a different energy demand profile. We disaggregated the environmental impacts showing the contribution of energy required for cell manufacturing and acknowledge that different assumptions in this respect could significantly alter the final results.

4.4.3 Future perspectives

As NMC technology is gaining increased market share in the Chinese LIB manufacturing market, an accurate quantification of the environmental impacts of LIB production is important in assessing the environmental implications of electric mobility. The inventories and environmental impact quantifications of this study for current and novel NMC batteries could provide an accurate estimation of the battery production impacts in studies focusing on electric vehicles in China and be used for future assessments on the production impacts of next-generation LIBs manufacturing in concert with projections on the electricity mix. The environmental burdens of novel LIBs manufacturing were predicted to decrease by at least 25% on a kW h basis due to increased storage capacities. However, as the initial lifespan of novel electrode batteries might be significantly lower than those already commercialised, it is questionable if the implementation of newly emerging electrodes will lead to reduced impact intensity over the whole cycle life.

Presently, the lack of real-life data, combined with complex degradation mechanisms, prevent the accurate prognosis of the battery lifetime of novel-electrode chemistries. On a per battery pack basis, increasing the nickel content caused an increase of the impact intensity of the production phase. As increased nickel content is favourable from a cost perspective, the compromise between cost and environmental performance should be investigated. For all scenarios, lithium products had a less than 5% contribution towards all impact categories. As lithium resources are not expected to be limiting (Grosjean et al., 2012), the low contribution of lithium products to the overall environmental burden of LIBs and the difficulty of recovering lithium, the environmental benefit of recycling lithium should be examined carefully.

4.5 Conclusions

An up-to-date, fully reproducible inventory for the production of lithium-ion batteries in China was constructed and the environmental impacts of novel electrode chemistries were compared to those of commercialised NMC technology under the same model and assumptions. In a LIBs manufacturing world dominated by China, the GWP of producing a lithium-ion battery is 40% higher than estimated previously in the literature (Ellingsen et al., 2014). Additionally, the production of next generation batteries will not lead to significant increases in GWP, which, therefore, is expected to decrease as a result of increased production and economies of scale. The production of copper for the current collector is the most important contribution towards all human toxicity and ecotoxicity categories with the next most important contribution coming from nickel sulphate production. It was shown that decreases in the impact-intensity of LIBs production will occur mainly from the increased capacities resulting from novel electrode chemistries. A quantification of the environmental impacts of the production of batteries with novel electrode chemistries was performed, offering robust means of decision making that complement scientific and engineering developments, aiming to decrease costs and increase LIB performance.

Chapter 5 Reducing the GHG intensity of battery manufacturing

After discussing the development of the LIB LCA model in Chapter 4, this Chapter looks at the energy use and associated GHG emissions of battery cell production. This is a key topic of research, as the energy use for cell production has been identified as a dominant contribution to the cradle-to-gate environmental footprint of automotive LIBs. Here, published data on the energy use of battery Gigafactories are meta-analysed and filtering criteria are suggested based on energy density and production scale. Additionally, energy use numbers for Giga-scale battery manufacturing facilities characteristics are used as input to the LIB LCA model, presented in Chapter 4, to estimate the environmental benefit of upscaling battery manufacturing operations. The Chapter ends with proposing a series of measures that would lead to reduced GHG intensities for battery cell manufacturing. Results presented in this Chapter form part of Kallitsis (2022), which was recently published in the Journal of Cleaner Production, and original research performed in the framework of the White Paper "Safe and sustainable lithium-ion batteries" (Kallitsis et al., 2022b). This Chapter utilises the LIB LCA model developed in Chapter 4, therefore, methods are not repeated.

5.1 Background and motivation

In recent years, a series LCA studies on LIB production have been published as shown in **Table 1** and discussed in Section 3.3. Recent studies from Degen & Schütte (2022) and Jinasena et al. (2021) have provided interesting insights on the energy use of Giga-scale automotive LIB cell production and the associated GHG emissions. This is a key topic of research, as the energy use for cell production has been identified as a dominant contribution to the cradle-to-gate environmental footprint of automotive LIBs. Due to varying and diverging data, the landscape

regarding the energy use of battery Gigafactories should be further clarified as it provides an important resource for LCA studies accounting for the production of LIBs used in electric vehicles. Additionally, the effect of upscaling LIB manufacturing to the cradle-to-gate GHG footprint of LIBs should be quantified, together with other measures such as sourcing less GHG intensive materials and increasing the energy density of battery cells.

5.1.1 Critical literature review

Degen & Schütte (2022) employ a gate-to-gate scheme in their study, from the point of active material mixing to end-of-line tests for automotive LIB cells; similar system boundaries were applied in Jinasena et al. (2021). While this allows the authors to provide sufficient detail on the energy consumption of machinery used in LIB manufacturing which provides a great resource for the community, it omitts a series of energy demanding processes included in the cradle-to-gate LIB production system. Specifically, Dai et al. (2019a) reported that producing the cathode active material consumes more energy than the cell manufacturing process itself. Their study reported that producing a 23.5 kW h, 165 kg LIB pack consumes 54 kW h_{energy} (kW h_{pack})$^{-1}$ for the cathode material preparation compared to 47.2 kW h_{energy} (kW h_{pack})$^{-1}$ for the cell manufacturing process. The cathode material preparation stage was also found to be a significant contributor to the cradle-to-gate energy use for LIB production in the studies of Kallitsis et al. (2020) and Sun et al. (2020). As modern day battery Gigafactories tend to integrate the active material preparation process with cell manufacturing and battery pack assembly (Kurland, 2019), it should be made clear to the reader that the gate-to-gate energy demand for cell production is only a fraction of the overall energy demand of a battery Gigafactory. Therefore, specifying accurately the system and the sub-systems that make up the production chain is important in order to avoid confusion, and requires listing of all the processes included in the system boundary, especially as active material preparation tends to get vertically integrated with battery cell production and battery pack assembly.

5.1.2 Pack vs cell level

Misinterpretations of pack level results as cell level and vice versa have led to confusion regarding the energy demand of battery Gigafactories. For example, in figure 9 of their original study, which summarises the energy consumption and associated greenhouse-gas emissions of battery cell production, Degen & Schütte (2022) include an energy consumption of 60.05 kW h_{energy} (kW h_{cell})$^{-1}$ for the study of Dai et al. (2019a). However, Dai et al. (2019a) explicitly

stated that the total energy requirement for cell manufacturing was 170 MJ (kW h_{cell})$^{-1}$ (47.2 kW h_{energy} (kW h_{cell})$^{-1}$; this was confirmed in the study of Jinasena et al. (2021). A possible pathway to miscalculation of this number comes from converting the energy consumption from a kW h basis to mass of battery and vice versa. While a kW h of pack capacity is the same as a kW h of cell capacity, the same can not be said on a mass basis as cells typically make up 60 % to 80 % of the battery pack's mass. For example, the 47.2 kW h_{energy} (kW h_{cell})$^{-1}$ reported by Dai et al. (2019a) would be converted to 9.3 kW h_{energy} (kg_{cell})$^{-1}$, accounting for their cell energy density of 0.197 kW h kg^{-1}. Calculating back to mass basis using their pack energy density (0.143 kW h kg^{-1}) results in an energy consumption of 65 kW h_{energy} (kW h_{cell})$^{-1}$ which is close to what Degen & Schütte (2022) reported. This is not the first time that the conversion of cell level numbers to pack level leads to miscalculations. In a letter to Dunn et al. (2015), Ellingsen et al. (2015) explained how the authors of the former study miscalculated the reported energy requirement of Ellingsen et al. (2014) by simply not accounting for the fact that battery cells make up 60 % of the total battery pack mass. For the sake of completeness, **Table 7** reports cell energy requirement numbers on both a kW h_{cell} and kg_{cell} across Giga-scale battery production studies, together with relevant parameters. The latter might be a more physically correct metric to include in battery LCA studies as bottom-up energy consumption studies produce their results based on material flows (Degen and Schütte, 2022; Jinasena et al., 2021) which then get converted to kW h basis based on the energy density. Also, life cycle inventories in LCA are commonly developed based on mass flows and reporting energy consumption data on a mass basis can avoid the miscalculation issues discussed above.

Whether studies focus on pack or cell level can also have a small but noticeable effect on the reported energy consumption. For example, Dai et al's. (2019a) reported energy requirement is focused solely on cell level, similarly to Jinasena et al. (2021) and Degen & Schütte (2022), while Sun et al. (2020) included the energy requirement for module and pack assembly, similarly to Ellingsen et al. (2014). However, the latter studies have shown that energy requirement for module and pack assembly is quite low.

5.1.3 GHG footprint of battery materials and the effect of energy density

Aluminium and copper are used in increased amounts in the battery pack's supporting structures and the current collectors. The former has been identified as the material with the greatest contribution to the battery pack's GHG footprint (Kallitsis et al., 2020), while producing the latter from sulfide ores includes a series of energy intensive processes such as

smelting, converting, fire- and electrolytic refining. Additionally, producing cathode materials in the form of $NiSO_4$, $MnSO_4$ and $CoSO_4$ includes a series of energy intensive processes, as discussed in Section 2.4.1. Such materials can be sourced from a series of locations, with production processes varying significantly, leading to fundamentally different GHG production footprints; the effect of materials sourcing to the overall GHG footprint of the battery pack remains to be understood.

As reported in Chapter 4, energy density plays an important role in determining the cradle-to-gate environmental footprint of LIBs, as a smaller amount of materials is used to produce a kW h of energy storage capacity in more dense batteries. As NMC batteries shift to higher nickel variations such as NMC622 and NMC811, significant energy density improvements are achieved. Additionally, mixing silicon in graphitic anodes is the most promising measure to increase the energy density. Here, an effort is made to quantify the combined effect of upscaling LIB manufacturing, sourcing low carbon materials and increasing energy density to the cradle-to-gate GHG footprint of LIBs.

5.2 Results and analysis

5.2.1 Meta-analysing literature data on the energy use of battery Gigafactories

Dunn et al. (2015), initiated the discussion on the role of facility scale in the overall energy consumption for cell manufacturing. Since then, the literature tends to agree that battery plants on the MW h scale exhibit a larger energy intensity compared to Gigafactories (Dai et al., 2019a; Kurland, 2019). Also, efforts to increase the energy density by altering the underlying electrode materials have been demonstrated to result in a net cradle-to-gate environmental benefit as simply less material is used to produce a kW h of battery storage capacity (Kallitsis et al., 2022b; Mohr et al., 2020). Therefore, studies aiming to explore the energy intensity of Giga-scale battery cell manufacturing should filter out studies that refer to MW h scale plants (Ellingsen et al., 2014; Kallitsis et al., 2020; Majeau-Bettez et al., 2011) and apply filtering criteria regarding similar battery chemistry types, focusing for example on NMC LIBs, which are particularly relevant for automotive applications (Lander et al., 2021b; World Economic Forum, 2019), and exclude studies that refer to batteries with significantly lower energy densities (Cusenza et al., 2019; Marques et al., 2019; Notter et al., 2010). **Table 7** is constructed

by applying those filters, reporting only studies that focus on NMC batteries with comparable energy densities and produced on the GW h scale.

Table 7. Reported energy use for cell production across studies focusing on NMC batteries produced in the Giga-scale (Kallitsis, 2022).

Study	**Battery chemistry**	**Cell energy density** [kW h kg^{-1}]	**Production scale** [GW h a^{-1}]	**Energy use of cell production** [kW h (kW h$_{cell}$)$^{-1}$]	[kW h (kg$_{cell}$)$^{-1}$]
Dai et al. (2019)	NMC333-Gr	0.197	2	47.2	9.3
Kurland (2019)[a]	NMC622-Gr	0.210[b]	8	50	10.5
Sun et al. (2020)	NMC622-Gr	0.180	30	30.6[d]	5.5
Jinasena et al. (2021)	NMC333-Gr	0.215[c]	2	45	9.7
Degen & Schütte (2022)	NMC622-Gr	0.210[b]	7	41.5	8.7

[a]Value for Northvolt Ett, [b]Energy density not disclosed directly, representative values for NMC622-Gr cyclindrical cells are included (Ciez and Whitacre, 2019),[c]Not disclosed directly, based on the fact that authors convert 44.6 W h (W h$_{cell}$)$^{-1}$ to 34.5 MJ (kg$_{cell}$)$^{-1}$,[d]includes 1 kW h for module and pack assembly

By inspecting **Table 7**, it immediately becomes evident that reported energy use for cell manufacturing falls within reasonable proximity in studies focusing on NMC batteries produced in Gigafactories. Specifically, estimates lie in the range of 30-50 kW h (kW h$_{cell}$)$^{-1}$ which indicates a significant convergence compared to the range of 83-700 kW h (kW h$_{cell}$)$^{-1}$ reported by Peters et al. (2016) a few years ago, accounting for different production scales and battery chemistries. Also, Kurland (2019) reported a range of 50-65 kW h (kW h$_{cell}$)$^{-1}$ but the upper limit of their study corresponded to energy consumption estimates for the Tesla Gigafactory I, which mainly produces NCA batteries. Indeed, varying process parameters, which Degen & Schütte (2022) and Jinasena et al. (2021) have covered in sufficient detail, and facility scale can cause different energy intensity profiles, even for the production of the same battery chemistry (Dunn et al., 2015). However, these differences are significantly smaller when employing the filtering criteria discussed herein. These issues have been discussed by a series of recent literature studies (Dai et al., 2019a; Kallitsis et al., 2020; Kurland, 2019) and cover LIBs utilising an NMC622 or NMC333 cathode combined with an anode made of

graphite (Gr). Also, Dunn et al. (2015) observed that in the past, employing a bottom-up approach versus collecting real-world energy consumption data resulted in very different energy intensities for battery cell manufacturing. However, as evident from **Table 6**, bottom-up studies (Degen and Schütte, 2022; Jinasena et al., 2021) now tend to converge with real-world energy consumption studies (Dai et al., 2019a; Sun et al., 2020), with the former providing an important resource to account for different production techniques and location-specific parameters when modelling the cradle-to-gate footprint of LIBs.

5.2.2 Reducing the cradle-to-gate carbon footprint of LIBs

As discussed in the previous section, the energy use of battery manufacturing plants has been reduced, mainly due to increased scale of production facilities. Here, the possible reductions to the cradle-to-gate Carbon Footprint (CF) of LIBs is quantified, together with other measures such as renewable energy integration, sourcing less carbon-intensive materials and increasing the energy density of battery cells. The calculations are based on the LIB production LCA model discussed in Chapter 4 and the main results are illustrated in **Figure 26**.

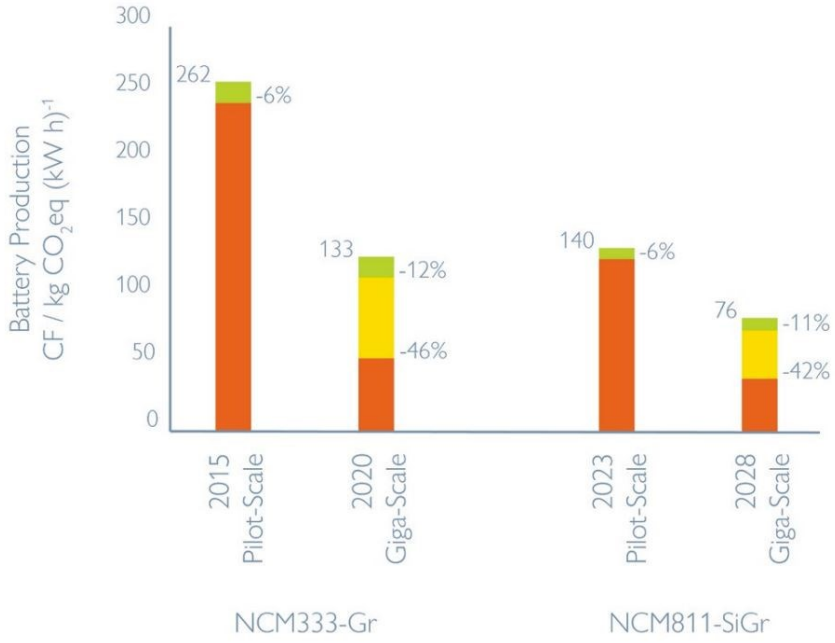


Figure 26. Battery production Carbon Footprint (CF) in kg CO_2 eq $(kW\ h)^{-1}$ predicted for NMC333-Gr and NMC811-SiGr, and pilot-/Gigascale. Green indicates CF reduction from European Al use; yellow indicates CF reduction from hydroelectric power use. Reference years are based on the battery commercialisation projections of the IEA (Kallitsis et al., 2022b).

Under baseline assumptions, a NMC333-Gr battery produced in China has a CF of 262 kg CO_2 eq $(kW\ h)^{-1}$, which is reduced to 246 kg CO_2 eq $(kW\ h)^{-1}$ when shifting the aluminium source from China to Europe. For Giga-scale battery manufacturing, reducing the energy requirement by 70% compared to pilot scale plants, to 47.2 kW h $(kW\ h_{cell})^{-1}$ based on the numbers reported by Dai et al. (2019), reduces the battery production footprint to 133 kg CO_2 eq $(kW\ h)^{-1}$, almost half of what is predicted for pilot-scale plants. Supplying the production chain with European aluminium further decreases the CF to 116 kg CO_2 eq $(kW\ h)^{-1}$, which is reduced to 64 kg CO_2 eq $(kW\ h)^{-1}$ when the battery Gigafactory's energy demand is fulfilled by hydroelectric power.

The scenario is similar for NMC811-SiGr chemistries, for which the pilot-scale footprint is estimated as 140 kg CO_2 eq $(kW\ h)^{-1}$, being further reduced to 67 and 39 kg CO_2 eq $(kW\ h)^{-1}$ for the Eruopean aluminium and hydroelectric power scenarios, respectively. Such magnitude of reductions compared to the NMC333-Gr chemistry are primarily attributed to the fact that energy density of the battery cells is doubled when shifting to high nickel chemistries utilising SiGr anodes. The results demonstrate that accounting for the increased scale of battery manufacturing, technological developments aiming at increased energy density and the possible transformation of the supply chain, reduces the cradle-to-gate CF of LIBs by 85%, from 262 kg CO_2 eq $(kW\ h)^{-1}$ in 2015 to 39 kg CO_2 eq $(kW\ h)^{-1}$ in 2028.

5.3 Discussion

The results of this chapter are combined with preceding literature studies in order to provide guidelines for minimising the environmental impact of battery production, which is a predominant industry goal in line with the urgent need for decarbonisation. As the LIB value chain is globally distributed, stakeholders seek ways to reduce their footprints. The most effective ways are discussed below.

Aluminium is a LIB constituent with a significant carbon footprint, which varies highly depending on the location. Specifically, North American and European aluminium production is powered by significant amounts of hydroelectric power, which is not the case for Chinese primary production, accounting for approximately half of the global supply. Inputting European-produced Al, instead of Chinese may decrease the overall carbon footprint of a battery by ~30% (Kelly et al., 2019). The same holds true, in a lower magnitude, for other

battery materials, it is, therefore, up to the battery manufacturer to source raw materials with a lower carbon footprint in order to reduce that of their batteries.

An additional strategy for reducing the carbon footprint of LIBs is powering the cathode powder production and cell manufacturing processes with renewable energy. Tesla has been committed to the target of powering the energy-intensive cell production process with 100% renewable energy, but the cathode powder production remains a challenge as it is produced externally. Recently, Northvolt announced plans to integrate the cathode powder production in the cell manufacturing facility and utilise hydropower in order to produce batteries with minimal carbon footprint. Powering cathode powder production with hydroelectricity holds the potential to reduce its footprint by 40%, while performing cell assembly with hydroelectric power can reduce the total carbon footprint of the battery by 30% (Kelly et al., 2019). However, the use of hydropower is associated with increased water depletion and the ultimate goal should be battery production supplied with 100% renewable energy, excluding hydropower.

A critical quantity contributing to the environmental footprint of battery production is the energy consumed during the cell assembly stage. The primary contribution comes from the requirement to power the energy-intensive dry room, which consumes the same amount of energy regardless of the number of batteries produced in the plant (Dunn et al., 2015). Therefore, operating a battery plant at full capacity in the Giga-scale reduces the energy required for cell assembly to 30 to 50 kW h per kWh cell produced from 163 kW h per kWh (Ellingsen et al., 2014). These reductions are already taking place in the Giga-scale battery manufacturing facilities.

An indirect way of lowering the environmental footprint of a battery, as illustrated in **Figure 26**, is by increasing its energy density with modifications in the underlying chemistry. Specifically, blending the graphitic anode with silicon has been demonstrated to cause a 32% reduction in the battery's carbon footprint and supplementing that with an increased nickel-content cathode (NMC811) leads to GHG emission reductions of 47% (Kallitsis et al., 2020). These benefits are associated with the increased energy density of those chemistries and extend to other environmental impact categories, as a reduced amount of energy and materials is required to produce a kWh of battery pack capacity.

Two additional ways to further reduce the carbon footprint of batteries include extending their lifetime and using increased amounts of recycled materials. The former has a key role as the

battery production footprint is compensated by an extended use phase, while in the latter recycled materials are known to come with a lower environmental burden than primary ones. As such strategies are associated with the use phase and end-of-life, they are explored in detail in subsequent chapters of this thesis.

5.4 Conclusions

This Chapter aimed at clarifying the landscape regarding the energy use of battery Gigafactories and quantifying the possible GHG intensity reductions in battery manufacturing. A series of filtering criteria regarding production scale and battery chemistry were applied regarding the energy use of battery Gigafactories revealling a range of 30-50 kW h (kW h_{cell})$^{-1}$, which contributes toward more accurate quantifications of the cradle-to-gate environmental footprint of NMC LIBs. Also, bottm-up energy consumption studies were found to converge with real-world data which was not the case in the past. However, as the gate-to-gate energy footprint for battery cell production only consists a fraction of the cradle-to-gate energy demand, further reductions in the cradle-to-gate footprint of LIBs should come throught the utilisation of renewable energy together with sourcing low-carbon materials and increasing the energy density of LIBs. Such advancements were demonstrated to hold the potential to reduce the CF of battery manufacturing by 85% by 2030 compared to 2015 levels. To date, manufacturers have not directly disclosed their energy demand and GHG intensity for cell manufacturing and have primarily relied on third party efforts. This is expected to change with the Batteries Regulation of the European Commission, which will require all electric vehicle batteries placed on the market by 2023 to come with a disclosure of their environmental footprint (Mathieu, 2021).

Chapter 6 Cost and carbon footprint modelling for electric vehicles

In this chapter, the development of an LCA and LCC model for the use phase of LIBs in EVs is presented and results on their overall cost and carbon footprint are discussed. The contribution of critical parameters such as the electricity mix used to charge the vehicle, the battery production footprint and the lifetime of the installed battery are analysed and their contribution to the total environmental footprint and cost of an EV is explored. The LCA results are focused only the CF of an EV, as it is the determinant quantity in comparing transportation alternatives as discussed in Section 3.4. This Chapter's results were published in Applied Energy (Lander et al., 2021b) with a focus on estimating the battery lifetime occurring from different thermal management systems and in determining the lifetime costs and CF of EVs utilising those systems. The modelling and results presented in this chapter were generated by the author in close collaboration with Dr. Laura Lander, except from the sensitivity studies shown in Sections 6.4.2 and 6.4.3, which were performed by my co-authors and are included here for completeness.

6.1 Background and Motivation

Decarbonisation of the transport sector is one of the most important steps in achieving the CO_2 emission reduction targets set by the Paris agreement in 2015, with a paradigm shift from ICEVs to EVs being essential. However, high purchase costs of EVs, caused by the costly LIBs are still detrimental to their large scale market penetration. Furthermore, the dependence of the carbon footprint of EVs on power decarbonisation reduces the efficacy of carbon intensity reductions in some regions (Knobloch et al., 2020). It is therefore crucial to find cost-cutting solutions for battery systems (International Energy Agency, 2019), as well as to accurately

account for their life-cycle carbon footprint of their use in EVs (Larcher and Tarascon, 2015; Peters et al., 2016).

Recent LCA studies of LIBs range from the quantification of environmental impacts of battery production to holistic assessments of the cradle-to-grave environmental impacts as discussed in Sections 3.3 and 3.4. Similarly, life cycle costing studies have been conducted to obtain a detailed insight into the cost implications and economic benefits of battery production, use and recycling (Berckmans et al., 2017; Nykvist and Nilsson, 2015). LCC studies of various vehicle technologies such as ICEVs, EVs and hybrid EVs (Offer et al., 2011; Wu et al., 2015) present important region-specific insights and cost-benefit analyses (Kara et al., 2017; Wong et al., 2010). This is crucial for the implementation of financing strategies and policy regulations to accelerate EV adoption (Zakeri and Syri, 2015). The LCC of an EV has a strong dependence on the specifics of the use phase, such as the distance travelled over its lifetime, external conditions, fuel efficiency and energy prices and it is, thus, important to assess the technologies in the context of their deployment on a case-by-case basis.

The question of whether EVs offer environmental benefits compared to ICEVs has been a long-lasting debate in the literature (de Souza, Picirelli Lora, Electo Palcio, Jose Rocha, Mateus Reno, Maria Venturini, 2018; Hawkins et al., 2013; Hoekstra, 2019; Holland et al., 2015; Ma et al., 2017; Qiao et al., 2019; Wu et al., 2018; Yu et al., 2018). A strong variability exists amongst LCA studies of BEVs with Hawkins et al. (2013), Ma et al. (2017), de Souza et al. (2018), Qiao et al. (2019) finding EVs to offer carbon emission reductions compared to ICEVs, while Yu et al. (2018) report otherwise. The relative benefits of EVs have also been questioned in the popular press (Lomborg, 2013; Sinn, 2019). The fact that the latter holds true only when EVs are powered by coal-intensive electricity has been underlined in the literature (Dunn et al., 2015), which was further confirmed by a more recent study reporting that even if future end-use electrification is not matched by rapid power-sector decarbonisation, EVs can still offer emission reductions across almost all world regions compared to ICEVs (Knobloch et al., 2020). The carbon intensity of the electricity mix is not the only quantity determining the environmental footprint of an EV, with the energy consumption, battery production footprint and the vehicle/battery lifetime having also an important role as discussed in Section 3.4. The dominant way of benchmarking transportation alternatives is based on a functional unit of 1 kilometre driven by the vehicle. Overall, the lens has recently been shifted from whether EVs offer environmental benefits to accepting their environmental superiority and quantifying the possible emission savings associated with their wide market adoption.

In modelling the operational phase of an EV, battery utilisation models are developed, which account for the vehicle energy consumption, battery and vehicle production footprint, electricity sources, battery lifetime and maintenance (Hawkins et al., 2013). Most of these quantities are improving in line with the wider tendency for decarbonisation; the environmental footprint of battery production is declining, the battery production costs are being driven down, electricity production mixes include an increasing share of renewable energy and the energy consumption of EVs is continuously improved.

A critical parameter in reducing the overall environmental impacts and costs of LIBs is the battery lifetime, as pressures on resources and negative impacts of both manufacturing and recycling can be counterbalanced by increasing the number of cycles that a battery is used during its lifetime. However, most studies focusing on the environmental impacts of electric vehicles arbitrarily determine a battery lifetime (Peters et al., 2016), failing to capture the impact of cycling conditions on it. Recently, researchers have become more aware of the importance of cycling conditions and battery lifetime to the overall cost and carbon footprint of an EV, with Yang et al. (2018) reporting on an analytical model to predict the lifetime of LMO-graphite batteries in order to improve the accuracy of the assessment of greenhouse-gas emissions. Also, Marques et al (2019) performed a comparative LCA of LMO and LFP batteries, addressing capacity fade based on experimental data of Wang et al. (2014; 2011). A similar approach has been applied for LCCA calculations by Liu et al. (2019), who implemented a capacity fade model to take into account degradation-related economic losses of automotive battery cells.

The lifetime of LIBs depends on various stress factors such as depth-of-discharge (DOD), state-of-charge (SOC), cycling rate (C-rate), storing conditions and operating temperature (Birkl et al., 2017). It has been shown that the optimal operating temperature range for LIBs is 15-35 °C (Chen et al., 2016). Higher temperatures can lead to a rapid capacity fade caused by chemical side reactions, SEI growth on the anode and electrolyte decomposition, while lower temperatures result in lithium plating and a loss of lithium inventory. An efficient TMS is therefore crucial to keep the cell temperature in the desired range and to ensure optimal performance and safety of the battery. Currently deployed cooling strategies for battery packs in EVs include air cooling (AC) and indirect liquid cooling. The former uses an air flow to cool down the batteries, while the latter uses a liquid refrigerant, which is channelled through the battery pack to absorb the heat. Some advantages of AC include low cost and simple

implementation in a range of battery pack geometries. However, its ability to remove heat from the battery pack at a sufficient rate is worse than liquid cooling, with the latter being preferable in most EV packs. Indirect liquid cooling uses a complex system of flow channels which are complicated and expensive to build into the battery pack design (Chung and Kim, 2019). More recently, immersion cooling (IC) (Gils et al., 2014) and tab cooling (TC) (Hunt et al., 2016) systems, both sub-systems of liquid cooling, have attracted increased attention due to their high cooling efficiency (Wu et al., 2019; Xia et al., 2017).

In this part of the thesis, LCA and LCC models were developed in order to calculate the cost and carbon footprint of EVs under realistic lifetime calculations. Specifically, the impact of different TMS (AC, SC, IC, TC) on the battery cycling life and in consequence on the life cycle footprint and LCC of the battery pack utilised in an EV is determined. The significant contribution of this work to the current state of knowledge of LIB techno-economic and carbon footprint analysis is the demonstration that with engineering solutions, the economic and environmental benefits of LIB utilisation in EVs can improve significantly. Also, the direct link between battery pack design and life cycle cost and carbon footprint is bridged, which has been an open question in the literature. To do so, the battery capacity fade of an NMC333/Gr cell was modelled as a function of the maximum cell temperature for various TMS options. The cycling life was then implemented in the LCA and LCC models. This allows the 1) calculation of more accurate LCA and LCC results using a realistic battery lifetime and 2) the demonstration of the importance of an efficient TMS for cycling life, emissions and costs improvements. Moreover, an optimised cell design is presented, which enables the implementation of a more efficient tab cooling system and its impacts on the CF and LCC are discussed.

6.2 Methods

The modelling procedure to quantify the environmental and cost benefits of advanced TMS in LIBs is presented in **Figure 27** and is as follows: (i) LCA and LCC models are developed in order to quantify the carbon footprint and costs occurring throughout an EVs lifetime, the generalised equations together with the case specific inputs are presented in Section 6.2.1, (ii) the battery and TMS designs to be studied are clearly defined including all their operational

and geometrical parameters in Section 6.2.2, (iii) the four TMS systems taken into consideration, AC, SC, IC, TC, are associated to a specific maximum operating temperature in Section 6.2.3 and (iv) a capacity fade model is developed in order to associate the maximum cell operating temperature to the number of Full Equivalent Cycles (FECs) achieved by the battery before reaching its end-of-life criterion, which is presented in section 6.2.4. A detailed discussion on the systems and applied models of this work is presented below.

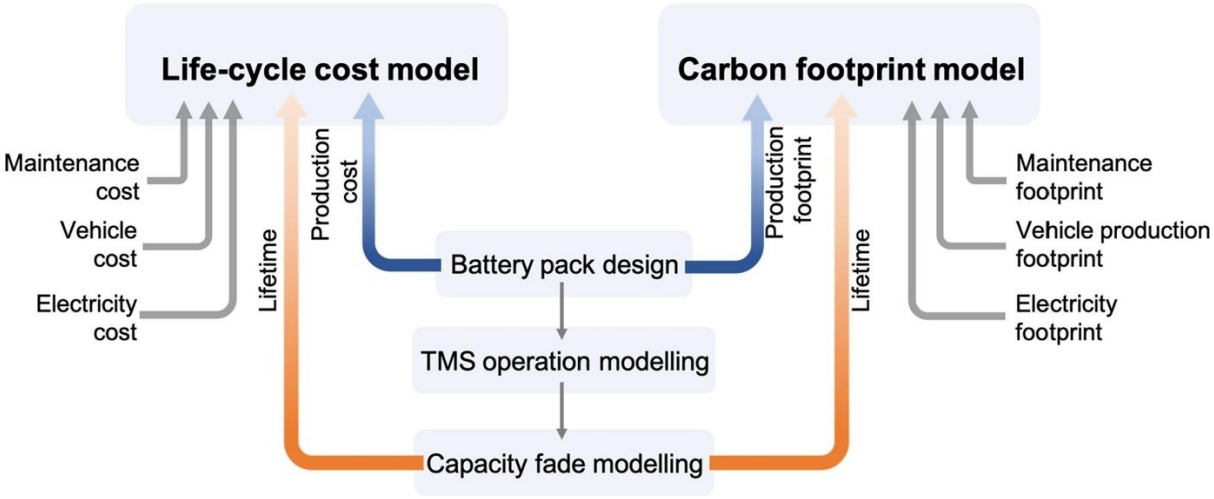


Figure 27. Methodological procedure for the life cycle cost and carbon footprint model applied in this study (Lander et al., 2021b).

6.2.1 Battery life cycle costs and emissions

The models were developed to calculate environmental impacts and costs for operating an electric vehicle by accounting for the battery, vehicle, electricity and maintenance costs and environmental impacts, which are representative of a compact sized EV. The functional unit was chosen as a km driven by the vehicle and the geographical boundary was set as global, as the battery production is performed in China while the EV is operated in the UK. The technology boundary was based on the current status for EVs and is representative of a compact vehicle utilising a NMC333-Gr battery chemistry. The system boundary for the components included in the vehicle, the vehicle body and the battery was set to cradle-to-gate, accounting for all the process steps included in the production of LIBs and the vehicle body. The system boundary for electricity was well-to-wheel, accounting for all the processes for delivering electricity to an EV, including production, transmission and charging. A particular focus was given to battery lifetime as it is an important quantity in the determination of the overall footprint of an EV. In this direction, the technology boundary was extended to include different cooling system options, which have a significant contribution to the lifetime of the battery. The

effects of the environmental emissions were assessed based on the ReCiPe 1.08 midpoint characterisation method, with a particular focus on the carbon footprint. The capital costs were calculated based on BatPac and literature data, while the cost to the consumer once ownership has been established was estimated through engineering calculations accounting for the energy required to power the electric vehicle and maintenance. All the inputs are representative for a compact size EV similar to Nissan Leaf and any recycling or end-of-life treatment was neglected.

Specifically, the lifetime costs associated to the EV production and use phase were calculated based on Eq. 6.1 for each battery/TMS system, which expresses the LCC in \$ km^{-1}. The LCC is calculated as a function of the battery pack cost (C_{bat}), the vehicle cost excluding the battery (C_{veh}) and the operational expenditures of supplying the vehicle with electricity throughout its lifetime (C_{elec}) and maintenance cost (C_{maint}), as shown in Eq. 6.1. C_{elec} is calculated as the total sum of the annual expenditure for supplying the vehicle with electricity ($C_{elec,n}$) over N_{veh} years of vehicle lifetime, which is discounted to present based on the discount factor (r), as shown in Eq. 6.2. The annual electricity cost is expressed in terms of the unit cost of a kW h of electricity ($C_{elec,kWh}$), the vehicle energy consumption (E_{veh}) and the average km distance driven by the vehicle per annum (d), as shown in Eq. 6.3. The years of vehicle lifetime are calculated as the fraction of the total distance driven by the vehicle (D_{km}) divided by the distance driven by the vehicle per annum, as shown in Eq. 6.4. D_{km} is assumed to be the same with the battery lifetime and is calculated in Eq. 6.5 based on the number of FECs delivered by the battery, the nominal energy storage capacity of the battery pack (NC_{bat}) and the vehicle energy consumption. Similarly to C_{elec}, C_{maint} is calculated as the discounted cash flow of the annual expenditure for maintaining a vehicle ($C_{maint,n}$) over N_{veh} years of vehicle lifetime, as shown in Eq. 6.6. $C_{maint,n}$ is expressed in Eq. 6.7 as a function of the maintenance cost of driving a km with the vehicle ($C_{maint,km}$) and the average distance driven by the vehicle per annum.

$$LCC = \frac{C_{bat} + C_{veh} + C_{elec} + C_{maint}}{D_{km}} \quad \text{Eq. 6.1}$$

$$C_{elec} = \sum_{n=1}^{N_{veh}} \frac{C_{elec,n}}{(1+r)^n} \quad \text{Eq. 6.2}$$

$$C_{elec,n} = C_{elec,kWh} \times E_{veh} \cdot d \quad \text{Eq. 6.3}$$

$$N_{veh} = \frac{D_{km}}{d} \quad \text{Eq. 6.4}$$

$$D_{km} = \frac{FEC \times NC_{bat}}{E_{veh}} \quad \text{Eq. 6.5}$$

$$C_{maint} = \sum_{n}^{N_{veh}} \frac{C_{maint,n}}{(1+r)^n} \quad \text{Eq. 6.6}$$

$$C_{maint,n} = C_{maint,km} \times d \quad \text{Eq. 6.7}$$

A summary of the inputs to the LCC model of Eqs. 6.1 to 6.7 is shown in **Table 8**. NC_{bat} is set to 26.6 kW h in line with literature values (Ellingsen et al., 2014; Kallitsis et al., 2020). The production costs to the original equipment manufacturer (OEM) for the battery pack (C_{bat}) are calculated with BatPaC. The original spread sheet was slightly modified in order to perform more detailed cost calculations of the various TMS. To do so, the base value for the thermal management system given in BatPaC was replaced by a breakdown of the sum of the TMS component costs. TMS costs were obtained by deriving the cost to OEM from component vendor prices by assuming a profit margin of 90%. The vehicle cost (C_{veh}) includes vehicle assembly costs and parts of the electric vehicle powertrain except for battery pack and TMS (Lutsey and Nicholas, 2019). $C_{elec,kWh}$ is based on prices for household consumers in the first half of 2019 (Eurostat, 2019). $C_{maint,km}$ is representative of a Nissan Leaf and includes service, maintenance and repair (FleetNews, 2019). The distance travelled by the car per year is assumed to be 15,000 km and the discount rate is assumed to be 2.5 %. Taxes are not considered in the LCC model.

Table 8. Summary of inputs to the utilisation LCC model (Lander et al., 2021b).

Input	Units	Value	Source
Energy consumption (E_{veh})	kW h km^{-1}	0.199	(Duce, 2014)
Battery pack cost (C_{bat})	$	6,950-7,140	Section 6.2.2
Nominal capacity of battery pack (NC_{bat})	kW h	26.6	(Ellingsen et al., 2014)
Vehicle cost (C_{veh})	$	15,000	(Lutsey and Nicholas, 2019)
Unit electricity cost ($C_{elec,kWh}$)	$ $(kW\ h)^{-1}$	0.21	(Eurostat, 2019)
Unit maintenance cost (C_{maint})	$ km^{-1}	0.063	(FleetNews, 2019)
Average distance per year (d)	km y^{-1}	15,000	Assumption
Discount rate (r)	%	2.5	Assumption

The carbon footprint of the EV is expressed as a function of the carbon footprint of battery and vehicle production (CF_{bat} and CF_{veh}), the well-to-wheel carbon footprint of a kWh of electricity (CF_{elec}), E_{veh} and the carbon footprint of maintenance (CF_{maint}), as shown in Eq. 6.8. CF_{bat} is defined in Eq. 6.9 as the product of the carbon footprint for producing a kg of battery pack ($CF_{batt,kg}$) with its mass (M_{bat}). CF_{veh} is defined in Eq. 6.10 as the product of the carbon footprint for producing a kg of the vehicle body ($CF_{veh,kg}$) with the overall vehicle mass, excluding the battery (M_{veh}). The carbon footprint of producing and transmitting a kW h of electricity ($CF_{elec,kW\,h}$) is multiplied by the vehicle energy consumption in order to express the well-to-wheel GHG emissions per km occurring from the vehicle's energy consumption. The carbon footprint of maintenance is expressed as a function of the units of maintenance (U_{maint}) and the carbon footprint of a maintenance unit ($CF_{maint,U}$) in Eq. 6.11. The maintenance unit is defined as the inverse fraction of D_{km} in Eq. 6.12 (Duce et al., 2016).

$$CF = \frac{(CF_{bat} + CF_{veh})}{D_{km}} + CF_{elec} \times E_{veh} + CF_{maint} \quad \text{Eq. 8}$$

$$CF_{bat} = CF_{bat,kg} \times M_{bat} \quad \text{Eq. 9}$$

$$CF_{veh} = CF_{veh,kg} \times M_{veh} \quad \text{Eq. 10}$$

$$CF_{maint} = U_{maint} \times CF_{maint,U} \quad \text{Eq. 11}$$

$$U_{maint} = \frac{1}{D_{km}} \quad \text{Eq. 12}$$

The main inputs to Eqs. 6.8 to 6.12 are summarised in **Table 9**. $CF_{bat,kg}$ was taken from Kallitsis et al. (2020), which is representative of an NMC333/Gr battery produced in China as presented in Chapter 4. The $CF_{veh,kg}$ is based on the Ecoinvent 3.5 database and, M_{bat} and M_{veh} are set to 253 kg and 918 kg respectively. The carbon footprint of different TMS options is assumed to remain unchanged across scenarios, as 94% of it comes from aluminium production which is used for the radiator, and is included in $CF_{bat,kg}$. The emission factor for electricity generation corresponds to consumed electricity in the UK in 2017 (including grid losses) consisting of 7% coal, 42% gas, 6% thermal and 45% nuclear and renewables (BEIS, 2019). $CF_{maint,U}$ is retrieved from Ecoinvent. E_{veh} is identical to the value used in the LCC, which is defined in **Table 8**.

Table 9. Summary of inputs to the utilisation LCA model (Lander et al., 2021b).

Input	Units	Value	Source
Battery production footprint ($CF_{bat,kg}$)	kg CO_2 eq kg^{-1}	29.1	(Kallitsis et al., 2020)
Vehicle production footprint ($CF_{veh,kg}$)	kg CO_2 eq kg^{-1}	7.3	Ecoinvent 3.5
Battery mass (M_{bat})	kg	253	(Kallitsis et al., 2020)
Vehicle mass (M_{veh})	kg	918	(Duce et al., 2016)
Electricity footprint (CF_{elec})	kg CO_2 eq $(kW\ h)^{-1}$	0.2766	(BEIS, 2019)
Maintenance footprint ($CF_{maint,U}$)	kg CO_2 eq pcs^{-1}	5.98×10^{-6}	Ecoinvent 3.5

The model is set up to include the electricity production and transmission losses in CF_{elec} and the efficiency of the entire vehicle powertrain in E_{veh}. The latter is calculated based on an average efficiency of 73.5% for the entire powertrain chain, which includes the charging/discharging efficiency of the battery, the efficiency of the charger and the energy recovery through regenerative braking (Duce et al., 2016). E_{veh} is assumed to not change significantly between scenarios.

So far, all the inputs to the LCA and LCC models have been defined except from the FECs, which are calculated for each TMS, while the cost of the battery pack has been given as a range. In the following sections, the properties of the studied battery pack are described and the calculation methodology for the FECs is summarised. The FECs and the battery pack costs are

presented in the results section, as they vary for each TMS design and were calculated for the purpose of this research.

6.2.2 Battery and TMS technologies

The battery cell and pack properties of the studied system are shown in **Table 10**. The cell design of the NMC333/Gr pouch cells was adopted from De Hoog et al. (2017) and the configuration of the 26.6 kW h battery pack from Ellingsen et al. (2014). Consequently, the pack voltage and pack dimensions were calculated using BatPaC. The pack dimensions and weight are given for a liquid cooled battery pack and vary for an air-cooling system since it requires additional air channels leading to a slightly larger pack.

The liquid cooling and AC circuits are made of two-loop systems including a coolant and refrigerant loop as shown in **Figure 10**. The liquid cooling system is further divided into SC, TC and IC. For the SC system, a set-up similar to the one integrated in the Chevrolet Volt is assumed, including pairs of pouch cells sandwiching one cooling plate resulting in single surface cooling. TC differs from SC as the heat is extracted via the cell tabs as opposed to the cell surface (**Figure 10**). IC describes a system where the cells are submerged directly in the refrigerant. To ensure a safe set-up even in case of cell damages, IC uses a dielectric refrigerant liquid, such as 3M™ Novec™ Engineered Fluid (Gils et al., 2014). A refrigerant volume of 0.5 L/kWh for IC is assumed, derived from expert indications. While indeed, TMS includes cooling and heating of the battery, in this study, only the cooling task is taken into account and the impact of low temperatures and the battery heating system was omitted.

Table 10. Cell and pack properties for an NMC333/Gr chemistry (Ellingsen et al., 2014; Hoog et al., 2017).

Chemistry	**NMC333/Gr**
Cell properties	
Cell type	Pouch
Nominal cell capacity [Ah]	20
Nominal cell voltage [V]	3.65
Length [mm]	217
Width [mm]	130
Thickness [mm]	7.1
Weight [g]	428
Tab length [mm]	40
Tab width [mm]	45
Pack properties	
Number of cells per module	30
Number of modules per pack	12
Total number of cells in pack	360
Pack capacity [Ah]	80.8
Pack voltage [V]	330
NC [kW h]	26.6
Length [mm]	1,437
Width [mm]	488
Height [mm]	167
Weight [kg]	204
Volume [L]	121

6.2.3 Determination of the maximum cell temperature

The maximum cell temperature T_{max} associated with a certain cooling method is determined based on Eq. 6.13, using the cell cooling coefficient (CCC) introduced by Hales et al. (2019), which describes the temperature gradient required for a given rate of heat rejection from a cell. The heat generation rate, Q_{gen}, per cell was obtained from BatPaC for the pack design described above. CCC_{tab} and $CCC_{1\ surf}$ (representing tab cooling and single surface cooling, respectively) have been reported previously for a 20 Ah pouch cell (A123 Nanophosphate® AMP20M1HD-A) that has comparative geometry to the cell used in this study from Hales et al. (2020, 2019). Given the small differences in each parameter, applying the literature CCC values to the here presented NMC333/Gr cell is justifiable.

$$T_{max} = T_{inlet} + \Delta T = T_{inlet} + \dot{Q}/CCC_i \qquad \text{Eq. 6.13}$$

Ongoing experiments by the authors of Lander et al. (2021b) have demonstrated that multiplying $CCC_{1\,surf}$ by 3.02 outputs $CCC_{2\,surf}$ (representing two-sided surface cooling). For a large format pouch cell such as that in the present study, where the sides of the cell are very small in comparison to the cell surfaces, $CCC_{2\,surf}$ may be assumed to be approximately equal to CCC_{imm}. **Table 11** lists the heat generation Q_{gen} per cell, refrigerant inlet temperature (assumed to be 298 K) and CCC for the respective TMS. For the purpose of this study, the energy demand for cooling was integrated within the total energy consumption of the vehicle, assuming that the additional energy requirement to keep a battery at lower temperatures is negligible compared to the energy required for traction. Therefore, the energy consumption was kept unchanged between scenarios.

Table 11. Heat generation Q_{gen}, refrigerant inlet temperature and CCC for surface, tab and immersion cooling (Lander et al., 2021b).

TMS	Heat generation (Q) [W]	Refrigerant inlet temperature (T_{inlet}) [K]	CCC_i [W K^{-1}]
Surface	1.664	298	4.08
Tab	1.664	298	0.24
Immersion	1.664	298	12.69

6.2.4 Capacity fade modelling

Analysing the battery capacity fade is important for estimating the number of cycles delivered during the battery lifetime and therefore the distance travelled during its service life in different operating temperatures. Since the capacity fade at elevated temperatures is caused by chemical side reactions such as SEI formation, an empirical Arrhenius law-based correlation between the relative capacity degradation (RCD) (%) and operating temperature T (K) is assumed based on the study of Wang et al. (2011) in Eq. 6.14. Q is the charge throughput (kAh), E is the fraction of the activation energy (J mol^{-1}), z is the power law factor, R is the ideal gas constant (J mol^{-1} K^{-1}) and B is the pre-exponential factor which should come in kAh^{-z} for the equation to be dimensionally consistent. Q is associated to FEC based on Eq. 6.15, where Q_{cell} is the cell's nominal capacity in kAh and the two is included to account for charge/discharge cycles.

$$RCD = B \times \exp\left(-\frac{E}{RT}\right) Q^z \qquad \text{Eq. 6.14}$$

$$\mathrm{Q} = \ 2 \times Q_{cell} \times FEC \qquad \text{Eq. 6.15}$$

B, E and z were obtained by fitting experimental data by de Hoog *et al*. (2017), who studied the degradation of a NMC333/Gr 20 Ah pouch cell under various experimental conditions, with Eq. 6.14 using the non-linear regression tool as integrated in MATLAB. The charge throughput was correlated to FECs based on Eq. 6.15. The DOD, Mid-SOC and charge/discharge rate were fixed at 80%, 50% and 1C, respectively and the model was fitted to experimental data for the first 1,000 FECs for three different temperatures (298 K, 308 K, 318K). Eq. 6.14 is empirical, with such dependence on temperature being originally observed in performance tests ranging from 25°C to 70°C (Bloom et al., 2001), which is considered satisfactory for the purpose of this study, but should not be over extrapolated. It is noted that RCD does not converge to unity for very large numbers of Q, which is counter intuitive. This is connected with the fact that performance tests were performed within the operating range of battery cells in first-life applications, which do not exceed RCD values of 20 to 30%. Therefore, Eq. 6.14 is considered satisfactory for the comparative assessment performed in this study but should not be used to extrapolate for large RCD values as the capacity fade behaviour in such values is not sufficiently understood to date.

6.3 Results and analysis

6.3.1 Battery cycling life

The fitting of Eq. 6.14 to the experimental data is shown in **Figure 28**. The calculated values for B, E and z were 4.2×10^5, 4.23×10^4 J mol^{-1} and 1.58, respectively. Any calendar aging contribution was neglected based on the data of de Hoog *et al.* (2017), showing a negligible *RCD* after 600 days of storage in 298 K. The goodness of fit is evaluated in **Figure 29**. For the first 500 FECs, the model underpredicts the relative capacity degradation (RCD) for 298 K and 308 K and overpredicts for 318 K as illustrated in **Figure 29a**, showing the predicted *vs.* experimental *RCD*. **Figure 29a** shows the coefficient of variation (CV) as a function of FECs. For 298 K all the values are included within ±25% CV, for 308 K all the values are included within ± 21.5% CV and for 318 K all the values are included within ±15.5% CV. For all cases, the model predictions lie within ±28.5% of the experimental values. The fitting is considered to be satisfactory for the purpose of comparing the capacity fade behaviour in different temperatures.

It was assumed that the capacity fade behaviour of each cell in the battery pack is equal and that the entire battery pack ages at the same rate as its hottest cell. Previous reports have shown that usually the cells closer to the charge load age faster than those further away, due to interconnection resistances (Chen et al., 2017). This will influence thermal gradients and degradation rates within the pack. However, since herein a 2P pack (i.e., two cells in parallel) is modelled, the difference in degradation rate between the two cells is assumed to be negligible. Therefore, in this case, upscaling the RCD from a 20 Ah cell to a 26.6 kWh battery pack is considered to be a reasonable approximation of the pack RCD.

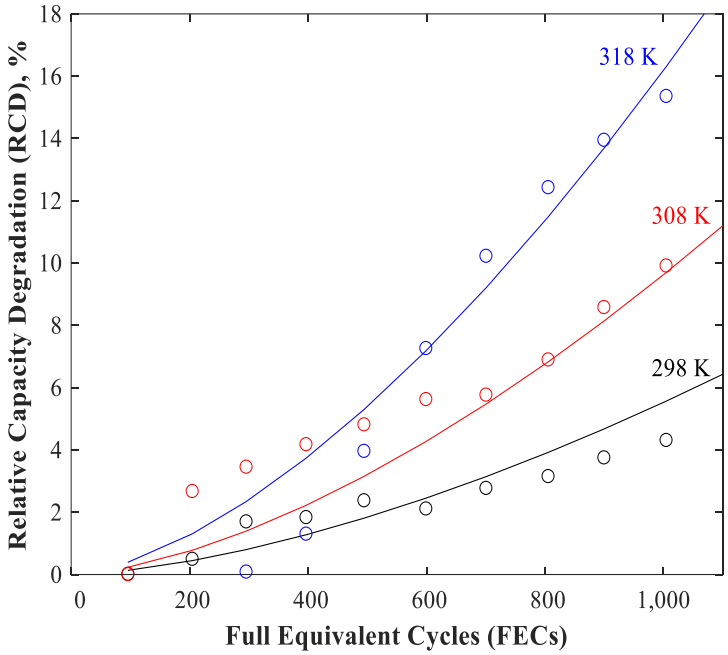


Figure 28. Experimental (dots) and fitted (solid line) data for NMC333/Gr cell at 298 K, 308 K and 318 K based on de Hoog et al. (2017), (Lander et al., 2021b).

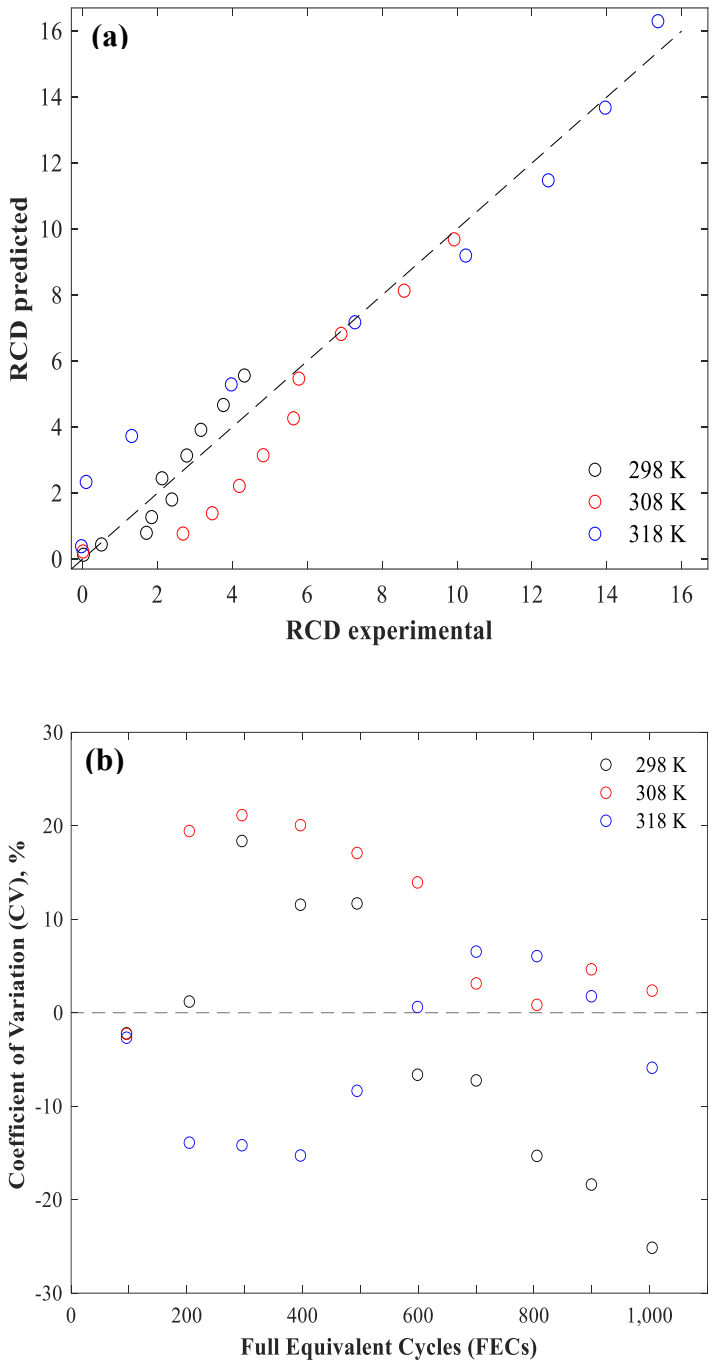


Figure 29. (a) predicted vs experimental RCD and (b) Coefficient of Variation (CV) vs FECs for fitting Eq. 6.14 to experimental data based on de Hoog et al. (2017), (Lander et al., 2021b).

This allows a scale-up from cells to battery pack by keeping the same *RCD* and increasing the nominal capacity. The capacity fade behaviour of the battery pack is estimated by accounting for the maximum cell operating temperature (T_{max}) for each TMS. The maximum cell temperatures for the LC TMS were calculated according to Eq. 6.13 and the results are summarized in **Table 12**. To the best of the author's knowledge no *CCC* has been reported for

air cooling. Therefore, a literature value for T_{max} based on experimental data has been used in the following (Dincer et al., 2016). The heat rejection capability (CCC) for IC is the highest amongst the TMS and thus leads to the lowest cell temperature. AC, given the low heat capacity of air ($C_{p,air}$=1.00 J g^{-1} K^{-1}) compared to the ethylene glycol/water-based refrigerant used for the liquid cooling ($C_{p,EG/water}$=3.26 J g^{-1} K^{-1}) leads to a significantly higher cell temperature (314 K) (Chen et al., 2017).

Table 12. ΔT and maximum cell temperature for each TMS under study (Lander et al., 2021b).

TMS	ΔT **[K]**	T_{max} **[K]**
Air	-	314.0
Tab	6.81	304.8
Surface	0.41	298.4
Immersion	0.13	298.1

The battery pack cycling life at the specific operating temperatures determined for each TMS (**Table 12**) was modelled using Eq. 6.14 and extrapolating to 2,500 FECs. It was assumed that the entire battery pack ages at the same rate as its hottest cell and thus the model was upscaled from a 20 Ah cell to the 26.6 kWh battery pack. The DoD was fixed at 80%, Mid-SoC at 50% and 1C charge/discharge rate. The battery end-of-life (EOL) criterion was set at 80% of the initial pack capacity.

Figure 30 shows the RCD in function of the number of full equivalent cycles. The AC TMS with an assumed cell temperature of 314 K results in the shortest cycling life (1,307 FECs), while IC and SC lead to the highest cycling numbers of 2,257 and 2,233 FECs, respectively. TC (T_{cell}=304.8 K) enables a battery cycling life of 1,781 FECs. This demonstrates that changing the TMS from AC to SC or IC increases the battery lifetime by around 40%. The FECs, travelled distance during lifetime (D_{km}) and lifetime in years (n) are summarised in **Table 13**.

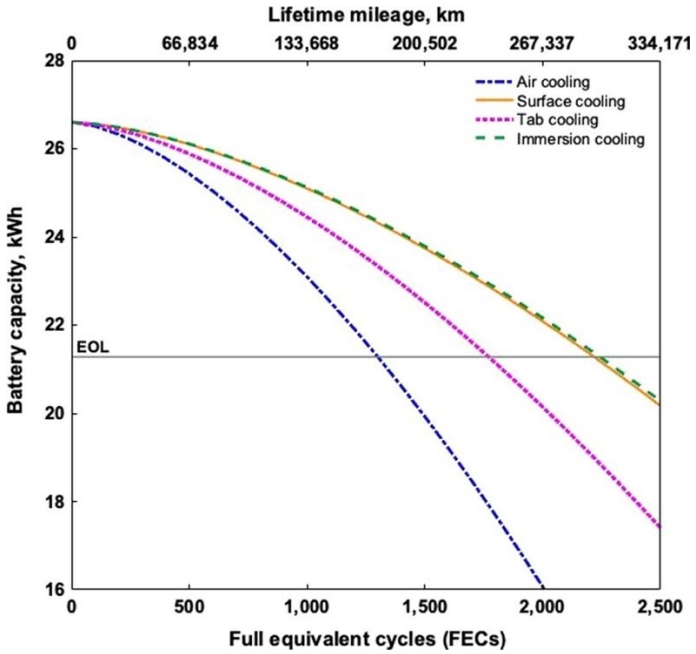


Figure 30. Battery capacity as a function of FECs for air (blue line), tab (pink line), surface (orange line) and immersion (green line) cooling (Lander et al., 2021b).

Table 13. Full Equivalent Cycles (FECs), travelled distance over lifetime (D_{km}) and lifetime in years (n) for a 26.6 kWh battery pack including air, tab, surface or immersion cooling (Lander et al., 2021b).

TMS	FECs [#]	D_{km} [km]	n [years]
Air	1,307	174,646	11
Tab	1,781	238,007	15
Surface	2,233	298,428	19
Immersion	2,257	301,686	20

6.3.2 Life cycle emissions and costs

The LIB pack's total cost, together with the contributions of the TMS in each case is shown in **Figure 31**. The total battery pack cost to OEM ranges between $6,670-6,870 for a 26.6 kW h pack, where the TMS amounts for 3-7% of the total cost in agreement with literature values (Dincer et al., 2016; Lutsey and Nicholas, 2019). Amongst the TMS considered here, AC is the cheapest design ($200) since refrigerant and cooling plates are not needed. Here, a system with an additional coolant loop was chosen; in case of an AC design without coolant the costs would further decrease, but also the cooling efficiency would diminish. IC is by far the most expensive solution ($470) due to the high cost of the refrigerant (in this case Novec™7000).

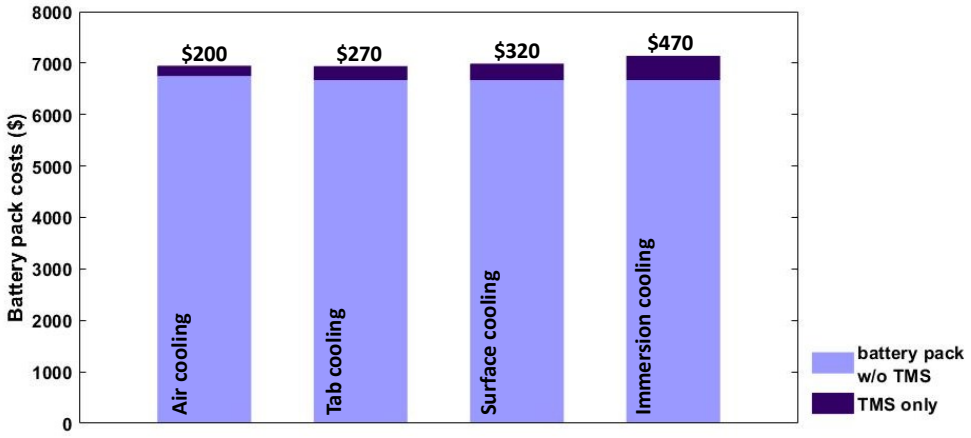


Figure 31. Battery pack costs excluding the TMS, together with the additional cost of TMS as estimated from BatPac (Lander et al., 2021b).

The calculated battery pack costs for each TMS were used as input to the LCC model described in Eqs. 6.1 to 6.7, obtaining LCC values of 0.22 $/km for AC and approximately 0.16 $/km for SC and IC **Figure 32a**. The contribution of battery pack cost and vehicle cost to the LCC of an AC system is quite significant and decreases with increased lifetime, making it less significant for an IC or SC system. As upfront battery pack costs and vehicle costs get diluted due to an increased lifetime of the LIB, the contribution of electricity and maintenance costs becomes more important as it is directly related to the EV and stays fixed through the scenarios considered here.

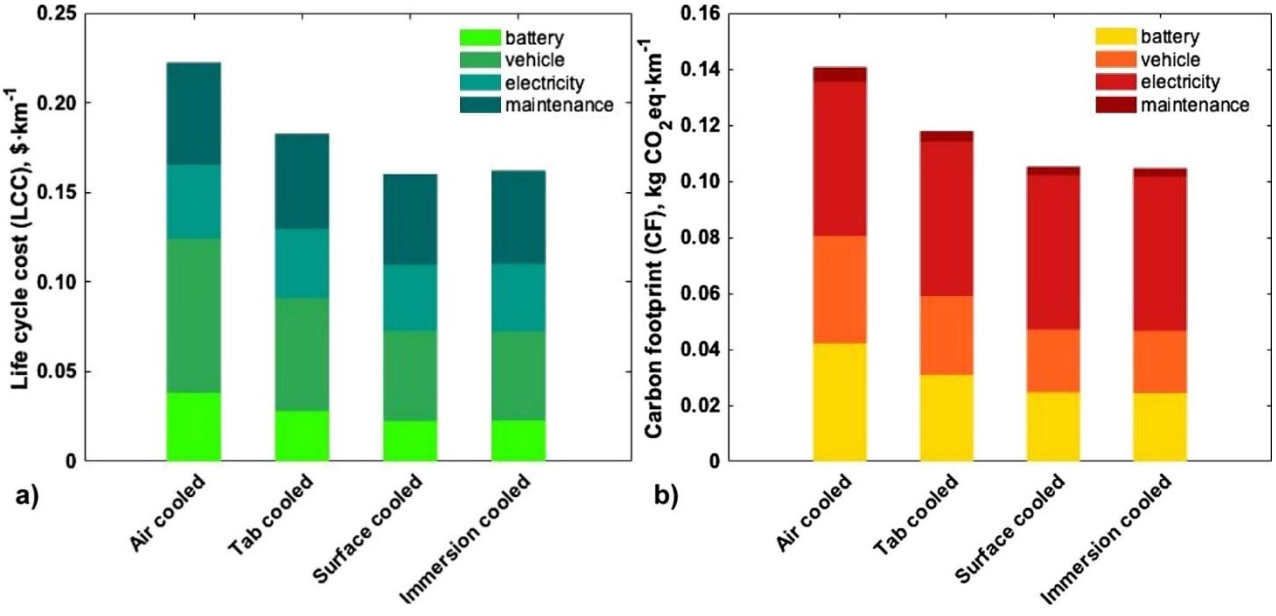


Figure 32. (a) LCC (in \$ km^{-1}) and (b) CF (in kg CO_2 eq km^{-1}) for AC, TC, SC and IC, with battery, vehicle, electricity and maintenance contributions (Lander et al., 2021b).

The CF per km (**Figure 32b**), calculated based on Eqs. 6.8 to 6.12, is dominated by the battery production, vehicle production and the electricity during the use phase. The increased lifetime achieved by an SC system causes a decline in the lifetime CF, from 0.141 kg CO_2 eq km^{-1} for AC to 0.105 kg CO_2 eq km^{-1} for SC. Moreover, the contribution of battery production to the total CF is cut in half due to the lifetime extension achieved by IC, compared to AC. An enhanced battery lifetime causes a decline in the battery and vehicle production footprint, as they are spread across a higher number of kilometres causing a decrease in the total CF. Since the electricity footprint remains unchanged across cases, its percentage contribution to the total CF increases with increased lifetime.

6.4 Discussion

6.4.1 Sensitivity analysis

To evaluate the impact of future developments in battery production and use phase on the LCC and CF, a sensitivity analysis of cost and CF for pack production (C_{bat}, $CF_{bat,kg}$), electricity (C_{elec}, CF_{elec}) and distance travelled over lifetime (D_{km}) was performed.

The reduction of battery pack costs and CF have been intensively pursued by researchers and manufacturers alike. As a result, battery pack costs have changed dramatically with time and prices have fallen significantly by 87% since 2010 (BloombergNEF, 2019). The effect of further production cost reductions is evaluated by reducing the calculated battery pack costs by 30% and 70%. According to Kelly et al. (2019), the assumed battery production CF baseline $CF_{bat,kg}$ of 29.1 kg CO_2 eq·kg^{-1} can be reduced by 30% as a result of energy savings occurring from upscaling battery manufacturing plants in China. A further reduction of 70% can be achieved by changing the supply chain and powering battery production with renewable energy. Therefore, a two-step reduction was assumed in the sensitivity analysis, by 30% and 80% compared to the baseline battery production CF.

Also, the electricity price and carbon intensity were varied in order to take into account different usage locations in Europe. For the electricity footprint CF_{elec}, the baseline value is reduced by 80% to reflect a low carbon electricity mix such as France's and is increased by 60% to reflect an electricity mix with approximately 30% coal such as Germany's. Similarly,

the electricity price $C_{elec,kWh}$ was reduced by 20% and increased by 45%, with the lower and upper values corresponding to France and Germany, respectively.

Furthermore, the impact of battery lifetime was evaluated. Harlow et al. (2019) predicted significant lifetime extensions to up to 1.2 million km distance driven throughout the battery lifetime . To reflect future battery lifetime trends in the sensitivity analysis, a lifetime extension of 100% for the NMC333/Gr battery was assumed. A battery lifetime reduction of 50% was also included, since new battery materials (high- nickel NMC chemistries) have reportedly shorter cycling lifetimes caused by material instabilities (Li et al., 2020).

EV manufacturers are focusing mostly on lowering battery pack production costs. However, this sensitivity analysis suggests that from the society and policy maker's point of view, the paramount priority in battery technology development should be to extend the battery lifetime as this has strong impacts on the LCC and CF of EV batteries. As shown in **Figure 33a**, doubling the lifetime results in a decrease of LCC and CF by 33% and 23%, respectively. A 50% lifetime reduction, on the other hand, causes an LCC and CF increase by 52% and 48%, respectively. Similar trends have been also demonstrated for batteries in grid-scale applications (Schmidt et al., 2019). On the other hand, reducing the pack production cost and production CF, have a much smaller effect on the overall LCC and CF compared to lifetime extension, although these aspects are understandably critical for battery producers. This sensitivity analysis also confirms that the life cycle CF is most sensitive to the footprint of the electricity mix supplied during the EV use phase, and this is more significant for longer lifetimes. An increasing contribution of renewable energies in the electricity mix will further reduce the overall CF (**Figure 33b**).

Understandably, OEMs might hesitate to accept higher upfront costs fearing lower profits. However, the upfront costs are largely outweighed by the reduced LCC. This in turn makes EVs more appealing to end users and might result in higher EV market penetration and hence larger production volumes. Moreover, given the rapidly increasing production scale of LIBs in the near future, an enhanced cycle lifetime will also help to reduce pressure on raw materials and battery waste.

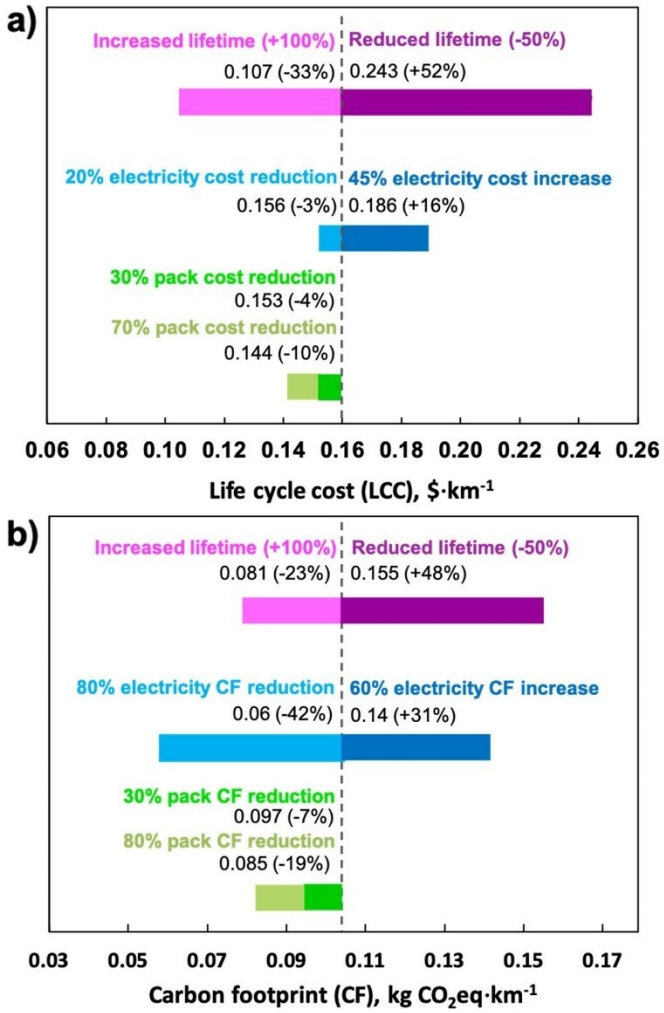


Figure 33. (a) LCC and (b) CF sensitivity analyses for surface cooling varying the battery pack cost/footprint (green), electricity cost/footprint (blue) and lifetime (purple) by ±50%; the dashed line indicates the base value for SC as shown in **Figure 32** (Lander et al., 2021b).

It is worth mentioning at this point that the driving pattern will also have an impact on the LCC and CF. The battery degradation rate and thus battery lifetime depends on the battery operation conditions in an EV such as speed, acceleration, regenerative breaking and distance travelled. Fast acceleration, for instance, requires fast discharge output (higher C rate) leading to a higher degradation rate (Jafari et al., 2015; B. Wang et al., 2014). This will, in turn, lead to a higher CF and LCC. Moreover, aggressive driving increases the vehicle energy consumption, leading to a more frequent need for battery charging and further increasing the CF and LCC related to the battery use phase (Egede et al., 2015).

6.4.2 Impact of thermal gradients on LCC and CF

In the case of IC, increased production costs were calculated as compared to SC, but no benefits in terms of battery lifetime, CF and LCC could be demonstrated. At this point, it is worth mentioning that the generation of cell thermal gradients and their impact on battery degradation has not been considered thus far in this paper. Cell thermal gradients lead to faster degradation due to inhomogeneous impedance and current distributions in the cell, which reduce usable capacity and lead to non-uniform ageing (Chiu et al., 2014; Fleckenstein et al., 2011). Therefore, cooling strategies which can minimise thermal gradients, are highly beneficial for the battery lifetime. A previous study by Hunt et al. (2016) demonstrated that using TC instead of SC can significantly reduce the thermal gradients and thus extend the battery lifetime threefold for a particular example. Similar observations have been made for IC systems (Gils et al., 2014). As a result, LCC and CF would further reduce, with regards to the values shown in **Figure 32** and hence make TC and IC more attractive than SC.

6.4.3 Modified cell design for tab cooling

In the previous sections, the performance of the various TMS based on currently employed pouch cell designs was discussed. Owing to their small thickness and large surface cooling areas, pouch cells are more suitable for SC than TC. It is impossible for a TC TMS to compete against an SC equivalent on such a cell. The cross-sectional area of the tabs is very small, meaning a significant temperature gradient is required, from the electrode stack to the external portion of the tabs, to establish the required rate of heat removal via TC. The result is a tab-cooled cell, which operates at a higher average temperature over its lifetime, compared with the surface-cooled cell. This in turn induces a higher rate of degradation in the tab-cooled cell (**Figure 30**). However, TC can have significant benefits over SC, because the heat is inherently removed from the pouch cell in such a manner that layer-to-layer temperature in- homogeneity is reduced (Hunt et al., 2016). This is directly linked to current in-homogeneity (Zhao et al., 2019), which strongly increases cell-wide degradation (Chiu et al., 2014). Several studies (Hunt et al., 2016; Zhao et al., 2019) in the computational and experimental domain have demonstrated that TC can increase the cell lifetime when a sufficient cooling rate, from the electrode stack to the external portion of the tabs, can be achieved with a reasonable temperature gradient.

Here, a first attempt is presented to quantify this effect with the limited information available. **Table 14** summarises two degradation studies comparing TC vs. two-sided SC. The first study was carried out on a small pouch cell (Kokam SLPB11543140H5), ideally designed for TC (Hunt et al., 2016). The second one was conducted on a large pouch cell (A123) not suitable for TC and geometrically similar to that used in the present study (Dondelewski et al., 2020). In each case, the cells were cycled at constant current between manufacturer voltage limits, at 20% of their discharge rate limit. Additionally, the two-sided surface and tabs cell cooling coefficients are presented for each cell, derived in previous studies (Dondelewski et al., 2020; Hales et al., 2020, 2019). The degradation rates and CCCs have been normalised against the respective cell capacity, so that the results can be directly compared. It is evident, through comparison of the CCCs, that the A123 cell is more suited to two-sided SC and the Kokam to TC. This is reflected in the degradation rates of each cell, under each TMS.

Figure 34 presents the normalised degradation rates against the normalised CCC (standardised by respective cell capacity) for each cell and TMS. The lowest of the four degradation rates is achieved through TC of the Kokam cell, while the highest is achieved through TC of the A123 cell. In simplified quantitative terms, this may be expressed via the magnitude of the gradient of the linear relationship. For TC, it is calculated to be 2.36 $(mAh \cdot cycle^{-1}) \cdot (W \cdot K^{-1})^{-1}$ whilst for SC it is only 0.41 $(mAh \cdot cycle^{-1}) \cdot (W \cdot K^{-1})^{-1}$.

Table 14. Summary of degradation results and cell cooling coefficients of two lithium-ion pouch cells with different geometry (Lander et al., 2021b).

Cell	**Kokam**	**A123**
BoL Capacity [Ah]	5	19.6
SC degradation rate [mAh $cycle^{-1}$ Ah^{-1}]	0.144	0.105
TC degradation rate [mAh $cycle^{-1}$ Ah^{-1}]	0.06	0.18
CCC_{2surf} [W K^{-1}]	3.07	13.86
CCC_{tabs} [W K^{-1}]	0.324	0.245

This study is based around the design of a battery pack that uses 20 Ah large format pouch cells. To predict what the required CCC_{tabs} for such a cell must be for effective tab cooling to be applied, the normalised CCC_{tabs} for the 5 Ah Kokam cell (0.0648 $W \cdot K^{-1} \cdot Ah^{-1}$) was used, since it is known that this is a cell that has been optimised for tab cooling. It is shown that

CCC_{tabs} for this 20 Ah cell must be 1.295 W·K^{-1} to bring its suitability for tab cooling in line with the 5 Ah Kokam cell. Assuming that CCC_{tabs} of 1.295 W·K^{-1} is achieved through cell redesign, the TC degradation rate of the 20 Ah cell should be reduced to 0.06 mAh·cycle^{-1}·Ah^{-1}, i.e. the TC degradation rate for the Kokam cell. This would be a reduction of 43% from the SC degradation rate of the 20 Ah cell.

According to Eq. 6.13, this new CCC_{tabs} gives a maximum cell temperature of 299.3 K. This is significantly reduced, compared with the temperature for a non-optimised TC system (304.8 K, **Table 12**). Including this temperature in the capacity fade model (Eq. 6.14) and taking into account the degradation rate reduction of 43% derived from the A123 SC and Kokam TC degradation rates (**Table 14**), a cycle lifetime of 3,088 FECs is obtained. This is 36% more than the FEC of a surface-cooled cell.

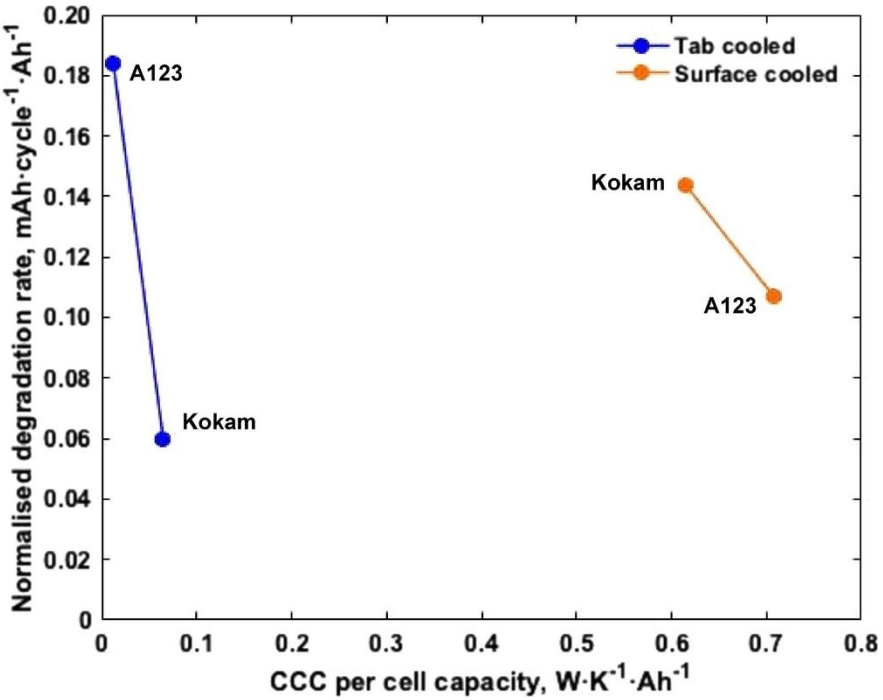


Figure 34. Degradation rate plotted against cell cooling coefficient (CCC) for two- sided SC and TC of two lithium-ion pouch cells (Lander et al., 2021b).

The resulting enhanced cycle lifetime has significant impacts on cost and environmental footprint (**Figure 35**). The total LCC drops to 0.133 \$·km^{-1}, which corresponds to a decrease of 40%, compared with the LCC for the air-cooled cell. The CF of the optimised TC accounts for 0.0913 kg CO_2 eq·km^{-1}, thus a reduction of 35% compared to the AC system.

The industry has focused on the optimisation of pouch cells for surface-cooled systems and as the results here show that further improvements will have only a marginal impact (**Figure 34**). Even though SC is currently the most deployed TMS, it is fundamentally flawed, due to the build-up of thermal gradients. The thickness of the lithium-ion pouch cells is therefore limited for an SC TMS since a thicker electrode stack would result in a more significant thermal gradient. This puts a limit on the energy density achievable at cell level.

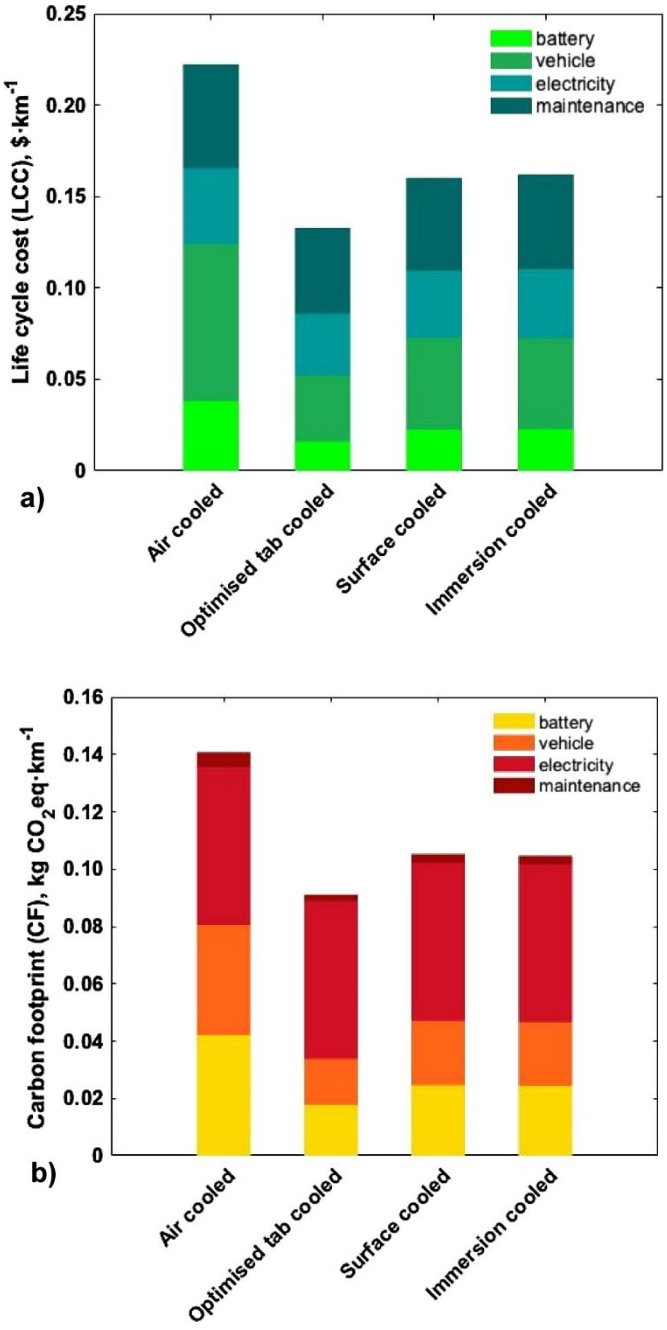


Figure 35. (a) LCC (in \$ km^{-1}) and (b) CF (in kg CO_2 eq km^{-1}) for different TMS cooling options, with battery, vehicle, electricity and maintenance contributions (Lander et al., 2021b).

In contrast, improving CCC_{tabs} has the potential of dramatically reducing the cell degradation rate and therefore life cycle cost and carbon footprint. Moreover, since the tab thickness should in theory be scalable, it enables the development of very thick electrode stacks. Numerical evidence has already been published to support the case for such a cell redesign (Zhao et al., 2019). However, little attention has been paid so far to the optimisation of TC and its potential is far from being exploited by manufacturers and cell designers.

6.5 Conclusions

In this study, the impact of thermal management strategies on the battery lifetime and their respective life cycle costs and carbon footprint was presented. It was demonstrated that through engineering solutions such as efficient thermal management systems, the life cycle costs and carbon footprint of electric vehicles batteries can be swiftly reduced. For example, implementing surface or immersion thermal management significantly decreases the cost and carbon footprint over the entire lifetime. The life cycle cost was shown to reduce by 27% from 0.22 \$·km^{-1} for air cooling to 0.16 \$·km^{-1} for surface cooling. The overall carbon footprint was reduced by 25% from 0.141 kg CO_2 eq·km^{-1} to 0.104 kg CO_2 eq·km^{-1}. Moreover, the proposed optimised cell design, which enables more efficient tab cooling and thus further extends the lifetime, was shown to have a life cycle cost of 0.133 \$·km^{-1} and a carbon footprint of 0.0913 kg CO_2 eq·km^{-1}, which is a reduction of 40% and 35%, respectively, compared to air cooling.

Improving the environmental benefits and economic viability of electric vehicle batteries is crucial to accelerate the adoption of electric vehicles. While the currently dominant research trend is mostly focused on energy density increase and production cost reductions, it is shown herein that battery lifetime is at least as important as a performance parameter. For instance, sensitivity analysis revealed that reducing battery pack costs has only a marginal impact on life cycle cost, compared to the extension of the battery lifetime which, if doubled, reduces the carbon footprint and life cycle cost by 23% and 33%, respectively. Similarly, reducing the pack production carbon footprint has a smaller impact on the overall life cycle footprint than battery lifetime extension. Shifting the research focus towards battery lifetime extension provides vast optimisation possibilities, ultimately improving the sustainability and cost of electric vehicle batteries. Therefore, the impact of improved cell and pack design, refined charging protocols,

advanced battery management systems and battery materials on battery lifetime and environmental and economic impact needs to be further assessed.

Chapter 7 Lithium-ion battery recycling LCA

In this section, the development of an LCA model for the end-of-life treatment of automotive battery packs is presented, taking into account market-leading hydrometallurgical and pyrometallurgical processes. Previously applied system boundaries across literature studies are expanded to describe the whole end-of-life treatment chain, from the point of collection of LIB packs to the recovery of secondary material. The specific literature gaps are identified, followed by a description of the LCI developed and of the various scenarios studied. Finally, the results are presented and discussed in detail and conclusions are made on the environmental competitiveness of hydrometallurgical and pyrometallurgical processes and the importance of recovering materials included in the LIB pack's supporting structures, i.e. BMS, TMS and packaging. This work has been peer-reviewed and recently published in the Journal of Cleaner Production (Kallitsis et al., 2022a).

7.1 Background and Motivation

Rapidly falling costs, a series of technological developments and the urgent need for decarbonisation have positioned EVs as the dominant choice for establishing widely accessible sustainable transport systems (Günther et al., 2015; Knobloch et al., 2020). Transforming the transport system requires an unprecedented increase on battery production capacity, with demand for EV batteries projected to increase twenty-fold by 2030 (International Energy Agency, 2021). This growth trajectory of the battery market creates an imperative need for effective EoL management of automotive lithium-ion batteries (LIBs) within the next decade. Battery recycling can divert batteries away from minor EoL treatment options, towards industrial-scale hydrometallurgical and pyrometallurgical processes, which are already being deployed around the world (Chen et al., 2019; Harper et al., 2019). Additionally, battery recycling offers a stream of raw materials, which is crucial in regions with limited availability

of primary resources, such as Europe, and provides efficient means of handling production scrap from battery Gigafactories (Peel and Sanderson, 2020).

The environmental impact reduction potential of recycling technologies is known to depend both on the specific processes used and the particulars of the value chain where recycling is implemented (Arshad et al., 2022; Rajaeifar et al., 2022). This has triggered a growing interest in the scientific community of using LCA to investigate the environmental benefits that battery recycling can achieve in different settings. Pyrometallurgical and hydrometallurgical treatments of NMC and LFP batteries are the most frequently assessed process options amongst LCA studies (Mohr et al., 2020). Such commercial processes have been discussed by recent reviews from Sommerville et al. (2021) and Neumann et al. (2022). As NMC is by far the most common positive electrode (hereby referred to as cathode) chemistry for automotive applications (Kallitsis et al., 2022b; World Economic Forum, 2019), its materials recovery processes have attracted increased attention.

Reported GWPs of LCA studies focusing on NMC battery recycling, alongside the respective battery production GWP, are shown in **Table 15**. Cusenza et al. (2019) performed a cradle-to-grave assessment of a LIB pack for hybrid electric vehicles utilising a LMO-NMC333 composite cathode material, demonstrating that utilising a pyrometallurgical-hydrometallurgical EoL treatment scheme reduces the production GWP by 5%. Ciez and Whitacre (2019) quantified, the net benefit of pyrometallurgical and hydrometallurgical recycling of NMC battery cells, amongst other battery chemistries, concluding that they do not reduce life cycle GHG emissions significantly. Dunn et al. (2015) calculated that producing a NMC battery with recycled material coming from pyrometallurgical processing, decreases its production GHG emissions by 20%, compared to production with primary material. Hao et al. (2017b) modelled an EV recycling chain in China and estimated that the most important source of environmental benefit from recycling an NMC battery comes from the recovery of cathode materials. Sun et al. (2020) performed a cradle-to-grave assessment of NMC333 battery packs in China, calculating that the battery production footprint of 124.5 kg CO_2-eq $(kW\ h)^{-1}$ can be reduced by 30.9 kg CO_2-eq $(kW\ h)^{-1}$ through the recovery of battery pack materials. More recently, Accardo et al. (2021) studied the production, use and recycling of an NMC333 battery pack, reporting that the introduction of EoL treatment results on a net 4.5% decrease in the LIB production GWP. A recent cradle-to-grave LCA for NMC333 battery packs by Quan et al. (2022) showed that recycling resulted in a small reduction of the production GWP (likely less than 5% judging qualitatively based on graphical illustrations in this work). Another recent

study by Du et al. (2022) provides valuable insights on the regeneration of NMC cathode material with a focus on the active material level, which explains why it is not included in **Table 15**. Jiang et al. (Jiang et al., 2022) predicted a -16.6 kg CO_2-eq $(kW\ h)^{-1}$ net benefit from hydrometallurgical recycling of NMC333 battery cells. Rajaeifar et al. (2021) performed an LCA of pyrometallurgical cell recycling using a mass functional unit, which is excluded from **Table 15** as this and the functional unit of other studies are not directly comparable. An earlier comprehensive review by Mohr et al. (2020) highlighted the varying system boundaries and functional units reported by different authors as a reason for the reported variability and the need for transparency amongst LCAs on LIB recycling. This study confirms this finding (**Table 15**). Only Ciez and Whitacre (2019) disclosed the unit process and background data used in their recycling inventory. While Quan et al. (2022) reported the foreground inventories used in their study in sufficient detail, the background data used in their work are hard to trace.

As evident from the information presented in **Table 15**, the reported achievable GWP reduction through battery recycling is highly variable in published studies, which presents a difficulty for industry and decision makers; this can also be extended to other impact categories. Part of this variability can be attributed to differences in the system boundaries considered. Specifically, literature reports focusing on the recovery of the battery electrode materials (Ciez and Whitacre, 2019; Mohr et al., 2020), which constitute less than half of a battery pack's mass, neglect significant fractions of aluminium, copper and steel that could be recovered from the battery pack's packaging, TMS and BMS. Therefore, an open question arises regarding the environmental benefit of a circular battery value chain when also accounting for the recovery of materials at pack level and for a series of processes involved including collection, transportation, sorting and dismantling, which are usually neglected. Additionally, part of the variability in the results shown in **Table 15** can be attributed to the different geographic locations of focus, given that different local electrical energy and material footprints influence the environmental burden of recycling chains, but also its benefit, as displaced material footprints differ significantly across locations (Kelly et al., 2019), with their relative differences remaining to be benchmarked under the same model and assumptions. In addition, evaluating other environmental impacts and benefits associated with LIB recycling, in addition to GHG emissions, is crucial (Ciez and Whitacre, 2019; Dunn et al., 2015) as water pollution from leachate, solid waste such as metal-rich ash, and air pollution impacts (Winslow et al., 2018) need to be considered when comparing potential management strategies for EoL LIBs.

Table 15. Reported GWP of NMC battery production and recycling across published studies (Kallitsis et al., 2022a).

Reference	Region	Cathode chemistry	Energy density [kW h kg^{-1}]	Focus	GWP [kg CO_2-eq (kW h)$^{-1}$]		
					Production	Recycling (net)[1]	
						Hydromet.	Pyromet.
Cusenza et al. (2019)	Europe	LMO-NMC333	0.065	Pack level	312.4	-15.4 (combination)	
Ciez and Whitacre (2019)	USA	NMC622	0.27[2]	Cell level	36.3	-1.3	6.4
			0.21[3]		42.4	-4.4	2.7
Sun et al. (2020)	China	NMC622	0.115	Pack level	124.5	-30.9	n/a
Mohr et al. (2020)	n/a	NMC333	0.174	Cell level	75.5	-16.4	-13.8
Accardo et al. (2021)	Europe	NMC333	0.111	Pack level	136[4]	-6.2 (combination)	
Quan et al. (2022)	China	NMC333	0.142	Pack level	87.1	n/a	n/a
Jiang et al. (2022)	China	NMC333	0.150	Cell level	n/a	-16.6	n/a

[1]Additional burden introduced for battery recycling inputs minus benefits through the displacement of primary material, [2]pouch and [3]cylindrical cells, [4]battery production assumed to take place in China.

The majority of non-energy-related environmental impacts in the life cycle of LIBs are linked with mining and materials processing operations (Porzio and Scown, 2021). The mining and materials processing impacts can be avoided to a certain extent when recycling is implemented, as suggested in recent studies aiming at extending the analysis beyond GHGs for a series of recycling processes (Jiang et al., 2022; Quan et al., 2022).

The above confirm the need for a LCA study that combines transparency, reproducibility of inventory, offers sufficient resolution to better understand the burdens and benefits of battery recycling options and evaluates a wide range of environmental categories. To this end, results from an attributional LCA model for materials recovery from spent automotive traction NMC battery packs are reported below, accounting for all the necessary steps to recover secondary

materials from the point of collection of EoL LIBs, to recovery, processing and displacement of primary material. The inventory developed in this study expands the system boundaries commonly used in battery recycling by compiling state-of-the art literature sources, original materials, and information sourced in the Ecoinvent database (Wernet et al., 2016). Dominant and mature hydrometallurgical and pyrometallurgical cell recycling schemes were modelled and complemented by pre-treatment and processing to recover the metal fractions of the battery pack in order to establish a realistic representation of the circularity in the LIB value chain that can be achieved through recycling. The direct recycling of LIBs, which aims at recovering active materials in the cathode and chemically upgrading these for new cathode manufacturing is also an important emerging opportunity (Gastol et al., 2022; Ji et al., 2021). However, the challenge of how to process different cathode chemistries together in direct recycling still needs to be solved and it is for this reason that direct recycling is not considered in this study.

The environmental burdens and benefits of the hydrometallurgical and pyrometallurgical recycling schemes were aggregated with the battery's production impact, to estimate the role recycling plays in reducing the overall environmental impact of the battery pack. The potential of battery recycling in reducing the GWP production impact was specifically explored for China, United States and Europe, enabling to account for the different electrical energy mixes and material production footprints relevant for each region. Moreover, an open issue regarding the role of recovered materials' quality on the overall environmental performance of battery recycling was explored through a sensitivity analysis on the 13 environmental impact categories under study. Finally, an in-depth analysis of unit process contributions to the environmental benefits and burdens of battery recycling options is provided herein, which contributes towards better understanding the environmental aspects of EoL treatment chains for LIBs.

7.2 Methods

7.2.1 LCA methodology

The LCA reporting guidelines according to the ISO 14040 standard series (ISO, 2014) were used in order to create a replicable, transparent and reliable inventory and results. The overarching objective was to develop a detailed Life Cycle Inventory (LCI) and assessment to

assess the environmental burdens and benefits associated with recycling of spent automotive traction battery packs. The functional unit was chosen as one kW h of nominal battery pack capacity, which is standard across literature studies on LIB production (Dai et al., 2019a; Kallitsis et al., 2020) and recycling (Ciez and Whitacre, 2019; Mohr et al., 2020). The technology boundaries were defined based on the current industrial practice, including either hydrometallurgical or pyrometallurgical processes for battery cell recycling (Mohr et al., 2020) and well-established aluminium (The Aluminumn Association, 2013), steel (Burchart-Korol, 2013) and copper recycling processes (Wernet et al., 2016). The battery technology was focused on a typical 253 kg NMC333 battery pack for automotive applications utilising an anode made of graphite with a storage capacity of 26.6 kW h, as this technology has been one of the first to be commercialised at scale, thus expected to constitute a large fraction of the first wave of EoL batteries (McKinsey&Company, 2018). Battery packs of similar type have been extensively studied in preceding literature studies on battery production (Ellingsen et al., 2014; Kallitsis et al., 2020), use (Lander et al., 2021b) and recycling (Mohr et al., 2020). While other battery chemistries such as LFP have been gaining increased attention for automotive traction applications, most commercial EVs currently include NMC formulations (Lima, 2022) which are projected to dominate the automotive sector (Walton et al., 2021; Xu et al., 2020). Within the NMC family of chemistries, we chose to focus on NMC333 as it has been commercialised widely in EVs, and excluded higher nickel chemistries, such as NMC622, as they are currently being deployed at scale and their availability for recycling is expected in more than a decade's time.

The baseline geographical boundary was limited to China, with materials and energy inputs, production processes and other LCI parameters reflecting the Chinese industrial averages. The environmental burdens and benefits of North American and European recycling chains were also investigated by adjusting key background inventories for Al, Cu and electricity production. A detailed depiction of the studied product system is given in **Figure 36**, which includes the (a) transportation of the spent battery pack from its end-user to the recycling facility, (b) dismantling of the battery pack to separate the battery modules from the TMS, BMS and packaging. The battery modules are then disassembled to battery cells, while the supporting structures, including the module and pack housing, which are considered part of the packaging, BMS and TMS, are sent for further treatment. (c) Next, the battery cells are discharged and fed to the recycling process, including either hydrometallurgical or pyrometallurgical processing. The former includes a mechanical treatment step (crushing), neutralisation and metallurgical

processing, while the latter includes a mechanical treatment step to separate Al and Cu with consequent metallurgical processing. The supporting structures are sent to a metals recycling facility, where the mixed scrap is shredded and sorted, and sent to metal recovery processes. Hence, this work analyses hydrometallurgical and pyrometallurgical processing of the spent battery cells, referred to as the hydrometallurgical and pyrometallurgical cases, with the remaining unit processes unchanged.

The EoL recycling approach was followed (Nordelöf et al., 2019), which considers that the recovered materials displace primary material upstream in the product system. The EoL treatment burden and benefit was calculated and then added to the production burden to yield the total environmental impact of production and recycling, which was then compared to the battery production impact to calculate the net environmental benefit or burden achieved through the introduction of LIB recycling across all impact categories of interest. The impact assessment was performed based on the ReCiPe 2016 Midpoint characterisation method (Huijbregts et al., 2017), given that it consists of one of the most widely used methods in battery production and recycling LCA studies (Ellingsen et al., 2014; Kallitsis et al., 2020; Oliveira et al., 2015; Sun et al., 2020). The environmental scores for GWP, FDP, stratospheric ozone depletion potential (SODP), POFP, fine particulate matter formation potential (FPMFP), TAP, FEP, MEP, FETP, METP, TETP, HTP and MDP were calculated which were presented in detail in **Table 1**. The LCA modelling was performed using the GaBi software with the background processes mainly being retrieved from the Ecoinvent version 3.5 database (Wernet et al., 2016).

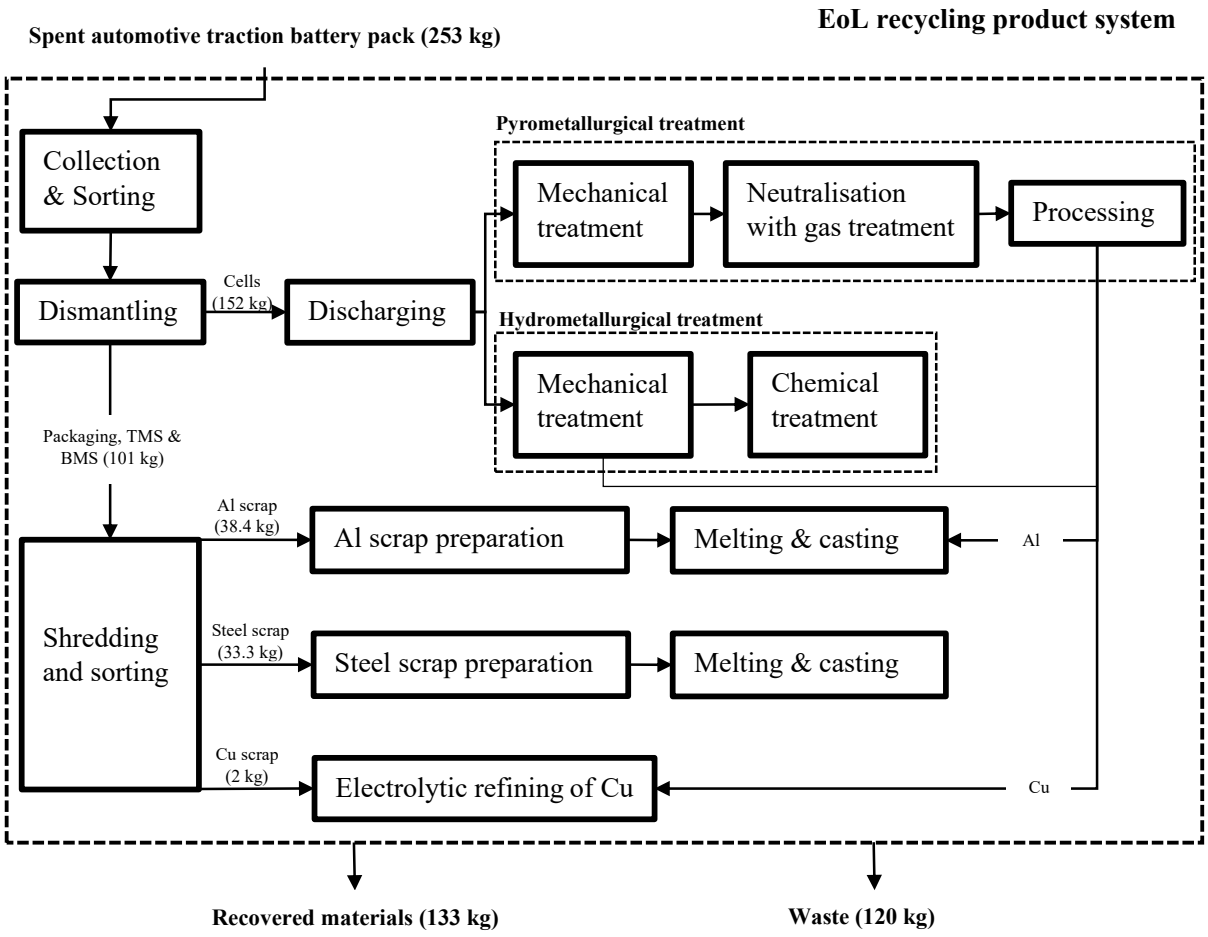


Figure 36. EoL recycling product system studied for the recovery of valuable metals from a spent automotive traction battery pack (collection of spent battery packs to generation of secondary materials) (Kallitsis et al., 2022a).

7.2.2 Inventory analysis

For the collection and sorting inventory, it was assumed that the battery pack is transported by first by freight rail and then by freight lorry to the sorting facility for 688 km and 174 km respectively, based on China's average transport distances (Jiang et al., 2022). Energy inputs associated with the sorting process were taken into account for powering a forklift and conveyor belt based on Fuc et al. (2016) and Fisher et al. (2006); the detailed calculation procedure is described in Appendix B. The dismantling process was modelled based on the studies of Choux et al. (2021) and Baazouzi et al. (2021). Specifically, this work modelled the power consumption of the robotic disassembly machinery used by Choux et al. (2021) based on the task planner of Choux et al. (2021); the detailed calculation procedure is described in Appendix B. Facility inputs associated with the collection and sorting, and dismantling processes were assumed to be insignificant due to their long lifetime. The LCI for the

discharging process was inspired by Yao et al. (Yao et al., 2020), who presented a quick discharge device based on the immersion of the battery in $FeSO_4$ solution. Salt-water discharge processes are the currently dominant option across industrial operations with a series of reagent options being reported across literature studies (Neumann et al., 2022; Shaw-Stewart et al., 2019; Zhong et al., 2020). The discharged battery cells are fed to cell recycling by hydrometallurgical or pyrometallurgical processes. The chemistry-specific foreground LCIs for those processes were taken from Mohr et al. (2020), who modified the corresponding Ecoinvent inventories in order to accurately account for the metal constituents included in the cathode material and the cell housing of NMC battery cells. The LCI for the hydrometallurgical process can be traced back to data from the company Recupyl and for the pyrometallurgical process to the company Batrec. Both processes are currently commercial and have been further discussed by Sommerville et al. (2021) and Neumann et al. (2022). The shredding and sorting of the mixed metal waste of the packaging, BMS and TMS was modelled through an Ecoinvent inventory. Consequently, the aluminium, copper and steel fractions are sent to materials recovery operations, while plastics, electronics, the electrolyte and the coolant are modelled as waste for further treatment. The pre-treatment of aluminium scrap was modelled using an Ecoinvent inventory, while the melting and casting LCI was based on the Aluminium Association's LCA report (The Aluminumn Association, 2013). Steel scrap is sorted and pressed and then fed to an electric arc furnace, with the latter being modelled based on the LCI of Burchart-Korol (2013). Copper scrap is treated by electrolytic refining, based on the corresponding Ecoinvent LCI. The main data sources and assumptions for the compilation of the inventory are shown in **Table 16** and inventory tables of the LCI are presented and further discussed in Appendix B.

7.2.3 Materials recovery and crediting

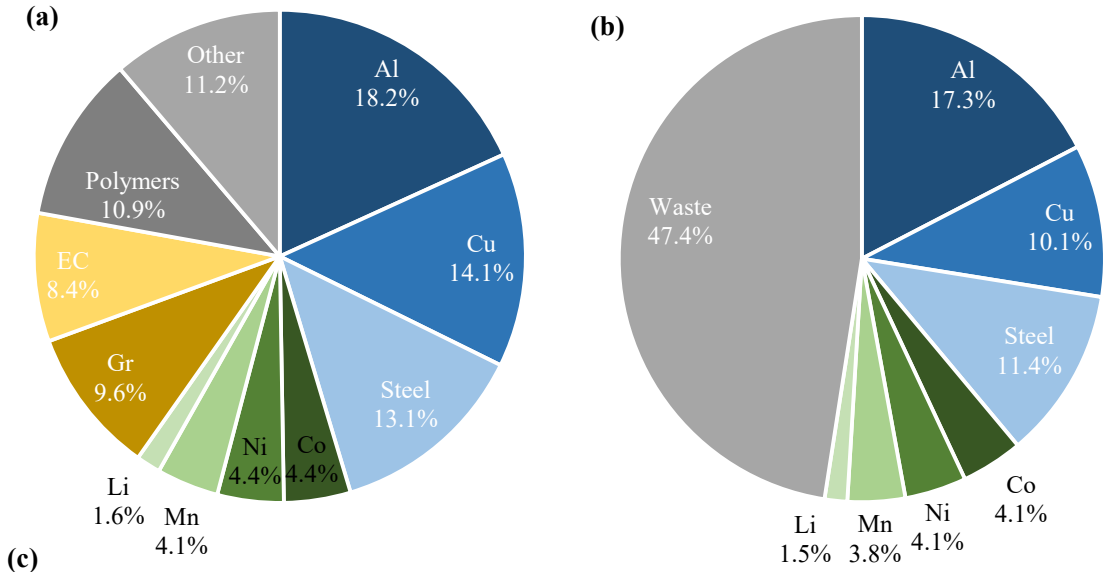
The 253 kg NMC333-Gr battery pack is broken down to its material composition in **Figure 37a**, which is in line with a series of preceding literature reports (Cusenza et al., 2019; Ellingsen et al., 2014; Kallitsis et al., 2020) . The EoL treatment chain shown in **Figure 36** recovers Al, steel and Cu from the battery's supporting structures, Li^{I} (as hydroxide), Co^{II}, Ni^{II} and Mn^{II} (all as sulfates) from the battery electrodes and elemental Cu, Al from the current collectors, with the recovery for the electrode materials being set to 93.6% and for Al, Cu to 93.8% for the hydrometallurgical process (Mohr et al., 2020). Similarly, the pyrometallurgical process recoveries were set to 93.6% for all materials (Mohr et al., 2020).

Table 16. Main data sources and assumptions for the compilation of the recycling LCI (Kallitsis et al., 2022a).

Unit process	Data source and assumptions
Collection & sorting	Battery transported firstly by freight rail and then by lorry with 32 tons load capacity based on Chinese average transport distance (Jiang et al., 2022)
	Estimated energy consumption for conveyor belt (Fisher et al., 2006) and electric forklift (Fuc et al., 2016) used in sorting.
Dismantling	Estimated energy consumption for robotic disassembly (Baazouzi et al., 2021; Choux et al., 2021)
Discharging	Inventory inspired by quick discharge device presented from Yao et al. (Yao et al., 2020)
Hydro-/Pyro-metallurgical treatment	Chemistry specific inventories for cell recycling are taken from Mohr et al. (2020)
Shredding and sorting	Material inputs and outputs complemented by Ecoinvent process: treatment of waste electric and electronic equipment, shredding
Al scrap preparation	Ecoinvent process: treatment of aluminium scrap, post-consumer, by collecting, sorting, cleaning, pressing, used to model processing inputs
Steel scrap preparation	Ecoinvent process: sorting and pressing of iron scrap, used to model processing inputs
Al melting and casting	Inventory inspired by The Aluminum Association (2013)
Steel melting and casting	Inventory inspired by Burchart-Korol (2013)
Electrolytic refining	Ecoinvent process: treatment of copper scrap by electrolytic refining, used to model processing inputs

Similar recovery rates for the electrode materials are considered realistic and have been adopted by a series of preceding studies, with the EverBatt model, for example, including recovery efficiencies of 98% for the key cathode materials (Dai et al., 2019b). Additionally, the recoveries for Al, steel and Cu from the Packaging, BMS and TMS were set to 95.5%, 86.8% and 76.3%, respectively. The recovered Al and Cu from the battery cells was fed to the corresponding melting and casting, and electrolytic refining processes in order to yield secondary materials with high purity. Materials available for recycling comprised 59.5% of the battery pack's mass (**Figure 37a**), with the remaining share modelled as waste for further treatment. **Figure 37b** presents the recovery of materials from hydrometallurgical recycling of the battery cells, with the combined recovery for each material resulting in the recovery of 52% of the battery pack's mass. Of those, 13.5% comprise cathode materials (Co^{II}, Ni^{II}, Mn^{II}, Li^{I}), while the highest share comes from the recovery of Al, steel and Cu, which are used widely in

the packaging, BMS, TMS and the current collectors. For the utilisation of a pyrometallurgical processing scheme, the recovery of Al and Cu from the current collectors are reduced by absolute 0.2%, having a negligible effect on the overall recovery for those metals, and Li^{I} is not recovered. The amounts of recovered materials for both cases are shown in Appendix B. The displaced materials shown in **Figure 37c** were modelled through corresponding Ecoinvent 3.5 datasets, with the exception of cobalt sulfate, which was modelled through the more recent Ecoinvent 3.8 dataset.



Recovered material	Al	Cu	Steel	Co^{II}	Ni^{II}	Mn^{II}	Li^{I}
Avoided material	Primary Al ingot	Primary Cu	Low-alloyed steel	$CoSO_4$	$NiSO_4$	$MnSO_4$	LiOH

Figure 37. (a) Mass composition of the 253 kg NMC333-Gr automotive traction battery pack, (b) recoverable fractions and waste occurring from the hydrometallurgical case and (c) displaced primary materials from the recovered metal fractions of the battery pack; stoichiometric elemental contributions are displayed for the cathode materials (Kallitsis et al., 2022a).

Figure 37c illustrates the displaced primary material from the recovery of metal fractions from the battery pack. For Al, Cu and steel, their recovery is followed by melting and casting or electrolytic refining as shown in **Figure 36**, which transform scrap to secondary material of sufficient quality to displace primary material. For battery electrode materials, recovered

material quality might not meet the requirements for battery production. This issue was addressed by assuming that recovered electrode materials are battery-grade as a baseline, in line with literature studies (Mohr et al., 2020), and further exploring the effect of recovered materials quality within a sensitivity analysis.



Figure 38. Schematic representation of the material and product flows of an integrated LIB production and recycling system; the utilisation phase is excluded from the calculations and is shown in grey (Kallitsis et al., 2022a).

Figure 38 provides further context on the crediting scheme employed in this study. After a battery is produced, it is utilised in an EV for over 10 years before reaching its EoL (as discussed in Chapter 6)(Lander et al., 2021b). Next, it can be repurposed for a second life or sent directly for recycling. Battery recycling introduces an additional environmental burden due to the materials and emissions associated with the processes implemented and a benefit due to the displacement of primary materials, upstream of the recycling product system. In order to estimate the net environmental benefit or burden of battery recycling the utilisation phase and second life must be excluded. The EoL treatment burden was then added to the production burden and any benefits are subtracted from the total. This yields the total environmental impact of production and recycling, which is then compared to the battery production impact to calculate the net environmental benefit or burden achieved through the introduction of LIB recycling across all impact categories of interest.

7.3 Results and analysis

7.3.1 Environmental impact of recycling

The environmental impact of battery recycling is presented in **Figure 39** for the pyrometallurgical and hydrometallurgical cases and broken down to the key contributing processes. Hydrometallurgical processing of the battery cells contributed 51% towards the GWP with an important contribution also arising from the electrolytic refining of copper

(19%). Similarly, 55% and 18% of the FDP arose from cell recycling and electrolytic refining of copper, respectively. The SODP was also dominated by the cell recycling (63%) and electrolytic refining of copper (23%) processes. Similarly, cell recycling and electrolytic refining of copper constituted the dominant contributions towards POFP, FPMFP, TAP and FEP. In the pyrometallurgical case, the GWP, FDP and POFP were increased by 25%, 21% and 30%, respectively, mainly attributed to the almost six times higher electrical energy consumption compared to the hydrometallurgical case; with the remaining impact categories variating by less than 5%.

The FEP was dominated by the electrolytic refining of copper, which contributed more than 75% in both cases. The MEP was built up from the shredding and sorting, aluminium melting and casting, and the cell recycling processes. More than 96% of the FETP and the METP arose from the preparation of aluminium scrap in both cases. The electrolytic refining of copper comprised the primary contribution towards TETP and MDP, while the steel melting and casting process dominated the HTP.

Impact of Recycling		Functional Unit Capacity [kW h]	Contribution Analysis
Hydrometallurgical Case			
GWP	*kg CO_2-eq*	12.7	
FDP	*kg oil-eq*	3.96	
SODP	*kg CFC-11-eq*	7.2×10^{-6}	
POFP	*kg NOx-eq*	0.04	
FPMFP	*kg $PM_{2.5}$-eq*	0.035	
TAP	*kg SO_2-eq*	0.076	
FEP	*kg P-eq*	0.018	
MEP	*kg N-eq*	3.21×10^{-3}	
FETP	*kg 1,4-DCB-eq*	19.1	
METP	*kg 1,4-DCB-eq*	23.0	
TETP	*kg 1,4-DCB-eq*	286	
HTP	*kg 1,4-DCB-eq*	5.02	
MDP	*kg Cu-eq*	0.299	
Pyrometallurgical Case			
GWP	*kg CO_2-eq*	15.8	
FDP	*kg oil-eq*	4.81	
SODP	*kg CFC-11-eq*	7.5×10^{-6}	
POFP	*kg NOx-eq*	0.05	
FPMFP	*kg $PM_{2.5}$-eq*	0.037	
TAP	*kg SO_2-eq*	0.074	
FEP	*kg P-eq*	0.018	
MEP	*kg N-eq*	3.21×10^{-3}	
FETP	*kg 1,4-DCB-eq*	19.1	
METP	*kg 1,4-DCB-eq*	22.9	
TETP	*kg 1,4-DCB-eq*	279	
HTP	*kg 1,4-DCB-eq*	5.07	
MDP	*kg Cu-eq*	0.308	

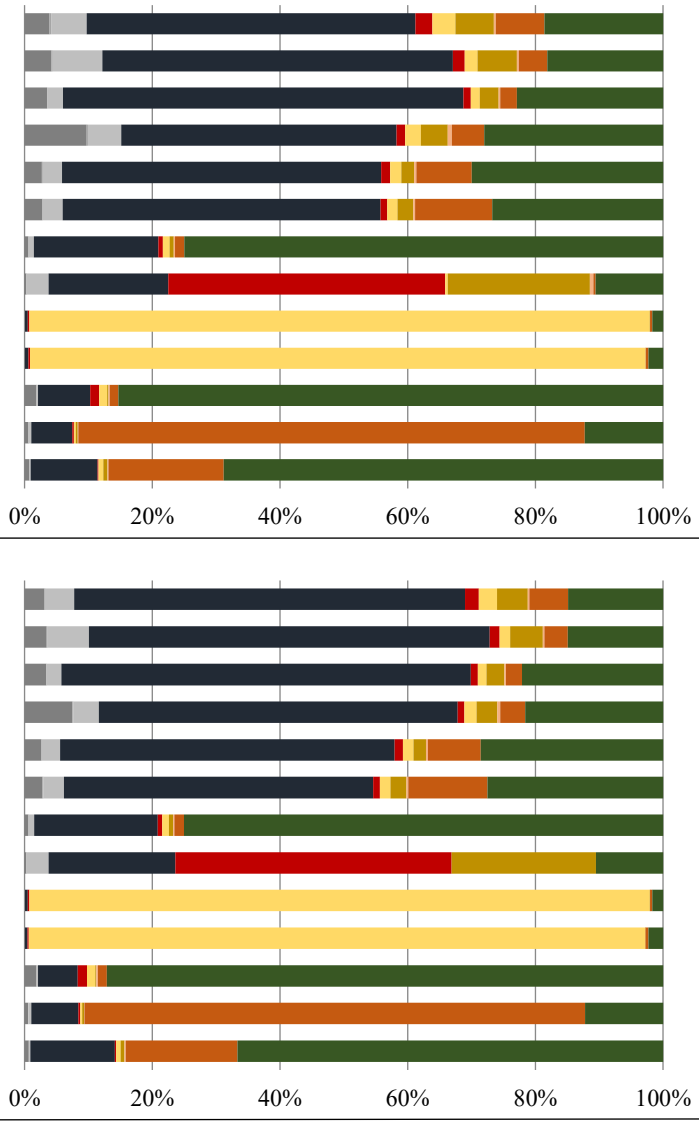


Figure 39. Environmental impacts of an NMC333-Gr battery pack recycling in China, disaggregated to key contributing processes. Battery cells are treated with either hydrometallurgical or pyrometallurgical processing in the two cases (Kallitsis et al., 2022a).

7.3.2 Environmental benefit of recycling

The recycling chain modelled in this study recovers Al, Cu and steel from the battery pack's supporting structures and Al, Cu, Ni^{II}, Co^{II}, Mn^{II} and Li^{I} from the battery cells, with the latter being recovered only in the case of hydrometallurgical processing. Specifically, the hydrometallurgical case recovered 26.1 kg of $NiSO_4$, 26.3 kg of $CoSO_4$, 25.5 kg of $MnSO_4$ and 12.4 kg of LiOH from the battery cells. Additionally, 44.5 kg of Al, 29 kg of steel and 26.2 kg of Cu were recovered from the 253 kg battery pack's supporting structures and the current collectors. The fraction of materials recovered in the pyrometallurgical case were very similar, as presented in Section 7.2.3, excluding LiOH, which was not recovered. More information on the background datasets used to model materials displacement is provided in Appendix B.

The environmental benefit arising from the recovery of the battery pack's materials is illustrated in **Figure 40**. The hydrometallurgical case resulted in a larger benefit by a maximum of 3% across all impact categories, with the exception of MEP (9%) and MDP (8%), due to the additional recovery of lithium as hydroxide. For both cases, approximately half of the GWP benefit was due to the recovery of aluminium, with the next most important contribution coming from the recovery of Co^{II}. Similarly, approximately half of the FDP benefit was due to the recovery of cobalt, with the next most important contribution coming from aluminium. Recovered copper, Co^{II} and aluminium provided the dominant contributions towards the POFP and SODP benefits. Recovered Ni^{II} provided the primary contribution towards the FPMFP and TAP benefits. The eutrophication and ecotoxicity impact categories were dominated by the recovery of copper and Co^{II}, with 9% of the MEP benefit arising from the recovery of Li^{I} in the hydrometallurgical case. The MDP benefit was dominated by the recovery of Co^{II}, with Ni^{II}, copper and Li^{I} having also important contributions. The percentage contribution of lithium recovery in MDP and MEP explains the larger benefit achieved in the hydrometallurgical case.

Benefit of Recycling		Functional Unit Capacity [kW h]	Contribution Analysis
Hydrometallurgical case			
GWP	*kg CO_2-eq*	-77.7	
FDP	*kg oil-eq*	-28.7	
SODP	*kg CFC-11-eq*	-5.8×10^{-5}	
POFP	*kg NOx-eq*	-0.278	
FPMFP	*kg $PM_{2.5}$-eq*	-0.672	
TAP	*kg SO_2-eq*	-2.01	
FEP	*kg P-eq*	-0.23	
MEP	*kg N-eq*	-0.013	
FETP	*kg 1,4-DCB-eq*	-10.0	
METP	*kg 1,4-DCB-eq*	-15.2	
TETP	*kg 1,4-DCB-eq*	-6,411	
HTP	*kg 1,4-DCB-eq*	-18.9	
MDP	*kg Cu-eq*	-13.4	
Pyrometallurgical case			
GWP	*kg CO_2-eq*	-74.9	
FDP	*kg oil-eq*	-27.8	
SODP	*kg CFC-11-eq*	-5.7×10^{-5}	
POFP	*kg NOx-eq*	-0.270	
FPMFP	*kg $PM_{2.5}$-eq*	-0.671	
TAP	*kg SO_2-eq*	-2.00	
FEP	*kg P-eq*	-0.23	
MEP	*kg N-eq*	-0.012	
FETP	*kg 1,4-DCB-eq*	-10.0	
METP	*kg 1,4-DCB-eq*	-15.1	
TETP	*kg 1,4-DCB-eq*	-6,398	
HTP	*kg 1,4-DCB-eq*	-18.7	
MDP	*kg Cu-eq*	-12.4	

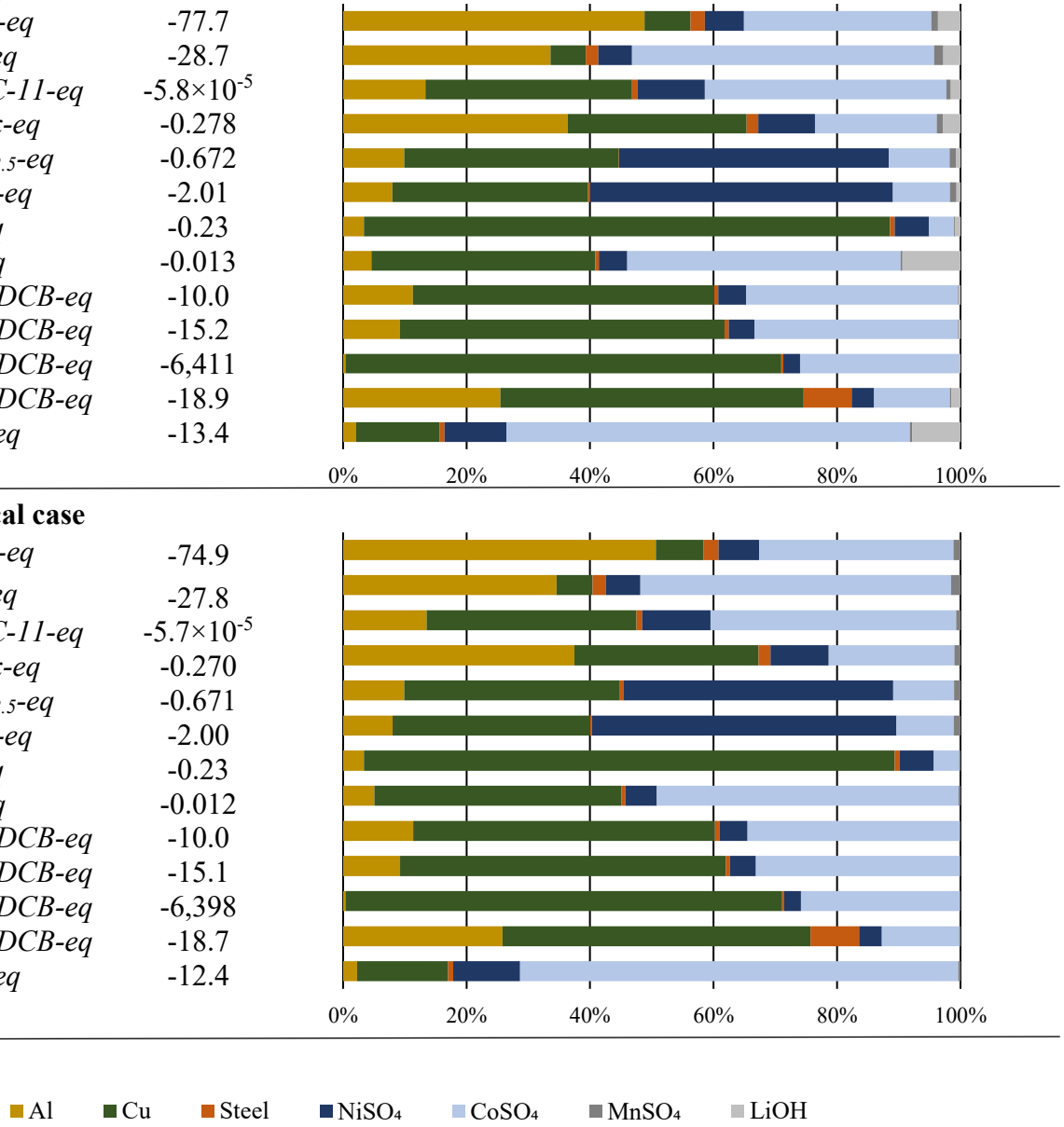


Figure 40. Environmental benefits of an automotive NMC333-Gr battery pack recycling in China, disaggregated to key contributing processes. Environmental benefits arose from the displacement of primary material based on the EoL recycling approach (Kallitsis et al., 2022a).

7.4 Discussion

7.4.1 Reducing the environmental impact of battery production

The net benefit of battery recycling is commonly accounted together with the environmental burden of LIB production to investigate to what extent the use of recycled material in the battery value chain reduces the production burden. The LIB production model of Kallitsis et al. (2020) was used here to calculate the environmental burden of battery production across the 13 impact categories of interest; the inventory model was modified to describe a giga-scale battery production plant (Kallitsis, 2022), to account only for primary material inputs and update the cobalt production inventory based on Ecoinvent 3.8. The combined production and recycling burden is shown in **Table 17**, including all the individual contributions. For both cases, accounting for battery pack recycling resulted in a net environmental benefit across 11 impact categories, with the exception of FETP and METP. The treatment of Al scrap introduced a significant burden to the latter two impact categories, resulting in a net increase of 61% and 35%. For the hydrometallurgical case, the GWP, FDP, SODP, POFP, FPMFP and TAP were reduced by 39%, 41%, 55%, 48%, 70% and 74%, respectively. As these impact categories had their most important contributions from the cell recycling process, the benefits were of slightly lower magnitude in the pyrometallurgical case, due to the increased energy consumption and the loss of Li^{I}. Benefits of more than 50% were achieved for FEP and TETP, with hydrometallurgical and pyrometallurgical cases resulting in quantitatively similar improvements. The MEP benefit of the hydrometallurgical case was 52%, absolute 7% higher than the pyrometallurgical case, with the variation in the former attributed solely to the recovery of Li^{I}, which also caused a higher MDP benefit of 84%, compared to 77% in the pyrometallurgical case. Finally, the HTP was approximately halved in both cases, with a slightly larger benefit predicted in the hydrometallurgical case, due to the additional recovery of lithium(I).

NMC battery packs have been shown to have significant GWP footprints, resulting from processing of energy intensive materials and the high energy demand of cathode preparation and cell manufacturing (Dai et al., 2019a; Ellingsen et al., 2014; Kallitsis, 2022; Kelly et al., 2019; Majeau-Bettez et al., 2011). This work has shown that establishing a circular battery value chain can reduce LIBs' production GWP footprint by more than 35%, with this benefit mostly due to the recovery of aluminium, which comes from recycling the battery packaging,

as its energy intensive primary production in China comes with a high GWP. Nickel and copper production have been identified as hotspots for sulfur dioxide emissions (Kallitsis et al., 2022b; Kelly et al., 2019) resulting from the battery production chain; the recovery of those materials was predicted to reduce the TAP by more than 70%. While earlier studies have raised concerns for the increased HTP occurring from the production of battery packs (Brennan and Barder, 2016; Hawkins et al., 2013), HTP was shown here to reduce by approximately 50% when including battery recycling, compared to Kallitsis et al.'s (2020) battery production model. LIB recycling was also shown to significantly avoid depletion of valuable metals, with the MDP reducing by 84% and 77% in the hydrometallurgical and pyrometallurgical case, respectively. Overall, EoL treatment of spent automotive traction battery packs was shown to mitigate the environmental impact across the majority of environmental categories.

Table 17. Environmental impact of battery production, burden and benefit of battery recycling and their combined effect in the environmental footprint of an NMC333-Gr battery pack. The "Total" is calculated as the sum of the production burden, recycling burden and benefit and "Net" refers to the net benefit on battery production when including recycled material,which is calculated as a percentage comparison between the "Total" and the production burden (Kallitsis et al., 2022a).

Impact per capacity [kW h]		**Production**	**Hydrometallurgical case**				**Pyrometallurgical case**			
	Units	Burden	Burden	Benefit	Total	Net [%]	Burden	Benefit	Total	Net [%]
GWP	*kg CO_2-eq*	168.8	12.7	-77.7	103.7	-39	15.8	-74.9	109.8	-35
FDP	*kg oil-eq*	59.8	3.96	-28.7	35.1	-41	4.81	-27.8	36.7	-39
SODP	*kg CFC-11-eq*	9.3×10^{-5}	7.2×10^{-6}	-5.8×10^{-5}	4.2×10^{-5}	-55	7.5×10^{-6}	-5.7×10^{-5}	4.32×10^{-5}	-54
POFP	*kg NOx-eq*	0.508	0.04	-0.278	0.265	-48	0.05	-0.270	0.283	-44
FPMFP	*kg $PM_{2.5}$-eq*	0.906	0.035	-0.672	0.269	-70	0.037	-0.671	0.271	-70
TAP	*kg SO_2-eq*	2.61	0.076	-2.01	0.68	-74	0.074	-2.00	0.69	-74
FEP	*kg P-eq*	0.32	0.018	-0.23	0.11	-67	0.018	-0.23	0.11	-66
MEP	*kg N-eq*	0.019	3.21×10^{-3}	-0.013	0.009	-52	3.21×10^{-3}	-0.012	0.011	-45
FETP	*kg 1,4-DCB-eq*	15.0	19.1	-10.0	24.1	60	19.1	-10.0	24.1	61
METP	*kg 1,4-DCB-eq*	22.1	23.0	-15.2	39.9	35	22.9	-15.1	30.0	35
TETP	*kg 1,4-DCB-eq*	7932	286	-6411.6	1806	-77	279	-6398.8	1813	-77
HTP	*kg 1,4-DCB-eq*	24.2	5.02	-18.9	12.2	-53	5.07	-18.7	12.5	-52
MDP	*kg Cu-eq*	6.09	0.299	-13.4	2.60	-84	0.308	-12.4	3.66	-77

7.4.2 Sensitivity analyses

The geographic specificity of the battery value chain is an important factor when estimating the environmental benefit and burden of battery recycling, as it affects emissions at local level, depends on a varying intensity of embodied emissions from local energy use, and also dictates the effective footprint adjustment required for the displaced material. Moreover, the effect of

recovered materials quality on the overall environmental benefit of battery pack recycling remains to be characterised. Here, two sensitivity analyses were performed concerning (a) the effect of geographic specificity on the combined production and recycling GWP and (b) the effect of recovered material's quality on all environmental impact categories studied. For the geographic specificity, GWP was chosen for the analysis as it reflects clearly the energy mix related benefits and impacts, which vary substantially across geographic locations.

The LIB production impact was combined with the recycling burden and benefit of this study to estimate the combined GWP of LIBs in China, North America and Europe, excluding the use phase. In order to calculate the LIB production impact, representative Ecoinvent inventories for each location were selected for electricity, aluminium and copper production, which are shown in Appendix B. The burden and benefit of battery recycling was calculated for each case by modifying the input electricity and the displaced primary material sourcing for Al and Cu, with the remaining materials being modelled through global Ecoinvent inventories across all scenarios. Al and Cu are considered specifically as their footprints vary highly across locations and they contribute substantially to the GWP. By modifying the background datasets for Al and Cu it is possible to provide a realistic comparison, as more than 55% of the GWP benefit arose from their recovery (see **Figure 40**). Remaining battery cell materials were produced through globally distributed supply chains. This is appropriate as active material mining and processing ($NiSO_4$ and $CoSO_4$) is geographically concentrated in only a few countries around the world; therefore, capturing any differences from sourcing of the active materials used in the US, China and Europe would only be due to transportation distance impacts, which are much smaller and also less variable than the footprint of production of the active materials. On the production side, approximately 60% of the NMC LIB production GWP was due to the energy requirement, Cu and Al inputs, based on the modified model of Kallitsis et al. (2020). This analysis assumes that only input materials and energy vary across locations, with the manufacturing and recycling technologies being practically the same. This assumption also allows to explore the effect of establishing regionalised battery production and recycling chains, considering that secondary material displaces the equivalent amount of primary material in the same region. The modifications for each scenario are described in detail in **Table 18**.

Table 18. Background Ecoinvent datasets used for the investigation of geographic specificity effects to the combined production and recycling GWP (Kallitsis et al., 2022a).

Dataset	China	North America	Europe
Electricity	CN: market group for electricity, medium voltage	RNA: market group for electricity, medium voltage	RER: market group for electricity, medium voltage
Aluminium	CN: aluminium production, primary, ingot	RNA: aluminium production, primary, ingot	IAI Area, EU27 & EFTA: aluminium production, primary, ingot
Copper	RAS: copper production, primary	RNA: copper production, primary	RER: copper production, primary

Figure 41 illustrates the GWP of battery production compared to the combined GWP of production and EoL recycling in China, North America and Europe. Including recycling resulted in a net benefit of 39% and 35% for the hydrometallurgical and pyrometallurgical cases in China, which was reduced to 34% and 30% for North America, and 30% and 27% for Europe, respectively. Evidently, larger GWPs of battery production offer a bigger opportunity for improvement, with a battery produced in Europe shown here to come with a 27% lower GWP compared to a battery produced in China, with the relative difference reduced to approximately 16% when recycling is considered. This demonstrates how regions with high battery production emissions such as China can utilise battery recycling as a method to catch up on the race to reduce the GWP of battery production.

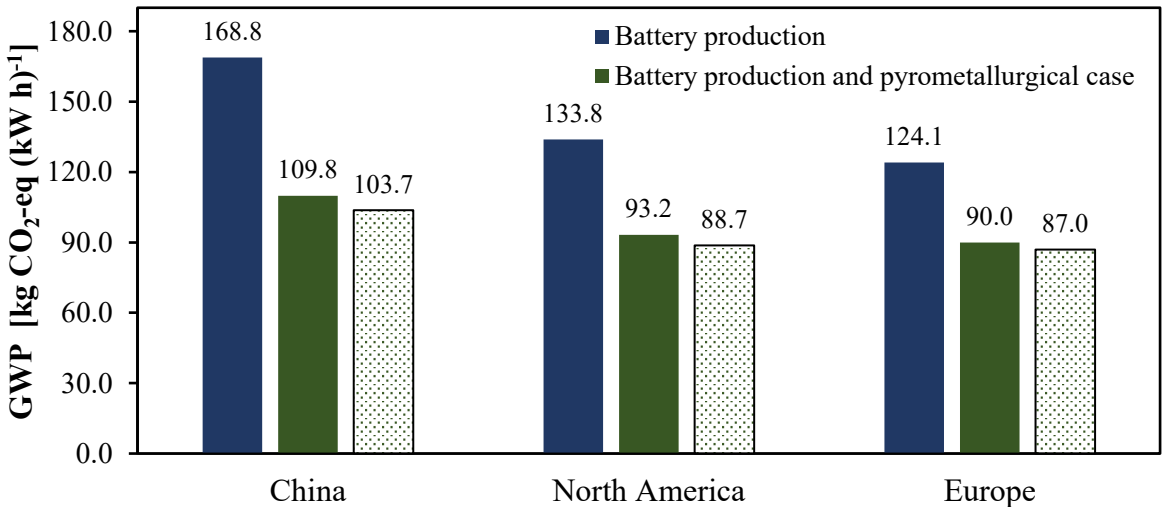


Figure 41. GWP of LIB production compared to production with EoL recycling for the hydrometallurgical and pyrometallurgical cases in China, North America and Europe (Kallitsis et al., 2022a).

The effect of recovered materials quality on the environmental benefit of LIB recycling was explored by displacing the equivalent amount of ore-grade (OG) materials instead of battery-

grade (BG) for Ni^{II}, Co^{II}, Mn and Li^{I}. The percentages of each metal included in the concentrated OG form was taken into account in order to convert the recovered materials in elemental form into ore grade materials as shown in **Table 19**. **Figure 42** presents the hydrometallurgical case, with the pyrometallurgical case not recovering lithium but being quantitatively similar for the recovery of the remaining materials.

Table 19. Displaced material datasets for the battery-grade (BG) vs ore-grade (OG) cases (Kallitsis et al., 2022a).

Recovered material	OG	Reference scenario (BG)
Ni	GLO: market for nickel ore, beneficiated, 16%	GLO: market for nickel sulfate
Co	GLO: market for cobalt	RoW: market for cobalt sulfate, ecoinvent 3.8
Mn	GLO: market for manganese concentrate	GLO: market for manganese sulfate
Li	GLO: market for lithium brine, 6.7% Li	GLO: market for lithium hydroxide

The POFP, FEP and HTP benefits were reduced by less than 15% when accounting for the recovery of OG material, due to the fact that the majority of the environmental benefit in those impact categories arose from the recovery of Al and/or Cu from the battery pack. The benefit in the ecotoxicity impact categories, SODP and GWP was reduced by 20% to 40%, which is reasonable given that electrode materials contribute to these impact categories significantly but are not the primary contributors. However, for those impact categories dominated by the recovery of cobalt and nickel (namely FDP, FPMFP, TAP, MEP and MDP) the benefit in the OG case was decreased by 40% to 60%. Specifically, the FPMFP and TAP benefits were reduced by 52% and 58%, respectively, in the OG case mainly due to the recovery of nickel of ore-grade quality, as the further processing of nickel ore is known to have a detrimental effect in those environmental impact categories (Norgate et al., 2007; Paulikas et al., 2020b). Similarly, cobalt refining is known to cause detrimental eutrophication impacts and consume fossil energy, which explains the large variability between the FDP and MEP benefits of the OG and BG cases (Paulikas et al., 2020b). A recent study by Rajaeifar et al. (2021) employed such multi-functionality approach in quantifying the impact of recovering OG materials versus BG materials. However, their system boundary was limited to pyrometallurgical cell recycling and only quantified implications associated with the GWP. Their findings showed that the GWP benefit reduces more than 50% when recovering lower grade materials in comparison to 28% decrease reported here. The difference can be attributed to the narrower system boundary

of Rajaeifar et al. (2021); our study showed that recovering cell materials is only a fraction of the benefit of recycling a battery pack. This work has also shown that the effect of recovering lower grade materials is much more evident in impact categories such as FDP, FPMFP, TAP, MEP and MDP, which was not captured by Rajaeifar et al. (2021).

Impact category	**Units**	**Benefit per capacity [kW h]**	
GWP	*kg CO_2-eq*	BG	-77.7
		OG	-52.5
FDP	*kg oil-eq*	BG	-28.7
		OG	-13.9
SODP	*kg CFC-11-eq*	BG	-5.8×10^{-5}
		OG	-3.9×10^{-5}
POFP	*kg NOx-eq*	BG	-0.278
		OG	-0.256
FPMFP	*kg $PM_{2.5}$-eq*	BG	-0.672
		OG	-0.322
TAP	*kg SO_2-eq*	BG	-2.01
		OG	-0.85
FEP	*kg P-eq*	BG	-0.23
		OG	-0.22
MEP	*kg N-eq*	BG	-0.013
		OG	-0.006
FETP	*kg 1,4-DCB-eq*	BG	-10.0
		OG	-6.4
METP	*kg 1,4-DCB-eq*	BG	-15.2
		OG	-9.8
TETP	*kg 1,4-DCB-eq*	BG	-6,411
		OG	-4,598
HTP	*kg 1,4-DCB-eq*	BG	-19.0
		OG	-16.2
MDP	*kg Cu-eq*	BG	-13.5
		OG	-7.97

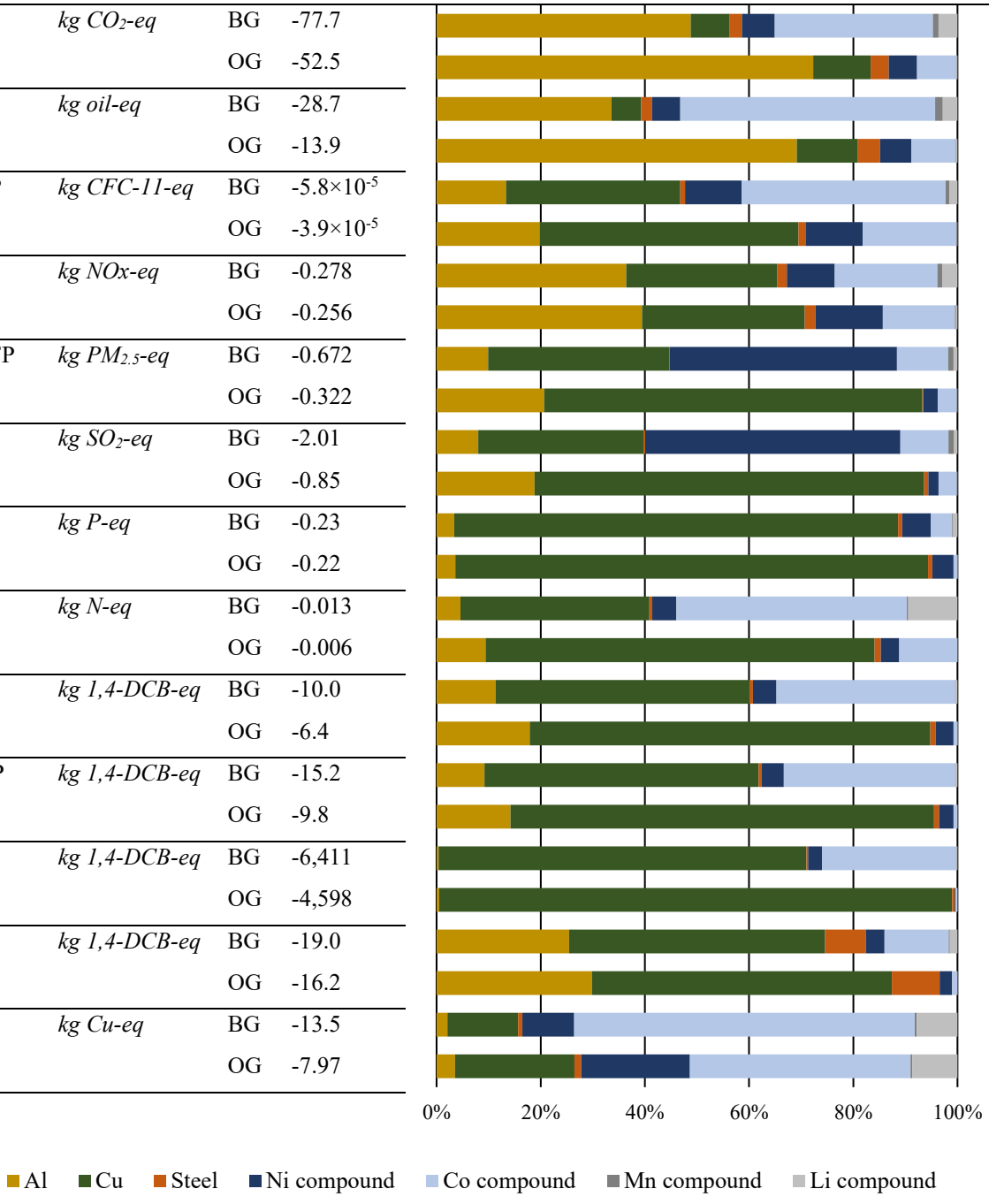


Figure 42. Environmental benefit for battery-grade (BG) vs ore-grade (OG) material recovery in the case of hydrometallurgical treatment (Kallitsis et al., 2022a).

Overall, this sensitivity analysis has shown that the positive impact of recycling is more significant when considering the effective displacement of BG quality materials in the value chain, especially in the FDP, FPMFP, TAP, MEP and MDP impact categories, thus supporting strongly the case for integration of regionalised battery production and recycling facilities. The quantitative evidence provided here offers a valuable methodological resource for LCA practitioners and supports decision making for recyclers and policy-makers interested in establishing sustainable battery recycling operations.

7.4.3 LIB recycling environmental performance and comparison with preceding studies

Two key observations are made based on the findings of this study, which help explain the variability on preceding literature studies that consider recycling, as shown in **Table 15**. Firstly, the majority of the environmental benefits of battery recycling arise from the recovery of Al and Cu fractions of the battery pack (**Figure 40**), with important contributions also arising from the recovery of nickel and cobalt from the electrodes. Therefore, studies focusing on the cell level only are expected to report lower benefits, as compared to those focusing on pack level recovery. Secondly, geographic specificity plays an important role on the calculated net benefit of battery recycling, with more environmentally burdening chains expected to come with higher net benefits when recycling is introduced (**Figure 41**). Ciez and Whitacre (2019) reported insignificant GWP intensity reductions achieved through hydrometallurgical and pyrometallurgical processing of NMC battery cells; the latter resulted in a net increase. More recently, Mohr et al. (2020) reported a -13.8 and -16.4 kg CO_2-eq $(kW\ h)^{-1}$ net benefit achieved through hydrometallurgical and pyrometallurgical processing of NMC battery cells. These observations are reasonable, given that these studies focused on cell level and modelled less environmentally burdening chains outside of China. Cusenza et al. (2019) reported a -15.4 kg CO_2-eq $(kW\ h)^{-1}$ net benefit for pack level recycling of a LMO-NMC333, while Sun et al. (2020) reported a -30.9 kg CO_2-eq $(kW\ h)^{-1}$ net benefit for hydrometallurgical recovery of NMC622. While both studies focused on pack level, the former modelled a European and the latter a Chinese recycling chain, so partly explaining the large variability together with the different chemistries modelled in each study. Additionally, Cusenza et al. (2019) modelled a combined hydrometallurgical-pyrometallurgical recycling scheme, which was also modelled by Zhou et al. (2021), and was more environmentally burdening. A similar scheme was modelled by Accardo et al. (2021), reporting recycling to come with a net benefit of -6.2 kg CO_2-eq $(kW\ h)^{-1}$ in Europe. This study's net benefit for pyrometallurgical recovery through a

European recycling chain was -34.1 kg CO_2-eq (kW h)$^{-1}$, with the difference attributed to the more environmentally burdening hydrometallurgical-pyrometallurgical recycling scheme modelled by Accardo et al. (2021). Moreover, in this study the displaced cobalt sulfate (based on the latest Ecoinvent 3.8 database) was shown to comprise the second most important contribution towards GWP reductions. The net recycling benefit for the hydrometallurgical case in China was -65.1 kg CO_2-eq (kW h)$^{-1}$ here, while Sun et al. (2020) reported a net benefit of -30.9 kg CO_2-eq (kW h)$^{-1}$ for similar parameters. Although the contributions of the recycling burden and benefit to the net benefit in Sun et al. (2020) were not reported, the difference can be mainly attributed to the updated cobalt sulfate inventory utilised herein, which was found to contribute 30% towards the GWP benefit. Another key source of variability is associated with varying NMC compositions resulting in different energy densities. This becomes more evident when looking at the sensitivity analysis performed by Mohr et al. (2020), who reported that increasing the energy density reduces the combined production and recycling burden given that under the same mass a higher capacity is achieved when shifting to higher nickel chemistries primarily affecting the kW h functional unit.

7.4.4 Recovered materials value

This study highlighted the need to recover the total set of battery pack materials in order to achieve maximum environmental benefits from LIB recycling. From an environmental perspective, benefits arise primarily from the recovery of Al and Cu from the battery pack. Here, the economic value for each recovered material in the hydrometallurgical and pyrometallurgical cases is calculated. Elemental prices were extracted from United States Geological Survey (USGS) (2020) for 2019 and multiplied by the amount of each recovered material to estimate the economic benefit achieved from the recovery of each battery material. The price of each recovered material is shown in **Table 20**. The average cash price of each material on the London Metal Exchange (LME) is also shown in **Table 20** for reference. Steel, Co, Ni, Al and Cu prices are similar, however this is not the case for Li. The USGS 2019 values were used in the calculations presented this study as they are an internally consistent set. The Mn price was sourced from (Federal Institute for Geosciences and Natural Resources, 2019) as it is not included in USGS source publication. The amount of recovered material was multiplied by its price to create **Figure 43**.

As currently recovered materials may not be of sufficient quality to displace primary material of the same price, **Figure 43** should be seen as an indication of what is possible, when recycled

material quality issues are resolved. Also, It should be noted that price volatility is typical in raw materials and is affected by many short- and longer-term geopolitical factors, thus the analysis of recovered materials value presented here should be taken as indicative snapshot in time, for the purpose of comparing the hydrometallurgical and pyrometallurgical options.

Table 20. Prices of recovered materials from the battery pack in 2019 (Kallitsis et al., 2022a).

Recovered material	USD kg^{-1}		Comments
	This study	LME	
Al	2.2	1.7	Based on U.S. annual average spot price of Al ingot
Cu	6.2	6.7	Based on U.S. annual average spot price for cathode Cu
Steel	0.266	0.289	Based on no.1 heavy melting composite annual price average
Co	37.5	33.5	Based on U.S. annual average spot price for cathode Co
Ni	14	14.9	Based on London Metal Exchange annual price average, contained Ni
Mn	1.82	n/a	Based on annual price average for electrolytic manganese, min. 99.7% pure (Federal Institute for Geosciences and Natural Resources, 2019)
Li	69	96	Based on U.S. annual price average of battery grade lithium carbonate, contained Li

The value of recovered material in the hydrometallurgical case was USD 1 079, 32% higher than in the pyrometallurgical case. This is connected directly to the additional recovery of Li^{I} through hydrometallurgical processing of the battery cells, which accounted for a quarter of the total (**Figure 43a**). The recovery of Ni^{II}, Co^{II}, Mn (as sulfates) and Li^{I} (as hydroxide) accounted for three quarters of the total economic value of recovered materials in the hydrometallurgical case (**Figure 43a**) and the recovery of Ni^{II}, Co^{II} and Mn^{II} (sulfates) accounted for 67.8% of the total in the pyrometallurgical case (**Figure 43b**). While the recovery of lithium (hydroxide) contributed less than 6% in 11 out of 13 environmental impact categories studied (**Figure 40**), it increased the economic value of recovered materials by 32% in the hydrometallurgical case. The two cases have different capital and operational cost patterns, which were not examined in this study, but the recovery of Li (hydroxide) is indeed an important factor on the economic viability of recycling operations. Finally, while environmental benefits primarily arose from the recovery of Al and Cu, economic benefits primarily arose from the recovery of cell materials, Ni^{II}, Co^{II} (sulfates) and Li^{I} (hydroxide), which highlights the need to target circularity at a pack level to unlock both the environmental and economic benefits of battery recycling.

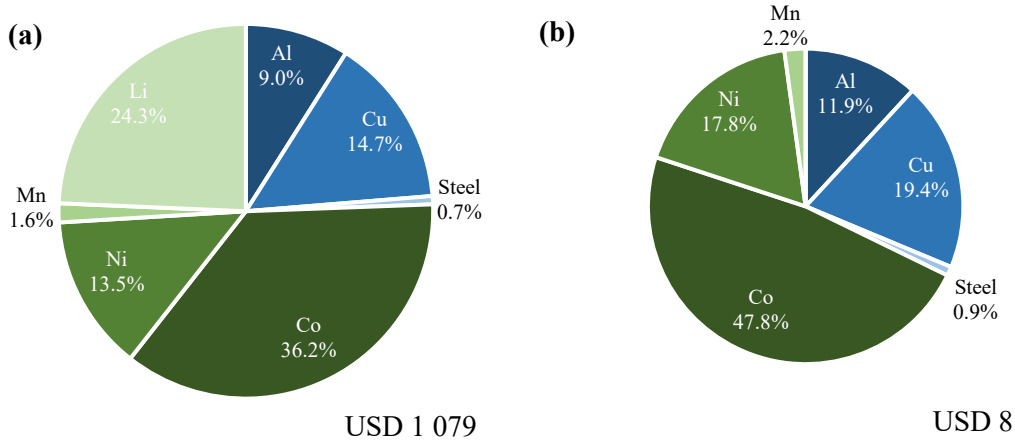


Figure 43. Economic value of recovered material for one battery pack using the (a) Hydrometallurgical (total: USD 1 079) and (b) Pyrometallurgical (total: USD 816) processes (Kallitsis et al., 2022a).

7.4.5 Data gaps, limitations and future perspectives

This study aimed to expand the description of the EoL treatment of automotive LIBs, from the point of collection to displacement of primary material, and to fill data gaps by combining a series of publicly available data sources. However, a series of improvements in the LCI could be made through the collection of process specific data. This study utilised Chinese average transport distances to model the collection of spent LIB packs and showed that its contribution to the overall environmental burden of battery recycling is insignificant, in line with Jiang et al. (2022). However, the collection process has been reported to be significant from an economic and safety perspective (Lander et al., 2021a; Slattery et al., 2021). As automotive LIB recycling is under development, average transportation distances could be confirmed through a more thorough investigation of EoL LIB collection and transportation networks. A first attempt to compile an inventory robotic disassembly was made in this study by calculating the energy inputs for robotic dismantling, assuming insignificant contributions from non-energy related inputs. As robotic dismantling is under development, with manual dismantling being the currently dominant practice (Sommerville et al., 2021) more complete inventories should be compiled as the technology matures. The dismantling process was found here have to have an insignificant contribution to the overall environmental burden of battery recycling. Rajaeifar et al. (2022) also indicate that the significance of dismantling is most evident with regard to the cost and safety perspectives. The discharging inventory was inspired from the quick discharge device presented by Yao et al. (2020), under the assumption that LIBs are

discharged on cell level. Different physical and chemical discharging techniques are being developed, which might dominate in the future and come with a different environmental profile.

The battery cell recycling inventory was inspired from Mohr et al. (2020), with the original data traced back to the Ecoinvent database. Currently, there is a lack of primary data regarding hydrometallurgical and pyrometallurgical cell recycling techniques which could be improved as more LIB recycling plants reach commercial scale. Also, the fate of the anode material in cell recycling operations is still uncertain, which explains why it has been treated as waste in this work. Current pyrometallurgical process usually burn graphite for energy, together with plastics and the electrolyte, while little is known regarding the fate of graphite in hydrometallurgical processes (Sommerville et al., 2021). More advanced options, which include the recovery of graphite and have been shown to be favourable from an environmental perspective have been discussed in recent studies (Mohr et al., 2020; Rey et al., 2021), however, whether these can be sustained at scale is unclear and would depend on the economics. Graphite has been recognised as a valuable waste stream from recycling processes (Rinne et al., 2021) but its recovery usually requires further process steps, which is indeed worth of further investigation as it is an important contribution to the overall mass of the battery pack (Porzio and Scown, 2021).

Also, the quality of recycled material is important, as it determines whether recovered cell materials can be recirculated to LIB production in a closed-loop system. Regarding the LIB pack's packaging, TMS and BMS, the process chains to recover Al, Cu and steel from them are well-established. An Ecoinvent inventory was used here to model shredding of this mixed metal waste. The different environmental profile achieved through the displacement of ore-grade materials was explored in the sensitivity analysis. The examination of locality effects on the environmental burdens and benefits of LIB recycling was found to be an important source of variability, mainly due to different footprints of displaced materials. As upstream battery material production chains emerge outside of China, the environmental benefit of battery recycling is expected to come with even higher variability across different locations.

7.5 Conclusions

Establishing a circular battery value chain was shown to mitigate the environmental impacts significantly across the majority of environmental impact categories considered. Specifically, employing hydrometallurgical or pyrometallurgical battery cell recycling schemes, together with the recovery of metal fractions from battery packs' supporting structures was shown to reduce the environmental burden of battery production by more than 35% across 11 out of 13 environmental impact categories considered. Pyrometallurgical processing of battery cells was associated with a greater GWP burden, so a slightly smaller benefit, mainly due to the almost six times higher electrical energy consumption. The hydrometallurgical case resulted in a larger benefit by a maximum of 9% for the MEP, due to the additional recovery of lithium hydroxide. The majority of the environmental burdens in the toxicity and ecotoxicity categories arose from the recovery chains for aluminium, copper and steel. Half of the GWP benefits were achieved from the recovery of aluminium, mainly included in the battery pack's packaging. Across the 13 impact categories considered, the recovery of Al and Cu provided more than half of the environmental benefit in 7 of them, highlighting their significance in reducing the total environmental impact of a battery pack. However, the recovery of battery cathode materials, especially nickel and cobalt, was shown to make an important contribution to the air quality, toxicity and resource depletion categories. These results highlight the importance of targeting circularity at the pack level to establish sustainable LIB recycling chains. The combination with the LIB production burden revealed that LIB recycling approximately mitigates the TAP by 74%, MDP by 77%, HTP by 50% and GWP by 35%. The investigation of geographic specificity effects on the combined production and recycling GWP revealed that more environmentally burdening chains offer a significantly higher potential for GWP reductions through battery recycling and that geographic specificity accounts for significant variability amongst LCA studies on LIB recycling. As a significant fraction of the environmental benefits arose from the recovery of Al and Cu from the battery pack, together with geographic specificity were found to constitute key sources of variability amongst literature studies reporting results for varying system boundaries and locations of focus.

Decision makers and other stakeholders concerned about the environmental impacts of the LIB value chain can take steps towards their reduction. Firstly, they should target circularity on a pack level, which was shown to unlock the environmental benefits potential of battery

recycling, as compared to the cell level. Starting a process of collecting, sorting and separating battery pack components and feeding the fractions in battery cell recycling and well-established metals recovery processes is a hugely important strategy towards the realisation of the environmental benefits of battery recycling; such business models are currently being explored (Berger et al., 2022; Wrålsen et al., 2021). The recovery of Al and Cu from the battery pack, together with the recovery of valuable battery cell materials Ni^{II}, Co^{II} (sulfates) and Li^{I} (hydroxide) can lead to economically beneficial and sustainable battery recycling. However, as recycling can be beneficial only upstream of the value chain, these efforts should be combined with sustainable battery production practices, the utilisation of renewable energy during battery production and the target to ensure longevity of battery systems. These, together with developments in battery technology, could lead to substantial reduction of the cradle-to-grave environmental footprint of LIBs in the near future.

Chapter 8 Innovation and contributions of this research

This thesis systematically investigated the different stages of the LIB value chain for automotive traction applications filling knowledge gaps regarding the environmental and cost aspects of LIB production, utilisation in EVs and recycling. Specifically, a detailed LCA model was developed for the cradle-to-gate LIB production system in order to (a) clarify the landscape regarding the environmental implications of the Chinese domination in LIB manufacturing and (b) assess the environmental impacts associated with high-nickel NMC cathodes and SiGr anodes (Chapter 4). In addition to making valuable recommendations and conclusions for policy making, the development of the LCA model was performed with increased transparency and shared through a peer-reviewed publication (Kallitsis et al., 2020), to allow for its reproduction by other researchers and LCA practitioners.

Closely connected with the LIB production modelling, an effort was made to apply filtering criteria regarding the energy use of battery Gigafactories in order to quantify the range of values expected in modern-day battery manufacturing plants (Chapter 5). A significant convergence was observed compared to the past, with numbers ranging from 30 to 50 kW h of energy used per kW h cell capacity produced, providing an important resource for the quantification of the environmental impact of battery manufacturing and the prediction of the energy footprint of the battery Gigafactory boom. By sharing such findings through a peer-reviewed publication (Kallitsis, 2022) additional observations were made, such as the tendency of bottom-up modelling studies to converge with real-world data, which are of timely importance to the current state-of-knowledge.

Proceeding to the utilisation phase of LIBs in electric vehicles, an analytical model was developed in order to quantify the contribution of the battery, vehicle, maintenance and electricity used for charging to the overall cost and carbon footprint of an EV (Chapter 6). Increased focus was given to the effect of adequate thermal management in increasing battery lifetime and, as a consequence, reducing the life cycle cost and carbon footprint of EVs. In performing such modelling exercise, experimental data were fitted in order to predict the

number of cycles delivered by a battery as a function of temperature. In addition, techno-economic calculations were performed to estimate the upfront cost of the EV and operational costs for maintenance and charging. This research went beyond traditional LCA boundaries by integrating techno-economic and capacity fade models with experimental data to quantify the importance of battery thermal management in establishing more environmentally-friendly and cost-efficient transport systems (Lander et al., 2021b).

In Chapter 7, publicly available data were synthesised in order to perform an LCA of end-of-life treatment chains for LIBs and assess the environmental effect of establishing circularity in the LIB value chain. The standard system boundary description across literature studies was expanded to include all the process contributions, from the point of collection of end-of-life LIB packs to materials recovery and displacement of primary materials. The LIB recycling and LIB production LCA models were integrated, in order to quantify the magnitude of environmental impact reductions achieved through the establishment of a circular battery value chain. The model was built with increased transparency and was shared with the scientific community through a peer-reviewed publication (Kallitsis et al., 2022a), providing an in-depth analysis of unit process contributions to the environmental benefit and burden of LIB recycling. Finally, market-standard pyrometallurgical and hydrometallurgical processes were compared in terms of economic and environmental benefit, providing valuable insights for policy makers and other shareholders interested in establishing a sustainable battery life-cycle.

In addition to the original research performed in the framework of this thesis, the "Safe and sustainable lithium-ion batteries" white paper (Kallitsis et al., 2022b) was compiled with direct input from the outcomes of this work. The paper outlined key processes involved in upstream battery material production, LIB manufacturing, utilisation in EVs and recycling. It also highlighted safety and environmental concerns from a life cycle perspective in an effort to inform stakeholders beyond traditional academic boundaries.

The main conclusions directly drawn from this thesis are as follows:

- In a manufacturing world dominated by China, the environmental cost of LIB production is much higher than estimated previously in the literature e.g. 40% higher for the GWP.
- Producing NMC batteries with increased nickel content in the cathode and/or graphitic anodes mixed with silicon is expected to lead to similar threats to humans and

ecosystems, with an obvious environmental benefit achieved through the improvement of their energy density.

- Filtering criteria regarding production scale and battery chemistry should be applied when studying the energy use of battery manufacturing plants, with their application revealing a range of values of 30 to 50 kW h of energy used per kW h battery capacity produced.
- Upscaling battery manufacturing plants results in an obvious environmental benefit, which together with other advancements such as the increase in energy densities and the decarbonisation of the supply chain could lead to an 85% decrease in the cradle-to-gate carbon footprint of LIBs by 2030.
- Engineering solutions such as efficient thermal management systems have a paramount effect in expanding the number of cycles delivered throughout a LIBs lifetime, leading to significant improvements in terms of the life cycle costs and carbon footprint of electric vehicles reducing them by 27% and 25%, respectively, for surface or immersion thermal management compared to air cooling.
- Further lifetime extensions and in turn life cycle cost and carbon footprint improvements can be achieved by optimising the cell design to increase its suitability for tab cooling.
- Pyrometallurgical processing of battery cells comes with a greater GWP burden, so a slightly smaller benefit, mainly due to the almost six times higher electrical energy consumption, while hydrometallurgical processing results in a larger benefit by a maximum of 9% for the MEP, due to the additional recovery of lithium hydroxide.
- The importance of recovering Al, Cu and steel from the battery pack's TMS, BMS and packaging should not be neglected, as they contributed to the majority of environmental impact categories considered in the LCA model.
- Establishing a circular value chain, where end-of-life LIBs are adequately handled and battery materials are recovered in a sufficient quality can lead to obvious benefits from both an environmental and cost perspective.

8.1 Recommendations for future research

In Chapter 4, it was shown that novel electrode NMC batteries exhibit a significantly environmental impact intensity than those already commercialised due to their improved energy density. However, it is questionable if the implementation of newly emerging electrodes will lead to reduced impact intensity over the whole cycle life, as early experimental data are showing reduced lifespans of such batteries. In this direction and as done to a certain extent in this thesis in Chapter 6, LCA studies on the LIB use phase should get information on the achievable lifespan of the battery through experimental or real-world data. Such efforts were limited to NMC333-Gr chemistries given the scarcity of degradation data. As new data comes to light regarding the capacity fade behaviour, similar research should be performed for NMC622 and NMC811 chemistries combined with Gr or SiGr anodes.

In Chapter 5, the energy use and GHG intensity of battery manufacturing was discussed. However, as the gate-to-gate energy consumption of battery cell manufacturing is only a fraction of the cradle-to-gate energy demand, the system boundary should be expanded in future studies on Giga-scale battery production to include the active material preparation stages, given the tendency to vertically integrate them to the cell production line. Additionally, the contribution of sourcing low-carbon materials in reducing the cradle-to-gate carbon footprint of LIBs was presented. Only aluminium sourced from different locations was taken into account to provide an indication of the reduction potential. However, as battery material production chains are a highly complex system, future studies should project the effect of materials sourcing from different locations in a much more detailed manner. In this direction, it should be mentioned that as sustainable practices are increasingly adopted throughout battery manufacturing operations, the contribution of battery materials to the overall environmental footprint of a LIB becomes increasingly important. Producing accurate representations of the environmental footprint of key battery materials using the LCA framework, such as Ni, Co, Li, Mn and graphite has a key role in more accurately quantifying the environmental footprint of LIBs.

As battery recycling is currently under development, different technological options are emerging across the end-of-life treatment chain. The LCA model developed in Chapter 7 should be seen as representative of the current industrial cell recycling processes. Therefore,

as different ways to recycle battery cells emerge, such as direct recycling, a detailed implementation in LCA models should be performed. This extends to unit processes beyond cell recycling, including discharging alternatives to immersion to salts, such as Ohmic discharge which are also explored. As recycling chains for LIBs get established, more detailed inventory data should be collected, ideally from industry, to inform LCA models and reduce uncertainties. In this direction, process specific data on LIB recycling would allow comparisons of similar processing techniques employed by different companies across different locations, such as comparing pyrometallurgical operations using high- vs low-carbon energy sources

References

Accardo, A., Dotelli, G., Musa, M.L., Spessa, E., 2021. Life cycle assessment of an NMC battery for application to electric light-duty commercial vehicles and comparison with a sodium-nickel-chloride battery. Appl. Sci. 11, 1–32. https://doi.org/10.3390/app11031160

Ahmadi, L., Young, S.B., Fowler, M., Fraser, R.A., Achachlouei, M.A., 2017. A cascaded life cycle: reuse of electric vehicle lithium-ion battery packs in energy storage systems. Int. J. Life Cycle Assess. 22, 111–124. https://doi.org/10.1007/s11367-015-0959-7

Ahmadian, A., Sedghi, M., Elkamel, A., Fowler, M., Aliakbar Golkar, M., 2018. Plug-in electric vehicle batteries degradation modeling for smart grid studies: Review, assessment and conceptual framework. Renew. Sustain. Energy Rev. 81, 2609–2624. https://doi.org/10.1016/j.rser.2017.06.067

Amarakoon, S., Smith, J., Segal, B., 2013. Application of life-cycle assessment to nanoscale technology: Lithium-ion batteries for electric vehicles, No. EPA 744-R-12-001.

Arshad, F., Lin, J., Manurkar, N., Fan, E., Ahmad, A., Tariq, M. un N., Wu, F., Chen, R., Li, L., 2022. Life Cycle Assessment of Lithium-ion Batteries: A Critical Review. Resour. Conserv. Recycl. 180. https://doi.org/10.1016/j.resconrec.2022.106164

Asadi, M., Sayahpour, B., Abbasi, P., Ngo, A.T., Karis, K., Jokisaari, J.R., Liu, C., Narayanan, B., Gerard, M., Yasaei, P., Hu, X., Mukherjee, A., Lau, K.C., Assary, R.S., Khalili-Araghi, F., Klie, R.F., Curtiss, L.A., Salehi-Khojin, A., 2018. A lithium–oxygen battery with a long cycle life in an air-like atmosphere. Nature 555, 502–506. https://doi.org/10.1038/nature25984

Baazouzi, S., Rist, F.P., Weeber, M., Birke, K.P., 2021. Optimization of disassembly strategies for electric vehicle batteries. Batteries 7. https://doi.org/10.3390/batteries7040074

Badin, F., Le Berr, F., Briki, H., Dabadie, J.C., Petit, M., Magand, S., Condemine, E., 2013. Evaluation of EVs energy consumption influencing factors: Driving conditions, auxiliaries use, driver's aggressiveness. World Electr. Veh. J. 6, 112–123. https://doi.org/10.1109/EVS.2013.6914723

Bak, S.-M., Hu, E., Zhou, Y., Yu, X., Senanayake, S.D., Cho, S.-J., Kim, K.-B., Chung, K.Y., Yang, X.-Q., Nam, K.-W., 2014. Structural Changes and Thermal Stability of Charged LiNixMnyCozO2 Cathode Materials Studied by Combined In Situ Time-Resolved XRD and Mass Spectroscopy. ACS Appl. Mater. Interfaces 6, 22594–22601. https://doi.org/10.1021/am506712c

Baumann, H., Tillman, A.-M., 2004. The hitch hiker's guide to LCA. Studentlitteratur, Lund.

BEIS, 2019. 2019 GOVERNMENT GREENHOUSE GAS CONVERSION FACTORS FOR COMPANY Methodology Paper for Emission Factors Final Report. London.

Berckmans, G., Messagie, M., Smekens, J., Omar, N., Vanhaverbeke, L., Mierlo, J. Van, 2017. Cost projection of state of the art lithium-ion batteries for electric vehicles up to 2030. Energies 10. https://doi.org/10.3390/en10091314

Berger, K., Schöggl, J.-P., Baumgartner, R.J., 2022. Digital battery passports to enable circular and sustainable value chains: Conceptualization and use cases. J. Clean. Prod. 353, 131492. https://doi.org/10.1016/j.jclepro.2022.131492

Bieker, G., 2021. A GLOBAL COMPARISON OF THE LIFE-CYCLE GREENHOUSE GAS EMISSIONS OF COMBUSTION ENGINE AND ELECTRIC PASSENGER CARS.

Birkl, C.R., Roberts, M.R., McTurk, E., Bruce, P.G., Howey, D.A., 2017. Degradation diagnostics for lithium ion cells. J. Power Sources 341, 373–386. https://doi.org/10.1016/j.jpowsour.2016.12.011

Bloom, I., Cole, B.W., Sohn, J.J., Jones, S.A., Polzin, E.G., Battaglia, V.S., Henriksen, G.L., Motloch, C., Richardson, R., Unkelhaeuser, T., Ingersoll, D., Case, H.L., 2001. An accelerated calendar and cycle life study of Li-ion cells. J. Power Sources 101, 238–247. https://doi.org/10.1016/S0378-7753(01)00783-2

BloombergNEF, 2019. Battery Pack Prices Fall As Market Ramps Up With Market Average

At $156/kWh In 2019 . URL https://about.bnef.com/blog/battery-pack-prices-fall-as-market-ramps-up-with-market-average-at-156-kwh-in-2019/ (accessed 3.10.20).

Bogacki, M., Oleniacz, R., Mazur, M., Szczyglowski, P., 2012. Air pollutant emissions during baking of semi-finished graphite products in a tunnel furnace. Environ. Prot. Eng. 38, 15–23.

Elvers, B., 1991. Ullmann's encyclopedia of industrial chemistry (Vol. 17, pp. 363-376). Hoboken, NJ: Verlag Chemie. Bouter, A., Guichet, X., 2022. The greenhouse gas emissions of automotive lithium-ion batteries: a statistical review of life cycle assessment studies. J. Clean. Prod. 344, 130994. https://doi.org/10.1016/j.jclepro.2022.130994

Brennan, J.W., Barder, T.E., 2016. Battery Electric Vehicles vs . Internal Combustion Engine Vehicles, Arthur D. Little.

Bruce, P.G., Freunberger, S.A., Hardwick, L.J., Tarascon, J.-M., 2012. Li–O2 and Li–S batteries with high energy storage. Nat. Mater. 11, 19–29. https://doi.org/10.1038/nmat3191

Burchart-Korol, D., 2013. Life cycle assessment of steel production in Poland: a case study. J. Clean. Prod. 54, 235–243. https://doi.org/10.1016/J.JCLEPRO.2013.04.031

Casals, L.C., Amante García, B., Canal, C., 2019. Second life batteries lifespan: Rest of useful life and environmental analysis. J. Environ. Manage. 232, 354–363. https://doi.org/10.1016/j.jenvman.2018.11.046

Chae, S., Ko, M., Kim, K., Ahn, K., Cho, J., 2017. Confronting Issues of the Practical Implementation of Si Anode in High-Energy Lithium-Ion Batteries. Joule 1, 47–60. https://doi.org/10.1016/j.joule.2017.07.006

Chagnes, A., Pospiech, B., 2013. A brief review on hydrometallurgical technologies for recycling spent lithium-ion batteries. J. Chem. Technol. Biotechnol. 88, 1191–1199. https://doi.org/10.1002/jctb.4053

Chen, D., Jiang, J., Kim, G.H., Yang, C., Pesaran, A., 2016. Comparison of different cooling methods for lithium ion battery cells. Appl. Therm. Eng. 94, 846–854. https://doi.org/10.1016/j.applthermaleng.2015.10.015

Chen, K., Wang, S., Song, M., Chen, L., 2017. Structure optimization of parallel air-cooled battery thermal management system. Int. J. Heat Mass Transf. 111, 943–952. https://doi.org/10.1016/j.ijheatmasstransfer.2017.04.026

Chen, M., Ma, X., Chen, B., Arsenault, R., Karlson, P., Simon, N., Wang, Y., 2019. Recycling End-of-Life Electric Vehicle Lithium-Ion Batteries. Joule 3, 2622–2646. https://doi.org/10.1016/j.joule.2019.09.014

Chiu, K.-C., Lin, C.-H., Yeh, S.-F., Lin, Y.-H., Huang, C.-S., Chen, K.-C., 2014. Cycle life analysis of series connected lithium-ion batteries with temperature difference. J. Power Sources 263, 75–84. https://doi.org/10.1016/j.jpowsour.2014.04.034

Chordia, M., Nordelöf, A., Ellingsen, L.A.W., 2021. Environmental life cycle implications of upscaling lithium-ion battery production. Int. J. Life Cycle Assess. 26, 2024–2039. https://doi.org/10.1007/s11367-021-01976-0

Choubey, P.K., Chung, K.S., Kim, M. seuk, Lee, J. chun, Srivastava, R.R., 2017. Advance review on the exploitation of the prominent energy-storage element Lithium. Part II: From sea water and spent lithium ion batteries (LIBs). Miner. Eng. 110, 104–121. https://doi.org/10.1016/j.mineng.2017.04.008

Choux, M., Bigorra, E.M., Tyapin, I., 2021. Task planner for robotic disassembly of electric vehicle battery pack. Metals (Basel). 11, 1–18. https://doi.org/10.3390/met11030387

Chung, Y., Kim, M.S., 2019. Thermal analysis and pack level design of battery thermal management system with liquid cooling for electric vehicles. Energy Convers. Manag. 196, 105–116. https://doi.org/10.1016/j.enconman.2019.05.083

Ciez, R.E., Whitacre, J.F., 2019. Examining different recycling processes for lithium-ion batteries. Nat. Sustain. 2, 148–156. https://doi.org/10.1038/s41893-019-0222-5

Cox, B., Mutel, C.L., Bauer, C., Mendoza Beltran, A., Van Vuuren, D.P., 2018. Uncertain Environmental Footprint of Current and Future Battery Electric Vehicles. Environ. Sci. Technol. 52, 4989–4995. https://doi.org/10.1021/acs.est.8b00261

Curran, M.A., 2017. Overview of goal and scope definition in life cycle assessment, in: Goal and Scope Definition in Life Cycle Assessment. Springer, pp. 1–62.

Cusenza, M.A., Bobba, S., Ardente, F., Cellura, M., Di Persio, F., 2019. Energy and environmental assessment of a traction lithium-ion battery pack for plug-in hybrid electric vehicles. J. Clean. Prod. 215, 634–649. https://doi.org/10.1016/j.jclepro.2019.01.056

Dai, Q., Kelly, C.J., Dunn, J., Benavides, T.P., 2018. Update of Bill-of-materials and Cathode Materials Production for Lithium-ion Batteries in the GREET Model. Argone Natl. Lab.

Dai, Q., Kelly, J.C., Gaines, L., Wang, M., 2019a. 1 Life Cycle Analysis of Lithium-Ion Batteries for Automotive Applications. Batteries 5, 48. https://doi.org/10.3390/batteries5020048

Dai, Q., Spangenberger, J., Shabbir Ahmed, L.G., Kelly, J., Wang, M., 2019b. EverBatt : A Closed-loop Battery Recycling Cost and Environmental Impacts Model. Argone Natl. Lab.

Daniel, C., Mohanty, D., Li, J., Wood, D.L., 2014. Cathode materials review. AIP Conf. Proc. 1597, 26–43. https://doi.org/10.1063/1.4878478

Dante, R.C., 2015. Handbook of friction materials and their applications. Woodhead publishing.

Dash, R., Pannala, S., 2016. Theoretical Limits of Energy Density in Silicon-Carbon Composite Anode Based Lithium Ion Batteries. Sci. Rep. 6, 6–12. https://doi.org/10.1038/srep27449

De Cauwer, C., Van Mierlo, J., Coosemans, T., 2015. Energy consumption prediction for electric vehicles based on real-world data. Energies 8, 8573–8593. https://doi.org/10.3390/en8088573

de Souza, Picirelli Lora, Electo Palcio, Jose Rocha, Mateus Reno, Maria Venturini, O., 2018. Comparative environmental life cycle assessment of conventional vehicles with different fuel options , plug-in hybrid and electric vehicles for a sustainable transportation system in Brazil 203, 444–468. https://doi.org/10.1016/j.jclepro.2018.08.236

Degen, F., Schütte, M., 2022. Life cycle assessment of the energy consumption and GHG emissions of state-of-the-art automotive battery cell production. J. Clean. Prod. 330, 129798. https://doi.org/10.1016/j.jclepro.2021.129798

Dincer, I., Hamut, H.S., Javani, N., 2016. Thermal management of electric vehicle battery systems. John Wiley & Sons.

Dondelewski, O., Szemberg O'Connor, T., Zhao, Y., Hunt, I.A., Holland, A., Hales, A., Offer, G.J., Patel, Y., 2020. The role of cell geometry when selecting tab or surface cooling to minimise cell degradation. eTransportation 5, 100073. https://doi.org/10.1016/j.etran.2020.100073

Du, S., Gao, F., Nie, Z., Liu, Y., Sun, B., Gong, X., 2022. Life cycle assessment of recycled NiCoMn ternary cathode materials prepared by hydrometallurgical technology for power batteries in China. J. Clean. Prod. 130798. https://doi.org/10.1016/j.jclepro.2022.130798

Duce, A. Del, Gauch, M., Althaus, H., 2016. Electric passenger car transport and passenger car life cycle inventories in ecoinvent version 3. Int. J. Life Cycle Assess. 1314–1326. https://doi.org/10.1007/s11367-014-0792-4

Dunn, J.B., Gaines, L., Kelly, J.C., James, C., Gallagher, K.G., 2015. The significance of Li-ion batteries in electric vehicle life-cycle energy and emissions and recycling's role in its reduction. Energy Environ. Sci. 8, 158–168. https://doi.org/10.1039/c4ee03029j

EC-JRC, 2012. Product Environmental Footprint (PEF) Guide. Ispra, European Commision Joint Research Centre.

EEA, 2017. Monitoring progress of Europe's transport sector towards its environment, health and climate objectives. Transport and Environment Reporting Mechanism (TERM).EEA, 2014. Emissions of air pollutants from transport. URL https://www.eea.europa.eu/data-and-maps/indicators/transport-emissions-of-air-pollutants-8/transport-emissions-of-air-pollutants-8 (accessed 3.11.21).

Egede, P., Dettmer, T., Herrmann, C., Kara, S., 2015. Life cycle assessment of electric vehicles–a framework to consider influencing factors. Procedia CIRP 29, 233–238. https://doi.org/10.1016/j.procir.2015.02.185

Element Energy, 2019. Forecasted breakdown of electric vehicle (EV) battery demand in Europe from 2017 to 2030, by chemical composition. Statista. URL https://www.statista.com/statistics/1039856/ev-batteries-demand-share-by-chemical-europe/ (accessed 12.29.21).

Ellingsen, L.A., Singh, B., Strømman, A.H., 2016. The size and range effect : lifecycle greenhouse gas emissions of electric vehicles The size and range effect : lifecycle greenhouse gas emissions of electric vehicles. Environ. Res. Lett. 11 054010. https://doi.org/10.1088/1748-9326/11/5/054010

Ellingsen, L.A.W., Majeau-Bettez, G., Singh, B., Srivastava, A.K., Valøen, L.O., Strømman, A.H., 2014. Life Cycle Assessment of a Lithium-Ion Battery Vehicle Pack. J. Ind. Ecol. 18, 113–124. https://doi.org/10.1111/jiec.12072

Ellingsen, L.A.W., Majeau-Bettez, G., Strømman, A.H., 2015. Comment on "The significance of Li-ion batteries in electric vehicle life-cycle energy and emissions and recycling's role in its reduction" in Energy & Environmental Science. J. Ind. Ecol. 19, 518–519. https://doi.org/10.1111/jiec.12309

Energy Systems Division Systems Assessment Group, 2016. Summary of Expansions, Updates, and Results in GREET® 2016 Suite of Models. Argonne Natl. Lab.

European Carbon and Graphite Association, 2018. Towards CO2 neutrality due to carbon and graphite.

Eurostat, 2019. Electricity price statistics [WWW Document]. URL https://ec.europa.eu/eurostat/statistics-explained/index.php/Electricity_price_statistics (accessed 2.25.20).

Fan, X., Sun, W., Meng, F., Xing, A., Liu, J., 2018. Advanced chemical strategies for lithium–sulfur batteries: A review. Green Energy Environ., Post Lithium ion batteries 3, 2–19. https://doi.org/10.1016/j.gee.2017.08.002

Federal Institute for Geosciences and Natural Resources, 2019. Preismonitor (Report) (in German).

Fetene, G.M., Kaplan, S., Mabit, S.L., Jensen, A.F., Prato, C.G., 2017. Harnessing big data for estimating the energy consumption and driving range of electric vehicles. Transp. Res. Part D Transp. Environ. 54, 1–11. https://doi.org/10.1016/j.trd.2017.04.013

Fisher, K., Collins, M., Laenen, P., Wallén, E., Peter, G., Aumônier, S., 2006. Battery waste management life cycle assessment. Environmental Resource Managment.

Fleckenstein, M., Bohlen, O., Roscher, M.A., Bäker, B., 2011. Current density and state of charge inhomogeneities in Li-ion battery cells with LiFePO4 as cathode material due to temperature gradients. J. Power Sources 196, 4769–4778. https://doi.org/10.1016/j.jpowsour.2011.01.043

FleetNews, 2019. Car running costs over 4 years and 80,000 miles. URL https://www.fleetnews.co.uk/car-running-costs-calculator (accessed 2.25.20).

Fotouhi, A., Auger, D.J., O'Neill, L., Cleaver, T., Walus, S., 2017. Lithium-Sulfur Battery Technology Readiness and Applications - A Review. Energies 10, 1937. https://doi.org/10.3390/en10121937

Fuc, P., Kurczewski, P., Lewandowska, A., Nowak, E., Selech, J., Ziolkowski, A., 2016. An environmental life cycle assessment of forklift operation: a well-to-wheel analysis. Int. J. Life Cycle Assess. 21, 1438–1451. https://doi.org/10.1007/s11367-016-1104-y

Gaines, L., 2014. The future of automotive lithium-ion battery recycling: Charting a sustainable course. Sustain. Mater. Technol. 1, 2–7. https://doi.org/10.1016/j.susmat.2014.10.001

Gastol, D., Marshall, J., Cooper, E., Mitchell, C., Burnett, D., Song, T., Sommerville, R., Middleton, B., Crozier, M., Smith, R., Haig, S., Mcelroy, C.R., Croft, P., Goodship, V., Kendrick, E., 2022. Reclaimed and Up-Cycled Cathodes for Lithium-Ion Batteries 2200046. https://doi.org/10.1002/gch2.202200046

Georgi-Maschler, T., Friedrich, B., Weyhe, R., Heegn, H., Rutz, M., 2012. Development of a recycling process for Li-ion batteries. J. Power Sources 207, 173–182. https://doi.org/10.1016/j.jpowsour.2012.01.152

Gils, R.W. Van, Danilov, D., Notten, P.H.L.L., Speetjens, M.F.M.M., Nijmeijer, H., Van Gils, R.W., Danilov, D., Notten, P.H.L.L., Speetjens, M.F.M.M., Nijmeijer, H., 2014. Battery thermal management by boiling heat-transfer. Energy Convers. Manag. 79, 9–17. https://doi.org/10.1016/j.enconman.2013.12.006

Goedkoop, M., Heijungs, R., Huijbregts, M., De Schryver, A., Struijs, J., Van Zelm, R., 2008. ReCiPe 2008: A life cycle impact assessment method which comprises harmonised category indicators at the midpoint and the endpoint level. Goedkoop, M.J., 1999. The Eco-indicator 99 a damage oriented method for life cycle impact assessment methodology

report. Pre Concultants.

Gopalakrishnan, R., Goutam, S., Miguel Oliveira, L., Timmermans, J.-M., Omar, N., Messagie, M., Van den Bossche, P., van Mierlo, J., 2017. A Comprehensive Study on Rechargeable Energy Storage Technologies. J. Electrochem. Energy Convers. Storage 13, 040801. https://doi.org/10.1115/1.4036000

Grolleau, S., Delaille, A., Gualous, H., 2013. Predicting lithium-ion battery degradation for efficient design and management. World Electr. Veh. J. 6, 549–554. https://doi.org/10.3390/wevj6030549

Guilmard, M., Pouillerie, C., Croguennec, L., Delmas, C., 2003. Structural and electrochemical properties of LiNi0.70Co0.15Al0.15O2. Solid State Ionics 160, 39–50. https://doi.org/10.1016/S0167-2738(03)00106-1

Günther, H.O., Kannegiesser, M., Autenrieb, N., 2015. The role of electric vehicles for supply chain sustainability in the automotive industry. J. Clean. Prod. 90, 220–233. https://doi.org/10.1016/j.jclepro.2014.11.058

Hales, A., Diaz, L.B., Marzook, M.W., Zhao, Y., Patel, Y., Offer, G., 2019. The Cell Cooling Coefficient: A Standard to Define Heat Rejection from Lithium-Ion Batteries. J. Electrochem. Soc. 166, A2383–A2395. https://doi.org/10.1149/2.0191912jes

Hales, A., Marzook, M.W., Bravo Diaz, L., Patel, Y., Offer, G., 2020. The Surface Cell Cooling Coefficient: A Standard to Define Heat Rejection from Lithium Ion Battery Pouch Cells. J. Electrochem. Soc. 167, 020524. https://doi.org/10.1149/1945-7111/ab6985

Hao, H., Mu, Z., Jiang, S., Liu, Z., Zhao, F., 2017a. GHG Emissions from the production of lithium-ion batteries for electric vehicles in China. Sustain. 9. https://doi.org/10.3390/su9040504

Hao, H., Qiao, Q., Liu, Z., Zhao, F., 2017b. Impact of recycling on energy consumption and greenhouse gas emissions from electric vehicle production: The China 2025 case. Resour. Conserv. Recycl. 122, 114–125. https://doi.org/10.1016/j.resconrec.2017.02.005

Harlow, J.E., Soc, J.E., Harlow, J.E., Ma, X., Li, J., Logan, E., Liu, Y., Zhang, N., Ma, L., Glazier, S.L., Cormier, M.M.E., Genovese, M., Buteau, S., Cameron, A., Stark, J.E.,

Dahn, J.R., 2019. A Wide Range of Testing Results on an Excellent Lithium-Ion Cell Chemistry to be used as Benchmarks for New Battery Technologies. J. Electrochem. Soc. 166, A3031. https://doi.org/10.1149/2.0981913jes

Harper, G., Sommerville, R., Kendrick, E., Driscoll, L., Slater, P., Stolkin, R., Walton, A., Christensen, P., Heidrich, O., Lambert, S., Abbott, A., Ryder, K., Gaines, L., Anderson, P., 2019. Recycling lithium-ion batteries from electric vehicles. Nature 575, 75–86. https://doi.org/10.1038/s41586-019-1682-5

Hawkins, T.R., Singh, B., Majeau-Bettez, G., Strømman, A.H., 2013. Comparative Environmental Life Cycle Assessment of Conventional and Electric Vehicles. J. Ind. Ecol. 17, 53–64. https://doi.org/10.1111/j.1530-9290.2012.00532.x

Helms, H., Pehnt, M., Lambrecht, U., Liebich, A., 2010. Electric vehicle and plug-in hybrid energy efficiency and life cycle emissions. Proc. 18th Int. Symp. Transp. Air Pollut. 113–124.

Hoekstra, A., 2019. The Underestimated Potential of Battery Electric Vehicles to Reduce Emissions. Joule 3, 1412–1414. https://doi.org/10.1016/j.joule.2019.06.002

Holland, S., Mansur, E., Muller, N., Yates, A., 2015. Environmental Benefits from Driving Electric Vehicles? National Bureau of Economic Research.

Hoog, J. De, Timmermans, J., Ioan-stroe, D., Swierczynski, M., Jaguemont, J., Goutam, S., Omar, N., Mierlo, J. Van, Bossche, P. Van Den, 2017. Combined cycling and calendar capacity fade modeling of a Nickel-Manganese-Cobalt Oxide Cell with real-life profile validation. Appl. Energy 200, 47–61. https://doi.org/10.1016/j.apenergy.2017.05.018

Huijbregts, M.A.J., Steinmann, Z.J.N., Elshout, P.M.F., Stam, G., Verones, F., Vieira, M., Zijp, M., Hollander, A., van Zelm, R., 2017. ReCiPe2016: a harmonised life cycle impact assessment method at midpoint and endpoint level. Int. J. Life Cycle Assess. 22, 138–147. https://doi.org/10.1007/s11367-016-1246-y

Huijbregts, M.A.J., Steinmann, Z.J.N., Elshout, P.M.F., Stam, G., Verones, F., Vieira, M.D.M., Hollander, A., Zijp, M., Van Zelm, R., 2016. ReCiPe 2016: A harmonized life cycle impact assessment method at midpoint and endpoint level Report I: Characterization.

Hunt, I.A., Zhao, Y., Patel, Y., Offerz, G.J., 2016. Surface cooling causes accelerated degradation compared to tab cooling for lithium-ion pouch cells. J. Electrochem. Soc. 163, A1846–A4852. https://doi.org/10.1149/2.0361609jes

Iclodean, C., Varga, B., Burnete, N., Cimerdean, D., Jurchiş, B., 2017. Comparison of Different Battery Types for Electric Vehicles. IOP Conf. Ser. Mater. Sci. Eng. 252. https://doi.org/10.1088/1757-899X/252/1/012058

International Energy Agency, 2021. Global EV Outlook 2021 - Accelerating ambitions despite the pandemic.

International Energy Agency, 2020. Global EV Outlook 2020.

International Energy Agency, 2019. Global EV Outlook 2019.

International Energy Agency, 2018. Global EV Outlook 2018.

International Energy Agency, 2017. CO_2 Emissions from Fuel Combustion 2017-Highlights.

IPCC, 2018. Global warming of 1.5°C, Report of the Intergovernmental Panel on Climate Change.

ISO, 2014. ISO 14040:2006 - Life Cycle Assessment: Principles and framework, Environmental management. International Organisation for Standardisation, Geneva.

ISO, 2006a. ISO14040:2006 Environmental management- Life cycle assessment- Principles and framework. International Organisation for Standardisation, Geneva.

ISO, 2006b. ISO14044:2006 Environmental management-Life cycle assessment-Requirements and guidelines. International Organisation for Standardisation, Geneva.

ISO, 2003. Environmental Management: Life Cycle Impact Assessment : Examples of Application of ISO 14042. International Organisation for Standardisation, Geneva.

ISO, 2001. Environmental Management - Life Cycle Assessment - Life Cycle Interpretation (ISO 14043: 2000, IDT)., Malaysian standard. Department of Standards Malaysia.

Itou, Y., Ukyo, Y., 2005. Performance of LiNiCoO2 materials for advanced lithium-ion batteries. J. Power Sources. 146, 39-44. https://doi.org/10.1016/j.jpowsour.2005.03.091

Jafari, M., Gauchia, A., Zhang, K., Gauchia, L., 2015. Simulation and Analysis of the Effect of Real-World Driving Styles in an EV Battery Performance and Aging. IEEE Trans. Transp. Electrif. 1, 391–401. https://doi.org/10.1109/TTE.2015.2483591

Jara, A.D., Betemariam, A., Woldetinsae, G., Kim, J.Y., 2019. Purification, application and current market trend of natural graphite: A review. Int. J. Min. Sci. Technol. 29, 671–689. https://doi.org/10.1016/j.ijmst.2019.04.003

Ji, Y., Kpodzro, E.E., Jafvert, C.T., Zhao, F., 2021. Direct recycling technologies of cathode in spent lithium-ion batteries. Clean Technol. Recycl. 1, 124–151. https://doi.org/10.3934/ctr.2021007

Jiang, S., Hua, H., Zhang, L., Liu, X., Wu, H., Yuan, Z., 2022. Environmental impacts of hydrometallurgical recycling and reusing for manufacturing of lithium-ion traction batteries in China. Sci. Total Environ. 811, 152224. https://doi.org/10.1016/j.scitotenv.2021.152224

Jinasena, A., Burheim, O.S., Strømman, A.H., 2021. A flexible model for benchmarking the energy usage of automotive lithium-ion battery cell manufacturing. Batteries 7, 1–21. https://doi.org/10.3390/batteries7010014

Kallitsis, E., 2022. On the energy use of battery Gigafactories. J. Clean. Prod. 364, 132573. https://doi.org/10.1016/j.jclepro.2022.132573

Kallitsis, E., Korre, A., Kelsall, G., Kupfersberger, M., Nie, Z., 2020. Environmental life cycle assessment of the production in China of lithium-ion batteries with nickel-cobalt-manganese cathodes utilising novel electrode chemistries. J. Clean. Prod. 254, 120067. https://doi.org/10.1016/j.jclepro.2020.120067

Kallitsis, E., Korre, A., Kelsall, G.H., 2022a. Life cycle assessment of recycling options for automotive Li-ion battery packs. J. Clean. Prod. 371, 133636. https://doi.org/10.1016/j.jclepro.2022.133636

Kallitsis, E., Lander, L., Edge, J., Bravo Diaz, L., Brown, A., Kelsall, G., Offer, G., Korre, A., 2022b. Safe and sustainable lithium-ion batteries. Imperial College London - Energy Futures Lab. https://doi.org/10.25561/95548

Kara, S., Li, W., Sadjiva, N., 2017. Life Cycle Cost Analysis of Electrical Vehicles in Australia. Procedia CIRP 61, 767–772. https://doi.org/10.1016/j.procir.2016.11.179

Kasemchainan, J., Bruce, P.G., 2018. All-solid-state batteries and their remaining challenges. Johnson Matthey Technol. Rev. 62, 177–180. https://doi.org/10.1595/205651318X696747

Keil, P., Schuster, S.F., Wilhelm, J., Travi, J., Hauser, A., Karl, R.C., Jossen, A., 2016. Calendar Aging of Lithium-Ion Batteries. J. Electrochem. Soc. 163, A1872–A1880. https://doi.org/10.1149/2.0411609jes

Kelly, J.C., Dai, Q., Wang, M., 2019. Globally regional life cycle analysis of automotive lithium-ion nickel manganese cobalt batteries. Mitig. Adapt. Strateg. Glob. Chang. 25, 371–396. https://doi.org/10.1007/s11027-019-09869-2

Kerman, K., Luntz, A., Viswanathan, V., Chiang, Y.-M., Chen, Z., 2017. Review—Practical Challenges Hindering the Development of Solid State Li Ion Batteries. J. Electrochem. Soc. 164, A1731–A1744. https://doi.org/10.1149/2.1571707jes

Kim, H.C., Wallington, T.J., Arsenault, R., Bae, C., Ahn, S., Lee, J., 2016. Cradle-to-Gate Emissions from a Commercial Electric Vehicle Li-Ion Battery: A Comparative Analysis. Environ. Sci. Technol. 50, 7715–7722. https://doi.org/10.1021/acs.est.6b00830

Klöpffer, W., Curran, A., 2021. LCA Compendium-The Complete World of Life Cycle Assessment Series Editors: Life Cycle Inventory Analysis Methods and Data. Springer.

Knobloch, F., Hanssen, S. V., Lam, A., Pollitt, H., Salas, P., Chewpreecha, U., Huijbregts, M.A.J., Mercure, J.-F., 2020. Net emission reductions from electric cars and heat pumps in 59 world regions over time. Nat. Sustain. 1–11. https://doi.org/10.1038/s41893-020-0488-7

Kurland, S.D., 2019. Energy use for GWh-scale lithium-ion battery production. Environ. Res. Commun. 2, 012001. https://doi.org/10.1088/2515-7620/ab5e1e

Lander, L., Cleaver, T., Rajaeifar, M.A., Nguyen-Tien, V., Elliott, R.J.R., Heidrich, O., Kendrick, E., Edge, J.S., Offer, G., 2021a. Financial viability of electric vehicle lithium-ion battery recycling. iScience 24, 102787. https://doi.org/10.1016/j.isci.2021.102787

Lander, L., Kallitsis, E., Hales, A., Edge, J.S., Korre, A., Offer, G., 2021b. Cost and carbon footprint reduction of electric vehicle lithium-ion batteries through efficient thermal management. Appl. Energy 289, 116737. https://doi.org/10.1016/j.apenergy.2021.116737

Larcher, D., Tarascon, J.M., 2015. Towards greener and more sustainable batteries for electrical energy storage. Nat. Chem. 7, 19–29. https://doi.org/10.1038/nchem.2085

Li, T., Yuan, X.-Z., Zhang, L., Song, D., Shi, K., Bock, C., 2020. Degradation Mechanisms and Mitigation Strategies of Nickel-Rich NMC-Based Lithium-Ion Batteries. Electrochem. Energy Rev. 3, 43–80. https://doi.org/10.1007/s41918-019-00053-3

Li, W., Stanula, P., Egede, P., Kara, S., Herrmann, C., 2016. Determining the Main Factors Influencing the Energy Consumption of Electric Vehicles in the Usage Phase. Procedia CIRP 48, 352–357. https://doi.org/10.1016/j.procir.2016.03.014

Lima, P., 2022. Comparison of different EV batteries in 2020 . PushEVs. URL https://pushevs.com/2020/04/04/comparison-of-different-ev-batteries-in-2020/ (accessed 5.30.22).

Linden, D., Reddy, T.B., 2002. Handbook of Batteries. 3rd. McGraw-Hill.

Liu, J., Bao, Z., Cui, Y., Dufek, E.J., Goodenough, J.B., Khalifah, P., Li, Q., Liaw, B.Y., Liu, P., Manthiram, A., Meng, Y.S., Subramanian, V.R., Toney, M.F., Viswanathan, V. V., Whittingham, M.S., Xiao, J., Xu, W., Yang, J., Yang, X.Q., Zhang, J.G., 2019. Pathways for practical high-energy long-cycling lithium metal batteries. Nat. Energy 4, 180–186. https://doi.org/10.1038/s41560-019-0338-x

Liu, K., Hu, X., Yang, Z., Xie, Y., Feng, S., 2019. Lithium-ion battery charging management considering economic costs of electrical energy loss and battery degradation. Energy Convers. Manag. 195, 167–179. https://doi.org/10.1016/j.enconman.2019.04.065

Liu, L., Wang, L.Y., Chen, Z., Wang, C., Lin, F., Wang, H., 2013. Integrated system identification and state-of-charge estimation of battery systems. IEEE Trans. Energy Convers. 28, 12–23. https://doi.org/10.1109/TEC.2012.2223700

Liu, X., Wang, H., Chen, J., He, Q., Zhang, H., Jiang, R., Chen, X., Hou, P., 2010. Method and basic model for development of Chinese reference life cycle database. Huanjing Kexue

Xuebao/Acta Sci. Circumstantiae 30, 2136–2144.

Lomborg, B., 2013. Green Cars Have a Dirty Little Secret. Wall Str. J. URL https://www.wsj.com/articles/SB10001424127887324128504578346913994914472 (accessed 3.8.20).

Long, L., Wang, S., Xiao, M., Meng, Y., 2016. Polymer electrolytes for lithium polymer batteries. J. Mater. Chem. A 4, 10038–10069. https://doi.org/10.1039/C6TA02621D

Lutsey, N., Nicholas, M., 2019. Update on electric vehicle costs in the United States through 2030. Int. Counc. Clean Transp. 1–12. https://doi.org/10.13140/RG.2.2.25390.56646

Lv, W., Wang, Z., Cao, H., Sun, Y., Zhang, Y., Sun, Z., 2018. A Critical Review and Analysis on the Recycling of Spent Lithium-Ion Batteries. ACS Sustain. Chem. Eng. 6, 1504–1521. https://doi.org/10.1021/acssuschemeng.7b03811

Ma, Y., Ke, R., Han, R., Tang, B., 2017. The analysis of the battery electric vehicle ' s potentiality of environmental effect : A case study of Beijing from 2016 to 2020. J. Clean. Prod. 145, 295-406. https://doi.org/10.1016/j.jclepro.2016.12.131

Madhavi, S., Subba Rao, G. V, Chowdari, B.V.R., Li, S.F.Y., 2001. Effect of aluminium doping on cathodic behaviour of LiNi0.7Co0.3O2. J. Power Sources 93, 156–162. https://doi.org/10.1016/S0378-7753(00)00559-0

Maiser, E., 2014. Battery packaging - Technology review. AIP Conf. Proc. 1597, 204–218. https://doi.org/10.1063/1.4878489

Majeau-Bettez, G., Hawkins, T.R., StrØmman, A.H., 2011. Life cycle environmental assessment of lithium-ion and nickel metal hydride batteries for plug-in hybrid and battery electric vehicles. Environ. Sci. Technol. 45, 1–51. https://doi.org/10.1021/es103607c

Manthiram, A., 2017. An Outlook on Lithium Ion Battery Technology. ACS Cent. Sci. 3, 1063–1069. https://doi.org/10.1021/acscentsci.7b00288

Manthiram, A., Fu, Y., Chung, S.-H., Zu, C., Su, Y.-S., 2014. Rechargeable Lithium–Sulfur Batteries. Chem. Rev. 114, 11751–11787. https://doi.org/10.1021/cr500062v

Manthiram, A., Yu, X., Wang, S., 2017. Lithium battery chemistries enabled by solid-state

electrolytes. Nat. Rev. Mater. 2, 1–16. https://doi.org/10.1038/natrevmats.2016.103

Marinescu, M., O'Neill, L., Zhang, T., Walus, S., Wilson, T.E., Offer, G.J., 2018. Irreversible vs Reversible Capacity Fade of Lithium-Sulfur Batteries during Cycling: The Effects of Precipitation and Shuttle. J. Electrochem. Soc. 165, A6107--A6118. https://doi.org/10.1149/2.0171801jes

Marques, P., Garcia, R., Kulay, L., Freire, F., 2019. Comparative life cycle assessment of lithium-ion batteries for electric vehicles addressing capacity fade. J. Clean. Prod. 229, 787–794. https://doi.org/10.1016/j.jclepro.2019.05.026

Mathieu, C., 2021. Green Batteries : A Competitive Advantage for Europe ' s Electric Vehicle Value Chain ?

McKinsey&Company, 2018. Lithium and cobalt-a tale of two commodities, McKinsey&Company Metals and Mining.

Melin, H.E., 2019. State-of-the-art in reuse and recycling of lithium-ion batteries-A research review, The Swedish Energy Agency. London.

Meshram, P., Pandey, B.D., Mankhand, T.R., 2014. Extraction of lithium from primary and secondary sources by pre-treatment, leaching and separation: A comprehensive review. Hydrometallurgy 150, 192–208. https://doi.org/10.1016/j.hydromet.2014.10.012

Mohr, M., Peters, J.F., Baumann, M., Weil, M., 2020. Toward a cell-chemistry specific life cycle assessment of lithium-ion battery recycling processes. J. Ind. Ecol. 1–13. https://doi.org/10.1111/jiec.13021

Mosaberpanah, M.A., Khales, S.D., 2012. The Role of Transportation in Sustainable Development. Icsdec 2012 441–448. https://doi.org/10.1061/9780784412688.053

Myung, S.T., Maglia, F., Park, K.J., Yoon, C.S., Lamp, P., Kim, S.J., Sun, Y.K., 2017. Nickel-Rich Layered Cathode Materials for Automotive Lithium-Ion Batteries: Achievements and Perspectives. ACS Energy Lett. 2, 196–223. https://doi.org/10.1021/acsenergylett.6b00594

Nealer, R., Hendrickson, T.P., 2015. Review of Recent Lifecycle Assessments of Energy and Greenhouse Gas Emissions for Electric Vehicles. Curr. Sustain. Energy Reports 2, 66–73.

https://doi.org/10.1007/s40518-015-0033-x

Nelson, P.A.P. a., Gallagher, K.G.K.G., Bloom, I.D., Dees, D.W.D.W., 2012. Modeling the Performance and Cost of Lithium-Ion Batteries for Electric-Drive Vehicles. Argonne Natl. Lab. 116. https://doi.org/10.2172/1209682

Neumann, J., Petranikova, M., Meeus, M., Gamarra, J.D., Younesi, R., Winter, M., Nowak, S., 2022. Recycling of Lithium-Ion Batteries—Current State of the Art, Circular Economy, and Next Generation Recycling. Adv. Energy Mater. 2102917. https://doi.org/10.1002/aenm.202102917

Nitta, N., Wu, F., Lee, J.T., Yushin, G., 2015. Li-ion battery materials: Present and future. Mater. Today 18, 252–264. https://doi.org/10.1016/j.mattod.2014.10.040

Noh, H.J., Youn, S., Yoon, C.S., Sun, Y.K., 2013. Comparison of the structural and electrochemical properties of layered Li[NixCoyMnz]O2 (x = 1/3, 0.5, 0.6, 0.7, 0.8 and 0.85) cathode material for lithium-ion batteries. J. Power Sources 233, 121–130. https://doi.org/10.1016/j.jpowsour.2013.01.063

Nordelöf, A., Messagie, M., Tillman, A.M., Ljunggren Söderman, M., Van Mierlo, J., 2014. Environmental impacts of hybrid, plug-in hybrid, and battery electric vehicles—what can we learn from life cycle assessment? Int. J. Life Cycle Assess. 19, 1866–1890. https://doi.org/10.1007/s11367-014-0788-0

Nordelöf, A., Poulikidou, S., Chordia, M., de Oliveira, F.B., Tivander, J., Arvidsson, R., 2019. Methodological approaches to end-of-life modelling in life cycle assessments of lithium-ion batteries. Batteries 5. https://doi.org/10.3390/batteries5030051

Norgate, T.E., Jahanshahi, S., Rankin, W.J., 2007. Assessing the environmental impact of metal production processes. J. Clean. Prod. 15, 838–848. https://doi.org/10.1016/j.jclepro.2006.06.018

Notter, D.A., Gauch, M., Widmer, R., Wäger, P., Stamp, A., Zah, R., Althaus, H.-J.J., 2010. Contribution of Li-ion batteries to the environmental impact of electric vehicles. Environ. Sci. Technol. 44, 6550–6556. https://doi.org/10.1021/es903729a

Nykvist, B., Nilsson, M., 2015. Rapidly falling costs of battery packs for electric vehicles. Nat.

Clim. Chang. 5, 329–332. https://doi.org/10.1038/nclimate2564

Offer, G.J., Contestabile, M., Howey, D.A., Clague, R., Brandon, N.P., 2011. Techno-economic and behavioural analysis of battery electric , hydrogen fuel cell and hybrid vehicles in a future sustainable road transport system in the UK. Energy Policy 39, 1939–1950. https://doi.org/10.1016/j.enpol.2011.01.006

Ohzuku, T., Makimura, Y., 2001. Layered Lithium Insertion Material of LiCo1/3Ni1/3Mn1/3O2 for Lithium-Ion Batteries. Chem. Lett. 30, 642–643. https://doi.org/10.1246/cl.2001.642

Oliveira, L., Messagie, M., Mertens, J., Laget, H., Coosemans, T., Van Mierlo, J., 2015. Environmental performance of electricity storage systems for grid applications, a life cycle approach. Energy Convers. Manag. 101, 326–335. https://doi.org/10.1016/j.enconman.2015.05.063

Opitz, A., Badami, P., Shen, L., Vignarooban, K., Kannan, A.M., 2017. Can Li-Ion batteries be the panacea for automotive applications? Renew. Sustain. Energy Rev. 68, 685–692. https://doi.org/10.1016/j.rser.2016.10.019

World Health Organization, 2014. 7 million premature deaths annually linked to air pollution. World Health Organization. Geneva, Switzerland.

Paulikas, D., Katona, S., Ilaves, E., Stone, G., O'Sullivan, A., 2020a. Where should metals for the green transition come from? DeepGreen.

Paulikas, D., Katona, S., Ilves, E., Ali, S.H., 2020b. Life cycle climate change impacts of producing battery metals from land ores versus deep-sea polymetallic nodules. J. Clean. Prod. 275, 123822. https://doi.org/10.1016/j.jclepro.2020.123822

Peel, M., Sanderson, H., 2020. EU sounds alarm on critical raw materials shortages. Financial Times. URL https://www.ft.com/content/8f153358-810e-42b3-a529-a5a6d0f2077f (accessed 15.11.2022)

Pesaran, A.A., Kim, G.H., Keyser, M., 2009. Integration issues of cells into battery packs for plug-in and hybrid electric vehicles. 24th Int. Batter. Hybrid Fuel Cell Electr. Veh. Symp. Exhib. 2009, EVS 24 3, 1924–1930.

Peters, J.F., Baumann, M., Zimmermann, B., Braun, J., Weil, M., 2016. The environmental impact of Li-Ion batteries and the role of key parameters – A review. Renew. Sustain. Energy Rev. 67, 491–506. https://doi.org/10.1016/j.rser.2016.08.039

Peters, J.F., Weil, M., 2018. Providing a common base for life cycle assessments of Li-Ion batteries. J. Clean. Prod. 171, 704–713. https://doi.org/10.1016/j.jclepro.2017.10.016

Podias, A., Pfrang, A., Di Persio, F., Kriston, A., Bobba, S., Mathieux, F., Messagie, M., Boon-Brett, L., 2018. Sustainability assessment of second use applications of automotive batteries: Ageing of Li-ion battery cells in automotive and grid-scale applications. World Electr. Veh. J. 9, 24. https://doi.org/10.3390/wevj9020024

Porzio, J., Scown, C.D., 2021. Life-Cycle Assessment Considerations for Batteries and Battery Materials. Adv. Energy Mater. 11, 2100771. https://doi.org/10.1002/aenm.202100771

Qiao, Q., Zhao, F., Liu, Z., He, X., Hao, H., 2019. Life cycle greenhouse gas emissions of Electric Vehicles in China: Combining the vehicle cycle and fuel cycle. Energy 177, 222–233. https://doi.org/10.1016/j.energy.2019.04.080

Qiao, Q., Zhao, F., Liu, Z., Jiang, S., Hao, H., 2017. Cradle-to-gate greenhouse gas emissions of battery electric and internal combustion engine vehicles in China. Appl. Energy 204, 1399–1411. https://doi.org/10.1016/j.apenergy.2017.05.041

Quan, J., Zhao, S., Song, D., Wang, T., He, W., Li, G., 2022. Comparative life cycle assessment of LFP and NCM batteries including the secondary use and different recycling technologies. Sci. Total Environ. 819, 153105. https://doi.org/10.1016/j.scitotenv.2022.153105

Rajaeifar, M.A., Ghadimi, P., Raugei, M., Wu, Y., Heidrich, O., 2022. Challenges and recent developments in supply and value chains of electric vehicle batteries: A sustainability perspective. Resour. Conserv. Recycl. 180, 106144. https://doi.org/10.1016/j.resconrec.2021.106144

Rajaeifar, M.A., Raugei, M., Steubing, B., Hartwell, A., Anderson, P.A., Heidrich, O., 2021. Life cycle assessment of lithium-ion battery recycling using pyrometallurgical technologies. J. Ind. Ecol. 1–12. https://doi.org/10.1111/jiec.13157

Rey, I., Vallejo, C., Santiago, G., Iturrondobeitia, M., Lizundia, E., 2021. Environmental Impacts of Graphite Recycling from Spent Lithium-Ion Batteries Based on Life Cycle Assessment. ACS Sustain. Chem. Eng. 9, 14488–14501. https://doi.org/10.1021/acssuschemeng.1c04938

Rinne, M., Elomaa, H., Porvali, A., Lundström, M., 2021. Simulation-based life cycle assessment for hydrometallurgical recycling of mixed LIB and NiMH waste. Resour. Conserv. Recycl. 170. https://doi.org/10.1016/j.resconrec.2021.105586

Romare, M., Dahllöf, L., 2017. The Life Cycle Energy Consumption and Greenhouse Gas Emissions from Lithium-Ion Batteries, IVL Swedish Environmental Research Institute. https://doi.org/978-91-88319-60-9

Rosenman, A., Markevich, E., Salitra, G., Aurbach, D., Garsuch, A., Chesneau, F.F., 2015. Review on Li-Sulfur Battery Systems: an Integral Perspective. Adv. Energy Mater. 5, 1500212. https://doi.org/10.1002/aenm.201500212

Schmidt, T.S., Beuse, M., Zhang, X., Steffen, B., Schneider, S.F., Pena-Bello, A., Bauer, C., Parra, D., 2019. Additional Emissions and Cost from Storing Electricity in Stationary Battery Systems. Environ. Sci. Technol. 53, 3379–3390. https://doi.org/10.1021/acs.est.8b05313

Schmuch, R., Wagner, R., Hörpel, G., Placke, T., Winter, M., 2018. Performance and cost of materials for lithium-based rechargeable automotive batteries. Nat. Energy 3, 267–278. https://doi.org/10.1038/s41560-018-0107-2

Schnell, J., Günther, T., Knoche, T., Vieider, C., Köhler, L., Just, A., Keller, M., Passerini, S., Reinhart, G., 2018. All-solid-state lithium-ion and lithium metal batteries – paving the way to large-scale production. J. Power Sources 382, 160–175. https://doi.org/10.1016/j.jpowsour.2018.02.062

Scientific Applications International Corporation, 2006. Life-cycle assessment: principles and practice. National Risk Management Research Laboratory, Office of Research and Development US EPA, Cincinnati, Ohio.

Shaju, K.M., Subba Rao, G. V, Chowdari, B.V.R., 2002. Performance of layered Li(Ni1/3Co1/3Mn1/3)O2 as cathode for Li-ion batteries. Electrochim. Acta 48, 145–151.

https://doi.org/10.1016/S0013-4686(02)00593-5

Shaw-Stewart, J., Alvarez-Reguera, A., Greszta, A., Marco, J., Masood, M., Sommerville, R., Kendrick, E., 2019. Aqueous solution discharge of cylindrical lithium-ion cells. Sustain. Mater. Technol. 22, e00110. https://doi.org/10.1016/j.susmat.2019.e00110

Shin, S.M., Kim, N.H., Sohn, J.S., Yang, D.H., Kim, Y.H., 2005. Development of a metal recovery process from Li-ion battery wastes. Hydrometallurgy 79, 172–181. https://doi.org/10.1016/j.hydromet.2005.06.004

Si, Q., Mori, D., Takeda, Y., Yamamoto, O., Imanishi, N., 2017. Silicon-carbon composite electrode materials prepared by pyrolysis of a mixture of Manila hemp, silicon powder, and flake artificial graphite for lithium batteries. Energies 10, 1–9. https://doi.org/10.3390/en10111803

Sinn, H.-W., 2019. Are electric vehicles really so climate friendly?. Guard. URL https://www.theguardian.com/environment/2019/nov/25/are-electric-vehicles-really-so-climate-friendly (accessed 3.8.20).

Slattery, M., Dunn, J., Kendall, A., 2021. Transportation of electric vehicle lithium-ion batteries at end-of-life: A literature review. Resour. Conserv. Recycl. 174, 105755. https://doi.org/10.1016/j.resconrec.2021.105755

Sommerville, R., Zhu, P., Rajaeifar, M.A., Heidrich, O., Goodship, V., Kendrick, E., 2021. A qualitative assessment of lithium ion battery recycling processes. Resour. Conserv. Recycl. 165, 105219. https://doi.org/10.1016/j.resconrec.2020.105219

Sovacool, B.K., 2019. The precarious political economy of cobalt: Balancing prosperity, poverty, and brutality in artisanal and industrial mining in the Democratic Republic of the Congo. Extr. Ind. Soc. 6, 915–939. https://doi.org/10.1016/j.exis.2019.05.018

Sun, X., Luo, X., Zhang, Z., Meng, F., Yang, J., 2020. Life cycle assessment of lithium nickel cobalt manganese oxide (NCM) batteries for electric passenger vehicles. J. Clean. Prod. 273, 123006. https://doi.org/10.1016/j.jclepro.2020.123006

Surovtseva, D., Crossin, E., Pell, R., Stamford, L., 2022. Toward a life cycle inventory for graphite production. J. Ind. Ecol. 1–16. https://doi.org/10.1111/jiec.13234

Tagawa, K., Brodd, R.J., 2009. Production processes for fabrication of lithium-ion batteries, in: Lithium-Ion Batteries. Springer.

The Aluminumn Association, 2013. The Environmental Footprint of Semi- Finished Aluminum Products in North America, The Aluminum Association.

Tran, T., Luong, V.T., 2015. Lithium Production Processes, Lithium Process Chemistry: Resources, Extraction, Batteries, and Recycling. Elsevier Inc.

Turcheniuk, K., Bondarev, D., Singhal, V., Yushin, G., 2018. Ten years left to redesign lithium-ion batteries. Nature 559, 467–470. https://doi.org/10.1038/d41586-018-05752-3

Uddin, K., Perera, S., Widanage, W., Somerville, L., Marco, J., 2016. Characterising Lithium-Ion Battery Degradation through the Identification and Tracking of Electrochemical Battery Model Parameters. Batteries 2, 13. https://doi.org/10.3390/batteries2020013

United States Geological Survey (USGS), 2020. Mineral Commodity Summaries 2020, U.S Department of the Interior, U.S Geological Survey.

van Oers, L., 2016. CML-IA database characterisation and normalisation factors for midpoint impact category indicators v4.8.

Väyrynen, A., Salminen, J., 2012. Lithium ion battery production. J. Chem. Thermodyn. 46, 80–85. https://doi.org/10.1016/j.jct.2011.09.005

Vieceli, N., Nogueira, C.A., Guimarães, C., Pereira, M.F.C., Durão, F.O., Margarido, F., 2018. Hydrometallurgical recycling of lithium-ion batteries by reductive leaching with sodium metabisulphite. Waste Manag. 71, 350–361. https://doi.org/10.1016/j.wasman.2017.09.032

Walton, A., Anderson, P., Harper, G., Mann, V., Beddington, J., Abbott, A., Bloodworth, A., OudeNijeweme, D., Schofield, E., Wall, F., 2021. Securing technology-critical metals for Britain. University of Birmingham.

Wang, B., Xu, M., Yang, L., 2014. Study on the economic and environmental benefits of different EV powertrain topologies. Energy Convers. Manag. 86, 916–926. https://doi.org/10.1016/j.enconman.2014.05.077

Wang, J., Liu, P., Hicks-Garner, J., Sherman, E., Soukiazian, S., Verbrugge, M., Tataria, H., Musser, J., Finamore, P., 2011. Cycle-life model for graphite-LiFePO4 cells. J. Power Sources 196, 3942–3948. https://doi.org/10.1016/j.jpowsour.2010.11.134

Wang, J., Purewal, J., Liu, P., Hicks-garner, J., Soukazian, S., Sherman, E., Sorenson, A., Vu, L., Tataria, H., Verbrugge, M.W., 2014. Degradation of lithium ion batteries employing graphite negatives and nickel-cobalt-manganese oxide + spinel manganese oxide positives: Part 1, aging mechanisms and life estimation. J. Power Sources 269, 937–948. https://doi.org/10.1016/j.jpowsour.2014.07.030

Weaving, J.S., Coowar, F., Teagle, D.A., Cullen, J., Dass, V., Bindin, P., Green, R., Macklin, W.J., 2001. Development of high energy density Li-ion batteries based on LiNi1−x−yCoxAlyO2. J. Power Sources, Proceedings of the 10th International Meeting on Lithium Batteries 97–98, 733–735. https://doi.org/10.1016/S0378-7753(01)00700-5

Weiss, M., Cloos, K.C., Helmers, E., 2020. Energy efficiency trade-offs in small to large electric vehicles. Environ. Sci. Eur. 32. https://doi.org/10.1186/s12302-020-00307-8

Wernet, G., Bauer, C., Steubing, B., Reinhard, J., Moreno-Ruiz, E., Weidema, B., 2016. The ecoinvent database version 3 (part I): overview and methodology. Int. J. Life Cycle Assess. 21, 1218–1230. https://doi.org/10.1007/s11367-016-1087-8

Wild, M., O'Neill, L., Zhang, T., Purkayastha, R., Minton, G., Marinescu, M., Offer, G.J., 2015. Lithium sulfur batteries, a mechanistic review. Energy Environ. Sci. 8, 3477–3494. https://doi.org/10.1039/C5EE01388G

Winslow, K.M., Laux, S.J., Townsend, T.G., 2018. A review on the growing concern and potential management strategies of waste lithium-ion batteries. Resour. Conserv. Recycl. 129, 263–277.

Wong, Y.S., Lu, W., Wang, Z., 2010. Life Cycle Cost Analysis of Different Vehicle Technologies in Singapore World Electr. Veh. J. 4, .912-920. World Economic Forum, 2019. A Vision for a Sustainable Battery Value Chain in 2030 Unlocking the Full Potential to Power Sustainable Development and Climate Change Mitigation. Geneva, Switzerland.

Wrålsen, B., Prieto-Sandoval, V., Mejia-Villa, A., O'Born, R., Hellström, M., Faessler, B., 2021. Circular business models for lithium-ion batteries - Stakeholders, barriers, and

drivers. J. Clean. Prod. 317. https://doi.org/10.1016/j.jclepro.2021.128393

Wu, G., Inderbitzin, A., Bening, C., 2015. Total cost of ownership of electric vehicles compared to conventional vehicles : A probabilistic analysis and projection across market segments. Energy Policy 80, 196–214. https://doi.org/10.1016/j.enpol.2015.02.004

Wu, Weixiong, Wang, S., Wu, Wei, Chen, K., Hong, S., Lai, Y., 2019. A critical review of battery thermal performance and liquid based battery thermal management. Energy Convers. Manag. 182, 262–281. https://doi.org/10.1016/j.enconman.2018.12.051

Wu, Z., Wang, M., Zheng, J., Sun, X., Zhao, M., Wang, X., 2018. Life cycle greenhouse gas emission reduction potential of battery electric vehicle. J. Clean. Prod. 190, 462–470. https://doi.org/10.1016/j.jclepro.2018.04.036

Xia, G., Cao, L., Bi, G., 2017. A review on battery thermal management in electric vehicle application. J. Power Sources 367, 90–105. https://doi.org/10.1016/j.jpowsour.2017.09.046

Xiong, S., Ji, J., Ma, X., 2019. Comparative Life Cycle Energy and GHG Emission Analysis for BEVs and PhEVs: A Case Study in China. Energies 12, 834. https://doi.org/10.3390/en12050834

Xu, C., Dai, Q., Gaines, L., Hu, M., Tukker, A., Steubing, B., 2020. Future material demand for automotive lithium-based batteries. Commun. Mater. 1. https://doi.org/10.1038/s43246-020-00095-x

Xu, J., Lin, F., Doeff, M.M., Tong, W., 2017. A review of Ni-based layered oxides for rechargeable Li-ion batteries. J. Mater. Chem. A 5, 874–901. https://doi.org/10.1039/C6TA07991A

Xu, J., Thomas, H.R., Francis, R.W., Lum, K.R., Wang, J., Liang, B., 2008. A review of processes and technologies for the recycling of lithium-ion secondary batteries. J. Power Sources 177, 512–527. https://doi.org/10.1016/j.jpowsour.2007.11.074

Yabuuchi, N., Ohzuku, T., 2003. Novel lithium insertion material of LiCo1/3Ni1/3Mn1/3O2 for advanced lithium-ion batteries. J. Power Sources 119–121, 171–174. https://doi.org/10.1016/S0378-7753(03)00173-3

Yang, F., Xie, Y., Deng, Y., Yuan, C., 2018. Predictive modeling of battery degradation and greenhouse gas emissions from U.S. state-level electric vehicle operation. Nat. Commun. 9, 1–10. https://doi.org/10.1038/s41467-018-04826-0

Yao, L.P., Zeng, Q., Qi, T., Li, J., 2020. An environmentally friendly discharge technology to pretreat spent lithium-ion batteries. J. Clean. Prod. 245, 118820. https://doi.org/10.1016/j.jclepro.2019.118820

Yin, R., Hu, S., Yang, Y., 2019. Life cycle inventories of the commonly used materials for lithium-ion batteries in China. J. Clean. Prod. 227, 960–971. https://doi.org/10.1016/j.jclepro.2019.04.186

Yu, A., Wei, Y., Chen, W., Peng, N., Peng, L., 2018. Life cycle environmental impacts and carbon emissions: A case study of electric and gasoline vehicles in China. Transp. Res. Part D Transp. Environ. 65, 409–420. https://doi.org/10.1016/j.trd.2018.09.009

Yuan, C., Deng, Y., Li, T., Yang, F., 2017. Manufacturing energy analysis of lithium ion battery pack for electric vehicles. CIRP Ann. - Manuf. Technol. 66, 53–56. https://doi.org/10.1016/j.cirp.2017.04.109

Zackrisson, M., Avellán, L., Orlenius, J., 2010. Life cycle assessment of lithium-ion batteries for plug-in hybrid electric vehicles-Critical issues. J. Clean. Prod. 18, 1519-1529. https://doi.org/10.1016/j.jclepro.2010.06.004

Zakeri, B., Syri, S., 2015. Electrical energy storage systems : A comparative life cycle cost analysis. Renew. Sustain. Energy Rev. 42, 569–596. https://doi.org/10.1016/j.rser.2014.10.011

Zhao, Y., Diaz, L.B., Patel, Y., Zhang, T., Offer, G.J., 2019. How to Cool Lithium Ion Batteries: Optimising Cell Design using a Thermally Coupled Model. J. Electrochem. Soc. 166, A2849–A2859. https://doi.org/10.1149/2.0501913jes

Zhong, X., Liu, W., Han, J., Jiao, F., Qin, W., Liu, T., 2020. Pretreatment for the recovery of spent lithium ion batteries: theoretical and practical aspects. J. Clean. Prod. 263, 121439. https://doi.org/10.1016/j.jclepro.2020.121439

Zhou, Z., Lai, Y., Peng, Q., Li, J., 2021. Comparative life cycle assessment of merging

recycling methods for spent lithium ion batteries. Energies 14, 1–18. https://doi.org/10.3390/en14196263

Appendices

Appendix A: LIB production inventory tables

Table A1. Battery pack production

Description	Input	Output	Unit	Ecoinvent 3.5 Process
Battery pack		1	kg	
Cooling system	0.041		kg	
Battery cell	0.6		kg	
Packaging	0.32		kg	
BMS	0.037		kg	
Electricity	1.44×10^{-3}		MJ	NO: market for electricity, medium voltage
Production facility	1.90×10^{-8}		pcs.	SE: precious metal refinery construction
Lorry transport	0.16		tkm	RER: transport, lorry >16t, fleet average [Street]
Ship transport	4.9		tkm	OCE: transport, transoceanic freight ship [Water]
Waste heat		0.0014	MJ	

Table A2. Battery cell production

Description	Input	Output	Unit	Ecoinvent 3.5 Process
Battery cell		1	kg	
Anode	0.39		kg	
Cathode	0.43		kg	
Electrolyte	0.16		kg	
Separator	0.022		kg	
Cell container	6.70×10^{-3}		kg	
Decarbonised water	3.80×10^{2}		kg	GLO: market for water, decarbonised, at user
Electricity	1.01×10^{2}		MJ	46%: KR: electricity production, hard coal 33%: KR: electricity production, nuclear, pressure water reactor 15%: KR: electricity production, natural gas, conventional power plant 4.4%: KR: electricity production, oil 1.4%: KR: electricity production, hydro, run-of-river 0.15%: KR: electricity production, wind, 1-3MW turbine, onshore 0.05 % KR: electricity production, photovoltaic, 570kWp open ground installation, multi-Si
Rail transport	0.26		tkm	RER: market group for transport, freight train
Lorry transport	0.1		tkm	RER: market for transport, freight, lorry >32 metric ton, EURO3
Waste heat		100	MJ	

Table A3. Anode production

Description	Input	Output	Unit	Ecoinvent 3.5 Process
Anode		1	kg	
Negative electrode paste	0.43		kg	
Negative current collector Cu	0.57		kg	
Rail transport	0.37		tkm	RER: market group for transport, freight train
Lorry transport	0.1		tkm	RER: market for transport, freight, lorry >32 metric ton, EURO3

Table A4. Sheet rolling - copper

Description	Input	Output	Unit	Ecoinvent 3.5 Process
Negative current collector Cu		1	kg	
Primary copper	0.85		kg	RLA: copper production, primary
Secondary copper	0.15		kg	RER: treatment of copper scrap by electrolytic refining
Production of current collector	1		kg	RER: sheet rolling, copper
Rail transport	0.2		tkm	RER: market group for transport, freight train
Lorry transport	0.1		tkm	RER: market for transport, freight, lorry >32 metric ton, EURO3

Table A5. Mixing of anode active material

Description	Input	Output	Unit	Ecoinvent 3.5 Process
Negative electrode paste		1	kg	
graphite, battery grade	0.96		kg	CN: graphite production, battery grade
Acrylic acid	0.02		kg	RER: acrylic acid production
Carboxymethyl cellulose	0.02		kg	RoW: carboxymethyl cellulose production, powder
Rail transport	1.2		tkm	RER: market group for transport, freight train
Lorry transport	0.19		tkm	RER: market for transport, freight, lorry >32 metric ton, EURO3
Chemical plant	4×10^{-10}		pcs.	RER: chemical factory construction, organics
1-Methyl-2-pyrrolidinone		0.94	kg	1-Methyl-2-pyrrolidone [Group NMVOC to air]

Table A6. Cathode production

Description	Input	Output	Unit	Ecoinvent 3.5 Process
Cathode		1	kg	
Positive electrode paste	0.89		kg	
Positive current collector Al	0.11		kg	
Rail transport	0.55		tkm	RER: market group for transport, freight train
Lorry transport	0.1		tkm	RER: market for transport, freight, lorry >32 metric ton, EURO3

Table A7. Sheet rolling - aluminium

Description	Input	Output	Unit	Ecoinvent 3.5 Process
Positive current collector Al		1	kg	
Aluminium production mix	1		kg	68% from IAI Area, Russia & RER w/o EU27 & EFTA: aluminium production, primary, ingot 22% from RER: treatment of aluminium scrap, new, at refiner 10% from RER: treatment of aluminium scrap, post-consumer, by collecting, sorting, cleaning, pressing
Production of current collector	1		kg	RoW: sheet rolling, aluminium
Rail transport	0.2		tkm	RER: market group for transport, freight train
Lorry transport	0.1		tkm	RER: market for transport, freight, lorry >32 metric ton, EURO3
Facility	1.50×10^{-10}		pcs.	RoW: aluminium casting facility construction

Table A8. Mixing of cathode active material

Description	Input	Output	Unit	Ecoinvent 3.5 Process
Positive electrode paste		1	kg	
$Li[N_{1/3}C_{1/3}M_{1/3}]O_2$	0.94		kg	
N-methyl-2-pyrrolidone	0.002		kg	RER: N-methyl-2-pyrrolidone production
PVDF	0.04		kg	RoW: polyvinylfluoride production
Rail transport	0.46		tkm	RER: market group for transport, freight train
Lorry transport	0.14		tkm	RER: market for transport, freight, lorry >32 metric ton, EURO3
Chemical plant	4.0×10^{-10}		pcs.	RER: chemical factory construction, organics

Table A9. Positive active material production

Description	Input	Output	Unit	Ecoinvent 3.5 Process
$Li[N_{1/3}C_{1/3}M_{1/3}]O_2$		1	kg	
Lithium carbonate	0.38		kg	GLO: market for lithium carbonate
$N_{1/3}C_{1/3}M_{1/3}(OH)_2$	0.95		kg	
Chemical plant	4.6×10^{-10}		pcs.	RER: chemical factory construction, organics
Electricity	25.2		MJ	RAS: market group for electricity, low voltage

Table A10. NMC hydroxide production

Description	Input	Output	Unit	Ecoinvent 3.5 Process
$N_{1/3}C_{1/3}M_{1/3}(OH)_2$		1	kg	
Cobalt sulphate	0.56		kg	
Manganese sulphate	0.55		kg	GLO: market for manganese sulfate
Nickel sulphate	0.56		kg	GLO: market for nickel sulfate
Sodium hydroxide	0.89		kg	RER: soda production, solvay process
Chemical plant	4×10^{-10}		pcs.	RER: chemical factory construction, organics
Heat	42.6		MJ	RoW: market for heat, from steam, in chemical industry
Sodium sulphate		1.6	kg	Sodium sulphate [Inorganic emissions to fresh water]

Table A11. Electrolyte production

Description	Input	Output	Unit	Ecoinvent 3.5 Process
Electrolyte		1	kg	
Ethylene carbonate	0.88		kg	GLO: market for ethylene carbonate
Lithium hexafluorophosphate	0.12		kg	RoW: lithium hexafluorophosphate production
Chemical plant	4.0×10^{-10}		pcs.	RER: chemical factory construction, organics
Rail transport	0.6		tkm	RER: market group for transport, freight train
Lorry transport	0.1		tkm	RER: market for transport, freight, lorry >32 metric ton, EURO3

Table A12. Separator production

Description	Input	Output	Unit	Ecoinvent 3.5 Process
Separator		1	kg	
Polypropylene granulate	1		kg	RoW: polypropylene production, granulate
Injection moulding	1		kg	RER: injection moulding
Rail transport	0.2		tkm	RER: market group for transport, freight train
Lorry transport	0.1		tkm	RER: market for transport, freight, lorry >32 metric ton, EURO3
Plastics plant	7.4×10^{-10}		pcs.	RER: plastic processing factory construction

Table A13. Cell container production

Description	Input	Output	Unit	Ecoinvent 3.5 Process
Cell container		1	kg	
Tab, Aluminum	0.22		kg	68% from IAI Area, Russia & RER w/o EU27 & EFTA: aluminium production, primary, ingot 22% from RER: treatment of aluminium scrap, new, at refiner 10% from RER: treatment of aluminium scrap, post-consumer, by collecting, sorting, cleaning, pressing
Production of aluminum tab	0.22		kg	RoW: sheet rolling, aluminium
Tab, Copper	0.38		kg	85% RLA: copper production, primary 15% RER: treatment of copper scrap by electrolytic refining
Production of copper tab	0.38		kg	RER: sheet rolling, copper
Multilayer pouch	0.4			34% from IAI Area, Russia & RER w/o EU27 & EFTA: aluminium production, primary, ingot 11% from RER: treatment of aluminium scrap, new, at refiner 5% from RER: treatment of aluminium scrap, post-consumer, by collecting, sorting, cleaning, pressing 8% from RER: nylon 6 production 7.8% from RoW: polyethylene terephthalate, granulate, bottle grade, recycled to generic market for bottle grade PET 32% from GLO: market for polypropylene, granulate 2.5% from RER: packaging film production, low density polyethylene
Production of nylon	0.188		kg	RER: injection moulding
Production of aluminum material in pouch	0.2		kg	RoW: sheet rolling, aluminium
Rail transport	0.32		tkm	RER: market group for transport, freight train
Lorry transport	0.16		tkm	RER: market for transport, freight, lorry >32 metric ton, EURO3
Aluminium tab plant	3.3×10^{-11}		pcs.	RoW: aluminium casting facility construction
Copper tab plant	1.75×10^{-10}		pcs.	RER: metal working factory construction
Pouch plant	1.4×10^{-10}		pcs.	RER: plastic processing factory construction

Table A14. Updated background processes for the production of Packaging/BMS/Cooling system. Original inventories can be found at Ellingsen et al. (2014)**.**

Ellingsen et al. (2014)	This study
Materials	
steel, low-alloyed, at plant/ RER/ kg	GLO: market for steel, low-alloyed
nylon 6, at plant/ RER/ kg	RER: nylon 6 production
nylon 66, glass-filled, at plant/ RER/ kg	RER: nylon 6-6 production, glass-filled
aluminium, production mix, at plant/ RER/ kg	68% from IAI Area, Russia & RER w/o EU27 & EFTA: aluminium production, primary, ingot 22% from RER: treatment of aluminium scrap, new, at refiner 10% from RER: treatment of aluminium scrap, post-consumer, by collecting, sorting, cleaning, pressing
copper, primary, at refinery/ GLO/ kg	RLA: copper production, primary
copper, secondary, at refinery/ RER/ kg	RER: treatment of copper scrap by electrolytic refining
acrylonitrile-butadiene-styrene copolymer, ABS, at plant/ RER/ kg	RER: acrylonitrile-butadiene-styrene copolymer production
synthetic rubber, at plant/ RER/ kg	RoW: synthetic rubber production
polypropylene, granulate, at plant/ RER/ kg	GLO: market for polypropylene, granulate
butyl acrylate, at plant/ RER/ kg	RoW: butyl acrylate production
printed wiring board, through-hole mounted, unspec., Pb free, at plant/ GLO/ kg	GLO: market for printed wiring board, through-hole mounted, unspecified, Pb free
integrated circuit, IC, logic type, at plant/ GLO/ kg	GLO: integrated circuit production, logic type
connector, clamp connection, at plant/ GLO/ kg	GLO: electric connector production, wire clamp
brass, at plant/ CH/ kg	RoW: brass production
tin, at regional storage/ RER/ kg	GLO: market for tin
cable, ribbon cable, 20-pin, with plugs, at plant/ GLO/ kg	GLO: cable production, ribbon cable, 20-pin, with plugs
electronic component, passive, unspecified, at plant/ GLO/ kg	GLO: market for electronic component, passive, unspecified
ethylene glycol, at plant/ RER/ kg	RER: ethylene glycol production
polyvinylchloride, at regional storage/ RER/ kg	RER: polyvinylchloride production, bulk polymerisation

silicon, electronic grade, at plant/ DE/ kg	DE: silicon production, electronics grade
glass fibre, at plant/ RER/ kg	RER: glass fibre production
Energy and processes	
steel product manufacturing, average metal working/ RER/ kg	RER: metal working, average for steel product manufacturing
injection moulding/ RER/ kg	RER: injection moulding
anodising, aluminium sheet/ RER/ m2	RoW: anodising, aluminium sheet
sheet rolling, aluminium/ RER/ kg	RoW: sheet rolling, aluminium
aluminium product manufacturing, average metal working/ RER/ kg	RER: metal working, average for aluminium product manufacturing
copper product manufacturing, average metal working/ RER/ kg	RER: metal working, average for copper product manufacturing
casting, brass/ CH/ kg	CH: casting, brass
Energy and processes	
steel product manufacturing, average metal working/ RER/ kg	RER: metal working, average for steel product manufacturing
injection moulding/ RER/ kg	RER: injection moulding
anodising, aluminium sheet/ RER/ m2	RoW: anodising, aluminium sheet
sheet rolling, aluminium/ RER/ kg	RoW: sheet rolling, aluminium
aluminium product manufacturing, average metal working/ RER/ kg	RER: metal working, average for aluminium product manufacturing
copper product manufacturing, average metal working/ RER/ kg	RER: metal working, average for copper product manufacturing
casting, brass/ CH/ kg	CH: casting, brass
Facilities	
facilities precious metal refinery/ SE/ unit	SE: precious metal refinery construction
metal working factory/ RER/ unit	RER: metal working factory construction
plastics processing factory/ RER/ unit	RER: plastic processing factory construction
aluminium casting, plant/ RER/ unit	RER:aluminium casting facility construction
electronic component production plant/ GLO/ unit	GLO: electronic component factory construction
Transportation	
transport, lorry >16t, fleet average/ RER/ tkm	RER: market for transport, freight, lorry 16-32 metric ton, EURO3
transport, transoceanic freight ship/ OCE/ tkm	GLO: transport, freight, sea, transoceanic ship

Table A15. Most important modifications of this study compared to Ellingsen et al**.** (2014)**.**

Study	Nickel sulphate production	Manganese sulphate production	Battery grade graphite	Lithium hexafluorophosphate
(Ellingsen et al., 2014)	Modified ecoinvent inventory for primary nickel (Majeau-Bettez et al., 2011)	Crude model based on (Majeau-Bettez et al., 2011)	Modified ecoinvent inventory for industrial graphite (Notter et al., 2010)	Production not modelled based on the assumptions of (Majeau-Bettez et al., 2011)
BCG scenario	GLO: market for manganese sulfate ecoinvent 3.5	GLO: market for nickel sulfate ecoinvent 3.5	GLO: market for graphite, battery grade	GLO: market for lithium hexafluorophosphate

Table A16. Anode production for NMC333-SiGr.

Description	Input	Output	Unit	Ecoinvent 3.5 Process
Anode		1	kg	
Negative electrode paste	0.255		kg	
Negative current collector Cu	0.745		kg	
Rail transport	0.37		tkm	GLO: market group for transport, freight train
Lorry transport	0.1		tkm	GLO: market for transport, freight, lorry >32 metric ton, EURO3

Table A17. Mixing of anode active material for NMC333-SiGr.

Description	Input	Output	Unit	Ecoinvent 3.5 Process
Negative electrode paste		1	kg	
graphite, battery grade	0.75		kg	CN: graphite production, battery grade
Silicon, electronics grade	0.21			GLO: market for silicon, electronics grade
Acrylic acid	0.02		kg	RoW: acrylic acid production
Carboxymethyl cellulose	0.02		kg	RoW: carboxymethyl cellulose production, powder
Rail transport	1.2		tkm	GLO: market group for transport, freight train
Lorry transport	0.19		tkm	GLO: market for transport, freight, lorry >32 metric ton, EURO3
Chemical plant	4×10^{-10}		pcs.	RoW: chemical factory construction, organics
1-Methyl-2-pyrrolidinone		0.94	kg	1-Methyl-2-pyrrolidone [Group NMVOC to air]

Table A18. Cathode production for NMC333-SiGr.

Description	Input	Output	Unit	Ecoinvent 3.5 Process
Cathode		1	kg	
Positive electrode paste	0.91		kg	
Positive current collector Al	0.09		kg	
Rail transport	0.55		tkm	GLO: market group for transport, freight train
Lorry transport	0.1		tkm	GLO: market for transport, freight, lorry >32 metric ton, EURO3

Table A19. Anode production for NMC622-SiGr

Description	Input	Output	Unit	Ecoinvent 3.5 Process
Anode		1	kg	
Negative electrode paste	0.265		kg	
Negative current collector Cu	0.735		kg	
Rail transport	0.37		tkm	GLO: market group for transport, freight train
Lorry transport	0.1		tkm	GLO: market for transport, freight, lorry >32 metric ton, EURO3

Table A20. Cathode production for NMC622-SiGr.

Description	Input	Output	Unit	Ecoinvent 3.5 Process
Cathode		1	kg	
Positive electrode paste	0.91		kg	
Positive current collector Al	0.09		kg	
Rail transport	0.55		tkm	GLO: market group for transport, freight train
Lorry transport	0.1		tkm	GLO: market for transport, freight, lorry >32 metric ton, EURO3

Table A21. NMC hydroxide production for NMC622-SiGr.

Description	Input	Output	Unit	Ecoinvent 3.5 Process
$NC_{1/3}M_{1/3}(OH)_2$		1	kg	
Cobalt sulphate	0.34		kg	
Manganese sulphate	0.33		kg	GLO: market for manganese sulfate
Nickel sulphate	1		kg	GLO: market for nickel sulfate
Sodium hydroxide	0.87		kg	RoW: soda production, solvay process
Heat	42.6		MJ	RoW: market for heat, from steam, in chemical industry
Chemical plant	4×10^{-10}		pcs.	RoW: chemical factory construction, organics
Sodium sulphate		1.6	kg	Sodium sulphate [Inorganic emissions to fresh water]

Table A22. Anode production for NMC811-SiGr

Description	Input	Output	Unit	Ecoinvent 3.5 Process
Anode		1	kg	
Negative electrode paste	0.292		kg	
Negative current collector Cu	0.708		kg	
Rail transport	0.37		tkm	GLO: market group for transport, freight train
Lorry transport	0.1		tkm	GLO: market for transport, freight, lorry >32 metric ton, EURO3

Table A23. Cathode production for NMC811-SiGr.

Description	Input	Output	Unit	Ecoinvent 3.5 Process
Cathode		1	kg	
Positive electrode paste	0.907		kg	
Positive current collector Al	0.093		kg	
Rail transport	0.55		tkm	GLO: market group for transport, freight train
Lorry transport	0.1		tkm	GLO: market for transport, freight, lorry >32 metric ton, EURO3

Table A24. NMC hydroxide production for NMC811-SiGr.

Description	Input	Output	Unit	Ecoinvent 3.5 Process
$NC_{1/4}M_{1/4}(OH)_2$		1	kg	
Cobalt sulphate	0.17		kg	
Manganese sulphate	0.16		kg	GLO: market for manganese sulfate
Nickel sulphate	1.34		kg	GLO: market for nickel sulfate
Sodium hydroxide	0.87		kg	RoW: soda production, solvay process
Heat	42.6		MJ	RoW: market for heat, from steam, in chemical industry
Chemical plant	4E-10		pcs.	RoW: chemical factory construction, organics
Sodium sulphate		1.6	kg	Sodium sulphate [Inorganic emissions to fresh water]

Appendix B: LIB recycling inventory tables

Table A25 summarises the collection and sorting inventory. The transport distances were based on Jiang et al. (.2022), who reported that batteries are transported firstly by freight rail (688 km) and then by lorry with a 32 tons load capacity (174 km) based on Chinese averages. Also, regarding the sorting process, the energy consumption of a conveyor belt of 2.4 W h per kg of batteries sorted is assumed based on Fisher et al. (2006). It is noted that Fisher et al. (2006) refer to cell level sorting, whereas in this study the same energy consumption by weight is assumed to be representative for battery packs. The energy consumption of a forklift was taken into account based on Fuc et al. (2016). The electric forklift ELE2 was chosen with 1.6 t capacity, which consumes 0.28 kWh $(t\ km)^{-1}$. Based on a 30 m distance from the point of collecting the load to unloading as described by Fuc et al. (2016) , the energy consumption of the forklift is estimated as 17×10^{-3} Wh.

Table A25. Collection & sorting

Description	Input	Output	Unit	Ecoinvent 3.5 Process
Spent battery pack, at end-user	1		kg	
Rail transport	0.688		t km	GLO: market group for transport, freight train
Lorry transport	0.174		t km	RoW: market for transport, freight, lorry >32 tonnes, EURO5
Conveyor belt operation	2.4		Wh	CN: market group for electricity, medium voltage
Forklift operation	0.017		Wh	CN: market group for electricity, medium voltage
Spent battery pack, at recycling facility		1	kg	Table A3

Table A26 summarises the dismantling inventory. It was assumed that robotic dismantling is performed using the IRB4400 robot by ABB with a power consumption of 1.33 kW based on Choux et al. (2021). The task planner of Baazouzi et al. (Baazouzi et al., 2021) was then used to calculate the average time that it takes to disassemble a battery pack. Based on their case study for the Audi A3 Sportback e-tron hybrid battery pack which includes 8 modules, it takes 31 min to dismantle the battery pack. The number was adjusted to account for the fact that the battery pack under study includes 12 modules, resulting in a disassembly time of 32 minutes. Multiplying the number with the robot's power consumption resulted in an energy consumption of 0.7 kW h to disassemble the 253 kg battery pack.

Table A26. Dismantling

Description	Input	Output	Unit	Ecoinvent 3.5 Process
Spent battery pack, at recycling facility	1		kg	
Robotic disassembly	2.8		Wh	CN: market group for electricity, medium voltage
Spent battery cells		0.6	kg	Table A4
Spent BMS, TMS and Packaging		0.4	kg	Table A7

Table A27 summarises the discharging inventory based on the study of Yao et al. (Yao et al., 2020) who modelled a quick discharge device based on the immersion of the battery in $FeSO_4$ solution. The bill of materials was directly retrieved from their study and was matched to equivalent background processes from the Ecoinvent database.

Table A27. Discharging

Description	Input	Output	Unit	Ecoinvent 3.5 Process
Spent battery cells	1		kg	
Chemicals	0.022		kg	GLO: market for chemical, organic
Water	0.003		m^3	Flow to the environment
Electricity	0.27		MJ	CN: market group for electricity, medium voltage
Wastewater	-0.00302		m^3	RoW: market for wastewater, average
Equipment	3.4×10^{-7}		m	GLO: market for conveyor belt
Discharged battery cells		1	kg	

The aggregated LCI for hydrometallurgical treatment of LIB cells is shown in Table A28. The process includes shredding and chemical treatment of waste batteries, with the material inputs/outputs based on Mohr et al. (2020).

Table A28. Hydrometallurgical processing of battery cells

Description	Input	Output	Unit	Ecoinvent 3.5 Process
Discharged battery cells	1		kg	
Sulfuric acid	0.213		kg	RoW: market for sulfuric acid
Lime	0.116		kg	RoW: lime production, hydrated, packed
Chemicals	0.025		kg	GLO: market for chemicals, inorganic
Electricity	0.504		MJ	CN: market group for electricity, medium voltage
Water	7.2×10^{-4}		m^3	Flow to the environment
Facility	4×10^{-10}		pcs.	GLO: market for chemical factory, organics
Metals for further treatment	-0.267		kg	GLO: market for non-Fe-Co-metals, from Li-ion battery, hydrometallurgical processing
Waste plastic	-0.0481		kg	RoW: market for waste plastic, mixture
Waste gypsum	-0.339		kg	RoW: market for waste gypsum
Inert waste	-0.202		kg	RoW: market for inert waste, for final disposal
Lithium(I) hydroxide*	**-0.082**		**kg**	**GLO: market for lithium hydroxide**
Nickel(II) sulfate*	**-0.172**		**kg**	**GLO: market for nickel sulfate**
Cobalt(II) sulfate*	**-0.173**		**kg**	**RoW: market for cobalt sulfate, ecoinvent 3.8**

Manganese(II) sulfate*	**-0.168**		**kg**	**GLO: market for manganese sulfate**
Aluminium scrap		0.0538	kg	Table A8
Copper scrap		0.238	kg	Table A10
Biological Oxygen Demand		6×10^{-5}	kg	Process emissions
Chemical Oxygen Demand		3×10^{-5}	kg	
Cobalt, to freshwater		1.7×10^{-8}	kg	
Copper, to freshwater		1.65×10^{-8}	kg	
Dissolved Organic Carbon		1.11×10^{-5}	kg	
Fluoride, to freshwater		3×10^{-8}	kg	
Hydrocarbons, to freshwater		10^{-8}	kg	
Nickel(II) to surface water		1.65×10^{-8}	kg	
NMVOC		2.5×10^{-6}	kg	
Solids, to freshwater		1.2×10^{-5}	kg	
Sulfur dioxide, to air		4.5×10^{-6}	kg	
Total organic bound carbon		1.11×10^{-5}	kg	
Wastewater		6.12×10^{-4}	m^3	
Water, to air		1.08×10^{-4}	m^3	

*Bold text indicates displaced materials

The aggregated LCI for pyrometallurgical treatment of LIB cells is shown in Table A29. The process includes mechanical treatment, neutralisation and processing, with material inputs/outputs based on Mohr et al. (2020).

Table A29. Pyrometallurgical processing of battery cells

Description	Input	Output	Unit	Ecoinvent 3.5 Process
Discharged battery cells	1		kg	
Sodium hydroxide	0.35		kg	GLO: market for sodium hydroxide, without water, in 50% solution state
Electrical energy	2.88		MJ	CN: market group for electricity, medium voltage
Water	0.001		m^3	Flow to the environment
Facility	5×10^{-10}		pcs.	GLO: market for blister-copper conversion facility
Metals for further treatment	-0.266		kg	GLO: market for non-Fe-Co-metals, from Li-ion battery, pyrometallurgical processing
Waste plastic	-0.0481		kg	RoW: market for waste plastic, mixture
Nickel(II) sulfate*	**-0.172**		**kg**	**GLO: market for nickel sulfate**
Cobalt(II) sulfate*	**-0.173**		**kg**	**RoW: market for cobalt sulfate, ecoinvent 3.8**
Manganese(II) sulfate*	**-0.168**		**kg**	**GLO: market for manganese sulfate**
Aluminium scrap		0.0537	kg	Table A8
Copper scrap		0.213	kg	Table A10
Chloride, to freshwater		0.04	kg	Process emissions
Sulfate, to freshwater		0.06	kg	
Particulates, <2.5 μm, to air		1.04×10^{-4}	kg	
Particulates, >10 μm, to air		1.04×10^{-5}	kg	
Particulates,>2.5 μm and <10 μm, to air		9.36×10^{-5}	kg	
Sulfur dioxide, to air		4.8×10^{-5}	kg	
Wastewater		8.5×10^{-4}	m^3	
Water, to air		1.5×10^{-4}	m^3	

*Bold text indicates displaced materials

Table A30. Shredding and sorting

Description	Input	Output	Unit	Ecoinvent 3.5 Process
Spent BMS, TMS and Packaging	1		kg	
Shredding and sorting	-1		kg	GLO: treatment of waste electric and electronic equipment, shredding
Waste plastic	-0.2		kg	RoW: market for waste plastic, mixture
Waste electric wiring	-0.01		kg	RoW: market for waste electric wiring
Electronic scrap	-0.01		kg	GLO: market for electronics scrap from control units
Used printed wiring boards	-0.01		kg	GLO: market for used printed wiring boards
Aluminium scrap		0.38	kg	Table A8
Copper scrap		0.02	kg	Table A10
Steel scrap		0.33	kg	Table A9
Waste, general		0.04	kg	Flow to the environment

Table A31. Aluminium scrap preparation

Description	Input	Output	Unit	Ecoinvent 3.5 Process
Aluminium scrap	1		kg	
Aluminium scrap processing	-1		kg	RoW: treatment of aluminium scrap, post-consumer, by collecting, sorting, cleaning, pressing
Aluminium scrap, prepared for melting		1	kg	Table A11

Table A32. Steel scrap preparation

Description	Input	Output	Unit	Ecoinvent 3.5 Process
Steel scrap	1		kg	
Steel scrap processing	-1		kg	RoW: sorting and pressing of iron scrap
Steel scrap, prepared for melting		1	kg	Table A12

Table A33. Electrolytic refining of copper

Description	Input	Output	Unit	Ecoinvent 3.5 Process
Copper scrap	1		kg	
Electrolytic refining	1		kg	RoW: treatment of copper scrap by electrolytic refining
Secondary copper*		**-0.76**	**kg**	**RAS: copper production, primary**

*Bold text indicates displaced materials

Table A34. Aluminium melting and casting

Description	Input	Output	Unit	Ecoinvent 3.5 Process
Aluminium scrap, prepared for melting	1		kg	
Argon	4.39×10^{-4}		kg	RoW: market for argon, liquid
Cryolite	5.44×10^{-4}		kg	GLO: market for cryolite
Filter media	1.11×10^{-4}		kg	GLO: air filter production
Hydraulic oil	4.17×10^{-5}		kg	GLO: market for chemical, organic
Quicklime	3.81×10^{-3}		kg	RoW: market for quicklime, milled, packed
Lubricant	2.77×10^{-5}		kg	GLO: market for chemical, organic
Nitrogen	0.016		kg	RoW: market for nitrogen, liquid
Oxygen	1.5×10^{-4}		kg	RoW: market for oxygen, liquid
Potassium chloride	5.44×10^{-4}		kg	GLO: market for potassium chloride, as K2O
Refractory	1.18×10^{-3}		kg	GLO: market for refractory, basic, packed
Sodium chloride	1.02×10^{-2}		kg	GLO: market for sodium chloride, powder
Sodium hydroxide	1.83×10^{-4}		kg	GLO: market for sodium hydroxide, without water, in 50% solution state
Sulfuric acid	2.89×10^{-5}		kg	RoW: market for sulfuric acid
Plastic packaging	1.15×10^{-5}		kg	RoW: polystyrene production, general purpose
Steel packaging	8.72×10^{-5}		kg	GLO: market for steel, low-alloyed
Wood packaging	3.39×10^{-4}		kg	RoW: market for cleft timber, measured as dry mass
Water	0.32		kg	

Electrical energy	0.11		kW h	CN: market group for electricity, medium voltage
Thermal energy, natural gas	4.57		MJ	GLO: market group for heat, district or industrial, natural gas
Metal scrap, for recovery	-7.25×10^{-4}		kg	RoW: treatment of scrap aluminium, municipal incineration
Dross, for recovery	-0.064		kg	GLO: market for dross from Al electrolysis
Used oil, for recovery	-5.3×10^{-5}		kg	RoW: treatment of bilge oil, hazardous waste incineration
Filter dust, for disposal	-6.88×10^{-3}		kg	RoW: treatment of filter dust from Al electrolysis, residual material landfill
Refractory, for disposal	-1.27×10^{-3}		kg	RoW: treatment of refractory spent pot liner from Al electrolysis, residual material landfill
Solid waste, for disposal	-2.5×10^{-5}		kg	GLO: solid waste, unsanitary landfill, dry infiltration class (100mm)
Saltcake, for disposal	-0.034		kg	GLO:treatment of refinery sludge, hazardous waste incineration
Al ingot*	**-0.96**		**kg**	**CN: aluminium production, primary, ingot**
Carbon dioxide, to air		6.96×10^{-6}	kg	Process emissions
Chlorine, to air		2.26×10^{-6}	kg	
Dust, to air		2.70×10^{-4}	kg	
Hydrogen chloride, to air		8.41×10^{-5}	kg	
Hydrogen fluoride, to air		2.46×10^{-5}	kg	
Lead, to air		1.03×10^{-6}	kg	
Mercury, to air		7.60×10^{-11}	kg	
Methane, to air		3.72×10^{-7}	kg	
Nitrogen dioxide, to air		2.03×10^{-4}	kg	

Nitrogen oxide, to air	3.53×10^{-7}	kg
Sulphur dioxide, to air	2.27×10^{-5}	kg
VOCs, to air	8.42×10^{-5}	kg
Al^{III}, to soil	7.29×10^{-5}	kg
Copper(II), to soil	2.01×10^{-6}	kg
Lead(II), to soil	3.64×10^{-8}	kg
Zinc(II), to soil	1.21×10^{-6}	kg

*Bold text indicates displaced materials

Table A35. Steel melting and casting

Description	Input	Output	Unit	Ecoinvent 3.5 Process
Steel scrap, prepared for melting	1		kg	
Quicklime	0.0372		kg	RoW: market for quicklime, milled, packed
Refractory	0.0495		kg	GLO: market for refractory, basic, packed
Electrode	0.0018		kg	GLO: electrode production, negative, Ni
Alloys	0.0019		kg	GLO: market for iron-nickel-chromium alloy
Electrical energy	0.35		kW h	CN: market group for electricity, medium voltage
Heat, natural gas	0.15		MJ	GLO: market group for heat, district or industrial, natural gas
Wastewater	-4.5×10^{-7}		m^3	RoW: market for wastewater, average
Refractory waste	-6.19×10^{-6}		kg	RoW: treatment of refractory spent pot liner from Al electrolysis, residual material landfill
EAF slag	-0.16		kg	RoW: treatment of slag, unalloyed electric arc furnace steel, residual material landfil
Crude steel*	**-0.87**		**kg**	**GLO: market for steel, low-alloyed**

*Bold text indicates displaced materials